Discrete Representation of Signals from
Infinite Dimensional Hilbert
Spaces with Application to Noise
Suppression and Compression

by A. Teolis
Advisors: J.J. Benedetto and S.A. Shamma

Report Documentation Page		*Form Approved* *OMB No. 0704-0188*

Public reporting burden for the collection of information is estimated to average 1 hour per response, including the time for reviewing instructions, searching existing data sources, gathering and maintaining the data needed, and completing and reviewing the collection of information. Send comments regarding this burden estimate or any other aspect of this collection of information, including suggestions for reducing this burden, to Washington Headquarters Services, Directorate for Information Operations and Reports, 1215 Jefferson Davis Highway, Suite 1204, Arlington VA 22202-4302. Respondents should be aware that notwithstanding any other provision of law, no person shall be subject to a penalty for failing to comply with a collection of information if it does not display a currently valid OMB control number.

1. REPORT DATE **1993**	2. REPORT TYPE	3. DATES COVERED **00-00-1993 to 00-00-1993**

4. TITLE AND SUBTITLE **Discrete Representation of Signals from Infinite Dimensional Hilbert Spaces with Application to Noise Suppression and Compression**	5a. CONTRACT NUMBER
	5b. GRANT NUMBER
	5c. PROGRAM ELEMENT NUMBER
6. AUTHOR(S)	5d. PROJECT NUMBER
	5e. TASK NUMBER
	5f. WORK UNIT NUMBER
7. PERFORMING ORGANIZATION NAME(S) AND ADDRESS(ES) **University of Maryland,The Graduate School,2123 Lee Building,College Park,MD,20742**	8. PERFORMING ORGANIZATION REPORT NUMBER
9. SPONSORING/MONITORING AGENCY NAME(S) AND ADDRESS(ES)	10. SPONSOR/MONITOR'S ACRONYM(S)
	11. SPONSOR/MONITOR'S REPORT NUMBER(S)

12. DISTRIBUTION/AVAILABILITY STATEMENT
Approved for public release; distribution unlimited

13. SUPPLEMENTARY NOTES

14. ABSTRACT
see report

15. SUBJECT TERMS

16. SECURITY CLASSIFICATION OF:			17. LIMITATION OF ABSTRACT	18. NUMBER OF PAGES **220**	19a. NAME OF RESPONSIBLE PERSON
a. REPORT **unclassified**	b. ABSTRACT **unclassified**	c. THIS PAGE **unclassified**			

Standard Form 298 (Rev. 8-98)
Prescribed by ANSI Std Z39-18

ABSTRACT

Title of Dissertation: Discrete Representation of Signals from Infinite Dimensional Hilbert Spaces with Application to Noise Suppression and Compression

Anthony Teolis, Doctor of Philosophy, 1993

Dissertation directed by: Professor J. J. Benedetto
Department of Mathematics
and Professor S. A. Shamma
Department of Electrical Engineering

Addressed in this thesis is the issue of representing signals from infinite dimensional Hilbert spaces in a discrete form. The discrete representations which are studied come from the irregular samples of a signal dependent transform called the group representation transform, e.g., the wavelet and Gabor transforms. The main issues dealt with are (i) the recoverability of a signal from its discrete representation, (ii) the suppression of noise in a corrupted signal, and (iii) compression through efficient discrete representation.

The starting point of the analysis lies with the intimate connection between the Duffin-Schaeffer theory of (global) frames and irregular sampling theory. This connection has lead elsewhere to the formulation of iterative schemes for the reconstruction of a signal from its irregular samples. However, these schemes have not addressed such issues as digital implementability and reconstruction from perturbed representations. Here, iterative reconstruction algorithms are developed and implemented which recover a signal from its possibly perturbed discrete representation.

Robustness to perturbations occurring directly in the signal domain are also investigated. Based on the notion of coherence with respect to a frame, a simple non-linear thresholding scheme is developed for the rejection of noise.

The structure of the discretization has many free parameters including the choice of group representation transform, the analyzing function associated with the group representation transform, and the sampling set. Each choice of parameters leads to a different discrete representation and the specification of an underlying set of primitive functions. Reconstructability is directly related to the frame properties of this set of primitive functions.

Localized discrete representations around a particular signal are also investigated. Truncations and other signal dependent localization of global representations lead to finite representations. The approach to finite representations which is taken here can be stated in terms of *local* frames for the reproducing kernel Hilbert space formed by the range of the group representation transform.

Finally, numerical examples of discrete representations which are signal independent and new signal *dependent* discrete (positive extrema) wavelet representations are presented. Reconstruction, noise suppression, and compression experiments are conducted and demonstrated on numerical examples including speech and synthetic signals.

Discrete Representation of Signals from Infinite Dimensional Hilbert Spaces with Application to Noise Suppression and Compression

by

Anthony Teolis

Dissertation submitted to the Faculty of The Graduate School
of The University Of Maryland in partial fulfillment
of the requirements for the degree of
Doctor of Philosophy
1993

Advisory Committee:

Professor S. A. Shamma, Chairman/Advisor
Professor J. J. Benedetto, Advisor
Professor P. S. Krishnaprasad
Associate Professor W. Dayawansa
Assistant Professor B. Marasli

Dedication

To my Mom
In memory of my Dad

Acknowledgments

First and foremost I would like to express my gratitude to Dr. John J. Benedetto. It is he who introduced me to the topic of irregular sampling from a mathematically sophisticated viewpoint; and it is he who fostered a stimulating mathematical environment in which to work. I believe that our relationship epitomizes the great reward which may be reaped from the crossing of disciplinary boundaries. Our work together has been both exciting and gratifying. As a result, I expect that this thesis is just the beginning of a long and mutually beneficial collaboration.

Second, I would like to thank my EE advisor Dr. Shihab A. Shamma for serving as mentor and advocate alike. He has provided me with a constant source of support in both the financial and academic senses. Moreover, he has given me the freedom to pursue a non-standard research program.

Third, I am indebted to Dr. P. S. Krishnaprasad for allowing me access to the resources of the Intelligent Servosytems laboratory. He has had a positive influence on my graduate career from its very begining.

I also would like to express my appreciation to Dr. W. Dayawansa and Dr. B. Marasli for serving on my dissertation committee.

There are several colleagues and peers from whose interaction I have greatly benefited in one way or the other. Among those who deserve mention are Buno Pati, John Reilly, and John Bartusek.

Another individual I would like to thank is Dr. James S. Byrnes. Apart from providing auxiliary employment through work at Prometheus Inc., he has afforded me the opportunity to work with scientists and engineers from diverse parts of the globe. My relationship with Dr. Byrnes has been greatly fulfilling on both personal and professional levels.

Lastly, I would be remiss if I did not single out the one person to which I am most indebted: my wife, Carole. Aside from the obvious emotional and personal support that she has provided, I and this research alike have benefited immeasurably from her insight and technical prowess.

Table of Contents

List of Tables

List of Figures

Chapter 1

Introduction

In this dissertation we develop theory and implement algorithms regarding, first, the discrete representation of signals belonging to certain infinite dimensional Hilbert spaces, and second, the reconstruction of these signals from their discrete representations. Our formulation of the problem leads to applications including signal compression and noise suppression.

1.1 Motivation

Many infinite dimensional (Hilbert) spaces are full of redundancy in the sense that they consist of elements (signals) which admit complete discrete representations. That is, such spaces consist of signals which admit discrete representations which uniquely describe them. Let us call such spaces as compressible. The canonical example of compressible spaces are the Paley-Wiener spaces made up of all functions band-limited by a certain fixed constant. They are functional Hilbert spaces consisting of elements whose Fourier transforms have compact support.

Many signals which occur in nature may be considered to come from infinite dimensional spaces. For example, the variation in air pressure caused by a sound source or the intensity of electromagnetic energy reflected by an object illuminated by an active source, e.g., sunlight. Sound and sight are just two examples of natural mechanisms which contain and convey information. Because the mediums in which these signals exist are inherently analog their direct processing by digital means requires discretization.

Digital techniques have fast become the prefered technology in a wide range of practical applications. Perhaps the best example of this comes from the voice communication industry. For transmission of spoken messages, the superiority of digitally coded analog voice over straight analog transmission has been firmly established [Gib93]. Of the many benefits associated with digital coding the two foremost are low susceptability to noise in communication channels and the ability of manipulation of the data by digital computers. With communication constraints such as fixed capacity and limited bandwidth channels, high information content signals can not be transmitted directly over existing channels. A theory of discrete representations which addresses issues such as compression and reconstructions is directly applicable to this problem.

With the pervasiveness of digital processing which permeates modern engineering and industry, the fundamental understanding of discrete representations is of great practical importance.

1.2 Perspective

The most natural example of a discrete signal representation in an infinite dimensional Hilbert space is one where residing signals are evaluated at a discrete set of points, i.e. sampling. As such the theory of discrete representations and the theory of sampling are intimately related.

Uniform sampling on the space of band-limited functions, also called the Paley-Wiener space[1], offers a well-known example of a discrete representation. Known to Whittaker [Whi15] in 1915, and applied later in 1933 by Kotel'nikov [Kot33] to communication problems, the so called "Sampling Theorem" did not find fame until the 1949 landmark paper of Shannon [Sha49]. Recall that the Classical Sampling Theorem establishes that any function f, in the space of functions band-limited by Ω, can be represented in terms of its samples as

$$f(x) = T \sum f(nT) \frac{\sin(2\pi\Omega(x - nT))}{\pi(x - nT)}$$

(where the sum converges in L^2) provided that $2T\Omega \leq 1$. Note that in the case $2T\Omega = 1$ the set of functions $\left\{ \frac{\sin(2\pi\Omega(x-nT))}{2\pi\Omega(x-nT)} \right\}$ is an orthonormal basis for the space of functions band-limited by Ω.

Many of the developments in what we will call "discretization theory" can be viewed as generalizations to the Classical Sampling Theorem. In particular, one direction of generalization is to remove the restriction that the sampling sequence be regular. Marvasti [Mar87] offers an extensive, but dated, bibliography on problems related to irregular sampling. Irregular sampling theory for band-limited spaces has been studied extensively by Paley-Wiener [PW34], Levinson [Lev40], Beutler [Beu61], [Beu66], and Yao-Thomas [YT67]. And recently all of the afore-mentioned theory has been extended and unified by Benedetto-Heller [BH90],[Hel91], and Benedetto [Ben92] in the context of frames. Frames were originally introduced by Duffin and Schaefer [DS52] for use in problems related to non-harmonic Fourier series. The theory of frames plays a fundamental role in irregular sampling and discretization theory.

Developing sampling theorems for spaces other than those that are band-limited is an additional level of generalization to the Classical Sampling Theorem. Two types of spaces that are of particular interest are generated as the image of (i) the Gabor transform and (ii) the (affine) wavelet transform. The continuous wavelet and Gabor transforms are reviewed in Chapter 2. The first space has its roots with Gabor [Gab46] and the coherent states of quantum physics while the second, has seen recent and significant growth with Meyer and Daubechies [Mey90] [Dau] [DGM86] [Dau90]. Both of these transforms can be identified with groups: in the case of the Gabor transform the Weyl-Heisenberg group of modulations and translations and in the case of the wavelet transform the affine or $ax + b$ group of dilations and translations.

Both the wavelet transform and the Gabor transform have associated discretizations and sampling theorems. To see this, consider the case of the wavelet transform. An affine wavelet transform is a continuous transformation that maps, for example, $L^2(\mathbb{R})$, the space of finite energy signals of one real variable, to finite energy signals on the affine or $ax + b$ group. Sampling the wavelet transform "regularly" (with respect to the group structure), one obtains the (regular) discrete wavelet transform. Theorems for the reconstruction of a signal from its discrete

---

[1]Because of a result of Paley and Wiener which characterizes the band-limited functions as entire functions of exponential type, such band-limited spaces are labeled as Paley-Wiener spaces.

wavelet transform are sampling theorems; and the regularly sampled discrete wavelet transform of a signal f of finite energy is a discrete representation of f.

Irregular sampling in spaces associated with the Gabor transform and the wavelet transform has been addressed by Gröchenig [Grö92]. Introduced by Mallat [MZ92b] in the context of image processing, the wavelet maxima representation can be thought of as a specific irregular sampling of the continuous wavelet transform. In this work Mallat has employed the method of projection onto convex sets [YW91] to obtain reconstructions.

Another space of interest is that of the Bargmann-Fock space. Irregular sampling in the Bargmann-Fock spaces has been investigated by Seip [Sei92a],[Sei92b]. Ogawa [Oga89] has taken an operator theoretic approach to the sampling problem at the level of Reproducing Kernel Hilbert Spaces (RKHS). Venturing further, out of the realm of Hilbert spaces, into the realm of Banach spaces, Gröchenig and Feichtinger [FG89] provide an extensive theory of "atomic decompositions" as discrete representations. Here, inner product dependent properties are replaced by analogous convolution formulations. In this thesis we shall limit the scope of the discussion to discretization in the more practical Hilbert spaces and not consider sampling in general Banach spaces.

1.3   Objectives

As mentioned earlier our primary goal is to develop both theory and numerical algorithms for the representation and reconstruction of signals from (compressible) Hilbert spaces. In particular, the following are some of the major objectives of this research:

(i) To develop tools for the study of invertible and stable discrete representations of signals resident in certain Hilbert spaces (in particular, reproducing kernel Hilbert spaces (RKHS)).

(ii) To provide implementable methods for the reconstruction of these signals from their discrete representations and to provide bounds for the associated reconstruction error.

(iii) To develop efficient methods for determining *finite* representations from discrete representations and to provide bounds on the associated error in reconstructions due to truncation.

(iv) To identify properties of discrete representations which make them suitable for practical applications, e.g., robustness to noise and coefficient imprecision.

(v) To provide particular representations; for example, the wavelet extrema representation of Mallat [MZ92b].

(vi) To apply the theoretical analysis developed and to implement the associated algorithms in the particular signal processing applications of data compression and noise suppression.

1.4   Approach

This research has two distinct components. First, it has an analytic or theoretical component and, second, it has a computational or implementational component. Analytically it is

desirable to work at a level of sufficient generality as to capture the essential features of the subject. Computationally, it is desirable to draw algorithms from a theory which is directly implementable. We wish to find an intermediate ground in which a coherent and *implementable* theory can be successfully developed. Because of these issues we believe that a proper setting for our investigation is in the Reproducing Kernel Hilbert Spaces.

On the computational side, we are interested in developing and implementing algorithms for the reconstruction of signals taken from certain infinite dimensional Hilbert spaces. The reconstruction should use only knowledge of a particular signal's discrete representation. Our approach to this problem will involve reproducing kernel Hilbert spaces in a fundamental way. The two main examples of RKHS's which we will target numerically are the Paley-Wiener space and the image of wavelet transforms.

On the analysis side, the RKHS's of interest will be infinite dimensional (separable) compressible Hilbert spaces. This space is denoted $\mathcal{H}$. Discrete representations of elements in this space will reside in an infinite dimensional (discrete) space which has functions with support on a discrete lattice. This space is denoted $\ell^2(\mathbb{Z})$. Finally, finite discrete representations of elements in $\mathcal{H}$ will be derived as finite truncations of corresponding elements in $\ell^2(\mathbb{Z})$. This finite dimensional (discrete) space which has functions with support on a discrete lattice is denoted as $\mathcal{H}_f$.

We have thus associated with the three spaces $\mathcal{H}$, $\ell^2(\mathbb{Z})$ and $\mathcal{H}_f$ the notions of compressible, discrete, and finite representations, respectively. Now, we define the mappings L (discretization) and F (truncation) through the statement

$$\mathcal{H} \overset{L}{\mapsto} \ell^2(\mathbb{Z}) \overset{F}{\mapsto} \mathcal{H}_f.$$

The research described here can be thought of succinctly as a detailed study of the properties of the two operators L and F.

For instance, suppose L is an invertible bounded linear operator so that L is a topological isomorphism. Consequently, the two spaces $\mathcal{H}$ and $L(\mathcal{H})$ are topologically equivalent. Therefore there is no loss of information in the discrete representation. Thus, with respect to information preserving discretizations, there is no need to require the image $L(\mathcal{H})$ of the discretization operator L, to be the *whole* space $\ell^2(\mathbb{Z})$. [2] Hence, this freedom may be exploited to achieve certain goals, e.g., noise suppression and signal compression.

Example 1.4.1 identifies a discretization operator for the familiar case of uniform sampling in a Paley-Wiener space. We see that sampling rates strictly above the Nyquist rate imply the injectivity of the discretization operator; and that rates at the Nyquist rate further imply the surjectivity of the discretization operator.

We denote the Fourier transform of a signal f as $\widehat{f}$ and formally define it as

$$\widehat{f}(\gamma) = \int f(t)e^{-2\pi i \gamma t}dt,$$

where $i = \sqrt{-1}$. This definition is valid on $L^1(\mathbb{R})$ and can be extended to functions in $L^2(\mathbb{R})$, viz. Chapter 2.

---

[2]This situation is to be contrasted with the problem of interpolation in which one starts out with a representation in $\ell^2(\mathbb{Z})$ and asks to find an f in $\mathcal{H}$ which has this representation. For interpolation problems it is required that L be surjective.

Example 1.4.1 (Uniform Sampling in $\mathcal{H} = PW_\Omega$) Given $\Omega > 0$, the Paley- Wiener space, PW_Ω, is defined as

$$PW_\Omega \triangleq \left\{ f \in L^2(\mathbb{R}) : \text{supp } \hat{f} \subseteq [-\Omega, \Omega] \right\}.$$

It is a RKHS with kernel

$$K_x(y) = \frac{\sin(2\pi\Omega(y-x))}{\pi(y-x)}$$

and reproducing formula

$$\forall f \in PW_\Omega, \quad f(x) = \langle f, K_x \rangle.$$

For $2T\Omega \leq 1$, we have the well-known Whittaker-Kotelnikov-Shannnon formula

$$\forall f \in PW_\Omega, \quad f(x) = T \sum f(nT) \frac{\sin(2\pi\Omega(x-nT))}{\pi(x-nT)}$$

which may be rewritten as

$$\forall f \in PW_\Omega, \quad f = T \sum <f, K_{nT}> K_{nT}.$$

Hence for the case $\mathcal{H} = PW_\Omega$ we may define the discretization operator $L : PW_\Omega \mapsto \ell^2(\mathbb{Z})$ as the mapping

$$Lf = \left\{ <f, \sqrt{T} K_{nT}> \right\}$$

with the adjoint $L^* : \ell^2(\mathbb{Z}) \mapsto PW_\Omega$

$$L^*c = \sum c_n \sqrt{T} K_{nT}.$$

This L is an injective isomorphism when $2T\Omega \leq 1$ and is surjective when $2T\Omega = 1$. Thus, for the case $2T\Omega = 1$, L is bijective.

1.4.1 Discrete Representations and Frames

Let $\mathcal{H}$ denote a separable Hilbert space. The main tool which we employ in our investigation is the theory of (Hilbert space) frames due to Duffin and Schaeffer [DS52]. As we will subsequently show, the power of frame theory lies in the fact that the associated "frame operator" S has many important properties; these include the following:

(i) S has the factorization $S = L^*L$, e.g., [DGM86], [Dau90], where L is a "discretization" operator which associates with any $f \in \mathcal{H}$ the discrete representation Lf (L^* is its adjoint); and

(ii) S is invertible.

These two properties are key elements of our analysis. To begin with, we have

$$\forall f \in \mathcal{H}, \quad f = S^{-1}L^*Lf. \tag{1.4.1}$$

In this equation we see that any signal f can be fully represented by the discrete vector Lf; i.e. the original signal f can be recovered from the discrete representation Lf. In other words f and Lf contain the same information.

1.4.2 Finite Representations

Through frame theory we are able to achieve countable representations of signals resident in any separable Hilbert space; however, we are ultimately interested in the finite dimensional representations of signals. It is evident that a method to go from the countable to the finite is desired. We have previously introduced such a transformation as the mapping F. In this section we discuss some of the pertinent issues concerning the operator F.

We have seen that any signal in a compressible Hilbert space $\mathcal{H}$ has a representation in terms of a countable set of coefficients. However, we would like to represent signals in $\mathcal{H}$ in terms of a *finite* set of coefficients. This leads naturally to the following questions:

(i) How is a finite set of coefficients chosen?

(ii) What are bounds on the associated approximation error?

Here, approximation error refers to the error incurred by performing reconstruction based on the finite set of coefficients. To answer these questions we identify and analyze the properties of an appropriate operator, F.

In order to "truncate" representations in $\ell^2(\mathbb{Z})$ so that the resulting truncations are members of a finite dimensional Hilbert space $\mathcal{H}_f$, we introduce the truncation operator, $F : \ell^2(\mathbb{Z}) \mapsto \mathcal{H}_f \subseteq \ell^2(\mathbb{Z})$. We think of $\mathcal{H}_f$ as the representation space. The best representation space for a given signal $f_* \in \mathcal{H}$ will, of course, depend largely on the signal itself. Therefore the truncation operator F (respectively, the space $\mathcal{H}_f$) will depend on a specific $f_* \in \mathcal{H}$ and an error tolerance $\delta > 0$. When pertinent we will write F_{f_*} or $F_{f_*,\delta}$ (respectively, $\mathcal{H}_f(f_*)$ or $\mathcal{H}_f(f_*,\delta)$) to make the dependence explicit. The representation space $\mathcal{H}_f$ can then be characterized as

$$\mathcal{H}_f(f_*) = F_{f_*} L(\mathcal{H}),$$

the image of the composite operator $F_{f_*} L$. The signal dependence of the representation space is of great interest in applications such as signal compression and noise suppression. Along with the fact that FL is a continuous mapping, the fact that the representation space is signal dependent suggests that it may be useful as describing signals which are alike, i.e. classification based on representation.

1.5 Synopsis

Our methods are demonstrated on numerical examples including speech and synthetic signals.

In chapter 2 we present background material.

In chapter 3 we review the theory of frames and develop some useful theoretical tools.

In chapter 4 we develop discrete representations in a general setting of reproducing kernel Hilbert spaces and give specific examples of such spaces and their representation.

In chapter 5 we introduce the notion of a *local frame* and its relationship to various signal dependent representations.

In chapter 6 we provide numerical examples of discrete signal representations and their reconstructions. In addition, we apply our discrete representation theory to the areas of signal compression and noise suppression. In particular we demonstrate our approach on speech signals.

Chapter 2

Mathematical Preliminaries

This chapter introduces the basic notation, concepts, and tools which we shall employ throughout this thesis. In particular, we introduce the pertinent basic spaces with which we shall deal, the Fourier transform and some important basic theorems which are associated with it. In addition we present some concepts from group theory which are pertinent to the discrete representation of analog signals. Also we describe the continuous versions of the Gabor and Wavelet transforms. Finally some notions from sampling theory are reviewed. Most of the basic notation and concepts which we use may be found in standard texts on real analysis and operator theory, e.g., [Roy68] and [GG80]. Material dealing with groups and weighted spaces is in the same vain as [FG89] and [HW89] and much of the material on sampling may be found in [You80] or [Ben92].

2.1 Notation and Tools

2.1.1 Basic Symbols and Functions

$\mathbb{Z}$ denotes the integers.

$\mathbb{R}$ denotes the real numbers.

$\mathbb{R}^+ = \{t \in \mathbb{R} \ : \ t > 0\}$ denotes the strictly positive real numbers.

$\mathbb{R}^- = \{t \in \mathbb{R} \ : \ t < 0\}$ denotes the strictly negative real numbers.

$\mathbb{C}$ denotes the complex numbers and $i = \sqrt{-1}$.

The complex conjugate of $z \in \mathbb{C}$ is denoted $\bar{z}$ and the magnitude of z is denoted $|z|$.

$\mathbb{T} \overset{\triangle}{=} \{z \in \mathbb{C} \ : \ |z| = 1\}$ is the torus of complex numbers with unit magnitude, i.e. the unit circle in the complex plane.

If S is a set then the *characteristic* function 1_S of the set S is defined as

$$1_S(x) = \begin{cases} 1, & x \in S, \\ 0, & otherwise. \end{cases}$$

The function $\delta_{m,n}$ is the Kronecker delta function defined as

$$\delta_{m,n} = \begin{cases} 1, & m = n, \\ 0, & m \neq n. \end{cases}$$

7

The *Dirichlet kernel* or *sinc* function d is defined as

$$d(t) = \frac{\sin(t)}{\pi t},$$

and for a constant $\lambda > 0$ the L^1 norm preserving dilation d_λ of d is

$$d_\lambda(t) = \lambda d(\lambda t).$$

2.1.2 Basic Function and Operator Spaces

An essential requirement of the Hilbert spaces which are to be discretized is that they admit dense countable subsets, i.e. that they be *separable*. Because of this whenever the discussion entails an arbitrary Hilbert space that Hilbert space should be assumed separable. No further mention of the separability issue will be made.

The three fundamental Hilbert spaces with which we deal are $L^2(\mathbb{R})$, $\ell^2(\mathbb{Z})$, and PW_Ω. Also of interest is the Banach space of all linear bounded operators mapping one Hilbert space to another.

$L^2(\mathbb{R})$ is the space of complex-valued finite energy signals defined on the real line $\mathbb{R}$. The *norm* of an element $f \in L^2(\mathbb{R})$ is

$$\|f\| \equiv \left(\int |f(t)|^2 dt \right)^{\frac{1}{2}} < \infty,$$

where integration is over $\mathbb{R}$, and the *inner product* of $f, g \in L^2(\mathbb{R})$ is $\langle f, g \rangle = \int f(t)\overline{g}(t)dt$.

$\ell^2(\mathbb{Z})$ is the space of complex-valued finite energy sequences defined on the integers $\mathbb{Z}$. The *norm* of an element $c \in \ell^2(\mathbb{Z})$ is

$$\|c\| \equiv \left(\sum |c_n|^2 \right)^{\frac{1}{2}} < \infty,$$

where summation is over $\mathbb{Z}$, and the *inner product* of $c, d \in \ell^2(\mathbb{Z})$ is $\langle c, d \rangle = \sum c_n \overline{d}_n$.

$\mathcal{B}(\mathcal{H}_1, \mathcal{H}_2)$ is the space of bounded linear operators which map the Hilbert space $\mathcal{H}_1$ to the Hilbert space $\mathcal{H}_2$. The *norm* of an element $K \in \mathcal{B}(\mathcal{H}_1, \mathcal{H}_2)$ is

$$\|T\| = \sup_{x \in \mathcal{H}_1} \frac{\|Tx\|_{\mathcal{H}_2}}{\|x\|_{\mathcal{H}_1}} < \infty.$$

2.1.3 Bases and Completeness in Hilbert Space

Let $\mathcal{H}$ be a separable Hilbert space and $\{\phi_n\}$ be a sequence of elements in $\mathcal{H}$. $\overline{\{\phi_n\}}$ denotes the closure.

I. span $\{\phi_n\}$ is the set of vectors generated as linear combinations of the elements of $\{\phi_n\}$, i.e. span $\{\phi_n\} = \left\{ \sum_{n=1}^{N} c_n \phi_n : c_n \in \mathbb{C}, N \in \mathbb{Z} \right\}$.

II. $\{\phi_n\}$ is *dense* in $\mathcal{H}$ if $\overline{\text{span} \{\phi_n\}} = \mathcal{H}$.

III. $\{\phi_n\}$ is *complete* in $\mathcal{H}$ if $\langle f, \phi_n \rangle = 0$ if and only if $f = 0$.

IV. $\{\phi_n\}$ is *orthonormal* in $\mathcal{H}$ if $\langle \phi_m, \phi_n \rangle = \delta_{m,n}$.

V. $\{\phi_n\}$ is a *Schauder basis* or *basis* for $\mathcal{H}$ if for each $f \in \mathcal{H}$ there is a unique sequence $\{c_n\} \in \mathbb{C}$ such that $f = \sum c_n \phi_n$.

VI. An orthonormal set $\{\phi_n\}$ is an *orthonormal basis* for $\mathcal{H}$ if for every $f \in \mathcal{H}$ there is sequence $\{c_n\} \in \mathbb{C}$ such that $f = \sum c_n \phi_n$. If $\{\phi_n\}$ is an orthonormal basis then for every $f \in \mathcal{H}$

$$f = \sum_n \langle f, \phi_n \rangle \, \phi_n$$

and

$$\|f\|^2 = \sum_n |\langle f, \phi_n \rangle|^2 \qquad \text{(Parseval's equality.)}$$

VII. A basis $\{\phi_n\}$ is a *Riesz basis* for $\mathcal{H}$ if it is related to an orthonormal basis by a topological isomorphism, i.e. there is a topological isomorphism $T : \mathcal{H} \mapsto \mathcal{H}$ such that $\phi_n = Te_n$ for all n where $\{e_n\}$ is an orthonormal basis for $\mathcal{H}$.

VIII. A basis $\{\phi_n\}$ is an *unconditional basis* for $\mathcal{H}$ if every convergent series of the form $\sum c_n \phi_n$ is unconditionally convergent, i.e. every arrangement of its terms converges to the same element.

IX. An unconditional basis $\{\phi_n\}$ is a *bounded unconditional basis* for $\mathcal{H}$ if there are constants $0 < A \leq B < \infty$ such that $A < \|\phi_n\| < B$.

X. If $\{\psi_n\}$ is another sequence in $\mathcal{H}$ then $\{\phi_n\}$ and $\{\psi_n\}$ are *biorthogonal* if $\langle \phi_m, \psi_n \rangle = \delta_{m,n}$.

2.1.4 Fourier Transform

The *Fourier transform* is a mapping $\mathcal{F} : L^2(\mathbb{R}) \mapsto L^2(\widehat{\mathbb{R}})$ as follows. For $f \in L^1(\mathbb{R}) \subset L^2(\mathbb{R})$

$$\mathcal{F}f(\gamma) = \widehat{f}(\gamma) = \int f(t)e^{-2\pi i t \gamma} dt, \tag{2.1.1}$$

and for $f \in L^2(\mathbb{R}) \setminus L^1(\mathbb{R})$

$$\mathcal{F}f(\gamma) = \widehat{f}(\gamma) = \lim_{n \to \infty} \int_{-n}^{n} f(t)e^{-2\pi i t \gamma} dt, \tag{2.1.2}$$

for $\gamma \in \widehat{\mathbb{R}}(\equiv \mathbb{R})$. Convergence of the integrals to $\mathcal{F}f = \widehat{f}$ is in the L^2-sense.

We shall almost exclusively adopt the "$\widehat{}$" notation to indicate the Fourier transform.

The Fourier transform of $f \in L^2(\mathbb{R})$ may be represented as

$$\widehat{f}(\gamma) = \langle f, e_\gamma \rangle_{L^2(\mathbf{R})} \tag{2.1.3}$$

and consequently the inverse transform as

$$f(t) = \left\langle \widehat{f}, e_{-t} \right\rangle_{L^2(\widehat{\mathbf{R}})}. \tag{2.1.4}$$

Two fundamental results in Fourier theory are the Plancherel and Parseval relations. Let $f, g \in L^2(\mathbb{R})$.

Plancherel

$$\int |f(t)|^2 dt = \int |\widehat{f}(\gamma)|^2 d\gamma.$$

Parseval

$$\int f(t)\overline{g}(t)dt = \int \widehat{f}(\gamma)\overline{\widehat{g}}(\gamma)d\gamma.$$

The Plancherel and Parseval relations may be represented as $\|f\| = \|\widehat{f}\|$ and $\langle f, g\rangle_{L^2(\mathbb{R})} = \langle \widehat{f}, \widehat{g}\rangle_{L^2(\widehat{\mathbb{R}})}$ respectively. In this form the relations also hold for spaces other than $L^2(\mathbb{R})$. The Fourier transform is a unitary map from $L^2(\mathbb{R})$ to $L^2(\widehat{\mathbb{R}})$.

Two further spaces of interest are the Hardy spaces H_+^2 and H_-^2 given as

$$H_+^2 = \left\{ f \in L^2(\mathbb{R}) \; : \; \text{supp } \widehat{f} \subset [0, \infty) \right\}$$

and

$$H_-^2 = \left\{ f \in L^2(\mathbb{R}) \; : \; \text{supp } \widehat{f} \subset (-\infty, 0] \right\},$$

where supp $\widehat{f}$ is the support of $\widehat{f}$. Let f_+ be an arbitrary element of H_+^2 and f_- an arbitrary element of H_-^2. The Hardy space H_+^2 is a Hilbert space with norm

$$\|f_+\|_{H_+^2} = \left(\int_0^\infty |\widehat{f}_+(\gamma)|^2 \right)^{\frac{1}{2}}$$

with the inner product it induces. The Hardy space H_-^2 is a Hilbert space with norm

$$\|f_-\|_{H_-^2} = \left(\int_{-\infty}^0 |\widehat{f}_-(\gamma)|^2 \right)^{\frac{1}{2}}$$

with the inner product it induces. Also H_-^2 and H_+^2 are orthogonal complements in $L^2(\mathbb{R})$, i.e., $L^2(\mathbb{R}) = H_-^2 \oplus H_+^2$. Consequently, for an arbitrary element f in $L^2(\mathbb{R})$ there are elements $f_- \in H_-^2$ and $f_+ \in H_+^2$ so that $f = f_- + f_+$ and $\|f\|^2 = \|f_-\|_{H_-^2}^2 + \|f_+\|_{H_+^2}^2$.

Remark 2.1.1 Any real element of $L^2(\mathbb{R})$ may be associated with either H_+^2 or H_-^2 since all real functions have Fourier transforms which are involutive (conjugate symmetric), i.e., if f is real then $\widehat{f}(\gamma) = \overline{\widehat{f}}(-\gamma)$. Thus, real functions are uniquely determined by their Fourier transforms on $[0, \infty)$ or $(-\infty, 0]$.

2.1.5 Operators

Let $\mathcal{H}_1$ and $\mathcal{H}_2$ be arbitrary Hilbert spaces with norms $\|\cdot\|_1$ and $\|\cdot\|_2$ and inner products $\langle \cdot, \cdot \rangle_1$ and $\langle \cdot, \cdot \rangle_2$ respectively. Let $T : \mathcal{H}_1 \mapsto \mathcal{H}_2$.

I. The *range* of T is $T(\mathcal{H}_1) \overset{\triangle}{=} \{Tf \; : \; f \in \mathcal{H}_1\}$.

II. The *kernel* of T is $\ker T \overset{\triangle}{=} \{f \in \mathcal{H}_1 \; : \; Tf = 0\}$.

III. T is *injective* or *one-to-one* if $Tf = Tg$ if and only if $f = g$. If T is a linear operator then T is injective if and only if $\ker T = \{0\}$.

IV. T is *surjective* or *onto* if $T(\mathcal{H}_1) = \mathcal{H}_2$.

V. T is *bijective* if it is both injective and surjective.

VI. T has an *inverse* $T^{-1} : \mathcal{H}_2 \mapsto \mathcal{H}_1$ if T is bijective. In this case the inverse of T is defined as $T^{-1}g = f$ if $g = Tf$.

VII. T is *continuous* if $x_n \to x$ implies $Tx_n \to Tx$. A linear operator T is bounded if and only if T is continuous.

VIII. The *adjoint* of T is the unique operator $T^* : \mathcal{H}_2 \mapsto \mathcal{H}_1$ so that $\langle Tf, g \rangle_2 = \langle f, T^*g \rangle_1$ for all $f \in \mathcal{H}_1$ and $g \in \mathcal{H}_2$. T is *self adjoint* if $T^* = T$.

IX. $T \in \mathcal{B}(\mathcal{H}_1, \mathcal{H}_2)$ is a *compact* operator if for all sequences $\{f_n : \|f_n\| = 1\} \subseteq \mathcal{H}_1$ the sequence $\{Tx_n\}$ has a converging subsequence in $\mathcal{H}_2$.

X. T is a *topological isomorphism* if T is bijective, $T \in \mathcal{B}(\mathcal{H}_1, \mathcal{H}_2)$ and $T^{-1} \in \mathcal{B}(\mathcal{H}_2, \mathcal{H}_1)$. Thus, both T and T^{-1} are continuous linear mappings.

XI. T is an *isometry* if for all $f \in \mathcal{H}_1$, $\|Tf\|_2 = \|f\|_1$.

XII. T is a unitary map if it is linear, bijective, and an isometry. If T is unitary then $T^{-1} = T^*$.

Compositions of topological isomorphisms are again topological isomorphisms. Two Hilbert spaces $\mathcal{H}_1$ and $\mathcal{H}_2$ which are related by a topological isomorphism are topologically equivalent. Topologically equivalent spaces are in an abstract sense the same. A topological isomorphism which is norm preserving is a unitary map. Compositions of isometries are again isometries.

With $\mathcal{H}'$ a subspace of a Hilbert space $\mathcal{H}$ the operator $P_{\mathcal{H}'} : \mathcal{H} \mapsto \mathcal{H}'$ is the orthogonal projection operator onto $\mathcal{H}'$.

Fact 2.1.2 ([GG80, Theorem II.13.1]) $P \in \mathcal{B}(\mathcal{H}, \mathcal{H})$ is an orthogonal projection if and only if $P^2 = P$ and P is self adjoint.

Fact 2.1.3 ([GG80, Theorem III.4.1]) If $T \in \mathcal{B}(\mathcal{H}, \mathcal{H})$ is self adjoint then

$$\|T\| = \sup_{f \in \mathcal{H}} \frac{|\langle f, Tf \rangle|}{\|f\|^2}.$$

Let f be an arbitrary element of $L^2(\mathbb{R})$ and take a, b and $s > 0$ all to be real numbers.

I. The *involution* operator $\tilde{} : L^2(\mathbb{R}) \mapsto L^2(\mathbb{R})$ is a unitary map given by

$$\tilde{f}(t) \triangleq \overline{f}(-t).$$

II. The *translation* operator $\tau_a : L^2(\mathbb{R}) \mapsto L^2(\mathbb{R})$ is a unitary map given by

$$(\tau_a f)(t) \stackrel{\triangle}{=} f(t-a).$$

III. The *modulation* operator $e_b : L^2(\mathbb{R}) \mapsto L^2(\mathbb{R})$ is a unitary map given by

$$(e_b f)(t) \stackrel{\triangle}{=} e^{2\pi i b t} f(t).$$

IV. The *dilation* operator $D_s : L^2(\mathbb{R}) \mapsto L^2(\mathbb{R})$ is a unitary map given by

$$(D_s f)(t) \stackrel{\triangle}{=} s^{\frac{1}{2}} f(st).$$

Table 2.1 displays in a compact form these unitary operators on $L^2(\mathbb{R})$, their definitions, inverses, and Fourier transforms.

Of special interest are the composite relations:

$$e_a \tau_b = e^{2\pi i a b} \tau_b e_a \qquad \text{and} \qquad \tau_b D_a = D_a \tau_{ab}.$$

Name	Uf	$(Uf)(t)$	$U^* f = U^{-1} f$	$(Uf)\widehat{}$
translation	$\tau_a f$	$f(t-a)$	$\tau_{-a} f$	$e_{-a}\widehat{f}$
modulation	$e_a f$	$e^{2\pi i a t} f(t)$	$e_{-a} f$	$\tau_a \widehat{f}$
dilation	$D_s f$	$s^{\frac{1}{2}} f(st)$	$D_{s^{-1}} f$	$D_{s^{-1}} \widehat{f}$
involution	$\widetilde{f}$	$\overline{f}(-t)$	$\widetilde{f}$	$\widetilde{\overline{\widehat{f}}}$

Table 2.1: Unitary Operators $U : L^2(\mathbb{R}) \mapsto L^2(\mathbb{R})$, their inverses (equal to their adjoints), and their Fourier transforms. $f \in L^2(\mathbb{R})$, $a,b \in \mathbb{R}$ and $s \in \mathbb{R}^+$.

The *convolution* $f * g$ of two functions $f, g \in L^2(\mathbb{R})$ is

$$(f * g)(t) = \int f(x) g(t-x) dx.$$

Convolution may also be represented as

$$(f * g)(t) = \langle f, \tau_t \widetilde{g} \rangle.$$

By standard arguments $(f * g)\widehat{} = \widehat{f}\widehat{g}$. To see this explicitly write

$$
\begin{aligned}
f * g(t) &= \langle f, \tau_t \widetilde{g} \rangle \\
&= \langle \widehat{f}, e_{-t}\widehat{\widetilde{g}} \rangle \qquad \text{(by Parseval)} \\
&= \langle \widehat{f}\widehat{g}, e_{-t} \rangle = (\widehat{f}\widehat{g})^\vee(t)
\end{aligned}
$$

2.1.6 Bandlimited Spaces

Paley and Wiener [PW34] have made significant fundamental contributions to Fourier theory and, in particular, the understanding of bandlimited functions. For this reason we label spaces of bandlimited functions as "Paley-Wiener" spaces. Bandlimited functions are defined as those which have compact support in the frequency domain, i.e. their Fourier transforms vanish off some compact set. One result of Paley and Wiener characterizes any Ω bandlimited space as one consisting of entire functions of exponential type $2\pi\Omega$.

For $\Omega > 0$ PW_Ω is the *Paley-Wiener space* defined as

$$PW_\Omega \triangleq \left\{ f \in L^2(\mathbb{R}) \; : \; \operatorname{supp} \widehat{f} \subseteq [-\Omega, \Omega] \right\}.$$

Recall that a complex function $f : \mathbb{C} \mapsto \mathbb{C}$ is analytic at a point $z_0 \in \mathbb{C}$ if the complex derivative $f'(z)$ exists for all points in some open neighborhood containing z_0.

Definition 2.1.4 (Entire functions of exponential type) Let $f : \mathbb{C} \mapsto \mathbb{C}$.

  a. f is an *entire* function if it is analytic on all of $\mathbb{C}$.

  b. An entire function f is of *exponential type* A if

$$\forall z \in \mathbb{C}, \quad |f(z)| \leq M e^{B|z|}$$

for some positive constant $M = M(B)$ and all $B > A$.

Theorem 2.1.5 ([PW34, Theorem X]) A function is Ω bandlimited if and only if it is an entire function of exponential type $2\pi\Omega$. i.e.,

$$PW_\Omega = \{ f : f \text{ is an entire function of exponential type } 2\pi\Omega \}.$$

For $a < b \in \mathbb{R}$ $PW_{[a,b]}$ is the *Paley-Wiener space* defined as

$$PW_{[a,b]} \triangleq \left\{ f \in L^2(\mathbb{R}) \; : \; \operatorname{supp} \widehat{f} \subseteq [a, b] \right\}.$$

For $\Omega_2 > \Omega_1 > 0$, PW_{Ω_1, Ω_2} is the *Paley-Wiener space* defined as

$$PW_{\Omega_1, \Omega_2} \triangleq \left\{ f \in L^2(\mathbb{R}) \; : \; \operatorname{supp} \widehat{f} \subseteq [-\Omega_2, -\Omega_1] \cup [\Omega_1, \Omega_2] \right\},$$

Clearly $PW_{\Omega_1, \Omega_2} = PW_{[-\Omega_2, -\Omega_1]} \oplus PW_{[\Omega_1, \Omega_2]}$.

$L^2[a,b]$ is the space of finite energy signals defined on the interval $[a,b]$. The Fourier transform is an isomorphism between the spaces $PW_{[a,b]}$ and $L^2[a,b]$ and hence, they are topologically equivalent. In particular, the spaces $L^2[-\Omega, \Omega]$ and PW_Ω are topologically equivalent by the Fourier transform and we may write $\widehat{PW_\Omega} = L^2[-\Omega, \Omega]$.

2.2 Reproducing Kernel

For Hilbert spaces of functions, the Riesz representation theorem states that every bounded linear functional may be represented as an inner product with a particular element from the Hilbert space. Let $\mathcal{H}$ denote the Hilbert space. A functional on $\mathcal{H}$ is any mapping $F : \mathcal{H} \mapsto \mathbb{C}$. In particular, consider the collection of point mappings $\{F_x\}_{x \in \mathcal{G}}$ given as

$$\forall x \in \mathcal{G}, \quad F_x f = f(x),$$

where $\mathcal{G}$ is some domain on which functions in $\mathcal{H}$ are defined. Clearly the point mapping collection $\{F_x\}_{x \in \mathcal{G}}$ is a set of functionals on $\mathcal{H}$. It is easy to verify that each member of this set is also linear. If all members of the Hilbert space $\mathcal{H}$ satisfy a pointwise bound on $\mathcal{G}$

$$\forall x \in \mathcal{G}, \quad |f(x)| < M_x \|f\| \tag{2.2.1}$$

then the collection $\{F_x\}_{x \in \mathcal{G}}$ is a set of bounded linear functionals. By the Riesz representation theorem for each $x \in \mathcal{G}$ there is an element $K_x \in \mathcal{H}$ such that the functional F_x may be expressed as

$$F_x f = \langle f, K_x \rangle.$$

The *reproducing kernel* for a Hilbert space $\mathcal{H}(\mathcal{G})$ is a mapping $\mathcal{K} : \mathcal{G} \times \mathcal{G} \mapsto \mathbb{C}$ defined as

$$\mathcal{K}(x, y) \stackrel{\triangle}{=} \langle K_y, K_x \rangle_{\mathcal{H}(\mathcal{G})}.$$

If the pointwise bound of (2.2.1) holds over $\mathcal{G}$ then $K_y(x) = \mathcal{K}(x, y)$ for $x, y \in \mathcal{G}$ and $\mathcal{H}(\mathcal{G})$ is a reproducing kernel Hilbert space (RKHS).

Example 2.2.1 For $\Omega > 0$ the Paley-Wiener space PW_Ω is a RKHS with reproducing kernel $\mathcal{K}(s, t) = d_{2\pi\Omega}(t - s)$ since for all $f \in PW_\Omega$

$$\begin{aligned}
f(t) &= \left(\hat{f} 1_{[-\Omega, \Omega]} \right)^{\vee}(t) \\
&= (f * d_{2\pi\Omega})(t) \\
&= \langle f, K_t \rangle,
\end{aligned}$$

where $K_t = \tau_t d_{2\pi\Omega}$.

Example 2.2.2 For $\Omega_2 > \Omega_1 > 0$ the Paley-Wiener space PW_{Ω_1, Ω_2} is a RKHS with reproducing kernel $\mathcal{K}(s, t) = 2\cos(\pi(\Omega_1 + \Omega_2)(t - s)) \, d_{\pi(\Omega_2 - \Omega_1)}(t - s)$.

2.3 Group Representation

2.3.1 Groups

A group is a set $\mathcal{G}$ along with an identity element and an associative binary operation on $\mathcal{G}$ called the group action. The group action is denoted as the operation "$\cdot$" so that with $x, y \in \mathcal{G}$ then $x \cdot y \in \mathcal{G}$ denotes x acting on y. The identity element of the group is denoted as "e", and the inverse of an element $x \in \mathcal{G}$ is x^{-1}. To formally state the definition, a group is a pair $(\mathcal{G}, \cdot)$ where $\mathcal{G}$ is a set, "$\cdot$" is the group action and there is an $e \in \mathcal{G}$ so that

a. if $x \in \mathcal{G}$ then $x \cdot e = x$, and

b. if $x \in \mathcal{G}$ then there is a $x^{-1} \in \mathcal{G}$ so that $x \cdot x^{-1} = e$.

A group is *abelian* if the group action is commutative. For example, $(\mathbb{R}, +)$ is an abelian group with identity element $e = 0$. Non-abelian groups will be of use in the general approach to discrete signal representation presented here. Much of the set up which is presented is adopted from [HW89].

The two examples of groups which follow are are found in the background of both the Gabor and wavelet theory. The particular form of the associated group operations is justified in Appendix B, cf. Section 2.3.3.

Example 2.3.1 (Affine Group) The affine group is the upper half-plane $\mathcal{G}_A = \mathbb{R} \times \mathbb{R}^+$ along with the group action defined as follows. Let $x, y \in \mathcal{G}_A$ and $x = (t_x, s_x)$ and $y = (t_y, s_y)$ then

$$x \cdot y = (t_x, s_x) \cdot (t_y, s_y) = (t_x + s_x^{-1} t_y, s_x s_y)$$

and

$$x^{-1} = (t_x, s_x)^{-1} = (-s_x t_x, s_x^{-1})$$

so that the identity element is $e = (0, 1)$.

Example 2.3.2 (Weyl-Heisenberg Group) The Weyl-Heisenberg Group is $\mathcal{G}_H = \mathbb{T} \times \mathbb{R} \times \mathbb{R}$ with the following group action. Let $x, y \in \mathcal{G}_H$ so with $z_x, z_y \in \mathbb{T}$ and $t_x, \gamma_x, t_y, \gamma_y \in \mathbb{R}$ we have $x = (z_x, t_x, \gamma_x)$ and $y = (z_y, t_y, \gamma_y)$ then

$$x \cdot y = (z_x, t_x, \gamma_x) \cdot (z_y, t_y, \gamma_y) = (z_x z_y e^{-2\pi i \gamma_y t_x}, \gamma_x + \gamma_y, t_x + t_y)$$

and

$$(z_x, t_x, \gamma_x)^{-1} = (z_x^{-1} e^{-2\pi i \gamma_x t_x}, -t_x, -\gamma_x)$$

so that the identity element is $e = (1, 0, 0)$.

2.3.2 Weighted Spaces

Define the Hilbert space of μ-square integrable functions as

$$L_\mu^2(\mathcal{G}) \triangleq \left\{ F : \int_\mathcal{G} |F(x)|^2 d\mu(x) < \infty \right\}$$

Let $F, G \in L^2_\mu(\mathcal{G})$. The space $L^2_\mu(\mathcal{G})$ has the associated norm

$$\|F\|_{L^2_\mu(\mathcal{G})} = \left(\int_\mathcal{G} |F(x)|^2 d\mu(x) \right)^{\frac{1}{2}}$$

and the inner product

$$\langle F, G \rangle_{L^2_\mu(\mathcal{G})} = \int_\mathcal{G} F(x)\overline{G}(x)d\mu(x).$$

A measure μ on a group $\mathcal{G}$ is *left-invariant* if for every integrable function F on $\mathcal{G}$ and every $y \in \mathcal{G}$

$$\int_\mathcal{G} F(y^{-1}x)d\mu(x) = \int_\mathcal{G} F(x)d\mu(x).$$

Such a measure is called a *left Haar measure* and it is well known from measure theory that such a measure exists and is unique up to multiplication by a constant.

The *convolution* $F * G$ of F and G elements of $L^2_\mu(\mathcal{G})$ is defined as

$$F * G(x) = \int_\mathcal{G} F(y)G(y^{-1}x)d\mu(y).$$

For $x, y \in \mathcal{G}$, the *translation* operator $T_x : L^2_\mu(\mathcal{G}) \mapsto L^2_\mu(\mathcal{G})$ is

$$T_x f(y) = f(x^{-1}y).$$

If μ is the left Haar measure then T_x is unitary and $T_x^{-1} = T_x^* = T_{x^{-1}}$. The *involution* $\widetilde{F}$ of $F \in L^2_\mu(\mathcal{G})$ is

$$\widetilde{F}(x) = \overline{F}(x^{-1}).$$

A function F is *involutive* if $F = \widetilde{F}$. The convolution $F * G$ may also be written

$$(F * G)(x) = \left\langle F, T_x \widetilde{G} \right\rangle_{L^2_\mu(\mathcal{G})}.$$

In the case that $\mathcal{G} = (\mathbb{R}, +)$ these formulas reduce to the standard ones and involutive functions are those whose real parts are even and imaginary parts are odd.

2.3.3 Representation

Let $\mathcal{H}$ be a Hilbert space and $\mathcal{G}$ be a group. A *representation* of $\mathcal{G}$ on $\mathcal{H}$ is a mapping $\Pi : \mathcal{G} \mapsto \mathcal{B}(\mathcal{H}, \mathcal{H})$ which satisfies the relation

$$\Pi(x)\Pi(y) = \Pi(x \cdot y),$$

for all $x, y \in \mathcal{G}$. For example, with respect to the group $(\mathbb{R}, +)$, $\Pi(t) = \tau_t$ is a representation of $\mathbb{R}$ on $L^2(\mathbb{R})$ since $\tau_t \tau_s = \tau_{t+s}$ where $t, s \in \mathbb{R}$.

An element $g \in \mathcal{H}$ is *cyclic* if $\overline{\text{span} \{\Pi(x)g\}}_{x \in \mathcal{G}} = \mathcal{H}$. For example, $d_{2\pi\Omega} \in PW_\Omega$ is cyclic with respect to the group $(\mathbb{R}, +)$ with representation τ_x.

I. A representation Π is *irreducible* if every $g \in \mathcal{H} \setminus \{0\}$ is cyclic.

II. An element $g \in \mathcal{H}$ is *admissible* if

$$\int_{\mathcal{G}} |\langle g, \Pi(x)g \rangle|^2 d\mu(x) < \infty.$$

The set of admissible functions is denoted $\mathcal{A}_{\Pi,\mu}(\mathcal{H})$ so that

$$\mathcal{A}_{\Pi,\mu}(\mathcal{H}) \triangleq \left\{ g \in \mathcal{H} \setminus \{0\} \ : \ \int_{\mathcal{G}} |\langle g, \Pi(x)g \rangle|^2 d\mu(x) < \infty \right\}.$$

Note that $\mathcal{A}_{\Pi,\mu}(\mathcal{H}) \subseteq \mathcal{H}$.

III. A representation Π is *square-integrable* if it is irreducible and $\mathcal{A}_{\Pi,\mu}(\mathcal{H})$ is not empty.

2.4 Group Representation Transform

The basic approach to discrete representation in Hilbert spaces which is taken here involves the sampling of an auxiliary signal dependent function or transform. This transform is known as the group representation transform. It is a generalized transform which contains the wavelet and Gabor transforms as special cases. Feichtinger and Gröchenig [FG89] have developed this generalized approach in the setting of Banach spaces.

The *group representation transform* [FG89] of $f \in L^2(\mathbb{R})$ with respect to an admissible $g \in \mathcal{A}_{\Pi,\mu}(\mathcal{H})$ is a mapping $V_g : L^2(\mathbb{R}) \mapsto L^2_\mu(\mathcal{G})$ given as

$$(V_g f)(x) = \langle f, \Pi(x)g \rangle. \tag{2.4.1}$$

The group representation transform is the fundamental transformation from which all discretizations studied in this thesis will come. Discretizations which we will consider are of the form $\{(V_g f)(x)\}_{x \in \Gamma}$ where Γ is a countable subset of $\mathcal{G}$. It is expected that such samplings of the group representation transform will allow full recovery of f under certain density conditions on Γ. This is because the range $V_g(\mathcal{H})$ is a reproducing kernel Hilbert space. To see this, take $f, g \in \mathcal{H}$ and note that by Cauchy-Shwarz

$$|(V_g f)(x)| = |\langle f, \Pi(x)g \rangle| \le \|f\| \|\Pi(x)g\| < \|f\| \|g\| \|\Pi(x)\| < M_x,$$

where $M_x < \infty$ since $\Pi(x)$ is a bounded operator by definition. Thus, there is a pointwise bound of the form given in (2.2.1). From the discussion in Section 2.2 there is a reproducing kernel associated with V_g and the range $V_g(\mathcal{H})$ of V_g is a RKHS. Moreover with the aid of the following theorem it is possible to write down explicitly the reproducing kernel for $V_g(\mathcal{H})$.

Theorem 2.4.1 ([GMP85]) Let Π be a representation of the group $\mathcal{G}$ on the Hilbert space $\mathcal{H}$ with left Haar measure μ. If Π is square integrable then there exists a unique self-adjoint positive operator $T : \mathcal{A}_{\Pi,\mu}(\mathcal{H}) \mapsto \mathcal{H}$ such that for all $g_1, g_2 \in \mathcal{A}_{\Pi,\mu}(\mathcal{H})$ and for all $f_1, f_2 \in \mathcal{H}$

$$\langle V_{g_1} f_1, V_{g_2} f_2 \rangle_{L^2_\mu(\mathcal{G})} = \langle f_1, f_2 \rangle \langle Tg_1, Tg_2 \rangle.$$

As consequences of this theorem two corollaries are derived immediately. These corollaries may be thought of as counterparts of the Parseval and Plancherel relations. With T be the unique self-adjoint positive operator of Theorem 2.4.1 the positive scalar c_g is defined as $c_g = \|Tg\|$.

Corollary 2.4.2 ("Parseval") If $g \in \mathcal{A}_{\Pi,\mu}(\mathcal{H})$ and $f_1, f_2 \in \mathcal{H}$ then

$$\langle V_g f_1, V_g f_2 \rangle_{L^2_\mu(\mathcal{G})} = c_g^2 \langle f_1, f_2 \rangle.$$

Corollary 2.4.3 ("Plancherel") If $g \in \mathcal{A}_{\Pi,\mu}(\mathcal{H})$ and $f \in \mathcal{H}$ then

$$\|V_g f\|^2_{L^2_\mu(\mathcal{G})} = c_g^2 \|f\|^2.$$

The following theorem establishes that the range of the group representation transform is a reproducing kernel and gives explicitly the form of the kernel. Asserted as a corollary is the fact that convolution with this kernel performs the orthogonal projection onto the range of the group representation transform.

Theorem 2.4.4 Suppose the hypothesis of Theorem 2.4.1 are satisfied and Π is a unitary representation then $V_g(\mathcal{H})$ is a RKHS with kernel $\mathcal{K}(x,y) = T_y K(x)$ where

$$K(x) = \frac{1}{c_g^2}(V_g g)(x).$$

Proof:

Let $F \in L^2_\mu(\mathcal{G})$.

$$
\begin{aligned}
(F * K)(x) \;&\overset{\triangle}{=}\; \int_\mathcal{G} F(y) K(y^{-1}x) d\mu(y) \\
&= \int_\mathcal{G} F(y) \left(\frac{1}{c_g^2}(V_g g)(y^{-1}x) \right) d\mu(y) \\
&= \frac{1}{c_g^2} \int_\mathcal{G} F(y) \left\langle g, \Pi(y^{-1}x)g \right\rangle d\mu(y) \\
&= \frac{1}{c_g^2} \int_\mathcal{G} F(y) \left\langle \Pi(y)g, \Pi(x)g \right\rangle d\mu(y) \\
&= \frac{1}{c_g^2} \int_\mathcal{G} F(y) \overline{V_g(\Pi(x)g)} d\mu(y) \\
&= \frac{1}{c_g^2} \left\langle F, V_g(\Pi(x)g) \right\rangle_{L^2_\mu(\mathcal{G})}.
\end{aligned}
$$

Orthogonally decomposing F with respect to $V_g(\mathcal{H})$ as $F = V_g f + H$ where $H \in V_g(\mathcal{H})^\perp$ for some $f \in \mathcal{H}$ yields

$$
\begin{aligned}
(F * K)(x) \;&=\; \frac{1}{c_g^2} \left\langle V_g f, V_g(\Pi(x)g) \right\rangle_{L^2_\mu(\mathcal{G})} \quad (H \text{ is nullified}) \\
&= \langle f, \Pi(x)g \rangle \quad (\text{by Theorem 2.4.1}) \\
&= V_g f(x).
\end{aligned}
$$

18

Corollary 2.4.5 Convolution with the reproducing kernel K performs the orthogonal projection onto the range $V_g(\mathcal{H})$, i.e.,

$$\forall F \in L^2_\mu(\mathcal{G}), \quad F * K = P_{V_g(\mathcal{H})}F.$$

Note that the kernel K is involutive, i.e. $K = \widetilde{K}$. To see this we shall without loss of generality assume $c_g = 1$. Write

$$
\begin{aligned}
\widetilde{K}(x) = (V_g g)\widetilde{}(x) &= \overline{V_g g(x^{-1})} \\
&= \overline{\langle g, \Pi(x^{-1})g \rangle} \\
&= \overline{\langle \Pi(x)g, g \rangle} \\
&= \langle g, \Pi(x)g \rangle \\
&= (V_g g)(x) = K(x).
\end{aligned}
$$

Thus, $(F * K)(x) = \langle F, T_x K \rangle$.

2.4.1 Gabor Transform

With $g \in L^2(\mathbb{R})$, the continuous Gabor Transform $G_g f$ of a signal $f \in L^2(\mathbb{R})$ is

$$(G_g f)(t, \gamma) = \int f(x) e^{-2\pi i \gamma x} \overline{g}(x - t)dx.$$

The Gabor transform may be interpreted as time-varying Fourier transform where the function g acts a sliding window in time over f. At a particular time instant t_0 the Gabor transform of a function f is the Fourier transform of f modulated by a t_0 translated version of g, i.e.,

$$(G_g f)(t_0, \gamma) = (f \tau_{t_0} \overline{g})\widehat{}.$$

In this way the Gabor transform attempts to expose the time-frequency content of the underlying signal f. This transform is also called the "short-time Fourier transform".

Alternatively the Gabor transform may be written as

$$
\begin{aligned}
(G_g f)(t, \gamma) &= \langle f, e_\gamma \tau_t g \rangle \\
&= \langle f, \Pi(1, t, \gamma)g \rangle \\
&= \langle f, \Pi(x)g \rangle
\end{aligned}
$$

where $x = (1, t, \gamma) \in \mathcal{G}_H$, the Weyl-Heisenberg group, and $\Pi(z, t, \gamma) = z\tau_t e_\gamma g$ where $|z| = 1$ is a representation of $\mathcal{G}_H$ on $L^2(\mathbb{R})$ (See Appendix B for verification). This representation is denoted $\Pi = \Pi_H$. The Weyl-Heisenberg group action is given in Example 2.3.2. For the Gabor transform the associated left Haar measure is the product measure

$$d\mu(z, t, \gamma) = dz dt d\gamma.$$

Although the toral component z associated with the Weyl-Heisenberg group $\mathcal{G}_H$ is necessary to properly define the representation Π_H it can effectively be ignored. To see this, first note that $\Pi_H(z,t,\gamma) = z\Pi_H(1,t,\gamma)$. Hence, for any $g \in L^2(\mathbb{R})$

$$
\begin{aligned}
\int_{\mathcal{G}} \Pi(x)g\, d\mu(x) &= \int_{\mathbf{T}} \int_{\mathbf{R}} \int_{\mathbf{R}} \Pi_H(z,t,\gamma)g\, dz dt d\gamma \\
&= \int_{\mathbf{R}} \int_{\mathbf{R}} \int_{\mathbf{T}} z dz\, \Pi_H(1,t,\gamma)g\, dt d\gamma \\
&= \int_{\mathbf{R}} \int_{\mathbf{R}} \Pi_H(1,t,\gamma)g\, dt d\gamma.
\end{aligned}
$$

Theorem 2.4.6 ([HW89, Proposition 3.2.4],[DGM86]) If $f, g \in L^2(\mathbb{R})$ then

$$
\|G_g f\|_{L^2_\mu(\mathcal{G}_H)} = \|g\|\,\|f\|.
$$

This theorem may be used to show that Π_H is a square integrable representation of $\mathcal{G}_H$ on $L^2(\mathbb{R})$. Thus, Theorem 2.4.1 is applicable where $T = T_H = I$. All $g \in L^2(\mathbb{R})$ are admissible and G_g is a multiple of an isometry.

2.4.2 Wavelet Transform

For $s > 0$ the continuous wavelet transform $W_g f$ of a signal $f \in L^2(\mathbb{R})$ is

$$
(W_g f)(t,s) = s^{\frac{1}{2}} \int f(x)\overline{g}(s(x-t))dx.
$$

Alternatively, the wavelet transform may be written as

$$
\begin{aligned}
W_g f(t,s) &= \langle f, \tau_t D_s g \rangle \\
&= \langle f, \Pi(t,s)g \rangle \\
&= \langle f, \Pi(x)g \rangle
\end{aligned}
$$

where $x = (t,s) \in \mathcal{G}_A$, the affine group, and $\Pi(t,s) = \Pi_A(t,s) \stackrel{\triangle}{=} \tau_t D_s$ is a representation of $\mathcal{G}_A = \mathbb{R} \times \mathbb{R}^+$ on $L^2(\mathbb{R})$. The affine group action is given in Example 2.3.1. For the wavelet transform the associated left Haar measure is

$$
d\mu(t,s) = s^{-2} dt ds.
$$

See Appendix B for verification that this μ is the left Haar measure and that Π_A is a representation of $\mathcal{G}_A$ on $L^2(\mathbb{R})$.

Theorem 2.4.7 ([HW89, Theorem 3.3.5],[GM84]) If $f, g \in L^2(\mathbb{R})$ then

$$
\|W_g f\|_{L^2_\mu(\mathcal{G}_A)} = \|f\|^2_{H^2_+} \|T_A g\|^2_{H^2_+} + \|f\|^2_{H^2_-} \|T_A g\|^2_{H^2_-},
$$

where $T_A g = \left(|\gamma|^{-\frac{1}{2}} \widehat{g}(\gamma) \right)^{\vee}$.

This theorem may be used to show that Π_A is a square integrable representation of $\mathcal{G}_A$ on H_+^2 and H_-^2. Thus, Theorem 2.4.1 is applicable. A similar result can be developed for real signals, c.f. Remark 2.1.1. By Theorem 2.4.7 if f is a real signal then

$$\|W_g f\|_{L_\mu^2(\mathcal{G}_A)} = \|f\| \|\tfrac{1}{2} T_A g\|.$$

If g is admissible then $c_g = \|T_A g\| < \infty$ and W_g is a multiple of an isometry.

2.5 Sampling and Interpolation

Let $\mathcal{H}$ be an arbitrary Hilbert space, e.g. PW_Ω. Let $\mathcal{H}_d$ be an arbitrary discrete Hilbert space, e.g. $\ell^2(\mathbb{Z})$. A *sampling* operator is any mapping $L : \mathcal{H} \mapsto \mathcal{H}_d$. An *interpolating* operator for $\mathcal{H}$ is a mapping $A : \mathcal{H}_d \mapsto \mathcal{H}$.

2.5.1 Sequences in Hilbert space

Definition 2.5.1 (Bessel Sequence) a. $\{\phi_n\} \subseteq \mathcal{H}$ is a *Bessel sequence* for $\mathcal{H}$ if

$$\forall f \in \mathcal{H}, \quad \sum |\langle f, \phi_n \rangle|^2 < \infty.$$

b. $\{\phi_n\} \subseteq \mathcal{H}$ is a *Bessel sequence of uniqueness* if in addition to a. there is a constant $A > 0$ such that

$$A\|f\|^2 \le \sum |\langle f, \phi_n \rangle|^2.$$

Definition 2.5.2 (Riesz-Fischer sequence) $\{\phi_n\} \subseteq \mathcal{H}$ is a *Riesz-Fischer sequence* if

$$\forall c \in \ell^2(\mathbb{Z}), \quad \exists \, f \in \mathcal{H} \ni \, c = \{\langle f, \phi_n \rangle\}.$$

With respect to the sequence $\{\phi_n\} \subseteq \mathcal{H}$ define the sampling operator $L_\phi : \mathcal{H} \mapsto \ell^2(\mathbb{Z})$ as

$$L_\phi f = \{\langle f, \phi_n \rangle\}$$

where $f \in \mathcal{H}$. The notions of Bessel and Riesz-Fischer sequences may be directly related to properties of the mapping L_ϕ. Namely, $\{\phi_n\}$ is a Bessel mapping if and only if L_ϕ is injective and it is a Riesz-Fischer map if and only if L_ϕ is surjective.

2.5.2 Density of Sampling Sets

Let $\Gamma = \{t_n\} \subseteq \mathbb{R}$ be a real sampling set.

I. The sequence $\{t_n\}$ is *uniformly discrete* if there is a $d > 0$ so that $|t_n - t_m| > d$ for all $n \neq m$.

II. A uniformly discrete sequence $\Gamma = \{t_n\}$ is uniformly dense with density $\Delta\Gamma$ if there is an $L < \infty$ so that for all n

$$|t_n - n(\Delta\Gamma)^{-1}| < L.$$

Additional studies of sampling in Hilbert spaces can be found in [Beu61], [Yen56], [Beu66], [Yao67], [Jer77], and [CA87].

Chapter 3

Frames

In this chapter the theory of (global) Hilbert space frames is reviewed and some necessary tools are developed. The theory of frames is due to Duffin and Schaeffer [DS52], cf., [Dau92], [DGM86], [HW89], [You80]. Throughout the chapter $\mathcal{H}$ denotes a Hilbert space contained in $L_\mu^2(\mathcal{G})$, with norm $\|\ldots\| \overset{\triangle}{=} \|\ldots\|_{L_\mu^2(\mathcal{G})}$ induced from $L_\mu^2(\mathcal{G})$. Here, $\mathcal{G}$ is a group and μ is the left Haar measure.

3.1   Frame Basics

As a concept, frames provide an intermediate ground between the two related notions of *completeness* in a space and an orthonormal *basis* for a space. Recall, a set of functions $\{\phi_n\}$ is complete in a Hilbert space $\mathcal{H}$ if the closure of their span is the whole space $\mathcal{H}$, i.e. $\overline{\text{span}\,\{\phi_n\}} = \mathcal{H}$. A set $\{\phi_n\}$ is a Schauder basis for the space $\mathcal{H}$ if for any $f \in \mathcal{H}$ there is a unique set of coefficients $\{c_n\}$ such that $f = \sum c_n \phi_n$. As it shall be seen the statements that a set $\{\phi_n\}$ is

a. complete in $\mathcal{H}$,

b. a frame for $\mathcal{H}$,

c. a Riesz basis for $\mathcal{H}$, and

d. an orthonormal basis for $\mathcal{H}$

are progressively stronger. In other words d $\Longrightarrow$ c $\Longrightarrow$ b $\Longrightarrow$ a.

To any set $\{\phi_n\}$ one may associate the operator $S = S_\phi$ defined as

$$Sf \overset{\triangle}{=} \sum \langle f, \phi_n \rangle \, \phi_n.$$

The frame property can be equivalently characterized in terms of this operator S, and consequently has been called the frame operator. Specifically the set $\{\phi_n\}$ is a frame for $\mathcal{H}$ if and only if there are constants A, B

$$\forall f \in \mathcal{H}, \quad A\|f\|^2 \le \langle f, Sf \rangle \le B\|f\|^2$$

such that $0 < A \le B < \infty$. Note that the frame operator has many "nice" properties including linearity, continuity, and invertibility. Definition 3.1.1 gives the formal definition of a Hilbert space frame, its associated frame operator, and the notions of tightness and exactness.

Definition 3.1.1 a. A sequence $\{\phi_n\} \subseteq \mathcal{H}$ is a *frame* for $\mathcal{H}$ if there exist *frame bounds* $A, B > 0$ such that

$$\forall f \in \mathcal{H}, \quad A\|f\|^2 \le \sum |\langle f, \phi_n\rangle|^2 \le B\|f\|^2, \tag{3.1.1}$$

where summation is over $\mathbb{Z}$.

b. The *frame operator* of the frame $\{\phi_n\}$ is the function $S : \mathcal{H} \mapsto \mathcal{H}$ defined as $Sf = \sum \langle f, \phi_n\rangle \phi_n$.

c. A frame is said to be a *tight* if $A = B$.

d. A frame for $\mathcal{H}$ is said to be *exact* if the set determined by the removal of any one of its elements fails to be a frame for $\mathcal{H}$.

Some examples of frames are presented below. From these examples it is seen that tightness and exactness are independent properties.

Tight and Exact Frame Clearly any orthonormal basis $\{e_n\} \subseteq \mathcal{H}$ is a tight exact frame with bounds $A = B = 1$ since by Parseval's equality for orthonormal bases $\sum |\langle f, \phi_n\rangle|^2 = \|f\|^2$. It is exact since the elements are orthogonal and the removal of any one element will cause the reduced set to fail to be dense in $\mathcal{H}$.

Tight and Non-exact Frame The union of any finite number $N > 2$ of orthonormal bases in $\mathcal{H}$ yields a tight non-exact frame for $\mathcal{H}$ with frame bounds $A = B = N$. To see this, for each $m = 1, 2, \ldots, N$ let $\{e_{m,n}\}_n$ be an orthonormal basis for $\mathcal{H}$. Then by Parseval's equality for orthonormal bases

$$\sum_{m=1}^{N} \sum_n |\langle f, e_{m,n}\rangle|^2 = \sum_{m=1}^{N} \|f\|^2 = N\|f\|^2.$$

Since each basis $\{e_{m,n}\}_n$ is dense in $\mathcal{H}$ the removal of any one element from

$$\bigcup_{m=1}^{N} \{e_{m,n}\}$$

will result in a collection of vectors which contains at least one orthonormal basis for $\mathcal{H}$. Therefore it is dense in $\mathcal{H}$.

For example $\{e_1, e_1, e_2, e_2, e_3, e_3, \ldots\}$ is a tight non-exact frame with $A = B = 2$.

Non-tight and Exact Frame A non-tight and exact frame may be generated from $\{\phi_n\}$ as

$$\{a_n e_n\}$$

where $\{a_n\}$ is a sequence of scalars satisfying $0 < A \le a_n^2 \le B < \infty$ and there is a pair m, n such that $a_m \ne a_n$. Clearly then the set $\{a_n e_n\}$ is exact and

$$
\begin{aligned}
\sum_n |\langle f, a_n e_n\rangle|^2 &= \sum_n a_n^2 |\langle f, e_n\rangle|^2 \\
&\le \sum_n \left(\sup_k a_k^2\right) |\langle f, e_n\rangle|^2 \\
&\le B \sum_n |\langle f, e_n\rangle|^2 = B\|f\|^2.
\end{aligned}
$$

The lower bound is similar.

For example $\{2e_1, e_2, e_3, e_4, \ldots\}$ is a non-tight exact frame with $A = 1$ and $B = 2$.

Non-tight and Non-Exact Frame There are many ways to generate non-tight non-exact frames. For example, the union of a orthonormal basis with a scaled orthonormal basis. An example is
$$\{e_1, 2e_1, e_2, 2e_2, e_3, 2e_3, \ldots\}.$$

The following theorem exhibits the close relationship between exact frames and orthonormal bases. More precisely it states that exact frames are Riesz bases. Riesz bases are by definition related to orthonormal bases by a topological isomorphism. See [You80, p. 188] for a proof of the equivalence of parts a and b.

Theorem 3.1.2 Let $\mathcal{H}$ be an arbitrary Hilbert space and $\{\phi_n\}$ be a sequence of elements in $\mathcal{H}$. The following are equivalent:

a. $\{\phi_n\}$ is an exact frame for $\mathcal{H}$.

b. $\{\phi_n\}$ is a Riesz basis for $\mathcal{H}$.

c. $\{\phi_n\}$ is a bounded unconditional basis for $\mathcal{H}$.

The following theorem states some of the fundamental properties of frames.

Theorem 3.1.3 a. If $\{\phi_n\} \subseteq \mathcal{H}$ is a frame with frame bounds A, B, then S is a topological isomorphism with inverse S^{-1}, $\{S^{-1}\phi_n\}$ is a frame with frame bounds B^{-1} and A^{-1}, and

$$\forall f \in \mathcal{H}, \quad f = \sum \left\langle f, S^{-1}\phi_n \right\rangle \phi_n = \sum \left\langle f, \phi_n \right\rangle S^{-1}\phi_n \tag{3.1.2}$$

in $\mathcal{H}$.

b. If $\{\phi_n\} \subseteq \mathcal{H}$, let $L : \mathcal{H} \mapsto \ell^2(\mathbb{Z})$ be defined as $Lf = \{\langle f, \phi_n \rangle\}$, cf., (3.2.3). If $\{\phi_n\}$ is a frame then $S = L^*L$, where L^* is the adjoint of L.

Since the frame operator S may be factored [DGM86, Dau90] as L^*L an immediate consequence is that
$$\langle f, Sf \rangle = \langle f, L^*Lf \rangle = \langle Lf, Lf \rangle = \|Lf\|^2.$$

Since $\{\phi_n\}$ is a frame with frame bounds A and B this implies that
$$A\|f\|^2 \leq \|Lf\|^2 \leq B\|f\|^2.$$

Thus,
$$\|L\| \leq B^{\frac{1}{2}} \quad \text{and} \quad \|L^{-1}\| \leq A^{-\frac{1}{2}},$$

where L^{-1} is defined on the range $L(\mathcal{H})$.

It is clear that if A and B are frame bounds for a frame $\{\phi_n\}$ then any other pair A_1 and B_1 such that $0 < A_1 < A$ and $\infty > B_1 > B$ are also valid frame bounds for $\{\phi_n\}$. It is of interest to know the smallest upper bound and the largest lower bound which serve as frame bounds for a frame. This motivates the notion of the *best* frame bounds. Given a frame $\{\phi_n\}$ for a Hilbert space $\mathcal{H}$ with frame operator S, the *best bounds* A and B are

$$A = \inf_{f \in \mathcal{H}} \frac{\langle f, Sf \rangle}{\|f\|^2},$$

$$B = \sup_{f \in \mathcal{H}} \frac{\langle f, Sf \rangle}{\|f\|^2}.$$

Since $\|Lf\|^2 = \langle f, Sf \rangle$ it follows that the best bounds A, B are also $A = \|L^{-1}\|^{-2}$ and $B = \|L\|^2$.

3.2   Frame Representation

In this section the natural discretization suggested by the frame operator is exposed via Theorem 3.1.3b. Consider the operator L of Theorem 3.1.3 and its adjoint. The theorem asserts that L and its adjoint L^* are factors of the frame operator S. Explicitly, the operators $L : \mathcal{H} \mapsto \ell^2(\mathbb{Z})$, and $L^* : \ell^2(\mathbb{Z}) \mapsto \mathcal{H}$ are

$$Lf = \{\langle f, \phi_n \rangle\} \tag{3.2.1}$$

and

$$L^*c = \sum c_n \phi_n, \tag{3.2.2}$$

where $f \in \mathcal{H}$ and $c \in \ell^2(\mathbb{Z})$. It is easily verified that in fact $S = L^*L$ since for all $f \in \mathcal{H}$

$$Sf = \sum \langle f, \phi_n \rangle \phi_n = L^*Lf.$$

The desired discretization operator L is a mapping from $\mathcal{H}$ to $\ell^2(\mathbb{Z})$ and is defined as

$$\begin{aligned} L \;:\; \mathcal{H} &\to \ell^2(\mathbb{Z}) \\ f &\mapsto \{\langle f, \phi_n \rangle\}. \end{aligned} \tag{3.2.3}$$

Figure 3.1 depicts the mappings L and its adjoint L^*. If $\{\phi_n\}$ is a frame for $\mathcal{H}$ then the mapping defined in (3.2.3) is called the *frame representation* or *frame discretization* operator. The frame representation operator L plays a central role in Theorem 3.1.3. Part a of the theorem describes one method to recover a signal $f \in \mathcal{H}$ from its frame representation $Lf \in \ell^2(\mathbb{Z})$. In part b, the theorem indicates that the frame operator S has factors L and L^*. In addition, Theorem 3.2.1 below states that the frame representation operator L has an inverse when considered on the range $L(\mathcal{H})$. These facts form the basis for the iterative reconstruction scheme given in Proposition 3.4.3 and, in turn, the notion of the *frame correlation* operator discussed in Section 3.3.

A characterization of frame representation operators is given in the following theorem.
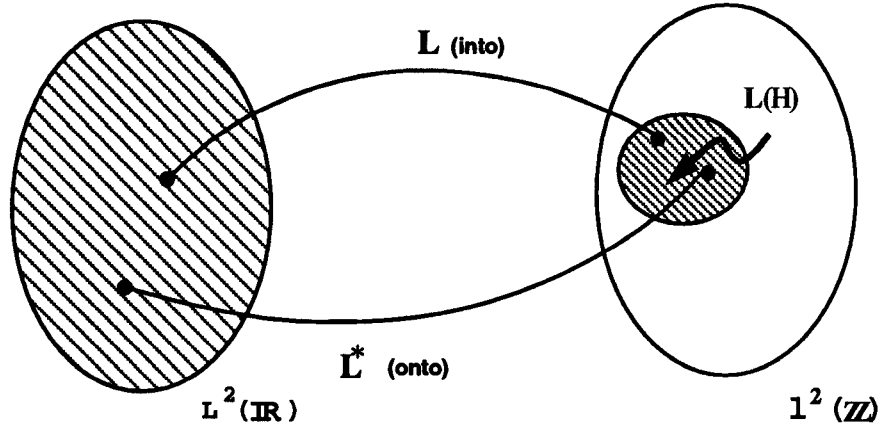
Figure 3.1: The mappings L and L^*

Theorem 3.2.1 ([Ben93, Theorem 3.6]) The sequence $\{\phi_n\}$ is a frame for $\mathcal{H}$ if and only if the mapping L given in (3.2.3) is a well defined topological isomorphism onto a closed subspace of $\ell^2(\mathbb{Z})$.

Theorem 3.2.1 has three significant consequences worthy of mention. Namely, if L is a frame representation operator then

a. L is injective (one to one),

b. $L(\mathcal{H})$ is closed, and

c. L^* is surjective (onto).

To see the injectivity of the map L suppose $\{\phi_n\}$ is a frame for $\mathcal{H}$ with bounds A and B and that $Lf_1 = Lf_2$. Then

$$0 = \|Lf_1 - Lf_2\|^2 = \|L(f_1 - f_2)\|^2 \geq A\|f_1 - f_2\|^2$$

which implies that $f_1 = f_2$. Thus, L is injective. Because L is an injective bounded linear operator whose range $L(\mathcal{H})$, is closed then L^* is onto by Proposition A.1.

3.3 Frame Correlation

A concept which arises naturally in frame theory is the notion of *frame correlation* given in Definition 3.3.1. It will be seen that the frame correlation is a crucial element in the process of reconstruction from frame representations, cf. Proposition 3.4.2.

Definition 3.3.1 (Frame Correlation) Let $\{\phi_n\}$ be a frame for the Hilbert space $\mathcal{H}$ with frame representation operator L. The *frame correlation* operator is defined as $R \stackrel{\triangle}{=} LL^*$.

27

The frame operator $S = L^*L$ and the frame correlation $R = LL^*$ are similar objects and play similar roles in the theory of frames. In fact, a reconstruction theory may be developed without ever introducing the frame correlation, cf. [FG92]. Hence, one may ask why the frame correlation is an important object to study? To answer this note that

$$S : \mathcal{H} \mapsto \mathcal{H},$$

while

$$R : L(\mathcal{H}) \mapsto L(\mathcal{H}).$$

In many cases of interest $\mathcal{H}$ will be an infinite dimensional Hilbert space having elements which can not be directly processed by a digital machine while $L(\mathcal{H})$ will consist of *discrete* elements, i.e. countable sets, which (if truncated) may be processed digitally. For example, such an $\mathcal{H}$ is the space of bandlimited functions PW_Ω, and $L(\mathcal{H}) = \{f(t_n) : f \in PW_\Omega\}$ for some sequence $\{t_n\}$. Thus the operator S does not admit a digital implementation while R does.

3.3.1 Properties

The frame correlation matrix R shares many properties of the frame operator S. For instance, they are both non-negative self adjoint operators which map bijectively onto their range. The crucial differences, however, are that

a. the range and domain of R is contained in $\ell^2(\mathbb{Z})$, and

b. the range of R need not be all of $\ell^2(\mathbb{Z})$.

These two differences directly relate to the issues of

a. digital implementability and

b. representation noise robustness

respectively. As discussed previously the fact that R operates on countable sequences, i.e. digital signals, immediately suggests that it is possible to implement R on a digital machine. This is not possible for S. Robustness to noise in the representation is directly related to the size of the kernel of R. This issue is addressed in Section 3.5.1.

This section is composed of several propositions which illustrate the properties of a frame correlation R. The first, Proposition 3.3.2 exposes the matrix representation of the frame correlation R (of a frame $\{\phi_n\}$ for a Hilbert space $\mathcal{H}$) as the Gram matrix associated with the sequence of elements $\{\phi_n\} \subseteq \mathcal{H}$. The second, Proposition 3.3.3 compiles a list of useful general properties of a frame correlation R. Thirdly, Theorem 3.3.4 establishes the ramifications for R and other equivalences if the underlying frame is exact.

Proposition 3.3.2 Given a frame $\{\phi_n\}$ for the Hilbert space $\mathcal{H}$, the frame correlation matrix R has the matrix representation

$$R = (\langle \phi_m, \phi_n \rangle) \stackrel{\triangle}{=} R_{m,n}.$$

Proof:

Take any $c \in \ell^2(\mathbb{Z})$. Then one can write

$$Rc = LL^*c = \{\langle L^*c, \phi_n \rangle\} = \left\{ \sum_m c_m \langle \phi_m, \phi_n \rangle \right\}$$

so that

$$(Rc)_n = (LL^*c)_n = \sum_m c_m \langle \phi_m, \phi_n \rangle, \qquad (3.3.1)$$

and

$$\begin{pmatrix} \vdots \\ (Rc)_{-1} \\ (Rc)_0 \\ (Rc)_1 \\ \vdots \end{pmatrix} = \begin{pmatrix} \ddots & & \vdots & & \\ & \langle \phi_{-1}, \phi_{-1} \rangle & \langle \phi_0, \phi_{-1} \rangle & \langle \phi_1, \phi_{-1} \rangle & \\ \cdots & \langle \phi_{-1}, \phi_0 \rangle & \langle \phi_0, \phi_0 \rangle & \langle \phi_1, \phi_0 \rangle & \cdots \\ & \langle \phi_{-1}, \phi_1 \rangle & \langle \phi_0, \phi_1 \rangle & \langle \phi_1, \phi_1 \rangle & \\ & & \vdots & & \ddots \end{pmatrix} \begin{pmatrix} \vdots \\ c_{-1} \\ c_0 \\ c_1 \\ \vdots \end{pmatrix}. \qquad (3.3.2)$$

∎

Proposition 3.3.3 Suppose $\{\phi_n\}$ is a frame for the Hilbert space $\mathcal{H}$ with frame representation operator L, correlation R and bounds A and B.

    a. If $\mathcal{H}$ is infinite dimensional then L is not compact; and thus, R is not compact.

    b. For each row m of R, $\lim_{n \to \infty} |R_{m,n}| \to 0$.

    For each column n of R, $\lim_{m \to \infty} |R_{m,n}| \to 0$.

    c. If the set $\{\phi_n\}$ is an orthonormal basis for $\mathcal{H}$ then the frame correlation operator is the identity.

    d. $\ker R = L(\mathcal{H})^\perp$.

    e. R maps $L(\mathcal{H})$ bijectively to itself.

    f. $R = P_{L(\mathcal{H})}R = RP_{L(\mathcal{H})}$

    g. R is self adjoint.

    h. $R \geq 0$.

Proof:

    a. To prove the non-compactness of L a normalized sequence $\{f_n\} \subseteq L^2(\mathbb{R})$ shall be chosen such that $\{Lf_n\}$ has no converging subsequence. Let $f_n = 1_{[n,n+1]}$ so that $\|f_n\| = 1$. For such a sequence one has

$$\|Lf_n - Lf_m\| = \|L(f_n - f_m)\| \geq A^{\frac{1}{2}} \|f_n - f_m\|,$$

where the equality holds by the linearity of L and the inequality holds by the frame condition applied to $f_n - f_m$. For our choice of $\{f_n\}$ it is easy to see that $\|f_n - f_m\| = 2(1 - \delta_{m,n})$. Thus one has that

$$\forall n \neq m, \quad \|Lf_n - Lf_m\| \geq 2A^{\frac{1}{2}}.$$

Since $\ell^2(\mathbb{Z})$ is complete one may conclude that $\{Lf_n\}$ has no converging subsequences. Hence L is not compact.

    To show R is not compact note that by part e. there is a well defined inverse R^{-1} of R on $L(\mathcal{H})$. With $\{f_n\}$ as in part a. define $c_n \triangleq \frac{R^{-1}Lf_n}{\|R^{-1}Lf_n\|} = R^{-1}L(f_n/a_n)$ where the normalization

is well defined since $a_n \overset{\triangle}{=} \|R^{-1}Lf_n\| = \|L_\psi f_n\| \geq B^{-\frac{1}{2}} > 0$. Also we have $a_n \leq A^{-\frac{1}{2}}$ or $a_n^{-2} \geq A$. As in part a. we may compute

$$\|f_n/a_n - f_m/a_m\| = (a_n^{-2} + a_m^{-2})(1 - \delta_{m,n}) \geq 2A(1 - \delta_{m,n}).$$

For the sequence $\{c_n\} \subseteq \ell^2(\mathbb{Z})$ then

$$\forall n \neq m, \quad \|Rc_n - Rc_m\| = \|L(f_n/a_n - f_m/a_m)\| \geq 2A^{\frac{3}{2}},$$

and one concludes that $\{Rc_n\}$ has no converging subsequences so that R is not compact.

b. Since $\{\phi_n\}$ is a frame for $\mathcal{H}$ then one must have in particular that

$$\forall m \quad \sum_n |\langle \phi_m, \phi_n \rangle|^2 \leq B\|\phi_m\|^2.$$

For the sum to converge it is necessary that $|\langle \phi_m, \phi_n \rangle| \to 0$ as $m \to \infty$.

c. Follows from Proposition 3.3.2 since $\langle \phi_m, \phi_n \rangle = \delta_{m,n}$.

d. i/ $\ker R \subseteq L(\mathcal{H})^\perp$

Let $c_0 \in \ker R$ so that $Rc_0 = 0$. We will show for all $f \in \mathcal{H}$ that $\langle c_0, Lf \rangle = 0$. Since L^* is onto then for all $f \in \mathcal{H}$ there is a $c \in L(\mathcal{H})$ so that $f = L^*c$. Thus,

$$\langle c_0, Lf \rangle = \langle L^*c_0, f \rangle = \langle L^*c_0, L^*c \rangle = \langle Rc_0, c \rangle = 0.$$

ii/ $\ker R \supseteq L(\mathcal{H})^\perp$

Let $c_\perp \in L(\mathcal{H})^\perp$. For any $c \in \ell^2(\mathbb{Z})$ we have

$$
\begin{aligned}
\langle Rc_\perp, c \rangle &= \langle c_\perp, Rc \rangle \\
&= \langle c_\perp, L(L^*c) \rangle = 0.
\end{aligned}
$$

Since $\langle Rc_\perp, c \rangle = 0$ for all $c \in \ell^2(\mathbb{Z})$ then $Rc_\perp = 0$.

e. Since L is a linear injective map, one need only demonstrate RL is an injective map from $L(\mathcal{H})$ to $L(\mathcal{H})$ to prove that R is injective on $L(\mathcal{H})$. Write $RL = LL^*L = LS$. Since both L and S are injective then $LS = RL$ is also. Thus R is 1-1. Since R is self adjoint and 1-1 then it must also be onto by Corollary A.2.

f. Let $c \in \ell^2(\mathbb{Z})$. Clearly, $Rc = LL^*c \in L(\mathcal{H})$. Thus, $R = P_{L(\mathcal{H})}R$ and by taking the adjoint $R = RP_{L(\mathcal{H})}$.

g. $R^* = (LL^*)^* = LL^* = R$.

h. Since L^* is surjective for all $f \in L^2(\mathbb{R})$ there is a $c \in L(\mathcal{H})$ such that $f = L^*c$. Thus, $0 \geq \|f\|^2 = \langle L^*c, L^*c \rangle = \langle c, LL^*c \rangle = \langle c, Rc \rangle$.

∎

We have seen in Proposition 3.3.3e that R maps $L(\mathcal{H})$ bijectively to itself. If $L(\mathcal{H})$ is all of $\ell^2(\mathbb{Z})$ (L is onto) then R is topological isomorphism on $\ell^2(\mathbb{Z})$. This can only happen if the underlying frame is a Riesz basis, i.e. an exact frame. This and other equivalences are the content of Theorem 3.3.4.

Theorem 3.3.4 Let $\{\phi_n\}$ be a frame for $\mathcal{H}$ with frame representation operator L, frame correlation R, and bounds A and B. The following are equivalent:

a. L is onto $\ell^2(\mathbb{Z})$.

b. L^* is one to one.

c. R is a topological isomorphism on $\ell^2(\mathbb{Z})$.

d. $R > 0$

e. $\{\phi_n\}$ is a Riesz-Fischer sequence.

f. $\{\phi_n\}$ is a Riesz basis.

Proof:
(a. $\Longrightarrow$ b.)

From elementary operator theory,

$$\ker L^* = L(\mathcal{H})^\perp = (\ell^2(\mathbb{Z}))^\perp = \{0\}$$

so that L^* (a linear operator) is one to one.

(b. $\Longrightarrow$ c.)

Clearly $R \in \mathcal{B}(\mathcal{H}, \mathcal{H})$ since $R = LL^*$ and $L \in \mathcal{B}(\mathcal{H}, \mathcal{H})$. R is one to one because L is one to one (always) and by assumption L^* is one to one so that the composition LL^* is also one to one. $R^* = R$ is onto by Proposition A.1 since $R(\mathcal{H}) = L(\mathcal{H})$ is closed (Theorem 3.2.1b). Thus R is bijective on $\ell^2(\mathbb{Z})$ and there exists an inverse R^{-1} on all of $\ell^2(\mathbb{Z})$. Moreover, $\|R^{-1}\| \le A^{-1}$ by dual frame arguments. Thus, R is a topological isomorphism on $\ell^2(\mathbb{Z})$.

(c. $\Longrightarrow$ a.)

Suppose R is a topological isomorphism and L is not onto $\ell^2(\mathbb{Z})$. But $R(\mathcal{H}) = L(\mathcal{H}) \ne \ell^2(\mathbb{Z})$ which means that R can not be onto. This contradicts the assumption that R is a topological isomorphism.

(b. $\Longrightarrow$ d.)

Write

$$\langle c, Rc \rangle = \langle c, LL^*c \rangle = \|L^*c\|^2 \ge 0.$$

Since L^* is one to one then $\langle c, Rc \rangle = 0$ if and only if $c = 0$. Thus, $R > 0$.

(d. $\Longrightarrow$ b.)

$R > 0$ means that for all non-zero $c \in \ell^2(\mathbb{Z})$

$$0 < \langle c, Rc \rangle = \|L^*c\|^2.$$

If $L^*c_1 = L^*c_2$ then

$$\langle c_1 - c_2, R(c_1 - c_2) \rangle = \|L^*c_1 - L^*c_2\| = 0$$

and we conclude that $c_1 = c_2$. Thus, L^* is one to one.

(a. $\Longleftrightarrow$ e.)

By definition $\{\phi_n\}$ is a Riesz-Fischer sequence means that for all $c \in \ell^2(\mathbb{Z})$ there is a $f \in \mathcal{H}$ such that $c = \{\langle f, \phi_n \rangle\}$. With L the frame representation $Lf = \{\langle f, \phi_n \rangle\}$ this translates equivalently to the statement that L is onto $\ell^2(\mathbb{Z})$.

31

(c. $\Longrightarrow$ f.)

Suppose R is a topological isomorphism on $\ell^2(\mathbb{Z})$. We have $Lf = \{\langle f, \phi_n \rangle\}$. Fix an integer N and define a new operator L_N as $L_N f = \{\langle f, \phi_n \rangle\}_{n \neq N}$. We will show that the removal of one element from the set $\{\phi_n\}$ will fail to be a frame by constructing a non-zero $f \in \mathcal{H}$ so that $L_N f = 0$. Let $\{e_n\}$ be an the standard orthonormal basis for $\ell^2(\mathbb{Z})$, i.e. $e_n = \{\delta_{m,n}\}$. Since R is a topological isomorphism on $\ell^2(\mathbb{Z})$ then R has an inverse R^{-1} on $\ell^2(\mathbb{Z})$. We may then pick

$$f = L^* R^{-1} e_N$$

so that for this choice of f

$$Lf = L(L^* R^{-1} e_N) = e_N$$

and hence $L_N f = 0$.

(f. $\Longrightarrow$ c.)

By definition $\{\phi_n\}$ is an exact frame means there exists a topological isomorphism T and an orthonormal basis $\{e_n\}$ for $\mathcal{H}$ so that for all n, $\phi_n = Te_n$. Let L_e be the frame representation associated with the orthonormal basis $\{e_n\}$. Since $\{e_n\}$ is an orthonormal basis then L_e is a topological isomorphism from $\mathcal{H}$ onto $\ell^2(\mathbb{Z})$. Similarly L_e^* is a topological isomorphism from $\ell^2(\mathbb{Z})$ onto $\mathcal{H}$. Noting that

$$L_e T^* f = \{\langle T^* f, e_n \rangle\} = \{\langle f, Te_n \rangle\} = \{\langle f, \phi_n \rangle\} = Lf$$

we conclude that $L = L_e T^*$ and $R = LL^* = L_e T^* T L_e^*$. Thus, since each factor of R is a topological isomorphism R is a topological isomorphism on $\ell^2(\mathbb{Z})$.

$\blacksquare$

3.3.2 Pseudo-Inverse

Proposition 3.3.3e implies that R has an inverse on $L(\mathcal{H})$. This inverse is denoted R^{-1} and

$$\forall c \in L(\mathcal{H}) \quad c = R^{-1} Rc = RR^{-1} c.$$

To extend the inverse to all of $\ell^2(\mathbb{Z})$ define the *pseudo inverse*

$$R^\dagger \overset{\triangle}{=} R^{-1} P_{L(\mathcal{H})} \tag{3.3.3}$$

where $P_{L(\mathcal{H})}$ is the orthogonal projection operator onto the image of L. Definition 3.3.5 gives a definition of pseudo-inverse. We note that there are several equivalent definitions with interesting interpretations of the pseudo-inversion process, viz. Appendix C.

Proposition 3.3.3f can be used to demonstrate that as defined in (3.3.3) $R^\dagger$ is in fact a bonified pseudo-inverse. Using Proposition 3.3.3f we have that for all $c \in \ell^2(\mathbb{Z})$

$$R^\dagger Rc = R^{-1} P_{L(\mathcal{H})} Rc = R^{-1} R P_{L(\mathcal{H})} c = P_{L(\mathcal{H})} c$$

and similarly

$$RR^\dagger c = RR^{-1} P_{L(\mathcal{H})} c = P_{L(\mathcal{H})} c.$$

We conclude that $R^\dagger R = R R^\dagger = P_{L(\mathcal{H})}$. This observation makes the verification of the defining conditions of a pseudo inverse in Definition 3.3.5 trivial. Thus, 3.3.3 does indeed give the pseudo-inverse of R. In Section 3.4 an iterative method for the construction of the pseudo-inverse is presented.

Definition 3.3.5[Gro77, Definition (P)] If $T \in \mathcal{B}(\mathcal{H}_1, \mathcal{H}_2)$ has closed range, then $T^\dagger$ is the unique operator in $\mathcal{B}(\mathcal{H}_2, \mathcal{H}_1)$ satisfying

(1) $TT^\dagger$ is self adjoint,

(2) $T^\dagger T$ is self adjoint,

(3) $TT^\dagger T = T$, and

(4) $T^\dagger T T^\dagger = T^\dagger$.

The following theorem shows that the best frame bounds of a frame are directly related to the operator norms of the frame correlation R and its pseudo inverse $R^\dagger$.

Theorem 3.3.6 Let $\{\phi_n\}$ be a frame for a Hilbert Space $\mathcal{H}$ with best frame bounds A and B and frame correlation R. Then the frame correlation R is related to the frame bounds A and B as

a. $A = \|R^\dagger\|^{-1}$

b. $B = \|R\|$.

Proof:

a. Since $\{\phi_n\}$ is a frame for $\mathcal{H}$ then L^* is surjective. Hence, for all $f \in \mathcal{H}$ there is a $c \in L(\mathcal{H})$ so that $f = L^*c$ and one may write for f not zero a.e.

$$\frac{\langle f, Sf \rangle}{\|f\|^2} = \frac{\langle L^*c, SL^*c \rangle}{\langle L^*c, L^*c \rangle} = \frac{\langle L^*c, L^*LL^*c \rangle}{\langle c, LL^*c \rangle} = \frac{\langle c, R^2 c \rangle}{\langle c, Rc \rangle} \tag{3.3.4}$$

for c off the $\ker L^* = L(\mathcal{H})^\perp$, i.e. $c \in L(\mathcal{H})$. The surjectivity of L^* then implies the best lower frame bound A is

$$A \stackrel{\triangle}{=} \inf_{f \in \mathcal{H}} \frac{\langle f, Sf \rangle}{\|f\|^2} = \inf_{c \in L(\mathcal{H})} \frac{\langle c, R^2 c \rangle}{\langle c, Rc \rangle}.$$

Since $R^\dagger$ is onto $L(\mathcal{H})$ for any $c \in L(\mathcal{H})$ there is a $c_0 \in L(\mathcal{H})$ so that $c = R^\dagger c_0$. With this substitution one has

$$\frac{\langle c, R^2 c \rangle}{\langle c, Rc \rangle} = \frac{\langle R^\dagger c_0, R^2 R^\dagger c_0 \rangle}{\langle R^\dagger c_0, RR^\dagger c_0 \rangle} = \frac{\langle c_0, c_0 \rangle}{\langle R^\dagger c_0, c_0 \rangle}.$$

Thus,

$$A = \inf_{c_0 \in L(\mathcal{H})} \frac{\langle c_0, c_0 \rangle}{\langle R^\dagger c_0, c_0 \rangle} = \left(\sup_{c_0 \in L(\mathcal{H})} \frac{\langle R^\dagger c_0, c_0 \rangle}{\langle c_0, c_0 \rangle} \right)^{-1} = \left(\sup_{c_0 \in L(\mathcal{H})} \frac{\left| \langle R^\dagger c_0, c_0 \rangle \right|}{\langle c_0, c_0 \rangle} \right)^{-1},$$

where the last equality follows since $R^\dagger$ is a non-negative operator. Further,

$$A = \left(\sup_{c_0 \in L(\mathcal{H}) \oplus \ker R^\dagger} \frac{\left| \left\langle R^\dagger c_0, c_0 \right\rangle \right|}{\langle c_0, c_0 \rangle} \right)^{-1} = \left(\sup_{c_0 \in \ell^2(\mathbb{Z})} \frac{\left| \left\langle R^\dagger c_0, c_0 \right\rangle \right|}{\langle c_0, c_0 \rangle} \right)^{-1} = \| R^\dagger \|^{-1}.$$

Where one has used the fact that $\ker R^\dagger = \ker R = L(\mathcal{H})^\perp$ from Proposition 3.3.3d. The last equality is a consequence of Fact 2.1.3.

b. The upper bound can be proven by via the dual frame $\{S^{-1}\phi_n\}$ with best bounds A', B' and frame correlation R'. Since $R' = R^\dagger$ and $A' = B^{-1}$ application of part a. to the dual frame yields $B^{-1} = \|(R')^\dagger\|^{-1}$ or $B = \|R\|$.

∎

3.3.3 Duality

From Theorem 3.1.3a a frame $\{\phi_n\}$ has an associated dual frame $\{\psi_n\}$, where $\psi_n \triangleq S^{-1}\phi_n$ and S is the frame operator. As a frame, $\{\psi_n\}$ also has a frame representation operator L_ψ, where $L_\psi f \triangleq \{\langle f, \psi_n \rangle\} = \{\langle f, S^{-1}\phi_n \rangle\}$. As a matter of notation we may write both L and L_ϕ to indicate the frame representation with respect to the frame $\{\phi_n\}$. Since S is a topological isomorphism clearly $L_\phi(\mathcal{H}) = L_\psi(\mathcal{H})$. With this notation, Equation 3.1.2 may be written as

$$\forall f \in \mathcal{H}, \quad f = L_\phi^* L_\psi f = L_\psi^* L_\phi f. \tag{3.3.5}$$

From this observation we may conclude that

$$L_\phi^* L_\psi = L_\psi^* L_\phi = I$$

where I is the identity operator on $\mathcal{H}$. Further, if attention is restricted to the range $L(\mathcal{H})$ we may write

$$L_\phi^{-1} = L_\psi^*$$

and

$$L_\psi^{-1} = L_\phi^*.$$

Moreover, the relation between the frame representation L_ϕ and its dual L_ψ is

$$L_\psi = R^{-1} R L_\psi = R^{-1} L_\phi \underbrace{L_\phi^* L_\psi}_{I} = R^{-1} L_\phi,$$

where R is the frame correlation associated with the frame $\{\phi_n\}$. Table 3.1 lists the relationships between the frame bounds A and B, frame operator S, frame representation L, and frame correlation R of a frame $\{\phi_n\}$ and its dual frame $\{S^{-1}\phi_n\}$. Dual quantities are denoted with $'$, e.g. S' is the dual frame operator.

Elements	Bounds	Operator	Representation	Correlation
$\{\phi_n\}$	(A, B)	S	L	R
$\{S^{-1}\phi_n\}$	(B^{-1}, A^{-1})	S^{-1}	$R^{-1}L$	$R^\dagger$

Table 3.1: Relation of frame objects and their duals.

3.4 Iterative Reconstruction

Let $\mathcal{H}$ be a Hilbert space and take $f_* \in \mathcal{H}$ arbitrarily. Assume also that $\{\phi_n\}$ is a frame for $\mathcal{H}$ with frame bounds A and B, frame representation L, and frame correlation R. This section details an iterative procedure for the recovery of a signal f_* from its frame representation Lf_*. The iterative procedure will generate a sequence $\{c_n\} \subseteq L(\mathcal{H})$ which converges to a $c_* \in L(\mathcal{H})$ such that $f_* = L^*c_*$. Moreover the sequence converges at an exponential rate. The algorithm for the computation of the sequence $\{c_n\}$ may be implemented digitally and identified with the computation of the inverse R^{-1} of the frame correlation R.

3.4.1 Frame Operator

It may be easily shown [Ben92, Algorithm 50] [Ben93, Section 6.6] that since $\{\phi_n\}$ is a frame for $\mathcal{H}$ with frame bounds A,B

$$\|I - \frac{2}{A+B}S\| \le \frac{B-A}{A+B} < 1,$$

so that by the Neumann expansion,

$$S^{-1} = \frac{2}{A+B}\sum_{j=0}^{\infty}(I - \frac{2}{A+B}S)^j, \tag{3.4.1}$$

where I is the identity operator in $\mathcal{H}$. For any $f_* \in \mathcal{H}$ applying (3.4.1) to Sf_* yields

$$f_* = \sum_{j=0}^{\infty}(I - \lambda S)^j(\lambda S)f_*, \tag{3.4.2}$$

where $\lambda = 2/(A + B)$.

An iterative procedure for the recovery of f_* from Sf_* could be constructed by 3.4.2 as a difference equation, e.g. [FG92], [CFS]. However, such a procedure would not be directly digitally implementable in the case that the underlying Hilbert space $\mathcal{H}$ consists of analog signals. Instead we will focus on iterative methods for reconstruction which are digitally implementable. These methods utilize not the frame operator S but the frame correlation R.

3.4.2 Frame Correlation

With a view toward digital implementation it is desirable to construct an iterative algorithm for the recovery of f_* from Lf_*. To do this we first shown that $I - \lambda R$ is a contraction on $L(\mathcal{H})$.

Lemma 3.4.1 Let $\{\phi_n\}$ be a frame for $\mathcal{H}$ with frame representation operator L, correlation R and bounds A, B. If $0 < \lambda < 2/B$ then $\|I - \lambda R\|_{L(\mathcal{H})} < 1$ and $\|I - \lambda R\|_{\ell^2(\mathbb{Z})} = 1$ if $\{\phi_n\}$ is not exact. In particular one may take $\lambda = 2/(A + B)$.

35

Proof:

Let L' and R' be the dual frame representation and correlation respectively. Since $(L')^*$ is surjective then for any $f \in \mathcal{H}$ there is a $c \in L'(\mathcal{H})$ so that $f = (L')^*c$. This together with the fact that $\{S^{-1}\phi_n\}$ is a frame for $\mathcal{H}$ yields

$$B^{-1}\langle c, R'c \rangle \le \langle c, (R')^2c \rangle \le A^{-1}\langle c, R'c \rangle. \quad \text{(c.f. Equation (3.3.4))}$$

Letting $c = (R')^\dagger c_0$ one has

$$B^{-1}\langle Rc_0, c_0 \rangle \le \langle c_0, c_0 \rangle \le A^{-1}\langle Rc_0, c_0 \rangle.$$

For all nonzero $c_0 \in L'(\mathcal{H})$ this means

$$A \le \frac{\langle Rc_0, c_0 \rangle}{\langle c_0, c_0 \rangle} \le B.$$

Thus one has for $\lambda > 0$

$$1 - \lambda B \le \frac{\langle (I - \lambda R)c_0, c_0 \rangle}{\langle c_0, c_0 \rangle} \le 1 - \lambda A$$

and combining the facts that $I - \lambda R$ is self adjoint, cf., Proposition 3.3.3g, and fact 2.1.3

$$\|I - \lambda R\|_{L(\mathcal{H})} = \sup_{c \in L(\mathcal{H})} \frac{|\langle (I - \lambda R)c, c \rangle|}{\langle c, c \rangle} \le \max\{|1 - \lambda A|, |1 - \lambda B|\}. \tag{3.4.3}$$

We would like to find a lambda such that $\|I - \lambda R\|_{L(\mathcal{H})} < 1$. This condition is satisfied for all $\lambda \in (0, 2/B)$. In particular if $\lambda = 2/(A + B)$ then

$$|1 - \lambda A| = |1 - \lambda B| = (B - A)/(A + B) < 1.$$

For this choice of λ we have proven that $\|I - \lambda R\|_{L(\mathcal{H})} < 1$. Clearly, for all nonzero c taken from $\ker R = L(\mathcal{H})^\perp$ one has $\frac{|\langle (I-\lambda R)c, c \rangle|}{\langle c, c \rangle} = 1$. Since $\ell^2(\mathbb{Z}) = L(\mathcal{H}) \oplus L(\mathcal{H})^\perp$ then $\|I - \lambda R\|_{\ell^2(\mathbb{Z})} = 1$ if $L(\mathcal{H})^\perp = \ker L^* \ne \{0\}$, i.e. by Theorem 3.3.4 $\{\phi_n\}$ is not exact.

■

Proposition 3.4.2 The signal f_* may be recovered from its frame representation Lf_* as

$$f_* = \lambda \sum_{j=0}^{\infty} L^*(I - \lambda R)^j Lf_*, \tag{3.4.4}$$

where $L^*c = \sum c_n \phi_n$ for $c = \{c_n\}$.

Proof: Since $\langle Lf, c \rangle \overset{\triangle}{=} \langle f, L^*c \rangle$ and

$$\langle Lf, c \rangle = \sum \bar{c}_n \langle f, \phi_n \rangle = \left\langle f, \sum c_n \phi_n \right\rangle,$$

one obtains the formula for L^*c.

Because of (3.4.2) and the fact that $S = L^*L$, it is sufficient to prove

$$\lambda \sum_{j=0}^{\infty} L^*(I - \lambda R)^j Lf_* = \sum_{j=0}^{\infty} (I - \lambda L^*L)^j (\lambda L^*L) f_*. \qquad (3.4.5)$$

The $j = 0$ terms are clearly the same in (3.4.5). Assume

$$\lambda L^*(I - \lambda R)^j Lf_* = (I - \lambda L^*L)^j (\lambda L^*L) f_*. \qquad (3.4.6)$$

Then, using (3.4.6), compute

$$\begin{aligned}
\lambda L^*(I - \lambda R)^{j+1} Lf_* &= \lambda L^*(I - \lambda R)^j Lf_* - \lambda L^*(I - \lambda R)^j \lambda RLf_* \\
&= \lambda (I - \lambda L^*L)^j L^* Lf_* - \lambda (I - \lambda L^*L)^j L^*L(\lambda L^* Lf_*) \\
&= \lambda (I - \lambda L^*L)^j (I - \lambda L^*L) L^* Lf_* \\
&= \lambda (I - \lambda L^*L)^{j+1} L^* Lf_*,
\end{aligned}$$

and the result follows by induction. ∎

Proposition 3.4.2 leads directly to Algorithm 3.4.3 which details an iterative reconstruction procedure for the recovery of the signal f_* from its frame representation Lf_*. Moreover, this iterative procedure will converge at an exponential rate.

Algorithm 3.4.3 Let $\{\phi_n\}$ be a frame for a Hilbert space $\mathcal{H}$ with frame representation L, correlation R and bounds A, B. Suppose $c_0 \triangleq Lf_*$ is the frame representation of a signal $f_* \in \mathcal{H}$. set $f_0 = 0$. If $\lambda = 2/(A + B)$ and h_n, c_n and f_n are defined recursively as

$$\begin{aligned}
h_n &\triangleq \lambda L^* c_n, \\
c_{n+1} &\triangleq c_n - Lh_n, \\
f_{n+1} &\triangleq f_n + h_n,
\end{aligned}$$

then

a. $\lim f_n = f_*$, and

b. $\frac{\|f_n - f_*\|}{\|f_*\|} < \frac{B}{A} \alpha^n$, where $\alpha \triangleq \|I - \lambda R\|_{L(\mathcal{H})} < 1$.

Proof:

a. An elementary induction argument shows that

$$\forall n, \quad f_{n+1} = \lambda L^* \left(\sum_{j=0}^{n} (I - \lambda R)^j \right) c_0.$$

Consequently, by Proposition 3.4.2, one has

$$\lim f_n = f_*.$$

b. Write

$$
\begin{aligned}
\|f_n - f_*\| &= \|(f_{n+1} - f_n) + (f_{n+2} - f_{n+1}) + (f_{n+3} - f_{n+2}) \cdots\| \\
&\leq \sum_{k \geq n} \|f_{k+1} - f_k\| \\
&= \sum_{k \geq n} \|\lambda L^*(I - \lambda R)^n L f_*\| \\
&\leq \sum_{k \geq n} \lambda \|L^*\| \|(I - \lambda R)^n\|_{L(\mathcal{H})} \|L\| \|f_*\| \\
&\leq \lambda B \left(\sum_{k \geq n} \alpha^n \right) \|f_*\| \\
&= \left(\frac{\alpha^n}{1 - \alpha} \right) \lambda B \|f_*\| \\
&\leq \frac{B}{A} \alpha^n \|f_*\| \quad \text{(by Equation (3.4.3).)}
\end{aligned}
$$

■

Algorithm 3.4.3 underscores the importance of the correlation frame operator R in the reconstruction process. Formally one may rewrite (3.4.4) as

$$
f_* = L^* R^{-1} L f_*. \tag{3.4.7}
$$

Note that if R is known apriori the inverse frame correlation R^{-1} can be computed once (off-line) and stored for future reconstruction computations via (3.4.7).

A crucial element in determining convergence of the algorithm presented in Algorithm 3.4.3 was the fact that $c_0 = L f_*$ and in particular that $c_0 \in L(\mathcal{H})$. In fact, if c_0 is not entirely in $L(\mathcal{H})$ then the algorithm will *not* converge, cf., Lemma 3.4.1. This issue is addressed in Section 3.5 where a second algorithm is presented which will converge on all of $\ell^2(\mathbb{Z})$.

Remark 3.4.4 It is important to note that Algorithm 3.4.3 may be implemented digitally. That is, the sequence $\{\sum_{k=1}^n c_k\}$ may be generated entirely on a digital processor from the initial representation c_0. In practice the iterative algorithm will be terminated at some finite iteration N. The sequence $\{\sum_{k=1}^N c_k\}$ is related to f_N as $f_N = L^* \sum_{k=1}^N c_k$. The final step in converting the digital representation $\sum_{k=1}^N c_k$ to f_N involves a generalized digital to analog procedure well determined by L^*.

3.5 Noise Robustness

With respect to frame representations of signals there are two domains in which noise may perturb a signal. The first space is the Hilbert space $\mathcal{H} \subseteq L^2(\mathbb{R})$ and the second is its image under L, i.e., $L(\mathcal{H}) \subseteq \ell^2(\mathbb{Z})$. The former space is called the *signal space* and the latter the *coefficient space*.

3.5.1 Coefficient Noise and Non-exactness

Suppose $f \in \mathcal{H}$ is a signal of interest with frame representation $Lf \in L(\mathcal{H})$. There are various sources of perturbation which may occur in the coefficient domain. For instance, the representation Lf may be communicated, stored, or retrieved incorrectly. A more direct issue is the representation of the real or complex valued coefficients Lf on a finite precision digital machine. Such a representation requires quantization of the coefficient sequence. Letting $Q : \mathbb{R} \mapsto \{l_1, l_2, \ldots, l_{2^N}\} \subseteq \mathbb{R}$ be quantization by a fixed number N of bits, we have at our disposal not Lf but $Q(Lf)$. Quantization may be viewed as noise in the coefficient domain.

It is natural to investigate the robustness of frame representations with respect to coefficient noise. Clearly, frame representations would be of little use if small perturbations in the coefficient domain destroyed large amounts of information in the signal domain. The following argument, cf., [DGM86] and [Dau92, Section 3.6], asserts that frames which are far from exact, i.e. have a large degree of linear dependence, exhibit robustness to noise in the coefficient domain.

Suppose one has a noise corrupted version $\tilde{c}$ of a signal f, so that

$$\tilde{c} = Lf + d,$$

where d is random noise which may be uniformly distributed. Reconstructing from $\tilde{c}$ entails

$$L^* R^\dagger \tilde{c} = L^* R^{-1} P_{L(\mathcal{H})}(Lf + d_\| + d_\perp) = L^* R^{-1}(Lf + d_\|),$$

where $d = d_\| + d_\perp$ is the orthogonal decomposition of d with respect to L, i.e. $d_\| \in L(\mathcal{H})$ and $d_\perp \in L(\mathcal{H})^\perp$. Thus, all the noise energy outside the range $L(\mathcal{H})$ is automatically nullified in the reconstruction process. For a uniformly distributed perturbation d, the larger the kernel of L^* the more energy in the noise will be nullified and the more noise tolerance will be achieved. Since the kernel of L^* being large is equivalent to the underlying frame having a large degree of linear dependence one may conclude that non-exactness yields robustness to coefficient imprecision.

Tacitly assumed in the above argument is a method for the reconstruction of a signal from its corrupted frame representation. The reconstructed version $f_\dagger$ from a noise perturbed frame representation $\tilde{c} = Lf + d$ is

$$f_\dagger \stackrel{\triangle}{=} L^* R^\dagger \tilde{c}.$$

Note that $\tilde{c}$ need not be in the range $L(\mathcal{H})$. In Section 3.4 an iterative algorithm, Algorithm 3.4.3, was presented for the reconstruction of a signal from its *uncorrupted* frame representation. However, as was shown earlier, this algorithm will not converge for arbitrary initial data, i.e., representations outside the range $L(\mathcal{H})$. Here, a second algorithm is provided which will converge on all of $\ell^2(\mathbb{Z})$. This algorithm is given as Algorithm 3.5.3.

Our approach is to modify Algorithm 3.4.3 so as to alleviate the problem of initialization with a coefficient sequence outside the range of L. As a first step note that $Rc \in L(\mathcal{H})$ for all $c \in \ell^2(\mathbb{Z})$. Thus, if c_0 were initialized to $R\tilde{c}$ then all that would be required is to provide an algorithm for the computation of R^{-2} on $L(\mathcal{H})$ instead of R^{-1} on $L(\mathcal{H})$. Before such an algorithm may be presented, it is necessary first to attend to some technical details.

Lemma 3.5.1 Let $\mathcal{H}_1$ and $\mathcal{H}_2$ be two Hilbert spaces. If $A \in \mathcal{B}(\mathcal{H}_1, \mathcal{H}_2)$ then

$$\|I - A^* A\| < 1 \quad \Longleftrightarrow \quad \forall x \in \mathcal{H}_1, \ 0 < \inf_{\|x\|=1} \|Ax\| \leq \sup_{\|x\|=1} \|Ax\| = \|A\| < \sqrt{2},$$

where I is the identity operator on $\mathcal{H}_1$.

Proof:

Since $I - A^*A$ is self adjoint, by Fact 2.1.3

$$\begin{aligned} \|I - A^*A\| &= \sup_{\|x\|=1} |\langle x, (I - A^*A)x \rangle| \\ &= \sup_{\|x\|=1} |1 - \|Ax\|^2|. \end{aligned}$$

Therefore the condition that $\|I - A^*A\| < 1$ is equivalent to the two conditions

$$\sup_{\|x\|=1} (1 - \|Ax\|^2) = 1 - \inf_{\|x\|=1} \|Ax\|^2 < 1$$

and

$$\sup_{\|x\|=1} (\|Ax\|^2 - 1) = \sup_{\|x\|=1} \|Ax\|^2 - 1 < 1,$$

which further translate to

$$\inf_{\|x\|=1} \|Ax\|^2 > 0 \quad \text{and} \quad \sup_{\|x\|=1} \|Ax\|^2 < 2.$$

■

With the aid of Lemma 3.5.1 it can easily be shown that the operator R^{-2} may be approximated as a Neumann series. To do this it is first shown that for a proper choice of relaxation parameter, e.g., $\lambda = \sqrt{2}/(A + B)$ the operator $I - (\lambda R)^2$ is a contraction on the range $L(\mathcal{H})$. This is the content of Lemma 3.5.2.

Lemma 3.5.2 Let $\{\phi_n\}$ be a frame for $\mathcal{H}$ with frame representation operator L, correlation R and bounds A, B. If $\lambda = \sqrt{2}/(A + B)$ then $\|I - (\lambda R)^2\|_{L(\mathcal{H})} < 1$.

Proof:

Take $A = \lambda R$ and $\mathcal{H}_1 = \mathcal{H}_2 = L(\mathcal{H})$ in Lemma 3.5.1. Then

$$\|A\| = \lambda \|R\| = \frac{\sqrt{2}}{A + B} B < \sqrt{2}$$

and

$$\inf_{c \in L(\mathcal{H}), \|c\|=1} \|\lambda Rc\| > 0$$

since by Proposition 3.3.3e R is 1-1 on $L(\mathcal{H})$ and $\|c\| = 1$. The result follows from application of Lemma 3.5.1.

■

Let $\lambda = \sqrt{2}/(A + B)$. Since $I - (\lambda R)^2$ is a contraction, the Neumann series

$$\lambda^2 \sum_{k=0}^{\infty} (I - (\lambda R)^2)^k$$

will converge to R^{-2} on $L(\mathcal{H})$. Formally, with $\tilde{c}$ an arbitrary element from $\ell^2(\mathbb{Z})$ and $c_0 \overset{\triangle}{=} R\tilde{c}$

$$\lambda^2 \sum_{k=0}^{n}(I - (\lambda R)^2)^k c_0,$$

will converge to $(R^{-2})R\tilde{c}$ since $c_0 \in L(H)$. In fact, it shall be seen that

$$R^\dagger = \lim_{n\to\infty} \lambda^2 \sum_{k=0}^{n}(I - (\lambda R)^2)^k R \qquad (3.5.1)$$

where $R^\dagger$ is the pseudo or *generalized* inverse [Gro77] of R. It is easy to check that as defined in Equation 3.5.1 $R^\dagger$ does indeed satisfy the requirements of Definition 3.3.5.

Algorithm 3.5.3 Let $\{\phi_n\}$ be a frame for a Hilbert space $\mathcal{H}$ with frame representation L, correlation R, and bounds A and B. Suppose $\tilde{c} \in \ell^2(\mathbb{Z})$ is the corrupted frame representation of a signal $f_* \in \mathcal{H}$. Set $c_0 = R\tilde{c}$ and $f_0 = 0$. If $\lambda = \sqrt{2}/(A+B)$ and h_n, c_n and f_n are defined recursively as

$$h_n \overset{\triangle}{=} \lambda^2 L^* c_n,$$
$$c_{n+1} \overset{\triangle}{=} c_n - RL h_n,$$
$$f_{n+1} \overset{\triangle}{=} f_n + h_n,$$

then

a. $\lim f_n = f_\dagger \overset{\triangle}{=} L^* R^\dagger \tilde{c}$ and

b. $\|f_\dagger - f_n\| < M\alpha^n$, where $M < \infty$ and $\alpha \overset{\triangle}{=} \|I - (\lambda R)^2\| < 1$.

Proof:

a. As in Algorithm 3.4.3, an elementary induction argument shows that

$$\forall n, \quad f_{n+1} = \lambda^2 L^* \left(\sum_{j=0}^{n}(I - (\lambda R)^2)^j\right) c_0.$$

Consequently one has

$$\lim f_n = L^* R^\dagger \tilde{c}.$$

b. Write

$$\|f_{n+1} - f_n\| = \|h_n\| = \|\lambda L^*(I - (\lambda R)^2)^n \tilde{c}\| \le \lambda^2 \|L^*\| \left(\|I - (\lambda R)^2\|\right)^n \|R\tilde{c}\| < M'\alpha^n,$$

where $M' = \lambda^2 B^{3/2}\|\tilde{c}\| < \infty$ since $\tilde{c} \in \ell^2(\mathbb{Z})$. Thus,

$$\|f_\dagger - f_n\| \le \sum_{k\ge n} M'\alpha^k = M'\frac{\alpha^n}{1-\alpha} = M\alpha^n.$$

∎

Iterative processes for the construction of generalized inverses have been well investigated, e.g., [Sho67], [Pet67], [Alt60], cf., [Gro77] for a broad overview.

3.5.2 Signal Noise and Frame Coherence

Intuitively, the noise in a signal is that part which lacks structure or coherence. For example, in auditory signals one can readily identify noise with incoherent garbled or hissing sounds. Implied in the use of the term "coherence" is some point of reference with which other points are coherent. It seems reasonable to adopt a (properly chosen) set of primitive functions as such a reference point. In speech, examples of coherent structures are the phonemic primitives which have been learned by the individual; and a pertinent collection of primitive functions may be extracted from the study of the cochlear mechanics of ear [BT92a, BT92b].

Suppose $\{\phi_n\}$ is a collection of appropriate primitive functions. In simple terms, a signal f is coherent with respect to the set $\{\phi_n\}$ if that signal may be approximated well by a linear combination of a relatively small number of members of $\{\phi_n\}$. Mallat [MZ92a] has used a similar notion with respect to arbitrary "dictionaries" of functions. Clearly such a primitive set can not be chosen arbitrarily if it is required that f may be approximated by a linear combination of its members. In addition, for practical implementations it is required that such approximations may be carried out in a numerically stable manner. Both of these requirements are satisfied if the reference set $\{\phi_n\}$ is a frame for a large enough Hilbert space, i.e. one which contains all signals of interest.

For these reasons attention shall be limited to collections $\{\phi_n\}$ which are frames. Consequently, considered as "non-noisy" are those signals which are coherent with respect to the frame $\{\phi_n\}$. This view of coherent signal versus noise admits a relatively simple procedure for the recovery of a signal embedded in noise. This procedure is now outlined.

Let $\mathcal{H} \subseteq L^2(\mathbb{R})$ be a Hilbert space of interest and $\{\phi_n\} \subseteq \mathcal{H}$ be a frame for $\mathcal{H}$ with frame representation operator L. Suppose one has a signal $f_* \in \mathcal{H}$ which is coherent with respect to $\{\phi_n\}$. Let f_w be a noise corrupted version of f_*, where $f_w = f_* + w$ and $w \in L^2(\mathbb{R})$ is non-coherent with respect to $\{\phi_n\}$. Note that f_w is not necessarily contained in $\mathcal{H}$.

From the discussions in Section 3.4 and Section 3.5.1, if $\{\phi_n\}$ were a frame for all of $L^2(\mathbb{R})$ then

$$f_w = L^* R^\dagger L f_w$$

would perfectly recover the noisy signal. Since our main objective is to reject the noisy portion w, this approach is clearly inappropriate without modification. The question naturally arises as to whether there is some processing which may be performed in the coefficient domain $L(\mathcal{H})$ which will act as a noise suppressant in the signal domain $\mathcal{H}$. This, in fact, is the crux of our approach.

Consider a truncation operator $F : L(\mathcal{H}) \mapsto FL(\mathcal{H})$ which nullifies or truncates coefficient sequences in places where the representation Lf_* of f_* has small coefficients (less than a small positive real number δ). That is for any $c \in L(\mathcal{H})$

$$(Fc)_n = \begin{cases} c_n, & |(Lf_*)_n| > \delta \\ 0, & \text{otherwise} \end{cases}$$

Clearly, the operator $F = F_{f_*,\delta}$ depends on the signal f_* and the threshold δ. It is easy to establish that F is a linear bounded operator. In fact $\|F\| = 1$. In Chapter 5 properties of such truncation operators are fully developed.

Now consider a reconstruction procedure which starts not from the whole sequence Lf_w but from the truncated sequence $F_{f_w,\delta} L f_w$. In this case we may define a reconstruction f_δ of the

coherent signal f_* from knowledge of its noise corrupted version f_w as

$$f_\delta \triangleq L^* R^\dagger F_{f_w,\delta} L f_w.$$

Define the δ truncated version of the sequence $L f_w$ as $c_\delta \triangleq F_{f_w,\delta} L f_w$. Expanding f_w and using the linearity of the operators $F_{f_w,\delta}$ and L we have

$$c_\delta = F_{f_w,\delta} L(f_* + w) = F_{f_w,\delta} L f_* + F_{f_w,\delta} L w.$$

The hope of this scheme for noise suppression lies in the expectations that

a. for a coherent signal f_* the truncation $F_{f_w,\delta} L f_* \approx L f_*$, and

b. for a non-coherent signal w the truncation $F_{f_w,\delta} L w \approx 0$.

Consequently we expect that $c_\delta \approx L f_*$. In this case we may view c_δ as a noisy version of $L f$ and use Algorithm 3.5.3 with initial data $c_0 = c_\delta$ to perform the noise suppression.

Let us look more deeply into the question of why this thresholding procedure should be expected to perform noise suppression. If $\{\phi_n\}$ is a frame for $\mathcal{H}$ with frame representation operator L then there is the following norm equivalence property. Namely, there are positive scalars A and B such that

$$\forall f \in \mathcal{H}, \quad A\|f\|^2 \leq \|Lf\|^2 \leq B\|f\|^2.$$

We may interpret such a relationship as an approximate energy preservation between the domains $\mathcal{H}$ and $L(\mathcal{H})$. Thus, for all signals $f \in \mathcal{H}$, the representation $L f$ must have approximately the same energy as the original signal; however, the distribution of the energy among the coefficients in $L f$ is dependent on the signal's degree of coherence with the underlying frame $\{\phi_n\}$. In fact, for a signal f_* which is coherent with respect to the frame $\{\phi_n\}$, i.e., one which is represented by a linear combination of a relatively few members, the frame representation norm equivalence necessarily implies that these few coefficients must contain most of the signal energy and hence have a relatively large magnitude. Similarly, a pure noise signal w, being incoherent with respect to the set $\{\phi_n\}$, must have a frame representation in which the noise energy is spread out over a very large numer of coefficients. Hence, these coefficients must have a relatively small magnitude. In light of this, if we now consider the noise corrupted signal $f_w = f_* + w$, for an appropriate value of the threshold δ the small coefficients in $L f_w$ due to the non-coherent portion w will be suppressed while the larger coefficients due to the coherent portion f_w will be preserved under truncation. Thus, the iterative Algorithm 3.5.3 initialized with $c_0 = F_{f_w,\delta} L f_w$ is in fact a technique for the suppression of noise.

Note that these arguments depend strongly on the notion of coherence, and more specificly coherence with respect to a particular frame. It should be clear that given a particular application appropriate frames must be chosen. For example, in the context of music processing there is a natural coherence with respect to the notion of time frequency evolution. A natural description of a piece of music involves the idea of frequencies moving in time. If our objective is to remove noise from music, or audible signals in general, then it seems reasonable to ask for frames which are well localized in both time and frequency. This naturally leads to incorporation of wavelet or Gabor frames as the reference for coherence.

Truncations of this form are one of the motivating factors spawning the notion of a "local" frame. Roughly speaking a local frame for a Hilbert space $\mathcal{H}$ is a frame for a much smaller

space $\mathcal{H}(f_*)$ in $\mathcal{H}$ generated by a specific signal $f_* \in \mathcal{H}$. It is also required that f_* be contained (almost) in $\mathcal{H}(f_*)$. Local frames are the subject of Chapter 5. We note that numerical examples of the performance of the noise suppression abilities of such a scheme are presented in Section 6.3.1.

3.6 Numerical Verification

In this chapter two algorithms have been presented for the recovery of a signal from its frame representation. It has been established that Algorithm 3.4.3 will converge to the original signal provided that it is initialized with a valid frame representation, i.e. a coefficient sequence entirely in the range of the frame representation operator L. If, however, the frame representation is perturbed so that it is no longer in the range of L then this algorithm will not converge. This situation spawned the development of a second algorithm which would contend with perturbations in the frames representation which fall outside the range of the operator L. It has been established that Algorithm 3.5.3 will always converge to a best approximation to the signal given its perturbed frame representation.

To illustrate the situation we perform the following experiment. We generate two frames Φ_1 and Φ_2 such that Φ_1 has no redundancy and that Φ_2 has a bit of redundancy. More precisely we construct a non-redundant frame $\Phi_1 = \left\{\phi_n^{(1)}\right\}_{n=1}^{20}$ for its span $\{\Phi_1\} \subseteq \mathbb{R}^{20}$ and a redundant frame $\Phi_2 = \left\{\phi_n^{(2)}\right\}_{n=1}^{20}$ for its span $\{\Phi_2\} \subseteq \mathbb{R}^{20}$ such that

- both Φ_1 and Φ_2 have the same frame bounds $(A, B) = (0.5, 1.5)$, and

- $\dim \ker R_1 = 20$ and $\dim \ker R_2 = 19$.

where R_1 and R_2 are the frame correlations of Φ_1 and Φ_2 respectively. Thus, there is no redundancy associated with the frame Φ_1 while there is one degree of redundancy associated with the frame Φ_2.

Let L_1 and L_2 be the respective frame representations associated with Φ_1 and Φ_2. Next we choose a $c_0 \in \mathbb{R}^{20}$ as

$$c_0 = (111\ldots1).$$

Thus c_0 is contained in $L_1(\mathcal{H})$ but c_0 is not contained in $L_2(\mathcal{H})$.

The results of initializing both Algorithm 3.4.3 and Algorithm 3.5.3 with c_0 is displayed in the figures. In Figure 3.2 the top graph displays the norm of the sequence $\{c_n\}$ as a function of the iteration number when Algorithm 3.4.3 is initialized with c_0 for the frame Φ_1. The bottom graph displays the norm of the sequence $\{c_n\}$ as a function of the iteration number when Algorithm 3.5.3 is initialized with c_0 for the frame Φ_1.

In Figure 3.3 the top graph displays the norm of the sequence $\{c_n\}$ as a function of the iteration number when Algorithm 3.4.3 is initialized with c_0 for the frame Φ_2. The bottom graph displays the norm of the sequence $\{c_n\}$ as a function of the iteration number when Algorithm 3.5.3 is initialized with c_0 for the frame Φ_2.

Recall that in each algorithm a sequence $\{f_n\}$ is generated which is given by

$$f_n = L^* \sum_{k=0}^{n} c_n.$$

$\|c_n\|$, wh/ c_1 = c, c (n+1) = (I-lambda1 R)c_n
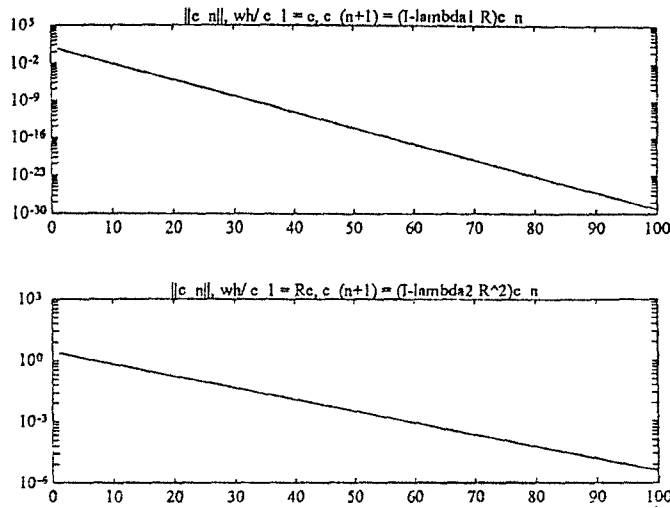
$\|c_n\|$, wh/ c_1 = Rc, c (n+1) = (I-lambda2 R^2)c_n

Figure 3.2: Comparison of the $\{\|c_n\|\}$ for the case of the non-redundant frame Φ_1.

Thus for convergence we must have $c_n \to 0$. In the figures we have plotted $\|c_n\|$ as a function of the iteration number. Since the vertical axis on the graph is logarithmic a negatively sloped line indicates an exponential rate of decay.

For the frame Φ_1 we can see from Figure 3.2 that both algorithms exhibit the predicted rate of exponential decay for $\{\|c_n\|\}$. Both algorithms are expected to converge because c_0 is in the range of L_1. For the frame Φ_2, however, c_0 is not in the range of L_2 and as a result it is expected that Algorithm 3.4.3 will not converge. These expectations are confirmed in Figure 3.3. Figure 3.3 clearly shows the following:

$\|c_n\|$, wh/ c_1 = c, c (n+1) = (I-lambda1 R)c_n

$\|c_n\|$, wh/ c_1 = Rc, c (n+1) = (I-lambda2 R^2)c_n
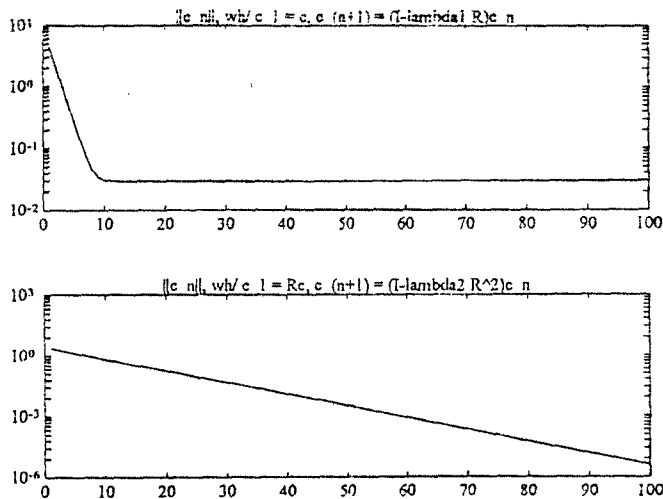
Figure 3.3: Comparison of the $\{\|c_n\|\}$ for the case of the redundant frame Φ_2.

a. Algorithm 3.5.3 convergence properties are identical to non redundant case, while

b. Algorithm 3.4.3 fails to converge since $\|c_n\|$ approaches a constant.

Thus, the experiment confirms the predictions of the theory.

Chapter 4

Sampling in RKHS

With the material of the previous chapter as motivation, a generic discrete represenation of analog signals is developed and relations are made to frames and irregular sampling in certain reproducing kernel Hilbert spaces. The discrete representations studied here come from samples of group representation transforms on lattices contained in appropriate groups. These representations are quite general and rely on a familiarity with the material in Section 2.3. In the last sections of this chapter three special cases of discrete representations are studied in detail. Respectively, these three special cases result in the study of Paley-Wiener frames, Gabor frames, and wavelet frames.

4.1   The Generic Representation

Let $\mathcal{H}$ be a Hilbert space contained in $L^2(\mathbb{R})$ and let $\mathcal{G}$ be a group with representation Π on $\mathcal{H}$. Suppose g is an admissible function, i.e. $g \in \mathcal{A}_{\Pi,\mu}(\mathcal{H})$ where μ is the left Haar measure. The generic discrete representation of a signal $f \in \mathcal{H}$ (in general) is an irregular sampling over the group $\mathcal{G}$ of its group representation transform $V_g f \in L^2_\mu(\mathcal{G})$. Recall that the group representation transform V_g is a mapping $V_g : \mathcal{H} \mapsto L^2_\mu(\mathcal{G})$ given by (2.4.1) redisplayed here for convenience

$$(V_g f)(x) = \langle f, \Pi(x)g \rangle .$$

For a generic discrete representation the sampling set Γ is some countable irregular set of points from the group $\mathcal{G}$

$$\Gamma = \{x_n\} \subseteq \mathcal{G}. \tag{4.1.1}$$

Thus, Γ is a discrete lattice contained in the group $\mathcal{G}$. The corresponding lattice-value pair $\Lambda(f)$ is

$$\Lambda(f) = (\Gamma, \{V_g f(x)\}_{x \in \Gamma}). \tag{4.1.2}$$

$\Lambda(f)$ is a lattice in $\mathcal{G}$ together with the group representation transform of f evaluated at all the points on that lattice. The fundamental concern of discretization theory is the following question:

What conditions on the sampling set Γ allow the recovery of f from $\Lambda(f)$?

As we shall see this question is related to the frame properties of the collection

$$\{\Pi(x)g\}_{x\in\Gamma}\,. \tag{4.1.3}$$

4.1.1 Frames and Sampling in $V_g(\mathcal{H})$

In Chapter 3 it was seen that collections of elements from a Hilbert space which are frames have associated discrete representations characterized by a topological isomorphism L on a closed subspace of $\ell^2(\mathbb{Z})$. As a result there are numerically stable iterative algorithms for the reconstruction of signals starting from their frame representations.

An underlying theme in sampling theory is the connection between boundedness, reproducing kernels, and sampling expansions. In Section 2.2 it is shown that, via the Riesz representation theorem, the condition that all members of a functional Hilbert space satisfy a pointwise bound implies a reproducing kernel for that space. Thus, loosely speaking we may say that boundedness leads to reproducing kernels. In Section 2.4 such a pointwise bound is easily established (via Cauchy-Shwarz) for members of $V_g(\mathcal{H})$. The reproducing kernel for $V_g(\mathcal{H})$ is given explicitly in 2.4.4 as

$$K = c_g(V_g g),$$

where c_g is some constant. The accompanying reproducing formula is

$$\forall F \in V_g(\mathcal{H}), \quad F(x) = (F * K)(x) = \langle F, T_x K\rangle_{L^2_\mu(\mathcal{G})}$$

for all $x \in \mathcal{G}$. From this we may conclude that knowledge of the samples $\{F(x_n)\}$ of a function $F \in V_g(\mathcal{H})$ is equivalent to knowledge of the inner products $\left\{\langle F, T_{x_n}K\rangle_{L^2_\mu(\mathcal{G})}\right\}$.

In the spirit of Chapter 3 this observation leads us to consider discretizations $\mathcal{L} : V_g(\mathcal{H}) \mapsto \ell^2(\mathbb{Z})$ defined as

$$\mathcal{L}F = \left\{\langle F, T_{x_n}K\rangle_{L^2_\mu(\mathcal{G})}\right\} = \{F(x_n)\}$$

with the adjoint $\mathcal{L}^* : \ell^2(\mathbb{Z}) \mapsto V_g(\mathcal{H})$

$$\mathcal{L}^* c = \sum c_n T_{x_n} K,$$

where $F \in V_g(\mathcal{H})$ and $c = \{c_n\} \in \ell^2(\mathbb{Z})$. Recall that for a fixed $x_0 \in \mathcal{G}$ the x_0-translation $T_{x_0}F$ of a function $F \in L^2_\mu(\mathcal{G})$ is $T_{x_0}F(x) = F(x_0^{-1}x)$. Because $\mathcal{L}F$ consists of irregular samples of F, this discretization allows us to develop expansions which recover F from its irregular samples in $\mathcal{G}$ provided the collection

$$\{T_{x_n}K\}$$

is a frame for a large enough subspace of $V_g(\mathcal{H})$. For example, if $\{T_{x_n}K\}$ were a frame for $V_g(\mathcal{H})$ then any $F \in V_g(\mathcal{H})$ could be reconstructed, viz. (3.4.7), from $\mathcal{L}F$ as

$$F = \mathcal{L}^*\mathcal{R}^\dagger(\mathcal{L}F),$$

where $\mathcal{R} = \mathcal{L}\mathcal{L}^*$ is the frame correlation. Since $\mathcal{L}F = \{F(x_n)\}$ this is a sampling expansion for reconstructing a function F which is an element of the reproducing kernel Hilbert space $V_g(\mathcal{H})$ from its sample values. Together with the previous boundedness arguments, this observation justifies the statement that boundedness implies RKHS implies sampling expansions.

Our main interest is, however, not to reconstruct group representation transforms from their irregular samples. Our main interest is, rather, to develop discrete representations of signals from $\mathcal{H}$ with associated reconstruction algorithms. It turns out that irregular samples of group representation transforms are in fact exactly the type of discrete representation which we seek. The two are essentially related by the group representation transform and its "inverse". To make this notion of inverse precise Proposition 4.1.1 identifies the proper spaces in which the group representation transform has an inverse.

Proposition 4.1.1 The group representation transform V_g has a well defined inverse when restricted to a subspace $\mathcal{H}_V \overset{\triangle}{=}$ span $\{\Pi(x)g\}_{x \in \mathcal{G}}$ mapping onto its closed range $V_g(\mathcal{H}_V) = V_g(L^2(\mathbb{R}))$.

Proof:

Clearly V_g maps onto its range. We show that $V_g : \mathcal{H}_V \mapsto V_g(\mathcal{H}_V)$ is one to one. Let $f_1, f_2 \in \mathcal{H}_V$ and suppose $V_g f_1 = V_g f_2$. This means that for all $x \in \mathcal{G}$

$$\langle f_1, \Pi(x)g \rangle = \langle f_2, \Pi(x)g \rangle$$

or

$$\langle f_1 - f_2, \Pi(x)g \rangle = 0.$$

From this we may conclude that $(f_1 - f_2) \perp \mathcal{H}_V$. Since $\mathcal{H}_V$ is a linear subspace $(f_1 - f_2) \in \mathcal{H}_V$. Thus, $f_1 - f_2$ must be zero. We have shown that $V_g : \mathcal{H}_V \mapsto V_g(\mathcal{H}_V)$ is bijective and therefore has a well defined inverse $V_g^{-1} : V_g(\mathcal{H}_V) \mapsto \mathcal{H}_V$.

∎

In specific cases, e.g. wavelet and Gabor, it can be shown by approximate identity arguments [HW89] that the group representation transform V_g has a well defined inverse on its range. In fact, if $f \in \mathcal{H}_V$ we may formally write

$$f = \frac{1}{c_g^2} \left\langle (V_g f)(x), \overline{\Pi(x)g} \right\rangle_{L^2_\mu(\mathcal{G})}$$

in L^2. Figure 4 depicts the group representation transform mapping V_g and its properties on different domains and ranges of interest.

In light of Proposition 4.1.1 and the operator $\mathcal{L}^*$ it is clear that only functions which are contained in $\mathcal{H}_V$ have any hope of being represented by linear combinations of $\{\pi(x_n)g\}$. Thus, we require that $\mathcal{H} \subseteq \mathcal{H}_V$.

To make the connection between irregular sampling in $V_g(\mathcal{H})$ and discrete representation in $\mathcal{H}$ fix $x_0 \in \mathcal{G}$ and consider the function $\Pi(x_0)g \in \mathcal{H}$. Since $\Pi(x_0)g$ is an element in $\mathcal{H}$ we may compute its group representation transform as

$$
\begin{aligned}
(V_g \Pi(x_0)g)(x) &= \langle \Pi(x_0)g, \Pi(x)g \rangle \\
&= \left\langle g, \Pi(x_0^{-1})\Pi(x)g \right\rangle \\
&= \left\langle g, \Pi(x_0^{-1}x)g \right\rangle \\
&= (V_g g)(x_0^{-1}x) = T_{x_0} V_g g(x) = c_g^2 T_{x_0} K(x).
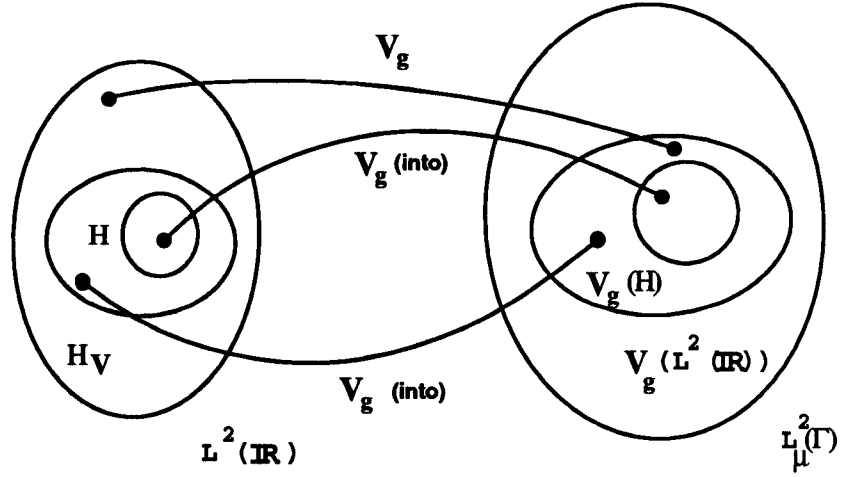\end{aligned}
$$

Figure 4.1: The group representation transform V_g on different domains.

From this calculation it follows that for fixed a $x \in \mathcal{G}$ the functions $\Pi(x)g$ and $c_g^2 \, T_x K$ are group representation transform pairs. This relationship is denoted as

$$\forall x \in \mathcal{G}, \quad \Pi(x)g \; \overset{V_g}{\longleftrightarrow} \; c_g^2 \, T_x K.$$

The sampling operator $\mathcal{L}$ whose domain is $V_g(\mathcal{H})$ has an associated discretization operator L whose domain is $\mathcal{H}$. Let $F = V_g f$. Then by the reproducing property and Corollary 2.4.2

$$F(x_n) = \langle F, T_{x_n} K \rangle_{L^2_\mu(\mathcal{G})} = \langle f, \Pi(x_n)g \rangle .$$

This suggests the discretization $L : \mathcal{H} \mapsto \ell^2 \, (\mathbb{Z})$ defined as

$$Lf = \{F(x_n)\}$$

with the adjoint

$$L^* c = \sum c_n \Pi(x_n)g.$$

Thus, questions about the frame properties of the sequence $\{T_{x_n} K\}$ in $L^2_\mu(\mathcal{G})$ may be translated to questions about the frame properties of the sequence $\{\Pi(x_n)g\}$ in $\mathcal{H}$.

At this point it may prove fruitful to present an example. Lets take g as the Dirichlet kernel $g = d_{2\pi\Omega}$ and $\mathcal{G} = (\mathbb{R}, +)$ having the group representation τ_x. With these choices we shall see that the situation reduces to the case of sampling in the bandlimited space PW_Ω. The group representation transform associated with these choices of g and $\mathcal{G}$ is

$$V_g f = \langle f, \Pi(x_n)g \rangle = \langle f, \tau_{x_n} d_{2\pi\Omega} \rangle = P_\Omega f,$$

where P_Ω is the orthogonal projection operator onto PW_Ω. Thus, V_g maps $L^2(\mathbb{R})$ onto PW_Ω. Now $\mathcal{H}_V = \text{span}\,\{\Pi(x)g\} = \text{span}\,\{\tau_x d_{2\pi\Omega}\} = PW_\Omega$. Thus, $V_g = P_\Omega$ trivially has a well defined inverse when considered as a map $V_g : \mathcal{H}_V \mapsto V_g(\mathcal{H}_V)$, i.e. $P_\Omega : PW_\Omega \mapsto PW_\Omega$, since it is the identity on PW_Ω. It is then evident that the discretization $L = \mathcal{L}$ is

$$Lf = \{\langle f, \tau_{x_n} d_{2\pi\Omega} \rangle\} = \{(P_\Omega f)(x_n)\}$$

Object	Group Transform Range	Group Transform Domain
Space	$V_g(\mathcal{H}_V) = \text{span}\,\{T_x K\}$	$\mathcal{H}_V = \text{span}\,\{\Pi(x)g\}$
Kernel	K	g
Translation	T_x	τ_x
Group/Representation	$(\mathcal{G}, \cdot),\ \Pi(x)$	$(\mathbb{R}, +),\ \tau_t$
Atoms	$\{T_{x_n} K\}$	$\{\pi(x_n)g\}$
Discretization	$\mathcal{L}F = \{F * K(x_n)\}$	$Lf = \{\langle f, \Pi(x_n)g\rangle\}$
Adjoint	$\mathcal{L}^* c = \sum c_n T_{x_n} K$	$L^* c = \sum c_n \pi(x_n)g$

Table 4.1: Group representation transform relations in the generic case.

with the adjoint

$$L^* c = \sum c_n \tau_{x_n} d_{2\pi\Omega}.$$

Thus, with these choices of g and $\mathcal{G}$ it is clear that it is only possible to reconstruct signals from their samples $\{f(x_n)\}$ if they are members of $\mathcal{H}_V = PW_\Omega$.

Object	Group Transform Range	Group Transform Domain
Space	$V_g(\mathcal{H}_V) = PW_\Omega$	$\mathcal{H}_V = PW_\Omega$
Kernel	$d_{2\pi\Omega}$	$d_{2\pi\Omega}$
Translation	τ_x	τ_x
Group/Representation	$(\mathbb{R}, +),\ \tau_t$	$(\mathbb{R}, +),\ \tau_t$
Atoms	$\{\tau_{x_n} d_{2\pi\Omega}\}$	$\{\tau_{x_n} d_{2\pi\Omega}\}$
Discretization	$\mathcal{L}f = \{P_\Omega f(x_n)\}$	$Lf = \{P_\Omega f(x_n)\}$
Adjoint	$\mathcal{L}^* c = \sum c_n \tau_{x_n} d_{2\pi\Omega}$	$L^* c = \sum c_n \tau_{x_n} d_{2\pi\Omega}$

Table 4.2: Group representation transform relations for the case $g = d_{2\pi\Omega}$ and $\mathcal{G} = (\mathbb{R}, +)$. The situation reduces to sampling in PW_Ω.

Similar tables may be constructed for the wavelet and Gabor cases where $\mathcal{G}$ is the affine group $\mathcal{G}_A$ in the wavelet case and $\mathcal{G}$ is the Heisenberg group $\mathcal{G}_H$ in the Gabor case. Since g may be taken as any admissible function (almost arbitrary) there are many such tables that may be generated. For the cases of the wavelet and Gabor transforms we shall refer to the generic Table 4.1. In the last sections of this chapter we will look in detail at three specific cases: Paley-Wiener, wavelet, and Gabor.

4.1.2 Weighted Frames

Let $\{w_n\} \subseteq \mathbb{R}^+$ be a sequence of strictly positive weights. In this section we derive operator theoretic characterizations for weighted sets

$$\{w_n \Pi(x_n)g\}$$

to form frames for $\mathcal{H}_V = \text{span}\,\{\Pi(x)g\}$. In other words, we are interested in sufficient conditions on a set $\Gamma = \{x_n\} \subseteq \mathcal{G}$ which insure that the set of functions $\{w_n \Pi(x_n)g\}$ is a frame for the

space $\mathcal{H}_V$. Recall that the measure of a set $E \subseteq \mathcal{G}$ is

$$\mu(E) = \int_E d\mu(x). \tag{4.1.4}$$

Let $\{V_n\} \subseteq \mathcal{G}$ denote a set of mutually disjoint connected regions from $\mathcal{G}$, corresponding to a set of sampling points $\{x_n : x_n \in V_n\}$. It is also required that the regions $\{V_n\}$ cover all of $\mathcal{G}$, i.e.

$$\overline{\bigcup V_n} = \mathcal{G}.$$

The sampling set $\{x_n\}$ is *regular* if there exists such a sequence of mutually disjoint connected regions from $\mathcal{G}$ and some compact set $V \subseteq \mathcal{G}$ such that

$$\forall n, \quad x_n^{-1} V_n = V.$$

For general irregular sampling sets it is required that there is a compact set $V \subseteq \mathcal{G}$ such that

$$\bigcup x_n^{-1} V_n = V.$$

In addition, to each region V_n we associate the characteristic $\chi_n \overset{\triangle}{=} 1(V_n)$ defined as the indicator function of the set V_n. Thus the set of functions $\{\chi_n\}$ forms an orthogonal partition of $L_\mu^2(\mathcal{G})$. We will call such $\{V_n\}$ a disjoint covering of $\mathcal{G}$ and such $\{x_n\}$ an *admissible sampling*.

Let $\mathcal{H}_V = \text{span}\{\Pi(x)g\} \subseteq L_\mu^2(\mathcal{G})$ where μ is the left Haar measure. Recall that $V_g(\mathcal{H}_V)$ is a reproducing kernel Hilbert space with kernel K, i.e.

$$\forall F \in \mathcal{H}, \quad F = F * K = \langle F, T_x K \rangle_{L_\mu^2(\mathcal{G})}.$$

Here, T_x is the translation operator in $\mathcal{G}$ and for convenience define $K_x \overset{\triangle}{=} T_x K$. The inner product for $V_g(\mathcal{H}_V)$ is inherited from $L_\mu^2(\mathcal{G})$.

Now, define the piecewise approximation operator $P : V_g(\mathcal{H}_V) \mapsto L^2(\mathcal{G})$ as

$$PF \overset{\triangle}{=} \sum \langle F, K_{x_n} \rangle_{L_\mu^2(\mathcal{G})} \chi_n \tag{4.1.5}$$

which depends on $\{x_n\}$. Note that its adjoint, $P^* : L^2(\mathcal{G}) \mapsto V_g(\mathcal{H}_V)$ is

$$P^* F \overset{\triangle}{=} \sum \langle F, \chi_n \rangle_{L_\mu^2(\mathcal{G})} K_{x_n}, \tag{4.1.6}$$

and of particular interest is the fact that

$$\forall F \in V_g(\mathcal{H}_V), \quad P^* P F = \sum \langle F, K_{x_n} \rangle_{L_\mu^2(\mathcal{G})} \|\chi_n\|^2_{L_\mu^2(\mathcal{G})} K_{x_n}. \tag{4.1.7}$$

From this calculation it can be seen that $P^* P$ is the frame operator S_w for the weighted collection $\{\mu(V_n) K_{x_n}\}$. This fact leads directly to Theorem 4.1.2.

Theorem 4.1.2 Let $V_g(\mathcal{H}_V)$ be a RKHS with reproducing kernel K. Let $\{x_n\} \subseteq \mathcal{G}$ be an admissible sampling. Then set $\{\mu(V_n) K_{x_n}\}$ is a frame for $V_g(\mathcal{H}_V)$ if and only if there exists constants $A > 0$ and $B < \infty$ such that

$$\forall F \in V_g(\mathcal{H}_V), \quad A\|F\|^2_{L_\mu^2(\mathcal{G})} < \|PF\|^2_{L_\mu^2(\mathcal{G})} < B\|F\|^2_{L_\mu^2(\mathcal{G})},$$

where $PF = \sum F(x_n) 1_{V_n}$.

Proof:

From (4.1.7) we have

$$\|PF\|^2_{L^2_\mu(\mathcal{G})} = \langle PF, PF \rangle_{L^2_\mu(\mathcal{G})} = \langle F, P^*PF \rangle_{L^2_\mu(\mathcal{G})} = \langle F, S_w F \rangle_{L^2_\mu(\mathcal{G})}.$$

∎

Corollary 4.1.3 With the hypotheses of Theorem 4.1.2 in place if

$$d \overset{\triangle}{=} \|I - P\|_{L^2_\mu(\mathcal{G})} < 1$$

then $\{\mu(V_n)K_{x_n}\}$ is a frame for $V_g(\mathcal{H}_V)$ with frame bounds $(1-d)^2$ and $(1+d)^2$.

Proof: For any $F \in V_g(\mathcal{H}_V)$ write

$$\left| \ \|F\|_{L^2_\mu(\mathcal{G})} - \|PF\|_{L^2_\mu(\mathcal{G})} \ \right|^2 \leq \|F - PF\|^2_{L^2_\mu(\mathcal{G})} \leq \|I - P\|^2_{L^2_\mu(\mathcal{G})}\|F\|^2_{L^2_\mu(\mathcal{G})} = d^2\|F\|^2_{L^2_\mu(\mathcal{G})}$$

so that

$$\forall F \in V_g(\mathcal{H}_V), \quad \left| \ \|F\|_{L^2_\mu(\mathcal{G})} - \|PF\|_{L^2_\mu(\mathcal{G})} \ \right| \leq d\|F\|_{L^2_\mu(\mathcal{G})}$$

leading to

$$\forall F \in V_g(\mathcal{H}_V), \quad (1-d)\|F\|_{L^2_\mu(\mathcal{G})} \leq \|PF\|_{L^2_\mu(\mathcal{G})} \leq (1+d)\|F\|_{L^2_\mu(\mathcal{G})},$$

and the result follows by invoking Theorem 4.1.2. ∎

The analog of Corollary 4.1.3 in the domain $\mathcal{H}_V$ is given below.

Corollary 4.1.4 With the hypotheses of Theorem 4.1.2 in place if $d \overset{\triangle}{=} \|I - P\|_{L^2_\mu(\mathcal{G})} < 1$ then $\{\mu(V_n)\Pi(x_n)g\}$ is a frame for $\mathcal{H}_V$ with frame bounds $(1-d)^2$ and $(1+d)^2$.

The following theorem is a slight generalization of the material appearing in [OS92].

Theorem 4.1.5 Let $\{V_n\}$ be a disjoint covering of the group $\mathcal{G}$ generated by the sampling set $\{x_n\} \subseteq \mathcal{G}$, and $V \overset{\triangle}{=} \bigcup x_n^{-1}V_n$. Let $V_g(\mathcal{H}_V) \subseteq L^2_\mu(\mathcal{G})$ be a RKHS having reproducing kernel K (μ is the left Haar measure). Define the quantities

$$d_1^2 \overset{\triangle}{=} sup_{x \in V} \int_{\mathcal{G}} |K_x - K| \, d\mu$$

$$d_2^2 \overset{\triangle}{=} sup_{\sigma \in \mathcal{G}} \sum_n \int_{V_n} |K_x(\sigma) - K_{x_n}(\sigma)| \, d\mu(x).$$

If $d_1 d_2 < 1$ then $\{\mu(V_n)\Pi(x_n)g\}$ is a frame for $\mathcal{H}_V$.

53

Proof:

With P as in 4.1.5, write

$$
\begin{aligned}
\|(I-P)F\|^2_{L^2_\mu(\mathcal{G})} &= \|F - \sum F(x_n)\chi_n\|^2_{L^2_\mu(\mathcal{G})} \\
&= \|\sum (F - F(x_n))\chi_n\|^2_{L^2_\mu(\mathcal{G})} \\
&= \int_{\mathcal{G}} \left|\sum (F(x) - F(x_n))\chi_n(x)\right|^2 d\mu(x) \\
&= \int_{\mathcal{G}} \left|\sum \langle F, K_x - K_{x_n}\rangle \chi_n(x)\right|^2 d\mu(x) \\
&= \int_{\mathcal{G}} \sum |\langle F, K_x - K_{x_n}\rangle|^2 \chi_n(x)\, d\mu(x),
\end{aligned}
$$

where the last step follows since χ_n may take only the values 1 or 0. Noting

$$
\langle F, K_x - K_{x_n}\rangle_{L^2_\mu(\mathcal{G})} \le \left\langle F|K_x - K_{x_n}|^{\frac{1}{2}}, |K_x - K_{x_n}|^{\frac{1}{2}}\right\rangle_{L^2_\mu(\mathcal{G})}
$$

and using Cauchy-Shwarz we further obtain

$$
\begin{aligned}
&\|(I-P)F\|^2_{L^2_\mu(\mathcal{G})} \\
&\le \int_{\mathcal{G}} \sum_n \| F|K_x - K_{x_n}|^{\frac{1}{2}}\|^2_{L^2_\mu(\mathcal{G})}\chi_n(x))\| |K_x - K_{x_n}|^{\frac{1}{2}}\|^2_{L^2_\mu(\mathcal{G})} d\mu(x) \\
&\le \int_{\mathcal{G}} \sum_n \left(\sup_{z\in\mathcal{G}} |K_z - K_{x_n}|\right) \|F\|^2_{L^2_\mu(\mathcal{G})} \left(\int_{\mathcal{G}} |K_x - K_{x_n}| d\mu\right) \chi_n(x) d\mu(x) \\
&= \sum_n \int_{V_n} \left(\sup_{z\in\mathcal{G}} |K_z - K_{x_n}|\right) \left(\int_{\mathcal{G}} |K_x - K_{x_n}| d\mu\right) d\mu(x) \|F\|^2_{L^2_\mu(\mathcal{G})} \\
&\le \sum_n \left(\sup_{x\in V_n} \int_{\mathcal{G}} |K_x - K_{x_n}| d\mu\right) \int_{V_n}\left(\sup_{z\in\mathcal{G}} |K_z - K_{x_n}|\right) d\mu(x) \|F\|^2_{L^2_\mu(\mathcal{G})}.
\end{aligned}
$$

In order to remove the dependence on n of the first product term in the sum we make the following estimate:

$$
\begin{aligned}
\sup_{z\in V_n}\left(\int_{\mathcal{G}} |K_z - K_{x_n}| d\mu\right) &= \sup_{z\in V_n}\left(\int_{\mathcal{G}} |T_z K - T_{x_n} K| d\mu\right) \\
&= \sup_{z\in V_n}\left(\int_{\mathcal{G}} |T_{x_n^{-1}z} K - K| d\mu\right) \\
&= \sup_{z\in x_n^{-1}V_n}\left(\int_{\mathcal{G}} |T_z K - K| d\mu\right) \\
&\le \sup_{z\in V}\left(\int_{\mathcal{G}} |T_z K - K|\right) d\mu,
\end{aligned}
$$

since $\forall n,\ x_n^{-1}V_n \subset V$. Which leads us to

$$
\begin{aligned}
\|(I-P)F\|^2_{L^2_\mu(\mathcal{G})} &\le \left[\sup_{x\in V}\left(\int_{\mathcal{G}} |K_x - K|\right) d\mu\right]\left[\sup \sum_n \int_{V_n} (|K_x - K_{x_n}|) d\mu(x)\right] \|f\|^2 \\
&= d_2^2 d_1^2 \|f\|^2.
\end{aligned}
$$

Invoking Corollary 4.1.4 we are done. ∎

54

Remark 4.1.6 As pointed out in [OS92] for the case of the discrete wavelet transform these estimates are not particularly good.

Suppose $\mathcal{H} = PW_\Omega$, which is a RKHS with reproducing kernel

$$K_x = \tau_x d_{2\pi\Omega}$$

and reproducing formula

$$\forall f \in PW_\Omega, \quad f(x) = \langle f, \tau_x d_{2\pi\Omega} \rangle .$$

Thus, PW_Ω is an example of a space which fits the hypotheses of all the above mentioned theorems. We could, in fact, invoke Theorem 4.1.5 and get (lousy) estimates for the frame bounds. Alternatively, though, we may use Corollary 4.1.4 directly along with a result of Gröchenig to conclude that the weighted set $\{w_n \, \tau_{t_n} d_{2\pi\Omega}\}$ is a frame for PW_Ω with the following estimates for the bounds.

From [Grö91] we have that with $\{t_n\}$ a sampling sequence such that $2T\Omega < 1$ and $T \overset{\triangle}{=} \sup |t_{i+1} - t_i|$ then

$$\|I - P\| \leq 2T\Omega \quad \text{on} \quad PW_\Omega$$

where P is the operator defined in 4.1.5 and the partition $\{V_n\}$ is the set of intervals having the midpoints $(t_{i+1} + t_i)/2$ as their end points and w_n as their length. Invoking Corollary 4.1.4 we obtain the result that the set

$$\{w_n \, \tau_{t_n} d_{2\pi\Omega}\}$$

is a frame for PW_Ω with frame bounds $(1 - 2T\Omega)^2$ and $(1 + 2T\Omega)^2$, or equivalently in the frequency domain the set

$$\{w_n \, e_{-t_n}\}$$

is a frame for $L^2[-\Omega, \Omega]$ with the same bounds $(1 - 2T\Omega)^2$ and $(1 + 2T\Omega)^2$.

4.2 Examples

As has been seen, the discrete representation of signals as irregular samples of their group representation transforms is a complete characterization provided certain countable sets of functions constitute frames for large enough spaces. Owing to the generality of the underlying square integrable group representations, the flexibility of this approach to signal representation is tremendous. This is manifested in the large number of free parameters in the representation. Each choice of group, group representation, analyzing function g, and discrete lattice leads to a discrete representation. Roughly speaking there are as many different discrete representations as there are groups, group representations, discrete lattices and functions g.

In this thesis we shall restrict ourselves to three classes of discrete representation. These classes correspond to the specific group representation transforms of (i) bandlimiting, (ii) Gabor

transform, and (iii) wavelet transform. Each of these classes is defined by specification of the group and the group representation, i.e. the pair $\{\mathcal{G}, \Pi\}$. Thus, within each class there is still considerable freedom, e.g. the choice of analyzing function g and the choice of discrete lattice Γ. For complete characterizations these choices can not, of course, be made arbitrarily. As discussed in previous sections, the frame properties of collections

$$\{\Pi(x)g\}_{x \in \Gamma}$$

are directly relevant. If this set were a frame then the group representation transform $V_g f$ of a signal f evaluated at points on the lattice Γ would be a complete characterization of f, viz. Chapter 3.

The corresponding group/group representation pair for the three special cases are

(i) bandlimiting: $\{(\mathbb{R}, +), \tau_t\}$,

(ii) Gabor transform: $\{\mathcal{G}_H, e_\gamma \tau_t\}$, and

(iii) wavelet transform: $\{\mathcal{G}_A, \tau_t D_s\}$,

where $\mathcal{G}_H$ and $\mathcal{G}_A$ are the Weyl-Heisenberg and affine groups respectively given in Examples 2.3.2 and 2.3.1. The common feature in each of these group representations is translation. In each case the group representation can be factored as $\Pi = U_x \tau_t$ where x and t are appropriate real values. Because translation in time acts as modulation by a complex exponential in frequency, the frame properties of sets of complex exponentials play a fundamental role in discrete representations of these types. The following lemma describes how frames of complex exponentials together with U_x can be used to generate frames for large spaces.

Lemma 4.2.1 Let supp $\widehat{g} = [a, b]$ where $a < b$ are real numbers. Also let U_x be a bounded linear operator for each real value x. Let $\{t_{m,n}\}$ and $\{x_m\}$ be real sequences. Suppose that

$$\{e_{-t_{m,n}}\} \text{ is a frame for } \widehat{V}_m \stackrel{\triangle}{=} (U_{x_m}(PW_{a,b}))^{\widehat{}}$$

with bounds A_m and B_m. If there are constants A and B such that for $\gamma \in \widehat{\mathbb{R}}$

$$0 < A \le G(\gamma) \stackrel{\triangle}{=} \sum_m |(U_{x_m} g)^{\widehat{}}(\gamma)|^2 \le B < \infty \quad \text{a.e.}$$

then $\quad \{\tau_{t_{m,n}} U_{x_m} g\}$ is a frame for $V \stackrel{\triangle}{=} \bigcup_m U_{x_m}(PW_{a,b}) \quad$ with bounds $A(\inf_m A_m)$ and $B(\sup_m B_m)$.

Proof:

For $f \in V$ write

$$
\begin{aligned}
\sum_{m,n} |\langle f, \tau_{t_{m,n}} U_{x_m} g \rangle|^2 &= \sum_{m,n} |\langle \widehat{f}, e_{-t_{m,n}} (U_{x_m} g)^{\widehat{}} \rangle|^2 \quad \text{(Parseval)} \\
&= \sum_{m,n} |\langle \widehat{f} \overline{(U_{x_m} g)^{\widehat{}}}, e_{-t_{m,n}} \rangle|^2 \\
&\le \sum_m B_m \| \widehat{f} \overline{(U_{x_m} g)^{\widehat{}}} \|^2
\end{aligned}
$$

$$= \sum_m B_m \int |\widehat{f}(\gamma)\overline{(\overline{U_{x_m}g})^{\widehat{\ }}}(\gamma)|^2 d\gamma$$

$$\leq \left(\sup_m B_m \right) \sum_m \int |\widehat{f}(\gamma)|^2 |(U_{x_m}g)^{\widehat{\ }}(\gamma)|^2 d\gamma$$

$$= \left(\sup_m B_m \right) \int |\widehat{f}(\gamma)|^2 \sum_m |(U_{x_m}g)^{\widehat{\ }}(\gamma)|^2 d\gamma$$

$$\leq B \left(\sup_m B_m \right) \int |\widehat{f}(\gamma)|^2 d\gamma$$

$$= B \left(\sup_m B_m \right) \|\widehat{f}\|^2$$

$$= B \left(\sup_m B_m \right) \|f\|^2 \qquad \text{(Plancherel)}$$

The first inequality follows from the assumption that $\{e_{-t_{m,n}}\}$ frames V_m and the fact that $\widehat{f}\,\overline{(U_{x_m}g)^{\widehat{\ }}} \in V_m$ for each m. The lower bound is analogous. ∎

It is clear from this lemma that for $\{\tau_{t_{m,n}}U_{x_m}g\}$ to be a tight frame then the function G must be constant a.e. The following corollary addresses the tightness issue.

Corollary 4.2.2 With the assumptions of Lemma 4.2.1 $\{\tau_{t_{m,n}}U_{x_m}g\}$ is a *tight* frame for $V \triangleq \bigcup_m U_{x_m}(PW_{a,b})$ if and only if G is constant a.e. and for all m the frame $\{e_{-t_{m,n}}\}$ is tight with $A_m = B_m = C$.

In the cases of the Gabor and wavelet transform Lemma 4.2.1 may be used to show that (under proper assumptions) irregular lattices exist which generate frames for $L^2(\mathbb{R})$ and $H^2_+(\mathbb{R})$ respectively. These results are stated in Theorems 4.2.9 and 4.2.10.

4.2.1 Paley-Wiener

Sampling in bandlimited spaces has been the subject of extensive study. Uniform or regular sampling in bandlimited spaces has been studied by Whittaker [Whi15] in 1915, Kotel'nikov [Kot33] in 1933, Shannon [Sha49] in 1949. The basic result of these studies is the widely known *classical sampling theorem*.

Theorem 4.2.3 (Classical Sampling Theorem) Let $\Omega > 0$ and $2\Omega T < 1$. Then any $f \in PW_\Omega$ may be reconstructed from its uniform samples $\{f(nT)\}$ as

$$f = T \sum f(nT)\tau_{nT}d_{2\pi\Omega},$$

where the sum converges in L^2 and $d_{2\pi\Omega}$ is the Dirichlet kernel.

Thus, the classical sampling theorem answers the following question:

What conditions on the set $\{nT\}$ allow the recovery of f from $\{\{nT\}, f(nT)\}$?

The condition that the Classical sampling theorem gives is that the sampling density T^{-1} must be at least as large as twice the value of the cutoff frequency Ω. i.e. $T^{-1} > 2\Omega$. The quantity 2Ω is called the *Nyquist density*.

Let us now relate the classical sampling theorem to the general RKHS approach taken in the begining of this chapter. In the case of uniform sampling the pertinent group is $(\mathbb{R}, +)$ and the sampling lattice is $\Gamma_T = nT$. In terms of the discrete representation and frame perspective the pertinent collection of elements is

$$\{\tau_{nT} d_{2\pi\Omega}\}.$$

In the case $2T\Omega = 1$ the set of functions $\left\{\frac{1}{2\Omega}\tau_{nT} d_{2\pi\Omega}\right\}$ is an orthonormal basis for PW_Ω. The discretization operator is

$$Lf = \{\langle f, \tau_{nT} d_{2\pi\Omega}\rangle\}$$

with the adjoint

$$L^*c = \sum c_n \tau_{nT} d_{2\pi\Omega}.$$

Note that the classical sampling theorem could be arrived at by considering the frame properties of the collection $\{\tau_{nT} d_{2\pi\Omega}\}$. In particular, if $2T\Omega = 1$ this set is a tight exact frame for PW_Ω with bounds $A = B = 2\Omega$, and correlation $R = 2\Omega I$ (I is the identity). In this case $R^\dagger = \frac{1}{2\Omega}I = TI$. Thus, we conclude that for any $f \in PW_\Omega$

$$f = L^* R^\dagger L f = T L^* L f = T \sum f(nT) \tau_{nT} d_{2\pi\Omega}.$$

4.2.1.1 Frames of Complex Exponentials

Consider now more general sampling sets which are not necessarily uniformly spaced. Irregular sampling in band-limited spaces has been studied extensively by Paley-Wiener [PW34], Levinson [Lev40], Beutler [Beu61],[Beu66], and Yao-Thomas [YT67]. And recently all of the afore-mentioned theory has been extended and unified by Benedetto-Heller [BH90], [Hel91], and Benedetto [Ben92] in the context of frames. In particular, much of the theory is developed in terms of frames of complex exponentials. Feichtinger and Gröchenig [FG92] have used the notion of weighted frames, cf. Section 4.1.2, (of complex exponentials) to achieve good convergence rates for iterative reconstructions from irregular samples where gaps in the sampling set are no larger than the Nyquist density.

Let us relate the situation to the general RKHS approach at the begining of the chapter. Suppose that $\Gamma = \{t_n\}$ is an irregular set of points from the real line $\mathbb{R}$ and f is a signal which is bandlimited by $\Omega > 0$, i.e. $f \in PW_\Omega$. For simplicity we shall again take $g = d_{2\pi\Omega}$. With these choices the fundamental question is the following:

What conditions on the set $\Gamma = \{t_n\}$ allow the recovery of f from $\{\{t_n\}, f(t_n)\}$?

In this case the discretization operator is

$$Lf = \{\langle f, \tau_{t_n} d_{2\pi\Omega}\rangle\} = \{f(t_n)\}$$

with the adjoint

$$L^*c = \sum c_n \tau_{t_n} d_{2\pi\Omega}.$$

In answer to the fundamental question we may state that a sufficient condition on $\{t_n\}$ is that the sequence

$$\{\tau_{t_n} d_{2\pi\Omega}\}$$

constitute a frame for PW_Ω. This is because in this case the discretization L is a frame representation making Proposition 3.4.2 applicable and in fact we may write for all $f \in PW_\Omega$

$$f = L^* R^\dagger L f.$$

The frame properties of the set $\{\tau_{t_n} d_{2\pi\Omega}\}$ are then of clear interest.

By Plancherel and Parseval it is clear from the definition of a frame, viz. 3.1.1, that a set $\{\phi_n\}$ is a frame for $\mathcal{H}$ if and only if $\{\hat{\phi}_n\}$ is a frame for $\hat{\mathcal{H}} \triangleq \{\hat{f} : f \in \mathcal{H}\}$. With this notation $\widehat{PW_\Omega} = L^2[-\Omega, \Omega]$. Because of the basic Fourier relation

$$(\tau_{t_n} d_{2\pi\Omega})\hat{} = e_{-t_n} 1_{[-\Omega,\Omega]},$$

the frame properties of the the set $\{\tau_{t_n} d_{2\pi\Omega}\}$ in PW_Ω are the same as the frame properties of the set $\{e_{-t_n} 1_{[-\Omega,\Omega]}\}$ in $L^2[-\Omega, \Omega]$. Thus, the frame properties of such sets of complex exponentials are of direct interest in sampling theory for bandlimited functions.

By definition, viz. Definition 3.1.1, a sequence constituting a frame for a Hilbert space must reside in that space. Notationally we may abuse this requirement and write that $\{e_{-t_n}\}$ is a frame for $L^2[a, b]$ meaning that $\{e_{-t_n} 1_{[a,b]}\}$ is a frame for $L^2[a, b]$. Here $a < b$ are real numbers. It is easy to see that if $\{e_{-t_n}\}$ is a frame for $L^2[a, b]$ then $\{e_{-t_n}\}$ is a frame for $L^2[a + c, b + c]$ for any real c. In the time domain this corresponds to the statement that $\{\tau_{t_n} e_{(a+b)/2} d_{2\pi[(b-a)/2]}\}$ is a frame for $PW_{[a,b]}$ if and only if $\{\tau_{t_n} e_c e_{(a+b)/2} d_{2\pi[(b-a)/2]}\}$ is a frame for $PW_{[a+c,b+c]}$.

Sets of complex exponentials $\{e_{-t_n}\}$ have been studied by Duffin and Schaeffer [DS52]. One of their fundamental results is a sufficient condition on a sampling set $\Gamma = \{t_n\}$ to generate a frame of complex exponentials for $L^2[-\Omega, \Omega]$. That is, a condition which insures that the set $\{e_{-t_n}\}$ forms a frame for $L^2[-\Omega, \Omega]$. This condition is related to the notion of uniform density. Recall that, in general, a set $\Gamma = \{t_n\}$ has uniform density $\Delta\Gamma$ if the two following conditions hold.

(i) Γ is uniformly discrete, i.e. there is a $d > 0$ so that for all $n \neq m$, $|t_n - t_m| > d$, and

(ii) $|t_n - n(\Delta\Gamma)^{-1}| < L$ for some constant $L < \infty$.

Since $|nT - mT| = |n - m|T$ and $|nT - n(1/T)^{-1}| = 0$ a uniform sampling set Γ_T with sampling period T is a uniformly dense sampling set with density $\Delta\Gamma_T = 1/T$.

Theorem 4.2.4 (Duffin-Schaeffer, [DS52, Theorem I]) If $\Gamma = \{t_n\}$ is a uniformly dense sequence with uniform density $\Delta\Gamma > 2\Omega > 0$ then $\{e_{-t_n}\}$ is a frame for $L^2[-\Omega, \Omega]$.

The following corollary is true by the Fourier transform isomorphism relating $L^2[-\Omega, \Omega]$ and PW_Ω.

Corollary 4.2.5 If $\Gamma = \{t_n\}$ is a uniformly dense sequence with uniform density $\Delta\Gamma > 2\Omega > 0$ then $\{\tau_{t_n} d_{2\pi\Omega}\}$ is a frame for PW_Ω.

It is interesting to note that a sequence which is uniformly dense may have arbitrarily large, though finite, gaps. The largest such gap is the parameter L in the definition of a uniformly dense sequence. For a uniformly dense sequence large gaps, however, must be compensated for by portions of high density elsewhere in the set. The uniform discreteness of such a sampling set prevents it from having any finite cluster points. Thus there can be no interval in which the density of sampling points is unbounded. Roughly speaking we can think of a uniformly dense sequence of uniform density Δ as a tesslation of the uniform sampling $\{n\Delta^{-1}\}$. By tesslation of the set $\{n\Delta^{-1}\}$ we mean a second set $\{t_n\}$ in which each sampling point t_n may be identified with a point $n\Delta^{-1}$ through the relation $|t_n - n\Delta^{-1}| < L$. Figure 4.1.2 illustrates a uniformly dense sequence derived as a tesslation of uniform sequence of density 1 on a compact interval.
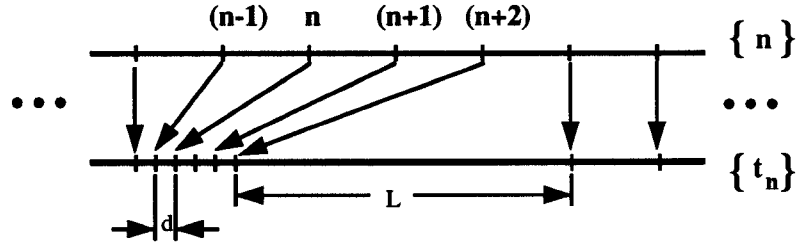
Figure 4.2: A uniformly dense sequence generated as a tesslation of a uniform sequence on a compact interval.

Jaffard [Jaf91] has characterized sampling sets $\Gamma = \{t_n\}$ which generate frames of complex exponentials $\{e_{-t_n}\}$ for $L^2[-\Omega, \Omega]$ in terms of unions of uniformly discrete and uniformly dense sampling sequences.

Although we have taken the analyzing function g to be $g = d_{2\pi\Omega}$ it should be evident that other analyzing functions can be used. In this case we are interested in the frame properties of the collection $\{\tau_{t_n} g\}$. This still leads to consideration of the frame properties of the complex exponentials since

$$(\tau_{t_n} g)\hat{} = e_{-t_n}\hat{g}.$$

For arbitrary functions g there is no reason that we should expect that this collection will form a frame for $L^2[-\Omega, \Omega]$. In fact such a collection could only possibly form a frame for $L^2(\text{supp } \hat{g})$. This is because if f is a function such that the support of $\hat{f}$ is exclusive of the support of $\hat{g}$, i.e. supp $\hat{f} \cap$ supp $\hat{g} = \emptyset$, then

$$\left\langle \hat{f}, e_{-t_n}\hat{g} \right\rangle = \left\langle \hat{f}\overline{\hat{g}}, e_{-t_n} \right\rangle = 0.$$

So that if the essential support of $\hat{g}$ does not cover $[-\Omega, \Omega]$ then there are non-zero functions $\hat{f} \in L^2[-\Omega, \Omega]$ for which there is no $A > 0$ so that

$$A\|\hat{f}\|^2 \le \sum | \left\langle \hat{f}, e_{-t_n}\hat{g} \right\rangle |^2.$$

4.2.1.2 Exact frames for PW_Ω

Definition 4.2.6 (Kadec-Levinson sequence) A real sequence $\{t_n\}$ is a *Kadec-Levinson sequence* if for some $\Omega > 0$ the condition

$$\sup_n |t_n - \frac{n}{2\Omega}| < \frac{1}{4}\left(\frac{1}{2\Omega}\right)$$

is satisfied.

Paley and Wiener first dealt with the question of when a set of complex exponentials $\{e_{-t_n}\}$ forms a basis for the space $L^2[-\Omega, \Omega]$. Levinson [Lev40] showed that the constant $1/4$ is the smallest such constant which insures the completeness of $\{e_{-t_n}\}$ in $L^2[-\Omega, \Omega]$. Later Kadec [Kad64] gave a direct proof that $\{e_{-t_n}\}$ is an exact frame. These results are stated in Theorem 4.2.7 which appears in [Ben92, Theorem 34].

Theorem 4.2.7 Suppose the sampling set $\{t_n\}$ is a Kadec-Levinson sequence for a given $\Omega > 0$. Then $\{e_{-t_n}\}$ is an exact frame for $L^2[-\Omega, \Omega]$.

A Kadec-Levinson sequence $\Gamma = \{t_n\}$ for $\Omega > 0$ is uniformly discrete with uniform density $\Delta\Gamma = 2\Omega$. Clearly, if the sequence were uniformly discrete the uniform density would be 2Ω. To see that a KL sequence is uniformly discrete assume without loss of generality that $t_m > t_n$ and write

$$
\begin{aligned}
t_m - t_n &\geq \inf(t_m - t_n) \\
&= \inf_m t_m - \sup_n t_n \\
&\geq (m - \frac{1}{4})\Delta - (n + \frac{1}{4})\Delta = (m - n - \frac{1}{2})\Delta,
\end{aligned}
$$

so that $|t_m - t_n| > d = \frac{1}{2}\Delta$. Figure 4.1.2 depicts sequences which are of the Kadec-Levinson type. Each element t_n in the sequence is restricted to lie within a region of length $1/(4\Omega)$ centered at $n\Delta$. This region is indicated by parentheses in the figure.
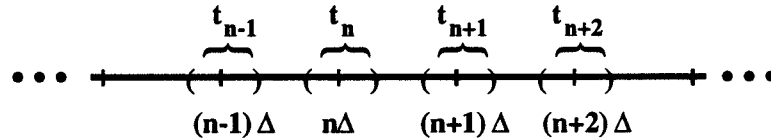
Figure 4.3: A Kadec-Levinson sequence $\{t_n\}$ for $\Omega > 0$ where $\Delta = \frac{1}{2\Omega}$.

4.2.2 Gabor

We have seen that the Gabor transform G_g is a special case of the group representation transform where the underlying group is the Weyl-Heisenberg group $\mathcal{G}_H = \mathbb{T} \times \mathbb{R} \times \hat{\mathbb{R}}$ and the

underlying representation is $\Pi_H(z, t, \gamma) = z e_\gamma \tau_t$. As previously noted the Gabor transform may be written as

$$G_g f(t, \gamma) = \langle f, \Pi_H(1, t, \gamma) g \rangle = \langle f, e_\gamma \tau_t g \rangle.$$

As a discrete representation of a signal f we shall consider an irregularly spaced sampling set $\Gamma = (t_n, \gamma_m)$ at which the Gabor transform will be evaluated. The discrete Gabor representation of a signal $f \in L^2(\mathbb{R})$ is then

$$\Lambda(f) = \{(t_n, \gamma_m), G_g f(t_n, \gamma_m)\}.$$

Thus, for the Gabor transform the fundamental question is the following:

What are conditions on the sampling set $\Gamma = (t_n, \gamma_m)$ such that an $f \in L^2(\mathbb{R})$ may be recovered from knowledge of $\Lambda(f) = \{(t_n, \gamma_m), G_g f(t_n, \gamma_m)\}$?

In keeping with our basic approach to discretization we are led to consider the frame properties of collections of the form

$$\{e_{\gamma_m} \tau_{t_n} g\}$$

which are the same as the frame properties for the collection

$$\{\tau_{t_n} e_{\gamma_m} g\}.$$

This is because the modulation and translation operators commute under magnitude, i.e. $|e_a \tau_b| = |\tau_b e_a|$. Appropriately, we call collections of this form *Gabor systems* and such collections which are frames *Gabor frames*. If the discrete lattice $\{(t_n, \gamma_m)\}$ is regular, i.e. there are real numbers a and b such that $(t_n, \gamma_m) = (na, mb)$ then we refer to the collection

$$\{\tau_{na} e_{mb} g\}.$$

as a *regular Gabor system* and if it is a frame a *regular Gabor frame*.

4.2.2.1 Regular Gabor Systems

There is a wealth of theory associated with the Gabor transform Gabor systems and their frame properties in the regular case. In this section we review some of the regular Gabor theory in as far as it is pertinent to our general irregular outlook.

For regular Gabor systems $\{\tau_{na} e_{mb} g\}$ there is a characterization their frame properties for $L^2(\mathbb{R})$ in terms of the product ab. Namely,

(i) if $ab > 1$ the regular Gabor system $\{\tau_{na} e_{mb} g\}$ is not a frame for $L^2(\mathbb{R})$ for any choice of g,

(ii) if $ab < 1$ then there exist analyzing functions g which generate regular Gabor frames $\{\tau_{na} e_{mb} g\}$ for $L^2(\mathbb{R})$, and

(iii) $ab = 1$ if and only if $\{\tau_{na} e_{mb} g\}$ is an exact regular Gabor frame for $L^2(\mathbb{R})$.

The Balian-Low theorem [Bal81], [Low85], [Dau90], viz. [BHW90] for a mathematically sound proof, is an uncertainty principle for exact Gabor frames. It says that an exact Gabor frame can not be generated from an analyzing function which is well localized in both time and frequency. For a function $g \in L^2(\mathbb{R})$ we can think of the quantity $\|tg(t)\|$ as a measure of its *localization* in time. Similarly, $\|\gamma \hat{g}(\gamma)\|$ can be thought of as a measure of its frequency localization.

Theorem 4.2.8 (Balian-Low) Let $g \in L^2(\mathbb{R})$. If $\{\tau_{na}e_{mb}g\}$ is an exact frame for $L^2(\mathbb{R})$ then

$$\|tg(t)\| \, \|\gamma\widehat{g}(\gamma)\| = \infty.$$

4.2.2.2 Irregular Gabor Systems

For $\widehat{g}$ compactly supported, the following theorem gives conditions on an irregular discrete lattice in the Weyl-Heisenberg group to give rise to a Gabor frame in $L^2(\mathbb{R})$. It is a direct consequence of Lemma 4.2.1. A theorem of this form which is due to Heller appears in [Hel91].
Theorem 4.2.9 With $[a,b] \subseteq \mathbb{R}$ a compact interval and $g \in PW_{[a,b]}$ with supp $\widehat{g} = [a,b]$ and $\widehat{g} \in L^\infty(\mathbb{R})$, suppose $\{t_n\}$ is a real sequence such that

$$\{e_{-t_n}\} \text{ is a frame for } L^2[a,b],$$

and $\{\gamma_m\}$ is a real sequence for which there is a d such that

$$\forall m, \quad 0 < d \le \gamma_{m+1} - \gamma_m \le b - a.$$

Then $\{e_{\gamma_m}\tau_{t_n}g\}$ is a frame for $L^2(\mathbb{R})$.

Proof:
In Lemma 4.2.1 let $U = U_\gamma = e_\gamma$ and $t_{m,n} = t_n$ so that

$$G = \sum_m |(e_{\gamma_m}g)\widehat{}|^2 = \sum_m |\tau_{\gamma_m}\widehat{g}|^2.$$

The condition that $\gamma_{m+1} - \gamma_m \le b - a$ for each m implies that each term in the sum has support which overlaps with at least one other. Thus there is an A such that $G > A > 0$ a.e. on $\widehat{\mathbb{R}}$. On the other hand, the condition that $\{\gamma_m\}$ is uniformly discrete together with the facts that $g \in PW_{[a,b]}$ and $\widehat{g} \in L^\infty(\mathbb{R})$ implies a B such that $G < B < \infty$ on $\widehat{\mathbb{R}}$. By Lemma 4.2.1

$$\{e_{\gamma_m}\tau_{t_n}g\}$$

is a frame for $\bigcup_m e_{\gamma_m}(PW_{[a,b]}) = L^2(\mathbb{R})$ since the supports of $(e_{\gamma_m}g)\widehat{}$ overlap and cover $\widehat{\mathbb{R}}$. ∎

We note that [Grö92] provides a similar theorem for irregular *weighted* Gabor systems, cf. Section 4.1.2, in which conditions on a sampling set in $\mathcal{G}_H$ are asserted which insure that the weighted system is a frame for $L^2(\mathbb{R})$. However, the conditions in [Grö92] are more restrictive than those of Theorem 4.2.9.

4.2.3 Wavelet

We have seen that the wavelet transform W_g is a special case of the group representation transform where the underlying group is the affine group $\mathcal{G}_A = \mathbb{R} \times \mathbb{R}^+$ and the underlying

representation is $\Pi_A(t,s) = \tau_t D_s$. As previously noted the wavelet transform may be written as

$$W_g f(t,s) = \langle f, \Pi_A(t,s)g \rangle = \langle f, \tau_t D_s g \rangle \, .$$

As a discrete representation of a signal f we shall consider an irregularly spaced sampling set $\Gamma = (t_{m,n}, s_m)$ at which the wavelet transform will be evaluated. The discrete wavelet representation of a signal $f \in L^2(\mathbb{R})$ is then

$$\Lambda(f) = \{(t_{m,n}, s_m), W_g((t_{m,n}, s_m))\} \, .$$

Thus, for the wavelet transform the fundamental question is the following:

What are conditions on the sampling set $\Gamma = (t_{m,n}, s_m)$ such that an $f \in L^2(\mathbb{R})$ may be recovered from knowledge of $\Lambda(f) = \{(t_{m,n}, s_m), W_g((t_{m,n}, s_m))\}$?

In keeping with our basic approach to discretization we are led to consider the frame properties of collections of the form

$$\left\{ \tau_{t_{m,n}} D_{s_m} g \right\} \, .$$

Collections of this form are called *wavelet systems* and such collections which are frames *wavelet frames*. If the discrete lattice $\{((t_{m,n}, s_m)\}$ is regular, i.e. there are real numbers a and b such that $(t_{m,n}, s_m) = (a^{-m}nb, a^m)$ then we refer to the collection

$$\left\{ \tau_{a^{-m}nb} D_{a^m} g \right\} \, .$$

as a *regular wavelet system* and if it is a frame a *regular wavelet frame*.

4.2.3.1 Regular Wavelet Systems

Recently regular wavelet systems have received an enormous amount attention. In fact, there are seminal developments of wavelet theory by Daubechies [Dau92], Mallat [Mal89c], [Mal89b], [Mal89a], and Meyer [Mey90]. The material in [Dau92] serves as an excellent backdrop to the recent developments in wavelet theory.

One particular area of interest is the existence and construction of orthonormal wavelet bases. In this regard the development of multi-resolution [Mal89c] analysis (MRA) has been a major advance. A further development [Dau88] has been the construction of orthonormal wavelet bases with compact support. As a result very fast algorithms, e.g. the fast wavelet transform, for the computation of the wavelet representation have been constructed.

Although such bases certainly lead to invertible discrete represenations with fast algorithms, we shall not consider such special cases in too much detail. For one thing, orthonormal bases preclude the benefits associated with redundant systems as discussed in Section 3.5.1. For another thing, in many applications the condition that the wavelet system must be regular is undesirable. For instance in pattern classification a desirable property of a representation of a signal is that it be translation invariant. In other words, translated versions of signals should yield translated versions of their discrete representations. This is clearly not satisfied for fixed sampling geometries such as are associated with regular wavelet systems. Moreover, there are still reasonably fast algorithms for the computation of the wavelet representation for irregular systems.

4.2.3.2 Irregular Wavelet Systems

In answer to the fundamental question, Theorem 4.2.10 gives conditions on a sampling set in $\mathcal{G}_A$ to give rise to a wavelet frame for $\mathcal{H}^2_+(\mathbb{R})$. It is a direct consequence of Lemma 4.2.1.

Theorem 4.2.10 Let $0 < a < b$ be two strictly positive real numbers and let $g \in PW_{[a,b]}$ and $\widehat{g} \in L^\infty(\mathbb{R})$ with supp $\widehat{g} = [a, b]$.

Suppose that $\{t_{m,n}\} \subseteq \mathbb{R}$ and $\{s_m\} \subseteq \mathbb{R}^+$ are two sequences such that

$$\{e_{-t_{m,n}}\} \text{ is a frame for } L^2[s_m a, s_m b]$$

and there is a d such that

$$\forall m, \quad 1 < d \le \frac{s_{m+1}}{s_m} \le \frac{b}{a}.$$

Then

$$\{\tau_{t_{m,n}} D_{s_m} g\} \text{ is a frame for } H^2_+(\mathbb{R}).$$

Proof:

In Lemma 4.2.1 let $U = U_s = D_s$ so that

$$G = \sum_m |(D_{s_m} g)\check{}|^2 = \sum_m |D_{s_m^{-1}} \widehat{g}|^2.$$

Since the support of $D_{s_m^{-1}} \widehat{g}$ is $I_m \overset{\triangle}{=} [s_m a, s_m b]$, the condition on $\{s_m\}$ that $s_{m+1}a \le s_m b$ insures that I_m and I_{m+1} have some overlap and are not identical. Since $g \in L^\infty(\mathbb{R})$ we may conclude that there are constants A and B so that $0 < A \le G \le B < \infty$. Clearly $\bigcup I_m = (0, \infty)$ so that $V = \bigcup_m D_{s_m}(PW_{[a,b]}) = PW_{(0,\infty)} = H^2_+(\mathbb{R})$ since identically constant functions are not in $L^2(\mathbb{R})$. Thus, by Lemma 4.2.1 $\{\tau_{t_{m,n}} D_{s_m} g\}$ is a frame for $H^2_+(\mathbb{R})$. ∎

Note that an identical theorem which concludes that $\{\tau_{t_{m,n}} D_{s_m} g\}$ is a frame for $L^2(\mathbb{R})$ can be arrived at by requiring the analyzing function g in Theorem 4.2.10 to be even. Finally, we note that as in the Gabor case [Grö92] provides a similar theorem for irregular *weighted* wavelet systems, cf. Section 4.1.2, in which conditions on a sampling set in $\mathcal{G}_A$ are asserted which insure that the weighted system is a frame for $L^2(\mathbb{R})$. However, the conditions in [Grö92] are more restrictive than those of Theorem 4.2.10.

Chapter 5

Local Frames

In previous chapters we have seen how it is possible to represent signals from an infinite dimensional Hilbert space using frames generated from irregular samplings of certain reproducing kernel Hilbert spaces. Because these are frame representations it follows that *every* signal in the Hilbert space can be reconstructed from its frame representation. With respect to the situation in which it is of interest to reconstruct only a specific single function in the Hilbert space, a full frame representation is much more than is needed. Moreover, even though frame representations are discrete, storage and manipulation on a digital machine, require not only a countable representation but also a finite representation. Both of these observations motivate the notion of a local frame. The chapter concludes with a scheme for signal compression using local frames.

5.1   Frame Localization

Suppose $\mathcal{H}$ is a Hilbert space of interest. On the one hand the global theory of frames, viz. Chapter 3, allows the reconstruction of *every* signal $f \in \mathcal{H}$ from its frame representation. On the other hand the fundamental goal of discretization theory is to reconstruct only a *particular* signal $f_* \in \mathcal{H}$ from its discrete representation. Although the global frame representation is a viable discrete representation which meets the mandate of the discretization theory, its ability to recover every signal is far more than is required. Since it is not necessary to reconstruct every signal in the entire Hilbert space $\mathcal{H}$ it is natural to ask if there is some method in which the global frame representation may be *localized* about a particular signal. These ideas lead directly to the notion of a *local frame*.

The distinguishing feature of a local frame for $\mathcal{H}$ is that it is dependent on a particular signal in $\mathcal{H}$. Thus, for every signal in $\mathcal{H}$ there is an associated local frame. In this section we examine two methods for frame localization: one entailing the signal dependent choice of frame elements, i.e. signal dependent sampling, and the other entailing the finite truncation of frame representations. The first method of localization involves the construction of a global frame which has elements which are signal dependent. With respect to the frame $\{\Pi(x)g\}_{x \in \Gamma}$ localizations of this form will come from sampling sets $\Gamma(f)$ which are signal dependent. The second method of frame localization is via truncation of a global frame. Truncation has the desirable property that it necessarily results in a finite discrete representation of a signal.

Localization can be viewed in terms of a decomposition of the Hilbert space $\mathcal{H}$ into two signal dependent subspaces. If $f_* \in \mathcal{H}$ is the particular signal of interest, localization results in a decomposition of $\mathcal{H}$ as

$$\mathcal{H} = \mathcal{H}(f_*) \oplus \mathcal{H}(f_*)^\perp$$

where f_* is (almost) contained in the finite dimensional subspace $\mathcal{H}(f_*)$.

In the following sections it is assumed that $\mathcal{H}$ is a Hilbert space contained in $L^2(\mathbb{R})$ and $\mathcal{G}$ is a group with representation Π on $\mathcal{H}$. Further g is assumed to be an admissible function, i.e. $g \in \mathcal{A}_{\Pi,\mu}(\mathcal{H})$ where μ is the left Haar measure. Recall that the generic representation of a signal $f \in \mathcal{H}$ is

$$\{\langle f, \Pi(x)g \rangle\}_{x \in \Gamma}$$

where $\Gamma \subseteq \mathcal{G}$ is a countable sampling set from $\mathcal{G}$. This representation may be thought of as the irregular sampling of the group representation transform $V_g : \mathcal{H} \mapsto L^2_\mu(\mathcal{G})$ given in Equation (2.4.1).

5.1.1 Signal Dependent Sampling

In previous discussions we have not addressed the issue of how the sampling set Γ arises. From a conventional point of view Γ would be considered to be fixed and given. Here, instead we view the sampling set Γ as a design parameter for signal representation. In particular, we may adapt the sampling set to fit particular signals of interest. As a result, we deal with signal dependent sampling sets $\Gamma(f)$ and study the frame properties of sequences

$$\{\Pi(x)g\}_{x \in \Gamma(f)}$$

for particular signals $f \in \mathcal{H}$. In general we look for signal dependent samplings $\Gamma(f) \subseteq \Gamma$ which are embedded in global samplings Γ which generate frames for the whole space $\mathcal{H}$. This is one method by which we may achieve frame localization.

As an example of a frame generated by a signal dependent sampling let's look at the familiar case of sampling in the bandlimited space $\mathcal{H} = PW_\Omega$. In this case, viz. Section 4.2, with $g = d_{2\pi\Omega}$ the sampling set $\Gamma = \{t_n\}$ is a sequence of real numbers and the representation of $f \in PW_\Omega$ is $\{f(t_n)\}$. Suppose that $f_* \in PW_\Omega$ is the particular non-zero signal of interest. Define the k-th moment sampling set $\Gamma^{(k)}(f_*)$ of f_* as

$$\Gamma^{(k)}(f_*) \triangleq \left\{ t : f_*^{(k)}(t) = 0 \right\},$$

where $f_*^{(k)}$ is the k-th derivative of f_*. Being in PW_Ω, f_* is analytic and the moment sampling sets $\left\{ \Gamma^{(k)}(f_*) \right\}$ are all well defined and countable. A nice feature of the moment sampling sets is that they are translation invariant, i.e. with $a \in \mathbb{R}$

$$\forall k, \quad \Gamma^{(k)}(\tau_a f_*) = \tau_a \Gamma^{(k)}(f_*).$$

According to the Duffin-Schaeffer theorem (Theorem 4.2.4) for $\{e_{-t}\}_{t \in \Gamma}$ to form a frame for PW_Ω it is needed that Γ have uniform density (Section 2.5.2) $\Delta\Gamma > 2\Omega$. We state without proof that such a sampling set may be generated as a finite union of moment sampling sets. That is, we construct a signal dependent sampling set $\Gamma(f_*)$ as

$$\Gamma(f_*) = \bigcup_{k \in F} \Gamma^{(k)}(f_*),$$

where $F \subseteq \mathbb{Z}$ is a finite set. The reader is referred to Section 6.2.1 for a numerical example of such a sampling scheme and its associated reconstructions.

5.1.2   Truncation

So far, our approach to discretization has resulted in representations of signals which are countable yet possibly infinite. For practical reasons it is also necessary to have representations which are finite. A natural procedure for going from a countably infinite representation to a finite representation is truncation. Such a truncation is necessarily signal dependent since it is the infinite representation of the signal on which the truncation is performed. In this section we shall assume that $\{\Pi(x)g\}_{x \in \Gamma}$ is a frame for $\mathcal{H}$ with frame representation L. If $\Gamma = \{x_n\}$ then L is given as

$$Lf = \{V_g f(x_n)\}$$

with the adjoint

$$L^* c = \sum c_n \Pi(x_n)g.$$

Define

$$\mathcal{H}_\delta(f_*) \stackrel{\triangle}{=} \operatorname{span} \{\Pi(x_n)g \; : \; |\langle f, \Pi(x_n)g\rangle| > \delta\} \tag{5.1.1}$$

We think of the space $\mathcal{H}_\delta(f_*)$ as the localized space around the signal f_* with respect to the frame $\{\Pi(x_n)g\}$. To further develop this idea we introduce the notion of a *frame truncation* operator.

Example 5.1.1 Let $J \subset \mathbb{Z}$. For localization around a specific f_* the set J will depend on f_*. A simple frame truncation operator, $F : \ell^2(\mathbb{Z}) \mapsto \ell^2(J)$ is

$$(Fc)_n = \begin{cases} c_n, & n \in J \\ 0, & \text{otherwise} \end{cases} \tag{5.1.2}$$

where $c \in \ell^2(\mathbb{Z})$. This F has the following properties:

 a. F is a linear operator,

 b. $\|F\| = 1$,

 c. $F = F^*$ is self adjoint,

 d. $F = F^2$, and

 e. F is the orthogonal projection operator onto the subspace $\ell^2(J)$.

Proof:

 a. With x, y elements of $\mathcal{H}$ and α, β complex scalars, clearly, $F(\alpha x + \beta y) = \alpha F x + \beta F y$.

 b. (i) $\|F\| \geq 1$
    Pick a $j^* \in J$ and let $c = (\delta_{j,j^*})$. Then we have

$$\|F\| \stackrel{\triangle}{=} \sup_{\|d\|=1} \|Fd\| \geq \|Fc\| = 1. \tag{5.1.3}$$

68

(ii) $\|F\| \leq 1$

$$\|Fc\|^2 = \sum_{j \in J} |c_j|^2 \leq \sum |c_j|^2 = \|c\|^2.$$

c.

$$\begin{aligned}
\langle Fc, c \rangle &= \sum (Fc)_j \bar{c}_j = \sum_{j \in J} |c_j|^2 \\
\langle c, Fc \rangle &= \sum c_j \overline{(Fc)}_j = \sum_{j \in J} |c_j|^2
\end{aligned}$$

d. Trivially, $F^2 x = F(Fx) = Fx$.

e. By Fact 2.1.2 items a. through d. imply e.

Example 5.1.2 As a more specific example of a frame truncation operator consider the following F defined with respect to a specific $f_* \in \mathcal{H}$ and $\delta > 0$. A family of truncations $\{F_{f_*,\delta}\}$ is given as

$$(F_{f_*,\delta} c)_n = \begin{cases} c_n, & |(c_*)_n| \geq \delta \\ 0, & \text{otherwise}, \end{cases} \tag{5.1.4}$$

where $c_* = L f_*$.

For all $c \in L(\mathcal{H})$ and $\delta > 0$, the truncation $F_{f_*,\delta}$ provides an orthogonal decomposition of c as

$$c = F_{f_*,\delta} c + (I - F_{f_*,\delta}) c$$

and

$$\|c\|^2 = \|F_{f_*,\delta} c\|^2 + \|(I - F_{f_*,\delta}) c\|^2.$$

Such an $F_{f_*,\delta}$ partitions c into two segments: one for which c_* has elements larger than δ and one for which c_* has elements less than or equal to δ. The two following lemmas show that (i) the former segment resides in a finite dimensional space and (ii) it is always possible to determine a δ which will ensure that an arbitrary percentage of the energy from the whole sequence c_* will be contained in this first finite dimensional segment.

Lemma 5.1.3 Suppose $F_{f_*,\delta}$ is as in Example 5.1.2 for a fixed $f_* \in \mathcal{H}$. For all $\delta > 0$

$$\dim \{F_{f_*,\delta} L(\mathcal{H})\} < \infty.$$

Proof:

69

We have

$$\|c_*\|^2 \geq \|F_{f_*,\delta}c_*\| \quad = \sum_{|(c_*)_n| \geq \delta} |(c_*)_n|^2$$

$$\geq \quad \delta^2 \, \mathrm{card} \, \{n : |(c_*)_n| \geq \delta\}$$

$$= \quad \delta^2 \, \dim \{F_{f_*,\delta}L(\mathcal{H})\},$$

so that

$$\dim \{F_{f_*,\delta}L(\mathcal{H})\} \leq \frac{\|c_*\|^2}{\delta^2} < \infty$$

since $c_* \in \ell^2(\mathbb{Z})$ and $\delta > 0$. ∎

Lemma 5.1.4 Suppose $F_{f_*,\delta}$ is as in Example 5.1.2. Given $\epsilon > 0$ there is a δ so that

$$\|(I - F_{f_*,\delta})c_*\|^2 < \epsilon\|c_*\|^2. \tag{5.1.5}$$

Proof:
Clearly,

$$\lim_{\delta \to 0} \|F_{f_*,\delta}c_*\|^2 = \|c_*\|^2 < \infty.$$

Therefore, for ϵ arbitrary there is some $\delta > 0$ so that

$$|\|c_*\|^2 - \|F_{f_*,\delta}c_*\|^2| < \epsilon\|c_*\|^2.$$

Since $\|c_*\|^2 = \|F_{f_*,\delta}c_*\|^2 + \|(I - F_{f_*,\delta})c_*\|^2$ we may conclude $\|(I - F_{f_*,\delta})c_*\|^2 < \epsilon\|c_*\|^2$. ∎

Equation (5.1.5) expresses the notion that the operator $F_{f_*,\delta}L$ extracts the most significant frame coefficients with respect to the specific signal f_*. Here the term "most significant" is quantified by the parameter $\epsilon \in (0,1)$. For example, a value of $\epsilon \approx 0$ indicates that almost every coefficient is significant, and a value of $\epsilon \approx 1$ indicates that almost every coefficient is insignificant. Via this lemma there is an interplay between the specified value of ϵ and δ. In fact, Lemma 5.1.4 implies the existence of a *truncation distribution* function $\nu(\epsilon)$ which serves as the boundary between acceptable and non-acceptable thresholds δ for a given ϵ. Given a particular $f_* \in \mathcal{H}$ define the truncation distribution function $\nu_{f_*} : (0,1) \mapsto [0, \|c_*\|_\infty]$ associated with the frame representation L as

$$\nu_{f_*}(\epsilon) = \inf \left\{ \delta \; : \; \|(I - F_{f_*,\delta})c_*\|^2 < \epsilon\|c_*\|^2 \right\}, \tag{5.1.6}$$

where $c_* = Lf_*$. A possible truncation distribution function is shown in Figure 5.1. Proposition 5.1.5 asserts that a truncation distribution function must be monotonically increasing.

Proposition 5.1.5 Given a signal $f_* \in \mathcal{H}$, a truncation distribution function ν_{f_*} as defined in (5.1.6) is a monotonically increasing function which is continuous from the left and

$$\lim_{\epsilon \to 0} \nu_{f_*}(\epsilon) = 0$$

$$\lim_{\epsilon \to 1} \nu_{f_*}(\epsilon) = \|c\|_\infty.$$

Proof:

We show ν is monotonically increasing. Let $\epsilon_1 < \epsilon_2$ and define the sets S_1 and S_2

$$S_i \triangleq \left\{ \delta \ : \ \|(I - F_{f_*,\delta})c_*\|^2 < \epsilon_i \|c_*\|^2 \right\}, \quad i = 1, 2.$$

Clearly $S_1 \subseteq S_2$ so that $\inf S_1 \leq \inf S_2$ and consequently $\nu_{f_*}(\epsilon_1) \leq \nu_{f_*}(\epsilon_2)$.   ∎
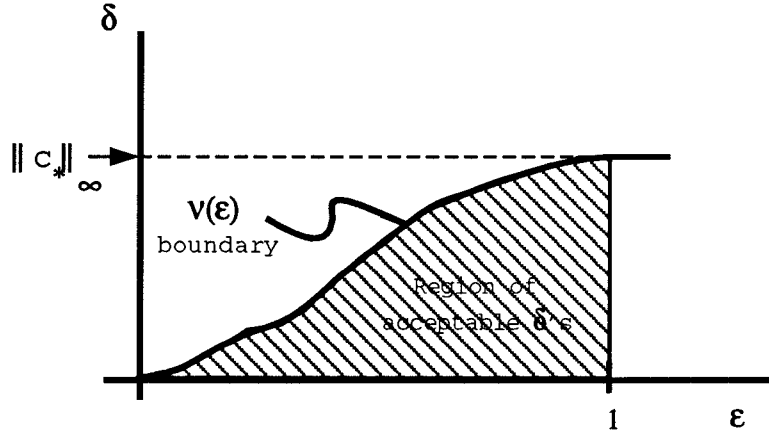
Figure 5.1: A possible truncation distribution function $\nu(\epsilon)$

The truncation distribution describes the relation between the necessary value for the truncation threshold δ and the desired percentage of energy preservation ϵ required after truncation. Typically, a value of ϵ is prescribed from which a compatible threshold δ is computed via the truncation distribution ν, i.e. $\delta = \nu(\epsilon)$. Suppose f_* is a particular signal in $\mathcal{H}$, L is the pertinent frame representation and ϵ is chosen as a fixed value between 0 and 1. With such a prescribed ϵ, if $\delta = \nu(\epsilon)$ it is assured that

$$\|(I - F_{f_*,\delta})Lf_*\|^2 < \epsilon\|Lf_*\|.$$

To see the ramifications of this requirement in the signal domain $\mathcal{H}$ let us first introduce the concept of "essential containment".

Definition 5.1.6 A signal $f \in \mathcal{H}$ is ϵ-contained in a subspace $\mathcal{H}' \subseteq \mathcal{H}$ if

$$\|(I - P_{\mathcal{H}'})f\|^2 < \epsilon\|f\|^2,$$

where $P_{\mathcal{H}'}$ denoted the orthogonal projection operator onto the subspace $\mathcal{H}'$, and we may write $f \widetilde{\in} \mathcal{H}'$ by ϵ.

By the previous discussion if $\delta = \nu(\epsilon)$ we may say that $F_{f_*,\delta}Lf_*$ is ϵ-contained in $F_{f_*,\delta}L(\mathcal{H})$. Moreover, the essential containment property can be related back to the signal domain by Theorem 5.2.1.

5.2 Finite Representation

In this section we examine localized frames resulting from truncation of a global frame for a Hilbert space $\mathcal{H}$. The truncation process results in a finite dimensional subspace of $\mathcal{H}$ which itself is framed by finitely many elements taken from the global frame. Being a frame for the localized space, the finite dimensional frame has an associated local frame representation. Reconstruction from local frame representations are examined and bounds for the corresponding error are developed.

5.2.1 Local Frame Representation

Assume that $\{\phi_n\}$ is a global frame for a Hilbert space $\mathcal{H} \subseteq L^2(\mathbb{R})$ with frame representation L and frame correlation R. In relation to previous material we may have $\phi_n = \Pi(x_n)g$, but this is not necessary for the discussion here. Fix $\delta > 0$ and consider a particular element $f_* \in \mathcal{H}$ and the localization associated with the truncation operator $F_{f_*,\delta}$ given in Example 5.1.2. From Lemma 5.1.3 we see that localization by truncation has the property that the truncated space $\mathcal{H}_\delta(f_*)$ is finite dimensional. Here

$$
\begin{aligned}
\mathcal{H}_\delta(f_*) &\stackrel{\triangle}{=} \operatorname{span}\{\phi_n \ : \ |\langle f_*, \phi_n\rangle| > \delta\} \\
&= \operatorname{span}\{\phi_n \ : \ n \in J_\delta(f_*)\} \\
&= F_{f_*,\delta}L(\mathcal{H}),
\end{aligned}
$$

where $J_\delta(f_*) = \{n \ : \ |\langle f_*, \phi_n\rangle| > \delta\}$ and $\operatorname{card} J_\delta(f_*) < \infty$.

Because any finite collection of functions is a frame for its span [Pat92] we conclude that

$$
\{\phi_n\}_{n \in J_\delta(f_*)}
$$

is a frame for $\mathcal{H}_\delta(f_*)$. Moreover the associated frame representation operator with respect to the truncated frame is $L_{f_*,\delta} = F_{f_*,\delta}L$ with local frame correlation $R_{f_*,\delta} = F_{f_*,\delta}RF_{f_*,\delta}$. A local reconstruction f_δ starting from an arbitrary $f \in \mathcal{H}$ is

$$
\begin{aligned}
f_\delta &= L_{f_*,\delta}^* R_{f_*,\delta}^\dagger L_{f_*,\delta} f \\
&= (F_{f_*,\delta}L)^*(F_{f_*,\delta}RF_{f_*,\delta})^\dagger F_{f_*,\delta}Lf \\
&= L^* F_{f_*,\delta}^2 R^\dagger F_{f_*,\delta}^2 Lf \\
&= L^* F_{f_*,\delta} R^\dagger F_{f_*,\delta} Lf
\end{aligned}
$$

because $F_{f_*,\delta}$ is an orthogonal projection, viz. Example 5.1.1. Thus, a local reconstruction may be thought of in terms of the truncation of the correlation matrix $R_{f_*,\delta}$. The L^2-error

associated with the local reconstruction is

$$
\begin{aligned}
\|f_* - f_\delta\| &= \|L^* R^\dagger L f_* - L^* R^\dagger F_{f_*,\delta} L f_*\| \\
&= \|L^* R^\dagger (I - F_{f_*,\delta}) L f_*\| \\
&\leq \|L^*\| \, \|R^\dagger\| \, \|(I - F_{f_*,\delta}) L f_*\| \\
&\leq \frac{B^{\frac{1}{2}}}{A} \|(I - F_{f_*,\delta}) L f_*\|.
\end{aligned}
$$

Thus, if $F_{f_*,\delta} L f_*$ is ϵ-contained in $F_{f_*,\delta} L(\mathcal{H})$ then f_δ is $\frac{B}{A^2}\epsilon$-contained in $\mathcal{H}_\delta(f_*)$ where $\mathcal{H}_\delta(f_*)$ is given in (5.1.1). In fact, Theorem 5.2.1 improves on this result with a tighter bound on the essential inclusion of $\frac{B}{A}$ instead of $\frac{B}{A^2}$.

Theorem 5.2.1 provides controllable error bounds on the local frame representation of a signal. More than this, it provides a precise statement of the notion that a signal can be well represented by the most important (e.g. largest) coefficients in its frame expansion and implies a natural decomposition of the space $\mathcal{H}$ as $\mathcal{H}_\delta(f_*) \oplus \mathcal{H}_\delta(f_*)^\perp$.

Theorem 5.2.1 Given a signal $f_* \in \mathcal{H}$, suppose $\{\phi_n\}$ is a frame for $\mathcal{H}$ with operator S, representation operator L, frame correlation R, and frame bounds A and B. Given $\epsilon > 0$, if $\delta = \nu(\epsilon)$ then

$$
\frac{\|f_* - f_\delta\|^2}{\|f_*\|^2} < \epsilon \frac{B}{A},
$$

where

$$
f_\delta \overset{\triangle}{=} L^*(F_{f_*,\delta} R^\dagger F_{f_*,\delta}) L f_* = S^{-1} L^* F_{f_*,\delta} L f_*.
$$

Proof:

First, we establish the formal identity $S^{-1} L^* F_{f_*,\delta} L f_* = L^*(F_{f_*,\delta} R^\dagger F_{f_*,\delta}) L f_*$. We have

$$
\begin{aligned}
S^{-1} L^* F_{f_*,\delta} L f_* &= S^{-1}(F_{f_*,\delta} L)^*(F_{f_*,\delta} L) f_* \\
&= \sum \lambda (I - \lambda L^* L)^j (F_{f_*,\delta} L)^*(F_{f_*,\delta} L) f_* \\
&= \sum (F_{f_*,\delta} L)^*(I - \lambda L L^*)^j (F_{f_*,\delta} L) f_* \\
&= (F_{f_*,\delta} L)^* R^\dagger (F_{f_*,\delta} L) f_* = L^*(F_{f_*,\delta} R^\dagger F_{f_*,\delta}) L f_*.
\end{aligned}
$$

Now, write

$$
f_* - f_\delta = S^{-1} S f_* - S^{-1} L^* F_{f_*,\delta} L f_* = S^{-1} L^*(I - F_{f_*,\delta}) L f_*. \tag{5.2.1}
$$

Because S is a frame operator we have that

$$
\forall g \in \mathcal{H}, \quad A\|g\|^2 \leq \langle S g, g \rangle \leq B\|g\|^2. \tag{5.2.2}
$$

In particular

$$
\begin{aligned}
A\|f_* - f_\delta\|^2 &\leq \left\langle L^*(I - F_{f_*,\delta}) L f_*, S^{-1} L^*(I - F_{f_*,\delta}) L f_* \right\rangle \\
&= \left\langle (I - F_{f_*,\delta}) L f_*, L S^{-1} L^*(I - F_{f_*,\delta}) L f_* \right\rangle \\
&\leq \|(I - F_{f_*,\delta}) L f_*\| \, \|L S^{-1} L^*(I - F_{f_*,\delta}) L f_*\|
\end{aligned}
$$

$$\leq \quad \|LS^{-1}L^*\| \, \|(I - F_{f_*,\delta})Lf_*\|^2$$
$$\leq \quad \|(I - F_{f_*,\delta})Lf_*\|^2$$
$$< \quad \epsilon \|Lf_*\|^2$$
$$\leq \quad \epsilon B \|f_*\|^2,$$

from which the result follows. The manipulations are justified respectively as frame definition, adjoint operator property, Cauchy-Schwarz (and the fact that $\langle f_*, S f_* \rangle$ is real and positive, i.e. S is a positive real operator), operator norm inequality, $\|LS^{-1}L^*\| \leq 1$ (by Fact 2.1.2 $LS^{-1}L^*$ is the orthogonal projection onto the range of L), application of Lemma 5.1.4, and finally $\|L\|^2 \leq B$. ∎

Theorem 5.2.1 shows that with

$$\mathcal{H}_\delta(f_*) \stackrel{\triangle}{=} \operatorname{span}\{\phi_n \;:\; |\langle f_*, \phi_n \rangle| > \delta\} = F_{f_*,\delta}L(\mathcal{H})$$

we have

$$f_* \widetilde{\in} \mathcal{H}_\delta(f_*) \text{ by } \epsilon\tfrac{B}{A},$$

where $\delta = \nu(\epsilon)$. We have decomposed the space $\mathcal{H}$ as

$$\mathcal{H} = \mathcal{H}_\delta(f_*) \;\oplus\; \mathcal{H}_\delta(f_*)^\perp,$$

where $f_* \widetilde{\in} \mathcal{H}_\delta(f_*)$ and $f_* \widetilde{\perp} \mathcal{H}_\delta(f_*)^\perp$.

5.2.2 Local Frame Correlation

In Section 3.3 we examined the properties of a general infinite dimensional frame correlation R. There we saw in Proposition 3.3.3a. that an infinite dimensional frame correlation R is not compact. Local frame correlations, however, are finite dimensional and therefore are compact. This implies the existence of eigenvalues and allows the incorporation of standard matrix techniques such as singular value decompositions to expose the eigen-structure of a local frame correlation matrix. From Proposition 3.3.2 local frame correlations $R_{f_*,\delta} = F_{f_*,\delta}RF_{f_*,\delta}$ are matrices given explicitly as

$$R_{f_*,\delta} = (\phi_{m,n})_{m,n \in J_\delta(f_*)}$$

where

$$J_\delta(f_*) \stackrel{\triangle}{=} \{n \;:\; |\langle f_*, \phi_n \rangle| > \delta\}.$$

The following theorem relates the frame bounds of a local frame to the eigenvalues of the local frame correlation matrix. In particular it shows that the maximum and minimum eigenvalues associated with eigenvectors in the range $L(\mathcal{H})$ are the values of the frame bounds.

Theorem 5.2.2 Let $\{\phi_n\}_{n \in J}$ be a local frame for the finite dimensional Hilbert Space $H = \mathcal{H}_\delta(f_*)$ with local best frame bounds A and B and frame correlation $R_{f_*,\delta}$. Then the frame correlation $R = R_{f_*,\delta}$ is related to the local frame bounds A and B as

$$
\begin{aligned}
A &= \min \sigma_L(R) \\
B &= \max \sigma_L(R),
\end{aligned}
$$

where $\sigma_L(\cdot)$ denotes the spectrum restricted to the range $L(H)$.

Proof:

This may be proven as a corollary to Theorem 3.3.6; however, we give the following direct proof. We shall show that $B = \max \sigma_L(R)$. The proof of the lower limit $A = \min \sigma_L(R)$ is analogous.

(i) $\max \sigma_L(R) \leq B$

Since $\{\phi_n\}$ is a frame for H then L^* is surjective. Hence, for all $f \in H$ there is a $c \in \ell^2(\mathbb{Z})$ so that $f = L^*c$ and by the frame property

$$
\forall c \in L(H) \quad A\|L^*c\|^2 \leq \langle L^*c, SL^*c \rangle \leq B\|L^*c\|^2,
$$

where $S = L^*L$ is the frame operator. This is equivalent to

$$
\forall c \in L(H) \quad A\langle c, LL^*c \rangle \leq \langle L^*c, L^*LL^*c \rangle \leq B\langle c, LL^*c \rangle,
$$

and so

$$
\forall c \in L(H) \quad A \leq \frac{\langle c, R^2c \rangle}{\langle c, Rc \rangle} \leq B.
$$

Letting λ be and eigenvalue of R in $L(H)$, i.e. for some $c \in L(H)$, $Rc = \lambda c$, we have

$$
A \leq \frac{\lambda^2\|c\|^2}{\lambda\|c\|^2} = \lambda \leq B.
$$

Therefore, in particular, $\max \sigma_L(R) \leq B$.

(ii) $\max \sigma_L(R) \geq B$

Now let c_i be the eigenvector associated with the eigenvalue λ_i of R. Since $\mathrm{span}\{c_i\} = L(H)$ then any $c \in L(H)$ may be written as $c = \sum \alpha_i c_i$ for some complex sequence $\{\alpha_i\}$. For all $c \in L(H)$,

$$
\begin{aligned}
\langle c, R^2c \rangle &= \left\langle \sum_i \alpha_i c_i, R^2 \sum_j \alpha_j c_j \right\rangle \\
&= \sum_i \sum_j \langle c_i, R^2 c_j \rangle \\
&= \sum_i \sum_j \lambda_j^2 \langle c_i, c_j \rangle \\
&\leq (\max_j \lambda_j) \sum_i \sum_j \lambda_j \langle c_i, c_j \rangle \\
&\leq \max \sigma_L(R) \langle c, Rc \rangle,
\end{aligned}
$$

so that $B \overset{\triangle}{=} \sup_c \frac{\langle c, R^2c \rangle}{\langle c, Rc \rangle} \leq \max \sigma_L(R)$. ∎

5.3   Compression

Compression of data is a natural goal in applications which seek to minimize the storage or medium capacity needed to hold the information contained in a signal. In this section we describe a general method for data compression using local frames. The method is constructed so that a local representation of an arbitrary signal satisfies a prescribed information constraint. The information constraint is assumed to be a fixed bit rate b_r (bits per second). Accordingly, compression comes from the quantization of local frame representations in such a way as to meet the information constraint. This compression method results in a coding scheme which is hierarchical in the sense that the code generated by the compression method with a low bit rate constraint is embedded in a code generated at higher bit rate constraint. Numerical reconstructions and performance evaluation of the compression method are detailed in Section 6.3.2.

5.3.1   Compression Ratios

When dealing with data and schemes for data compression it is natural to introduce a measure of compression. In simple terms, a "compression ratio" measures the relative decrease in complexity of data in a raw form as compared to the complexity of its new compressed form.

For speech it is customary to deal directly with bit rates instead of compression ratios. This is because the bandwidth of speech is a fixed constant which, for some practical purposes, may be taken to be $\Omega = 4000$ Hz. Consider the "raw" form of an analog speech signal f_* to be a sampled version with 8 bits per sample and a uniform sampling period of $T = 1/(2\Omega) = 1/8000$ seconds. In this case the required "raw" bit rate is 64Kbps. Since the hypotheses of the classical sampling theorem are satisfied, it is possible to reconstruct (modulo slight errors due to quantization) the original speech signal f_*. Any representation which allows for recovery of the original speech signal f_* and requires a bit rate less than 64Kbps is a compressed version of f_*. Consequently, a compression ratio of 10:1 will be achieved by a particular speech compression scheme if that scheme yields a bit rate of 6.4Kbps.

It is clear that a similar calculation can be made for signals from an arbitrary bandlimited space (with a bandlimit other than 4KHz). Since in practice we may consider all signals of interest to be bandlimited, we deal directly with bit rates instead of compression ratios.

5.3.2   Approach

Let us now return to the generic representations in the RKHS $V_g(\mathcal{H})$, viz. Section 4.1. Thus, we specialize to elements $\phi_n = \Pi(x_n)g$. With $\mathcal{H}_V \stackrel{\triangle}{=} \text{span} \{\Pi(x)g\}_{x \in \mathcal{G}}$, let $f_* \in \mathcal{H}_V$ be a signal on the interval I of duration $|I|$ and let L be the frame representation operator for the frame $\{\Pi(x_n)g\}$ so that

$$Lf_* = \{\langle f_*, \Pi(x_n)g \rangle\}$$

is the set of frame coefficients.

It is the frame coefficients which must be transmitted or stored. For representation in digital form, it is necessary that the frame coefficients be quantized. For simplicity, the quantization strategy which we employ is one which maps values uniformly along some interval. This uniform

76

mapping corresponds to specifying each coefficient with a fixed number of bits. The fixed number of bits which we allocate for the representation of each coefficient is denoted by b_c (bits/coef). Let the quantization level set $\{l_k\}_{k=1}^{2^{b_c}}$ be a sequence of increasing real numbers. The quantization function Q_{b_c} is defined in terms of the level set $\{l_k\}_{k=1}^{2^{b_c}}$ as

$$Q_{b_c}(x) = \begin{cases} l_1, & x < l_1, \\ l_k, & x \in [l_k, l_{k+1}), \\ l_{2^{b_c}}, & x \geq l_{2^{b_c}}, \end{cases} \tag{5.3.1}$$

For the values $(m, M) = (1, 2)$ and $b_c = 1, 2, 3$ the uniform quantization function is plotted in Figure 5.2. For quantization of the frame coefficients the dynamic range of interest is (m, M) and where

$$M \equiv \|Lf_*\|_\infty \equiv \sup_n \{|\langle f_*, \phi_n \rangle|\} \tag{5.3.2}$$

and m may be chosen in a number of ways, e.g., viz. Section 6.3.2. A uniform quantization is performed by the function Q_{b_c} if the level set $\{l_k\}_{k=1}^{2^{b_c}}$ has elements

$$l_k = m + \left(\frac{2k-1}{2^{b_c+1}}\right)(M - m).$$

We shall specify the inherent constraint on the amount of information which we can transmit per unit time as a maximum allowable bit rate of b_r bps (bits per second). For convenience, we do not fix this quantity explicitly. Instead, we specify a corresponding coefficient rate c_r, and vary the bit allocation b_c to meet the information rate constraint b_r, through the simple relation $b_r = c_r b_c$. With the coefficient rate fixed and specified, the maximum number of coefficients n_c that we are able to transmit for the function f_* of duration $|I|$ is

$$n_c = c_r |I|.$$

Thus, given the acoustic signal f_* of duration $|I|$ and a fixed coefficient rate, the maximum number of coefficients with which f_* may be represented, while still satisfying the information rate constraint, is given by n_c. With respect to the frame coefficients, this maximum number of coefficients n_c can further be related to a value for a threshold δ. To see this, we introduce the *coefficient distribution function*,

$$\lambda(\delta) \overset{\triangle}{=} \dim F_{f_*, \delta} L(\mathcal{H}) = \text{card}\{\langle f_*, \psi_{m,n}\rangle \geq \delta\}, \tag{5.3.3}$$

for $\delta \in [-M, M]$. The coefficient distribution function $\lambda : [-M, M] \mapsto \mathbb{N}$ is monotonically decreasing and continuous from the left. We may associate with λ an 'inverse' λ^{-1} defined as

$$\lambda^{-1}(n) \equiv \inf\{x \in [-M, M] : \lambda(x) < n\},$$

where $n \in \mathbb{N}$. If a threshold value δ is chosen as

$$\delta = \lambda^{-1}(n_c),$$

then the thresholded frame representation $F_{f_*, \delta} L(f_*)$ will have a cardinality

$$\dim F_{f_*, \lambda^{-1}(n_c)} L(\mathcal{H}) \leq n_c.$$
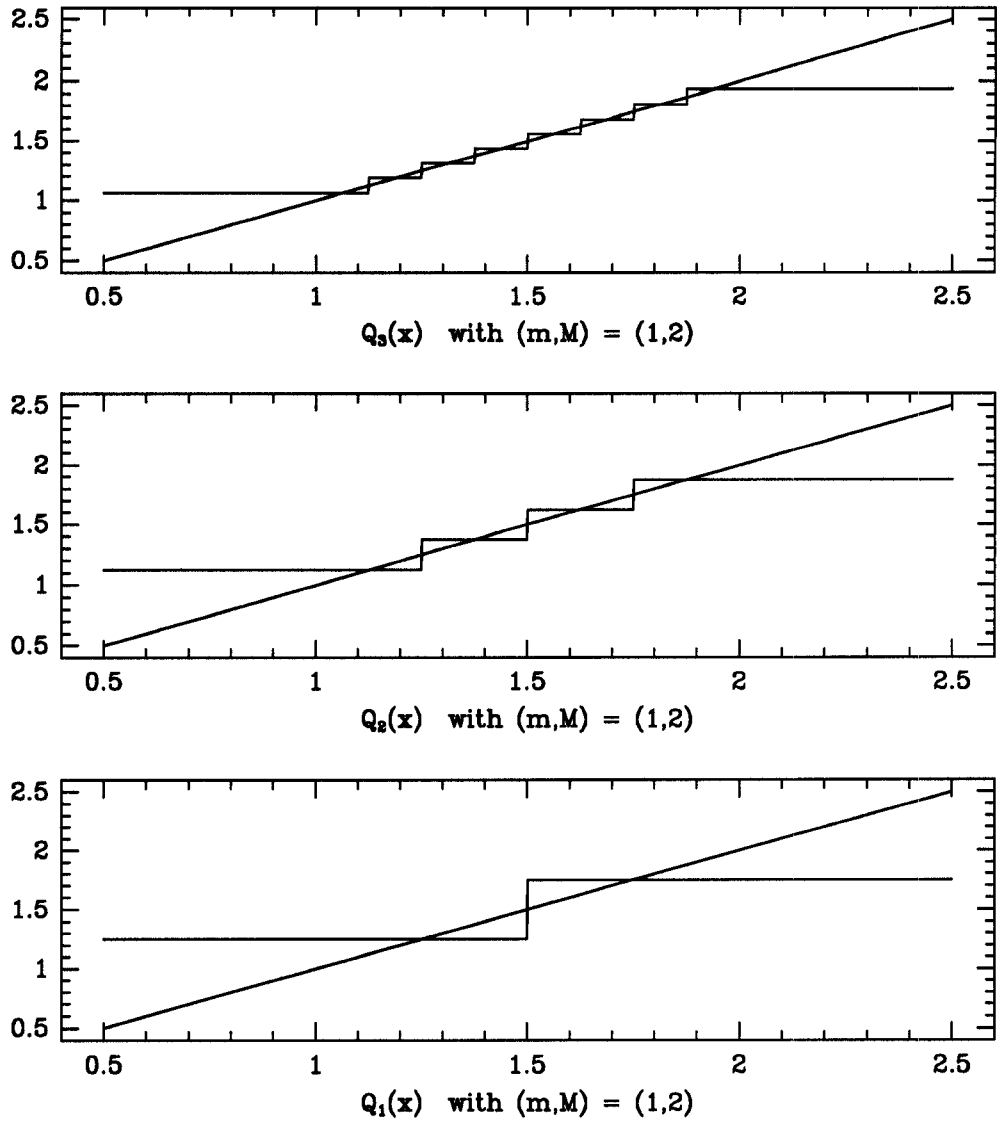
Figure 5.2: Uniform quantization with $(m, M) = (1, 2)$ for $b_c = 1, 2, 3$.

Consequently, the total bit requirement for representing the acoustic signal f_* of duration $|I|$ in b_c bits/coefficient is no greater than $n_c b_c$ bits. This, in turn, guarantees that the local frame encoding of the signal f_* is compatible with the bit rate constraint, i.e.,

$$b_c \ \dim F_{f_*, \lambda^{-1}(n_c)} L(\mathcal{H}) \leq b_r |I|.$$

A numerical experiment based on this scheme for data compression is detailed in Section 6.3.2. There the method is applied to real speech signals as well as synthesized data.

Chapter 6

Applications and Results

In this chapter we numerically validate and demonstrate the utility of the discrete representation theory developed in this thesis. For several test signals discrete representations are computed and displayed for the cases of Paley-Wiener and wavelet representations. Further, for the cases of the Paley-Wiener and wavelet representations the test signals are reconstructed from a variety of discrete representations. Finally, numerical experiments investigating the noise suppression and compression abilities of discrete positive extrema (PE) wavelet representations are presented.

6.1   Test Signals

To illustrate various discretizations and signal processing tasks, we have chosen a set of four basic test signals. Three of these four signals are synthetic and designed to have interesting time-frequency behavior. The third signal is a real speech signal taken from the TIMIT [1] speech corpus. These four signals are respectively labeled "chirp", "packet", "harmonic" and "water". Throughout this section the function A is a smooth positive window function of compact support which is realized as one half period of a sine wave centered about the origin, i.e.

$$A_L(t) \stackrel{\triangle}{=} \begin{cases} \sin\left(\frac{\pi}{L}(t + L/2)\right), & t \in (-L/2, L/2) \\ 0, & \text{otherwise,} \end{cases} \tag{6.1.1}$$

where L is the length of the interval of support of A_L. For convenience we define a second window function A_L^+ which is a shifted version of A_L having support starting at zero as

$$A_L^+ \stackrel{\triangle}{=} \tau_{L/2} A_L.$$

We now describe the test signals.

Sine Packet

Shown in Figure 6.1, is a synthetic signal which is a time progression of three windowed sine waves. We shall refer to this signal as "packet". Each successive windowed sine has a

---

[1]The TIMIT speech corpus is a data base consisting of phonemically balanced sentences spoken by people of different dialects throughout the United States.
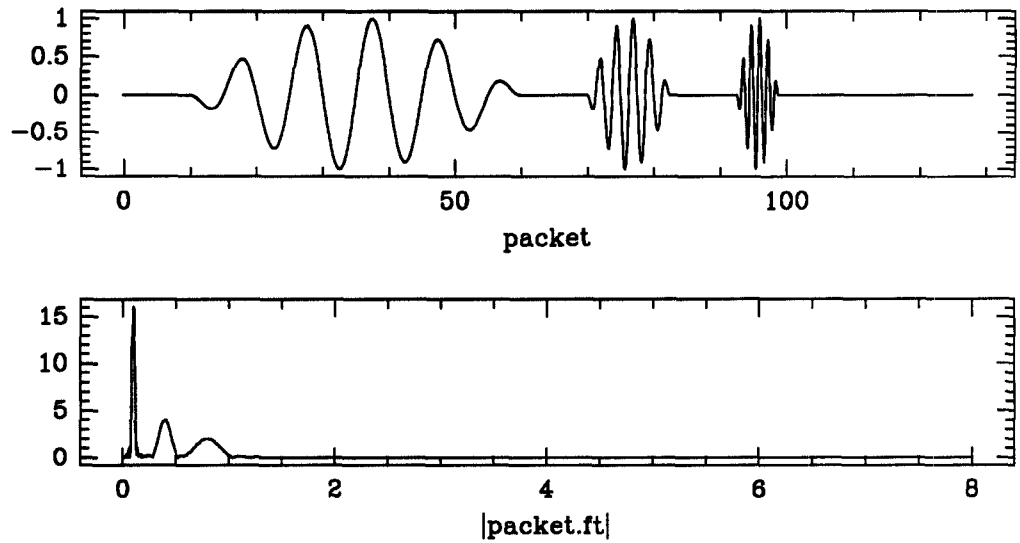
Figure 6.1: The signal "packet" and its magnitude Fourier transform.

higher frequency than then its predecessor. The windows are non-overlapping and compactly supported with an interval of support equal to 5 periods of the corresponding sine wave. The sine packet sequence is given by

$$\sum_{k=1}^{N} A_{5/\omega_k}(t - t_k)\sin(2\pi\omega_k t),$$

where $N = 3$, A_{5/ω_k} is the window function of (6.1.1) with $L = 5/\omega_k$ and $(\omega_1, \omega_2, \omega_3) = (100, 400, 900)$ Hz.

Chirp

In general, a chirp signal may be given by

$$A_L(t)\sin(at^\alpha),$$

where $a > 0$ and $\alpha > 1$ are constants and A_L is the window function with support on an interval of length L. Intuitively, the "instantaneous" frequency of a chirp signal as a function of time is increasing. The specific chirp signal which we use and refer to as "chirp" has the values $a = 0.03$, $\alpha = 1.8$. The signal "chirp" is plotted in Figure 6.2.

Harmonic

Figure 6.3 displays the second synthetic signal which we shall refer to as "harmonic". It consists of a windowed portion of the superposition of three sine waves with harmonically related frequencies. The harmonic signal is given by

$$A(t)\sum_{k=1}^{N} a_k \sin(2\pi k\omega_0 t)$$

where $N = 4$, A is the window function, $a_k = 1$, for $k = 1, 2, 4$, $a_3 = 0$ and $\omega_0 = 100$ Hz.

80
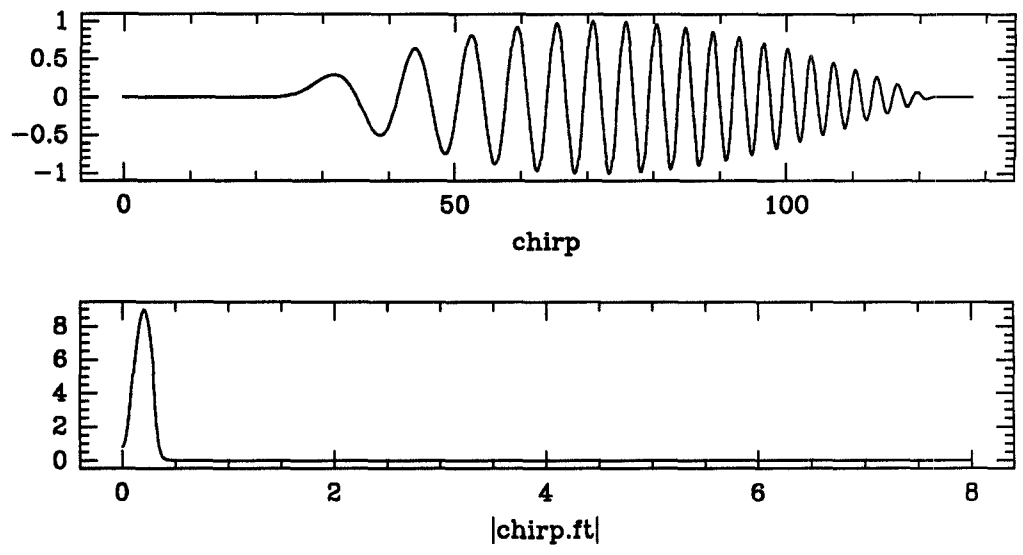
Figure 6.2: Chirp signal and its magnitude Fourier transform.

Female spoken "water"

The third signal is a real speech signal as spoken by a female speaker from the TIMIT data base. The word "water" is taken from the TIMIT sentence [2] "She had your dark suit in greasy wash water all year". This signal is depicted in Figure 6.4.

---

[2] The exact reference to the TIMIT data base is sentence "sa1", speaker "fdaw0".
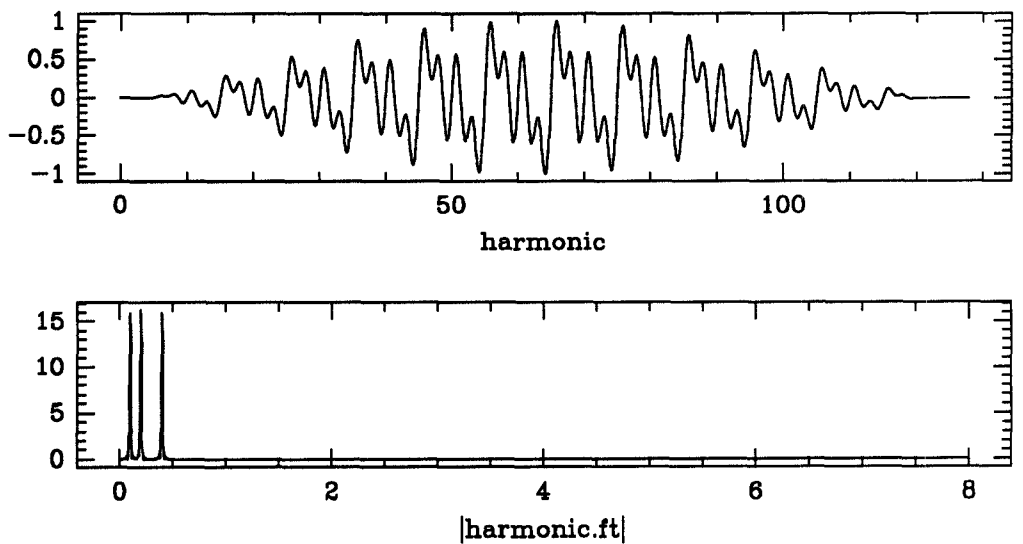
Figure 6.3: The signal "harmonic" and its magnitude Fourier transform.
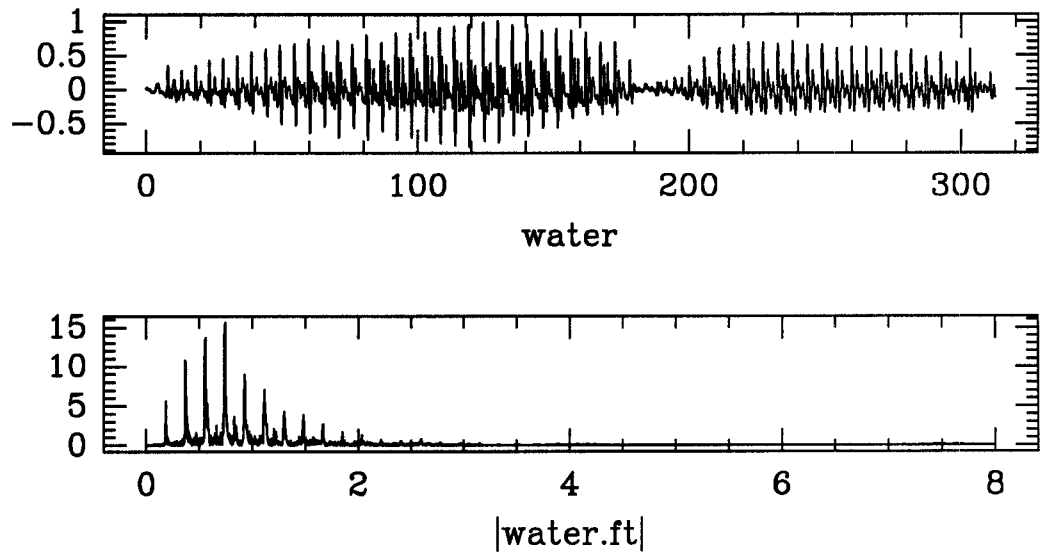
Figure 6.4: Female spoken "water" and its magnitude Fourier Transform.

6.2 Numerical Reconstruction

The main question put to test the validity of any discrete representation is whether it contains enough information about the underlying signal to be able to recover it. One goal of this section is to numerically illustrate the theory of discrete (local) representations developed in this thesis on real signals. In particular, we shall provide numerous examples of discrete representations and their corresponding reconstructions.

We first examine discrete representations in the Paley Wiener spaces. Here, we provide examples of discrete representations of bandlimited signals directly by its samples. Second, we provide discrete wavelet representations of the test signals and illustrate by example how such time-frequency discrete representations are useful in speech processing for noise suppression and compression.

6.2.1 Sampling in Paley-Wiener Spaces

The most natural discrete representation of a signal is through its direct sampling. For bandlimited signals there are direct sampling discrete representations which admit full reconstruction of the original signal, viz. Section 4.2.1. In this section we provide some examples of discrete representations in bandlimited spaces and numerically illustrate the iterative reconstruction process, viz. Algorithms 3.4.3 and 3.5.3.

Let $\Omega > 0$ be the finite constant bandlimit. The representation of a signal $f \in PW_\Omega$ is

$$Lf = \{f(t_n)\}, \tag{6.2.1}$$

where $\{t_n\} \subseteq \mathbb{R}$ is the sampling set and L is the representation operator, cf. Section 4.1 and Table 4.2. For the Paley-Wiener space PW_Ω we examine four different types of sampling:

uniform, Kadec-Levinson, jitter, and extrema. Each type of sampling is fully explained in the sections below. Except for the last type of sampling, all of these strategies are signal independent, i.e. global.

6.2.1.1 Uniform Sampling

Uniformly sampled representations of bandlimited signals is the most commonly employed representation for signal processing. The uniformly sampled representation of a signal $f \in PW_\Omega$ is given by (6.2.1) where the sampling set Γ is

$$\Gamma = \Gamma_T = \{nT\}$$

and where T is the sampling period. For perfect reconstruction of every signal in PW_Ω from its uniform samples on Γ_T the classical sampling Theorem 4.2.3 gives the necessary and sufficient condition that $2T\Omega < 1$.

Figures 6.5 through 6.8 illustrate the iterative reconstruction of the signals in the test set from their respective uniform samples. Each figure indicates the value of Ω used to determine the sampling period T. In each case the sampling period is taken to be $T = 1/2\Omega$.
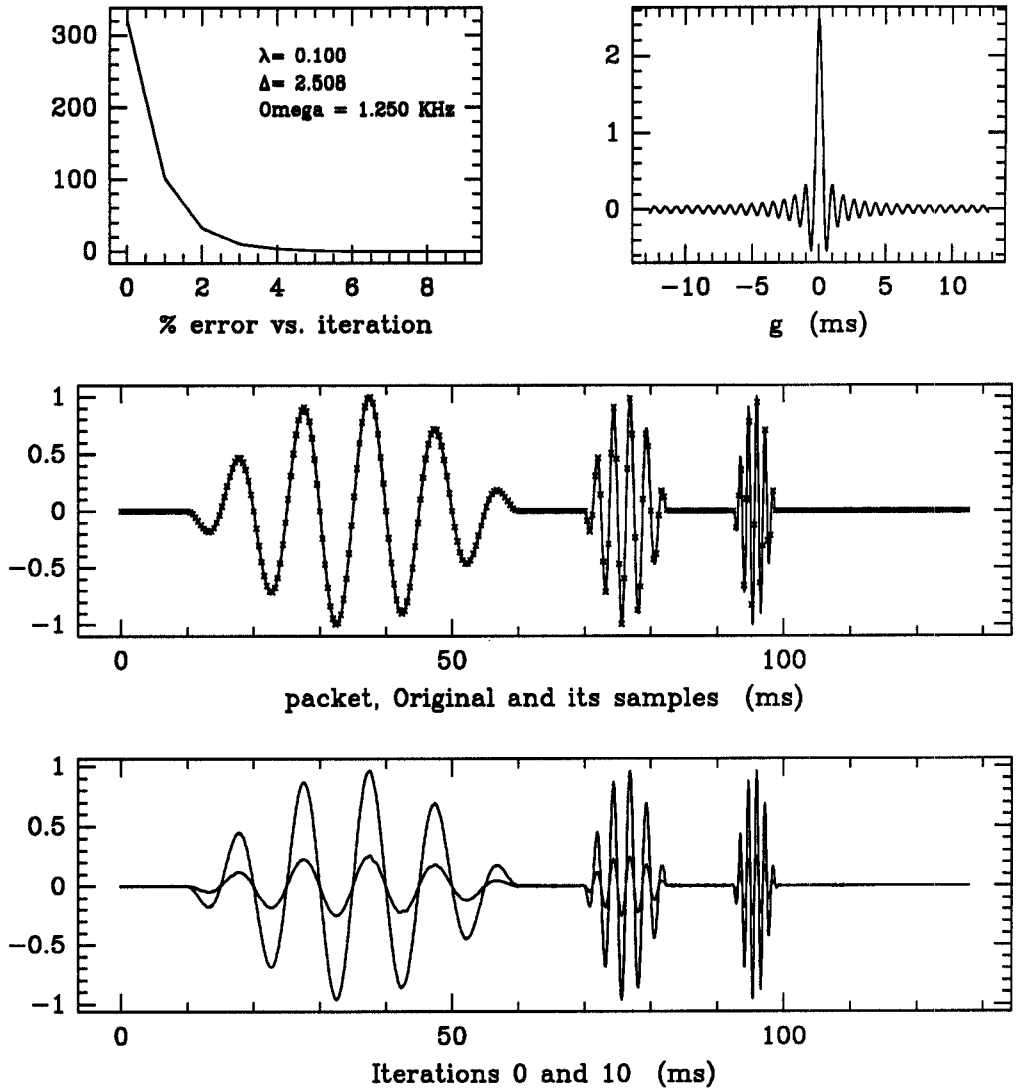
Figure 6.5: Reconstruction of "packet" from its uniform samples.

The above figure shows the uniform representation of the signal "packet" and its iterative reconstruction using Algorithm 3.4.3. The L^2-error is plotted as a function of the iteration number in the upper left graph which also contains the values of the simulation parameters. To its right is the reconstructing dirichlet function. The middle graph shows the original signal and its uniform samples and the iterative reconstruction is shown in the very bottom graph.
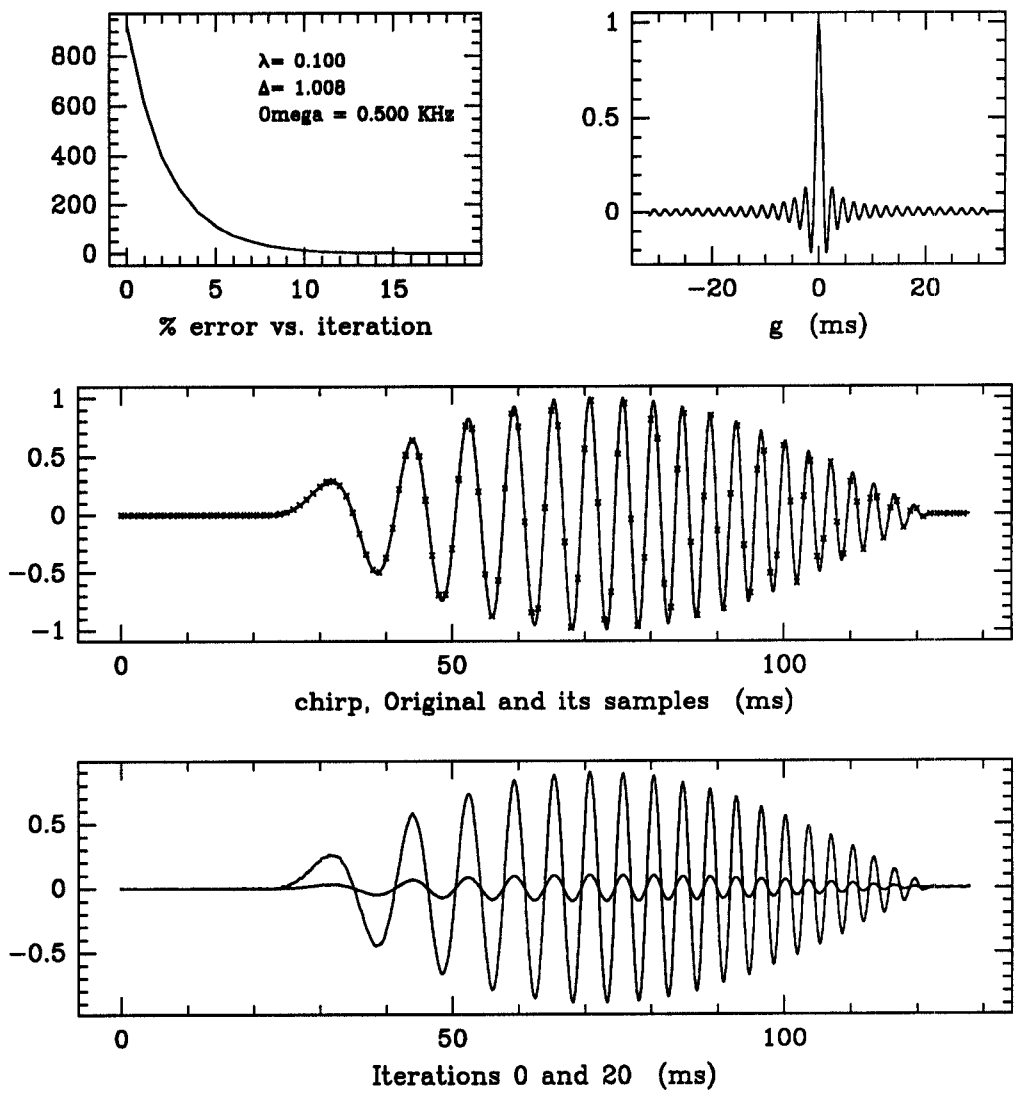
Figure 6.6: Reconstruction of "chirp" from its uniform samples.

The above figure shows the uniform representation of the signal "chirp" and its iterative reconstruction using Algorithm 3.4.3. The L^2-error is plotted as a function of the iteration number in the upper left graph which also contains the values of the simulation parameters. To its right is the reconstructing dirichlet function. The middle graph shows the original signal and its uniform samples and the iterative reconstruction is shown in the very bottom graph.
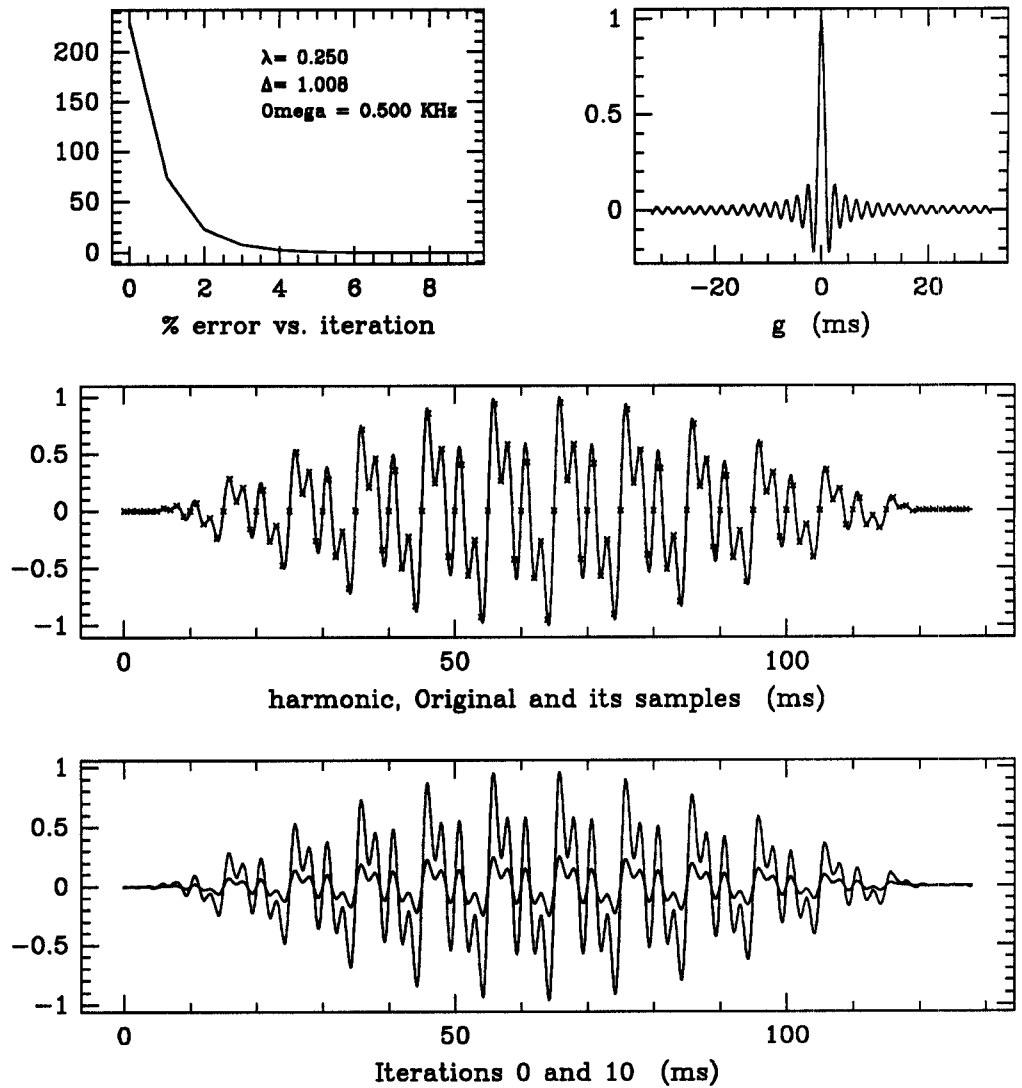
Figure 6.7: Reconstruction of "harmonic" from its uniform samples.

The above figure shows the uniform representation of the signal "harmonic" and its iterative reconstruction using Algorithm 3.4.3. The L^2-error is plotted as a function of the iteration number in the upper left graph which also contains the values of the simulation parameters. To its right is the reconstructing dirichlet function. The middle graph shows the original signal and its uniform samples and the iterative reconstruction is shown in the very bottom graph.
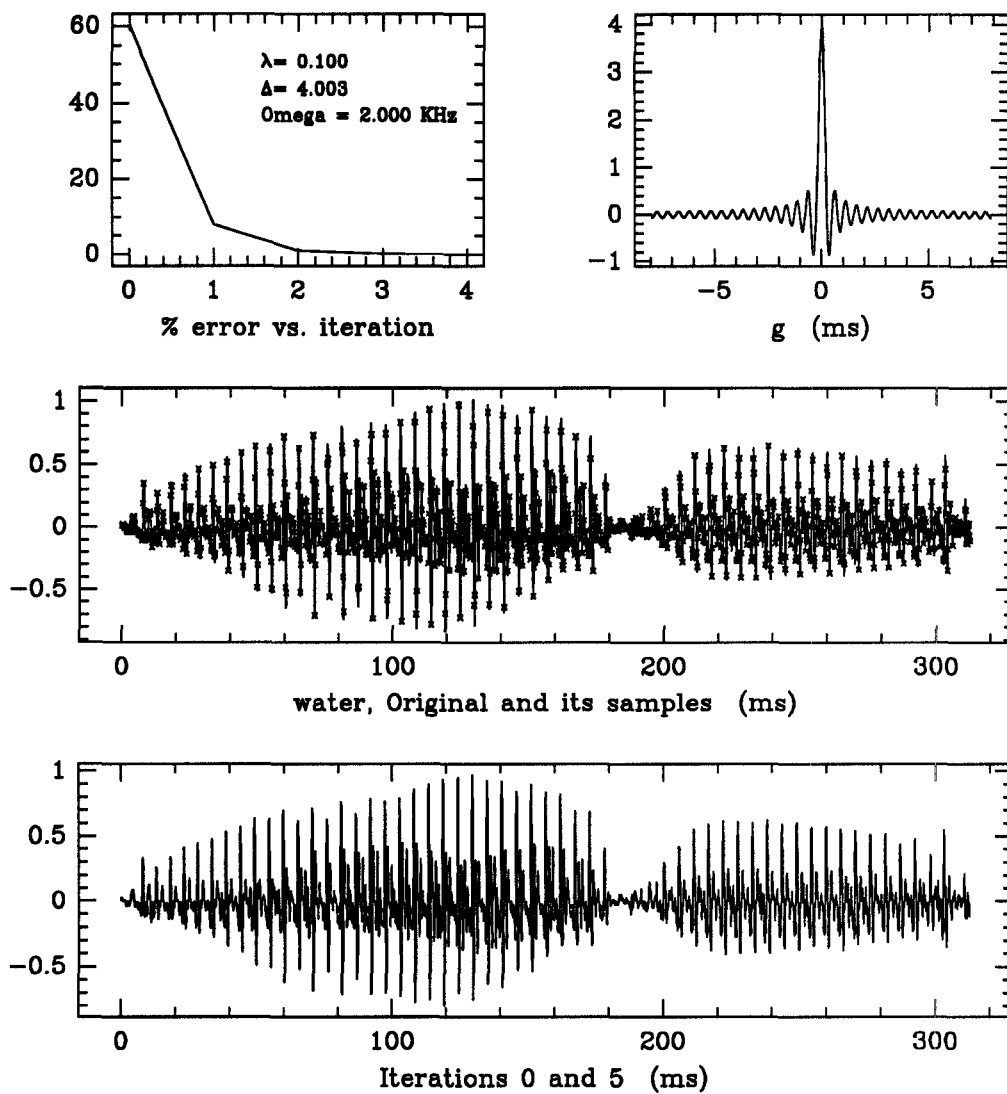
Figure 6.8: Reconstruction of "water" from its uniform samples.

The above figure shows the uniform representation of the signal "water" and its iterative reconstruction using Algorithm 3.4.3. The L^2-error is plotted as a function of the iteration number in the upper left graph which also contains the values of the simulation parameters. To its right is the reconstructing dirichlet function. The middle graph shows the original signal and its uniform samples and the iterative reconstruction is shown in the very bottom graph.

6.2.1.2 Kadec-Levinson Sampling

A Kadec-Levinson representation of a signal $f \in PW_\Omega$ is given by (6.2.1) where the sampling set $\Gamma = \{t_n\}$ satisfies

$$|t_n - \frac{n}{2\Omega}| < \frac{1}{4}\left(\frac{1}{2\Omega}\right)$$

for all n. viz. Definition 4.2.6. By Theorem 4.2.7 a Kadec-Levinson sequence implies that $\{e_{-t_n}\}$ is an exact frame for PW_Ω. Hence, we may reconstruct any signal $f \in PW_\Omega$ from its Kadec-Levinson representation using either Algorithm 3.4.3 or 3.5.3.

Figures 6.9 through 6.12 illustrate the iterative reconstruction of the signals in the test set from their respective Kadec-Levinson representations. Each figure indicates the value of Ω used to determine the Kadec-Levinson sampling. In each case the sample sequence is generated randomly to conform to the Kadec-Levinson condition as

$$t_n = \left(n + \sigma_n \frac{1}{4}\right)\frac{1}{2\Omega}$$

where $\{\sigma_n\}$ is a sequence of independently identically distributed random variables with uniform distribution on $(-1, 1)$.
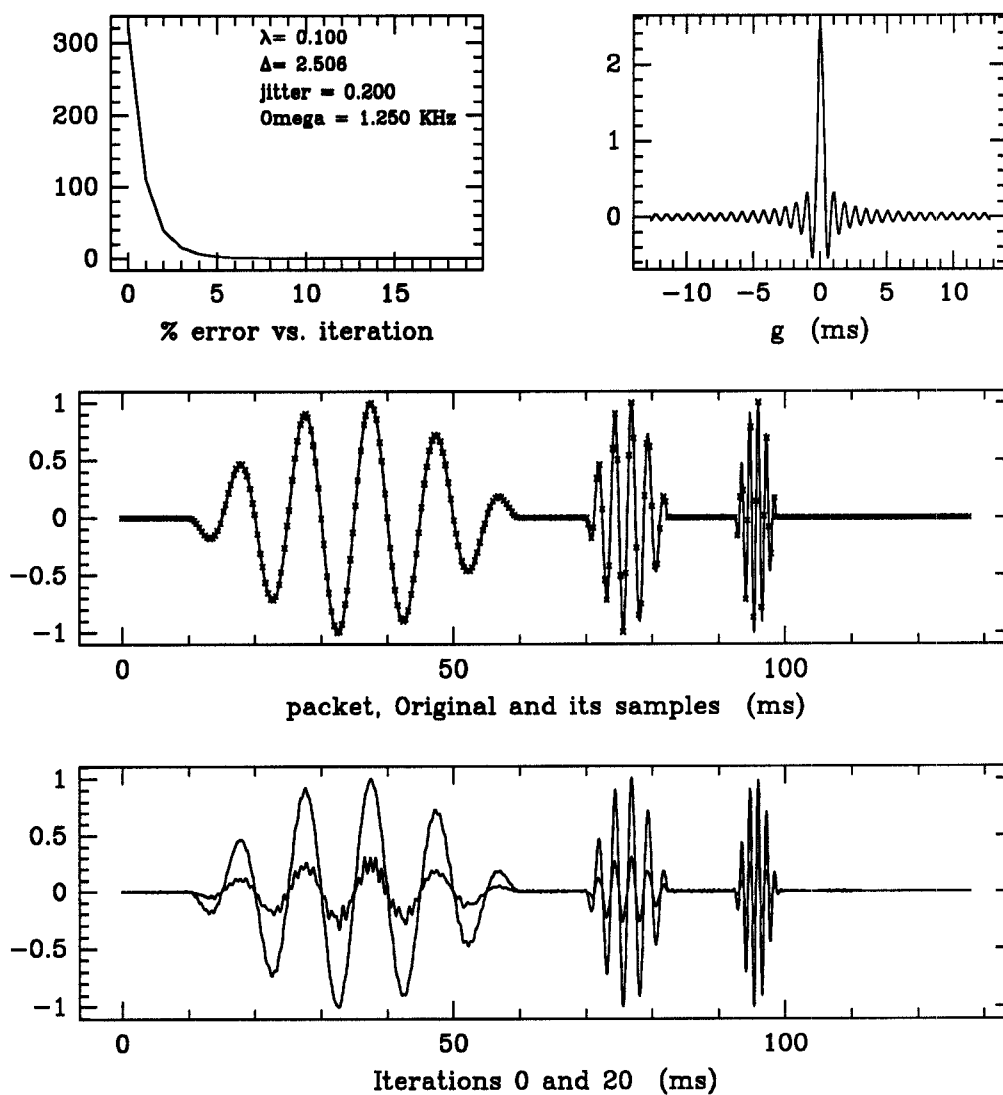
Figure 6.9: Reconstruction of "packet" from its Kadec-Levinson samples.

The above figure shows the Kadec-Levinson representation of the signal "packet" and its iterative reconstruction using Algorithm 3.4.3. The L^2-error is plotted as a function of the iteration number in the upper left graph which also contains the values of the simulation parameters. To its right is the reconstructing dirichlet function. The middle graph shows the original signal and its Kadec-Levinson samples and the iterative reconstruction is shown in the very bottom graph.
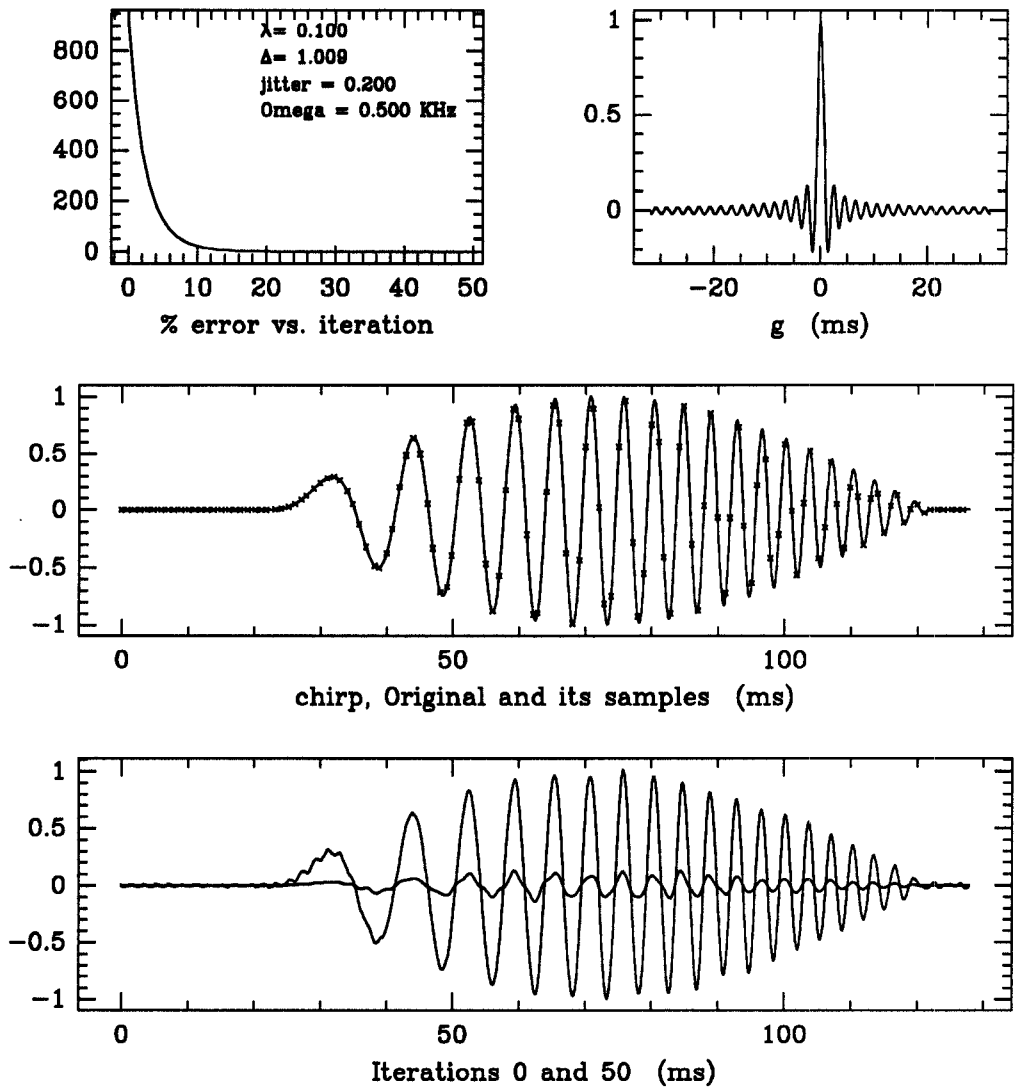
Figure 6.10: Reconstruction of "chirp" from its Kadec-Levinson samples.

The above figure shows the Kadec-Levinson representation of the signal "chirp" and its iterative reconstruction using Algorithm 3.4.3. The L^2-error is plotted as a function of the iteration number in the upper left graph which also contains the values of the simulation parameters. To its right is the reconstructing dirichlet function. The middle graph shows the original signal and its Kadec-Levinson samples and the iterative reconstruction is shown in the very bottom graph.
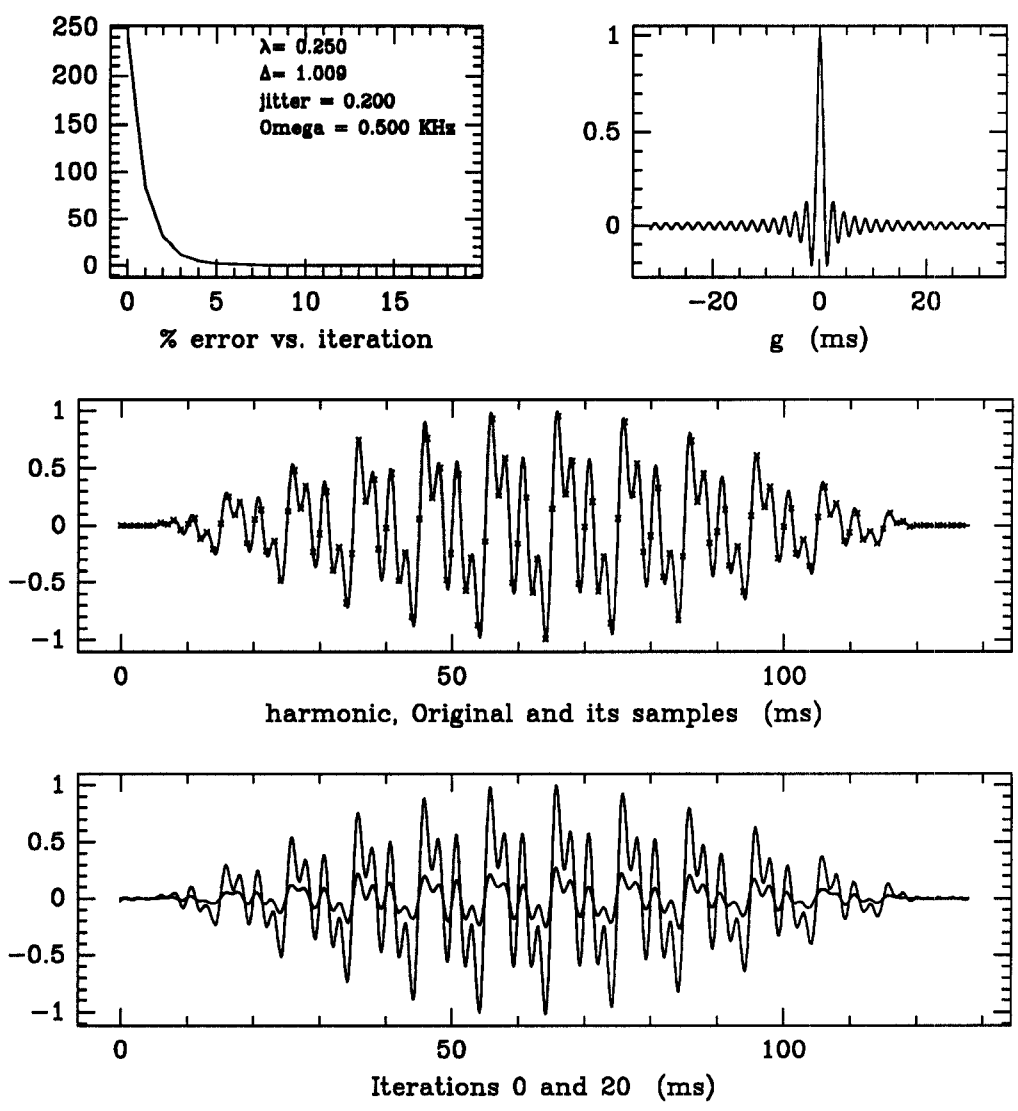
Figure 6.11: Reconstruction of "harmonic" from its Kadec-Levinson samples.

The above figure shows the Kadec-Levinson representation of the signal "harmonic" and its iterative reconstruction using Algorithm 3.4.3. The L^2-error is plotted as a function of the iteration number in the upper left graph which also contains the values of the simulation parameters. To its right is the reconstructing dirichlet function. The middle graph shows the original signal and its Kadec-Levinson samples and the iterative reconstruction is shown in the very bottom graph.
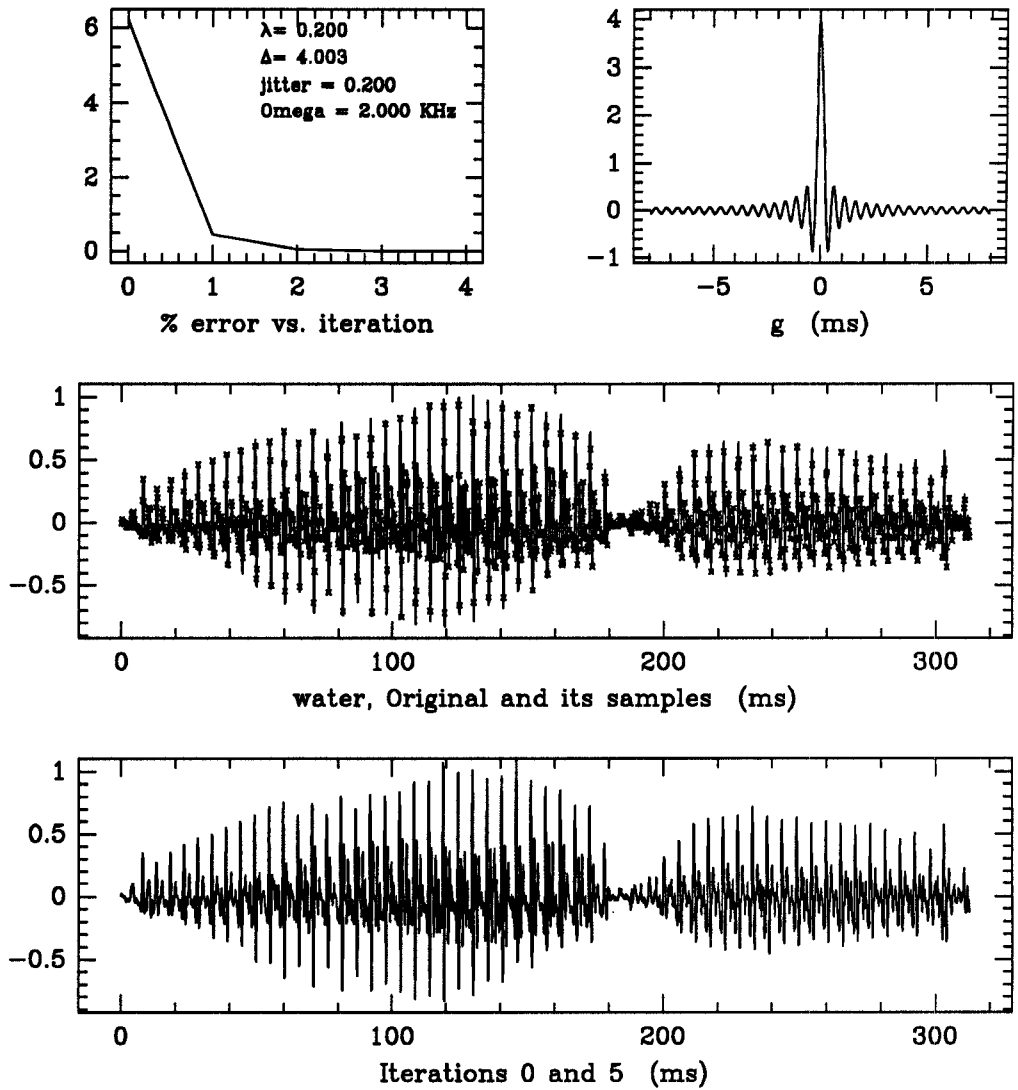
Figure 6.12: Reconstruction of "water" from its Kadec-Levinson samples.

The above figure shows the Kadec-Levinson representation of the signal "water" and its iterative reconstruction using Algorithm 3.4.3. The L^2-error is plotted as a function of the iteration number in the upper left graph which also contains the values of the simulation parameters. To its right is the reconstructing dirichlet function. The middle graph shows the original signal and its Kadec-Levinson samples and the iterative reconstruction is shown in the very bottom graph.

6.2.1.3 Jitter Sampling

Jitter sampling sequences are similar to Kadec-Levinson sequences except that they allow a larger constant than the constant 1/4 required in the Kadec-Levinson condition. However, it is still necessary that the jittered sequence be a uniformly discrete sequence, viz. Section 2.5.2. From the point of view of frame reconstructions, the Duffin and Schaeffer Theorem 4.2.4 requires that the uniform density $\Delta\Gamma$ of the sampling sequence Γ satisfy $\Delta\Gamma > 2\Omega$. If this condition is satisfied we may reconstruct any signal $f \in PW_\Omega$ from its jittered representation using either Algorithm 3.4.3 or 3.5.3.

Figures 6.13 through 6.16 illustrate the iterative reconstruction of the signals in the test set from their respective jittered representations. Each figure indicates the value of Ω used to determine the jittered sampling sequence. In each case the sample sequence is generated randomly as

$$t_n = (n + \sigma_n\beta)\frac{1}{2\Omega}$$

where $\{\sigma_n\}$ is a sequence of independently identically distributed random variables with uniform distribution on $(-1, 1)$ and $\beta = 0.4$.
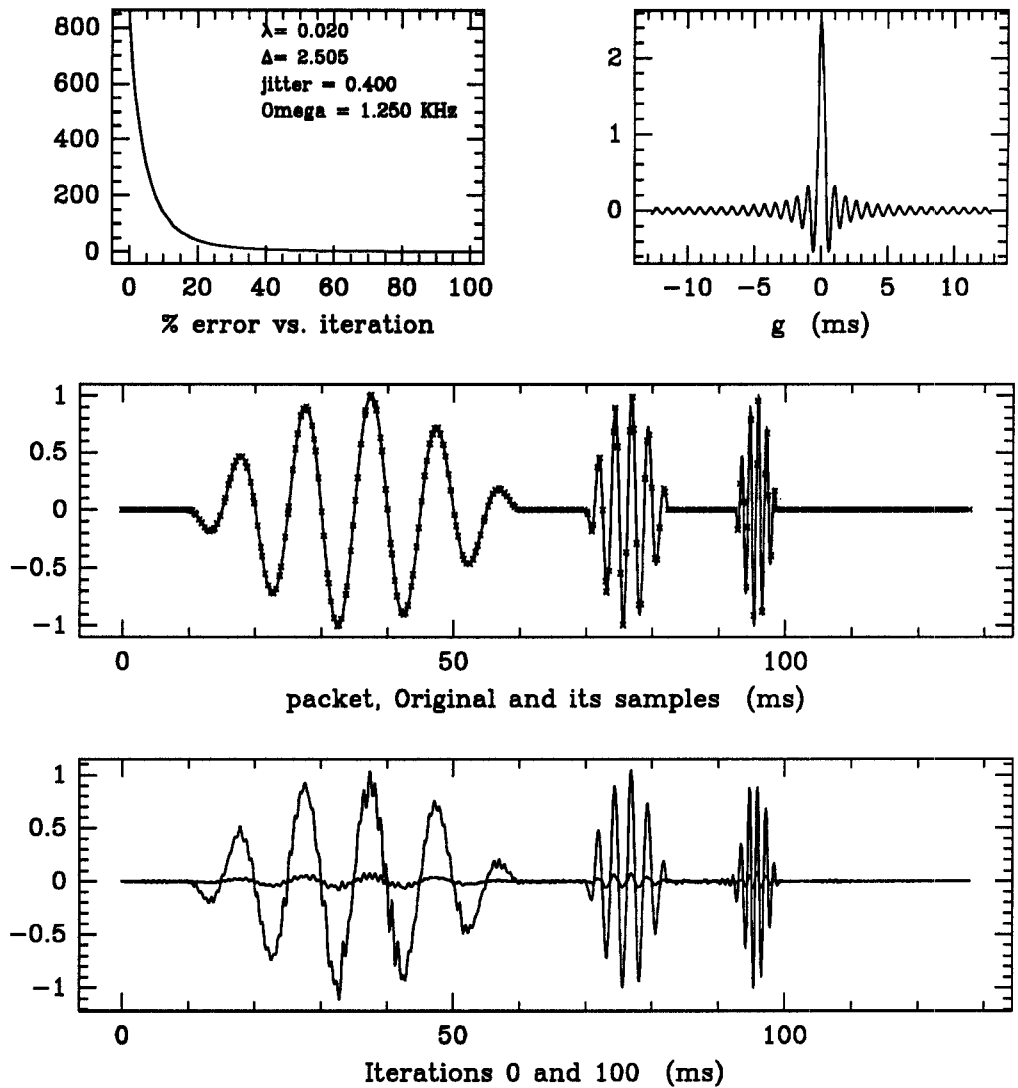
Figure 6.13: Reconstruction of "packet" from its jittered samples.

The above figure shows the jittered representation of the signal "packet" and its iterative reconstruction using Algorithm 3.4.3. The L^2-error is plotted as a function of the iteration number in the upper left graph which also contains the values of the simulation parameters. To its right is the reconstructing dirichlet function. The middle graph shows the original signal and its jittered samples and the iterative reconstruction is shown in the very bottom graph.
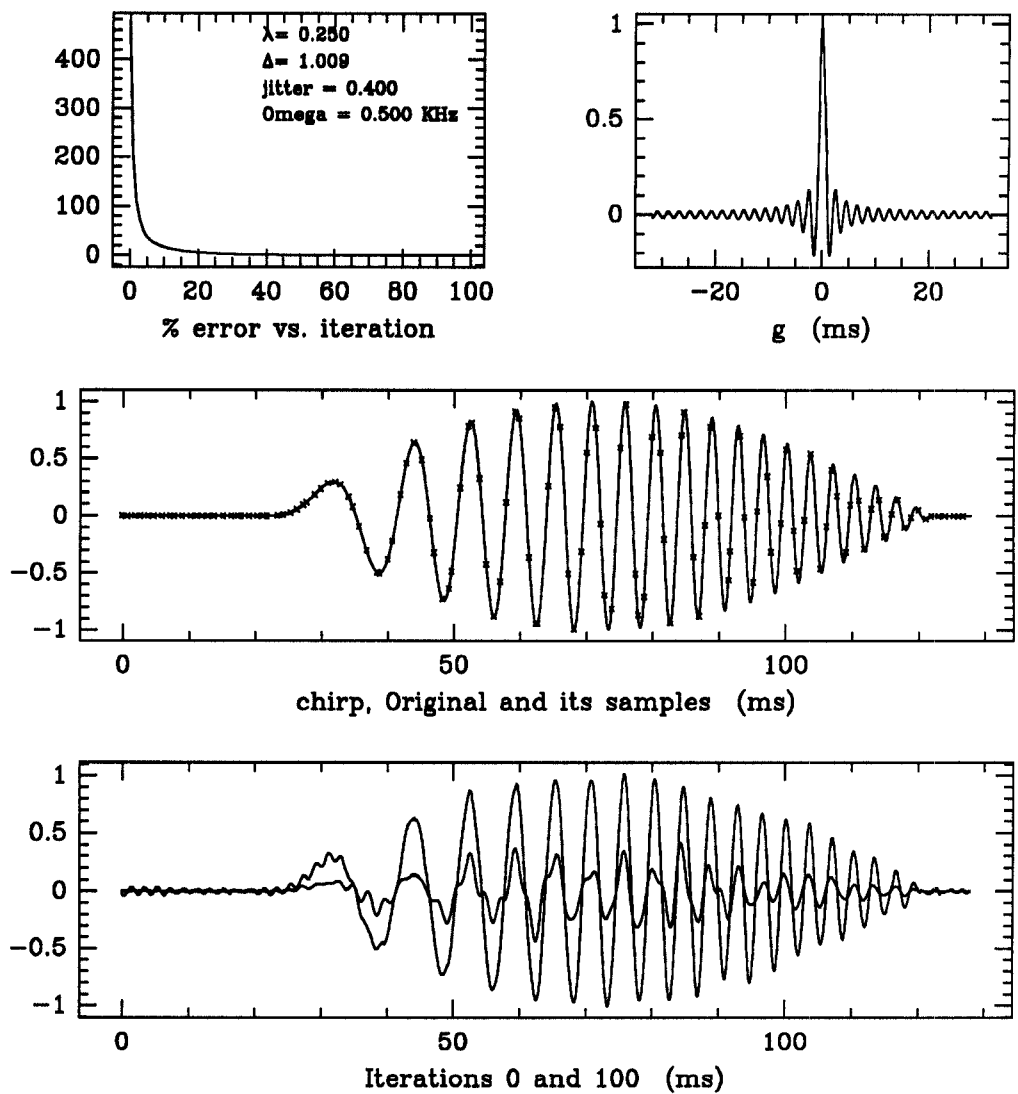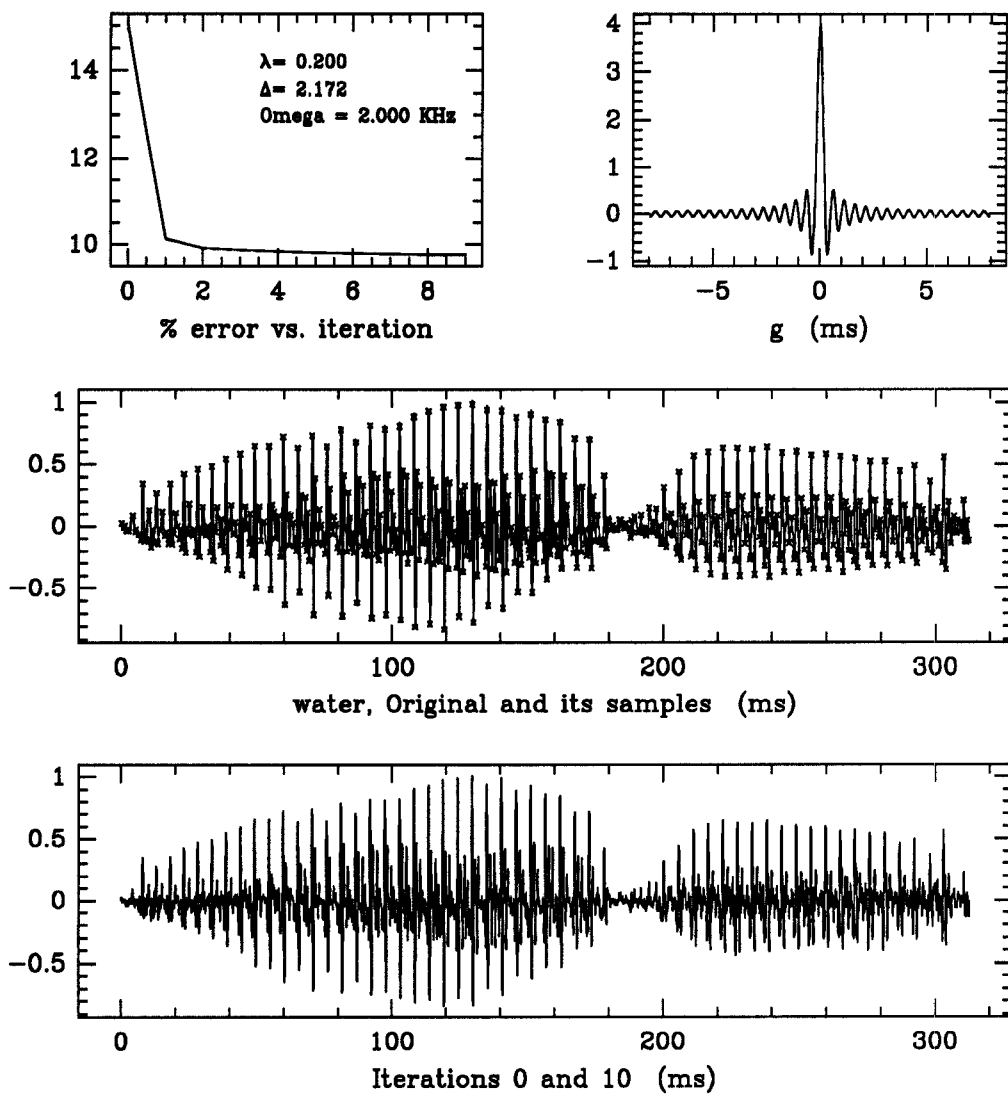
Figure 6.14: Reconstruction of "chirp" from its jittered samples.

The above figure shows the jittered representation of the signal "chirp" and its iterative reconstruction using Algorithm 3.4.3. The L^2-error is plotted as a function of the iteration number in the upper left graph which also contains the values of the simulation parameters. To its right is the reconstructing dirichlet function. The middle graph shows the original signal and its jittered samples and the iterative reconstruction is shown in the very bottom graph.
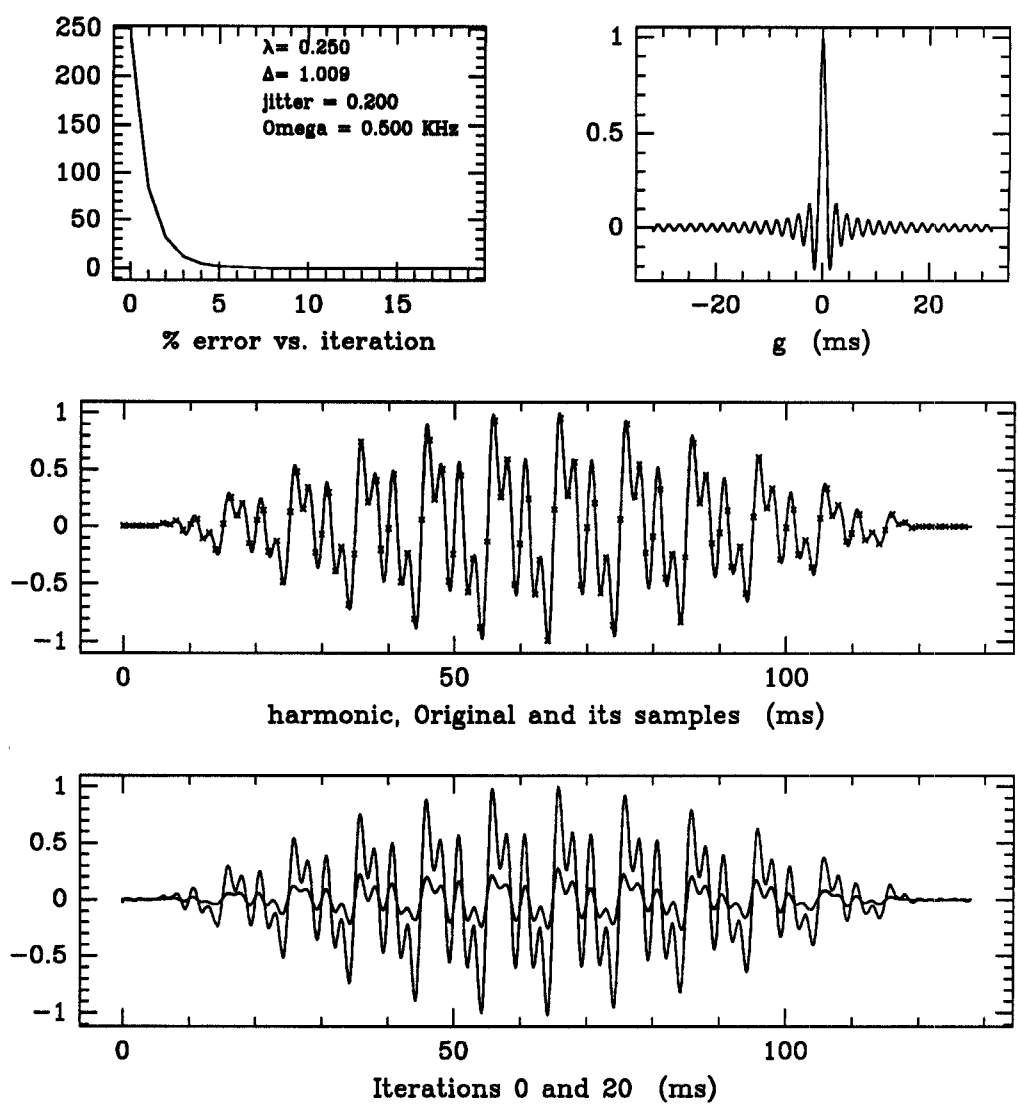
Figure 6.15: Reconstruction of "harmonic" from its jittered samples.

The above figure shows the jittered representation of the signal "harmonic" and its iterative reconstruction using Algorithm 3.4.3. The L^2-error is plotted as a function of the iteration number in the upper left graph which also contains the values of the simulation parameters. To its right is the reconstructing dirichlet function. The middle graph shows the original signal and its jittered samples and the iterative reconstruction is shown in the very bottom graph.
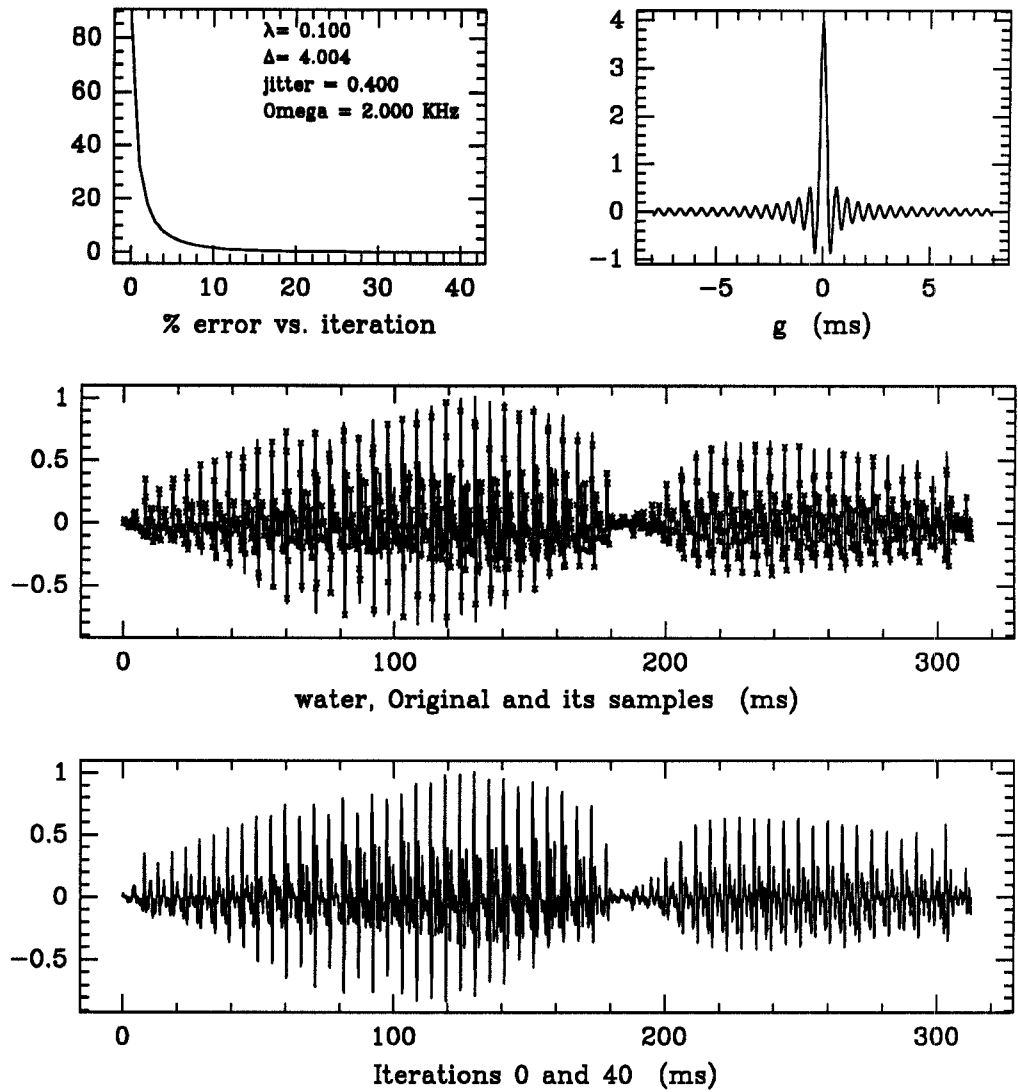
Figure 6.16: Reconstruction of "water" from its jittered samples.

The above figure shows the jittered representation of the signal "water" and its iterative reconstruction using Algorithm 3.4.3. The L^2-error is plotted as a function of the iteration number in the upper left graph which also contains the values of the simulation parameters. To its right is the reconstructing dirichlet function. The middle graph shows the original signal and its jittered samples and the iterative reconstruction is shown in the very bottom graph.

6.2.1.4 Extrema Sampling

Using the theory of local frames developed in Chapter 5, we argue that there are classes of signals for which their local extrema locations form local frames of complex exponentials around each signal in the class.

To see this, consider the windowed sine function $f_*(t) = A(t)\sin(2\pi\Omega_0 t)$ of frequency $\Omega_0 > 0$. Also consider the sampling set

$$\Gamma(f_*) = \Gamma^{(0)}(f_*) \bigcup \Gamma^{(1)}(f_*)$$

where $\Gamma^{(k)}(f_*) = \left\{ t \ : \ f_*^{(k)}(t) = 0 \right\}$ is the kth moment sampling set, viz. Section 5.1.1. Here we assume that A is a strictly positive window function which has compact support in frequency.

For this f_* we can easily determine the sampling set Γ to be $\Gamma(f_*) = \left\{ \frac{n}{4\Omega_0} \right\}$. Thus, $\Gamma(f_*)$ is a uniform sampling set with density $\Delta\Gamma(f_*) = 4\Omega_0$. With $\Omega < 2\Omega_0$, it follows from the Duffin-Schaeffer Theorem 4.2.4 that $\{e_{-t_n}\}$ is a frame for $L^2[-\Omega, \Omega]$ or equivalently that the set $\{\tau_{-t_n} d_{2\pi\Omega}\}$ is a frame for PW_Ω. Consequently any function in PW_Ω may be reconstructed from its sample values on $\Gamma(f_*)$. In particular, if f_* were in PW_Ω for some $\Omega < 2\Omega_0$ then it could be reconstructed from its extrema and zero crossing sampling set $\Gamma(f_*)$ as

$$f_* = L^* R^\dagger L f_*$$

where R is the frame correlation and L is the frame representation

$$\forall f \in PW_\Omega, \quad Lf = \{f(t)\}_{t \in \Gamma(f_*)}.$$

To complete the argument we need only note that for the particular signal f_*

$$L^* R^\dagger L f_* = L^* R^\dagger L_1 f_*$$

where L_1 is the representation associated with only the extrema set $\Gamma^{(1)}(f_*)$, i.e. $L_1 f = \{f(t)\}_{t \in \Gamma^{(1)}(f_*)}$. This statement can most easily be verified through the observation that for a general frame $\{\phi_n\}$ for a Hilbert space $\mathcal{H}$

$$\forall f \in \mathcal{H}, \quad f = L^* R^\dagger L f = L_\psi^* L f = \sum \langle f, \phi_n \rangle \psi_n$$

where $\{\psi_n\}$ is the dual frame with frame representation L_ψ. Thus, eliminating terms for which $\langle f, \phi_n \rangle = 0$ has no effect on the reconstruction.

If the window function is such that $f_* \in PW_\Omega$ for some $\Omega < 2\Omega_0$ then by the above arguments we may conclude that $\{\tau_t d_{2\pi\Omega}\}_{t \in \Gamma^{(1)}(f_*)}$ is a local frame for PW_Ω around f_* and moreover that f_* can be reconstructed from only its extrema values.

Remark 6.2.1 Note that the same conclusion can be made if the sample set is taken as only the maxima points and not *all* the extrema points. In the case of $f_*(t) = A(t)\sin(2\pi\Omega_0 t)$ the set of maxima locations together with the set of zero crossing locations will have a density of $3\Omega_0$.

It is clear that we can not expect arbitrary bandlimited functions to have extrema sampling sets which form local frames containing the signal itself. This is particularly true for signals with complicated time-frequency behavior, e.g. the chirp or sine packet signal. On the other hand, we can extend the previous argument fairly easily to apply to signals which are superpositions of finitely many sinusoidal signals. See, for example, Figure 6.19 in which the signal "harmonic" is perfectly reconstructed from its extreme points. The reason we expect to be able to reconstruct a finite superposition of windowed sinusoidals is that the highest frequency in the superposition will dominate the extrema set. Consequently the extrema plus zero set should have a density large enough to form a frame of complex exponentials for a bandlimited space which contains the original superposition. Based on experiments we conjecture that there are large classes of signals (other than finite superpositions of sinusoids) which admit such local extrema representations.

Consider now the signal "packet" and its extrema reconstruction in Figure 6.17. It is evident from the figure that the reconstruction failed to replicate the original signal; however, since the "packet" signal is a time progression of individual sinusoidals we are able to replicate any particular one by choosing the reconstruction filter g appropriately. In this figure $g = d_{2\pi(0.5)}$ to match the middle sinusoid. From the figure it is clear that the sampling for the lowest frequency sinusoid is too sparse for reconstruction with g while the highest frequency sinusoid has too high a bandlimit for reconstruction with g, i.e. it is not in $PW_{(0.5)}$. For the middle sinusoid, though, we are able to reconstruct perfectly using the filter g. Similar remarks can be made for the "chirp" signal in Figure 6.18.

This situation suggests the notion of incorporating different analyzing filters over different frequency bands. For instance, for the signal "packet" we might incorporate three different filters to reconcile each individual sine packet and subsequently reconcile (add) the three results to obtain the entire original signal. This observation hints strongly at the wavelet transform and in particular the discrete extrema or positive extrema or maxima wavelet representation for signals with complex time-frequency behavior. Discrete wavelet representations are numerically investigated in the next section. Numerical results for the discrete positive extrema wavelet representation are presented in Section 6.2.2.3.

Figures 6.17 through 6.20 illustrate the iterative reconstruction of the signals in the test set from their extrema representations.
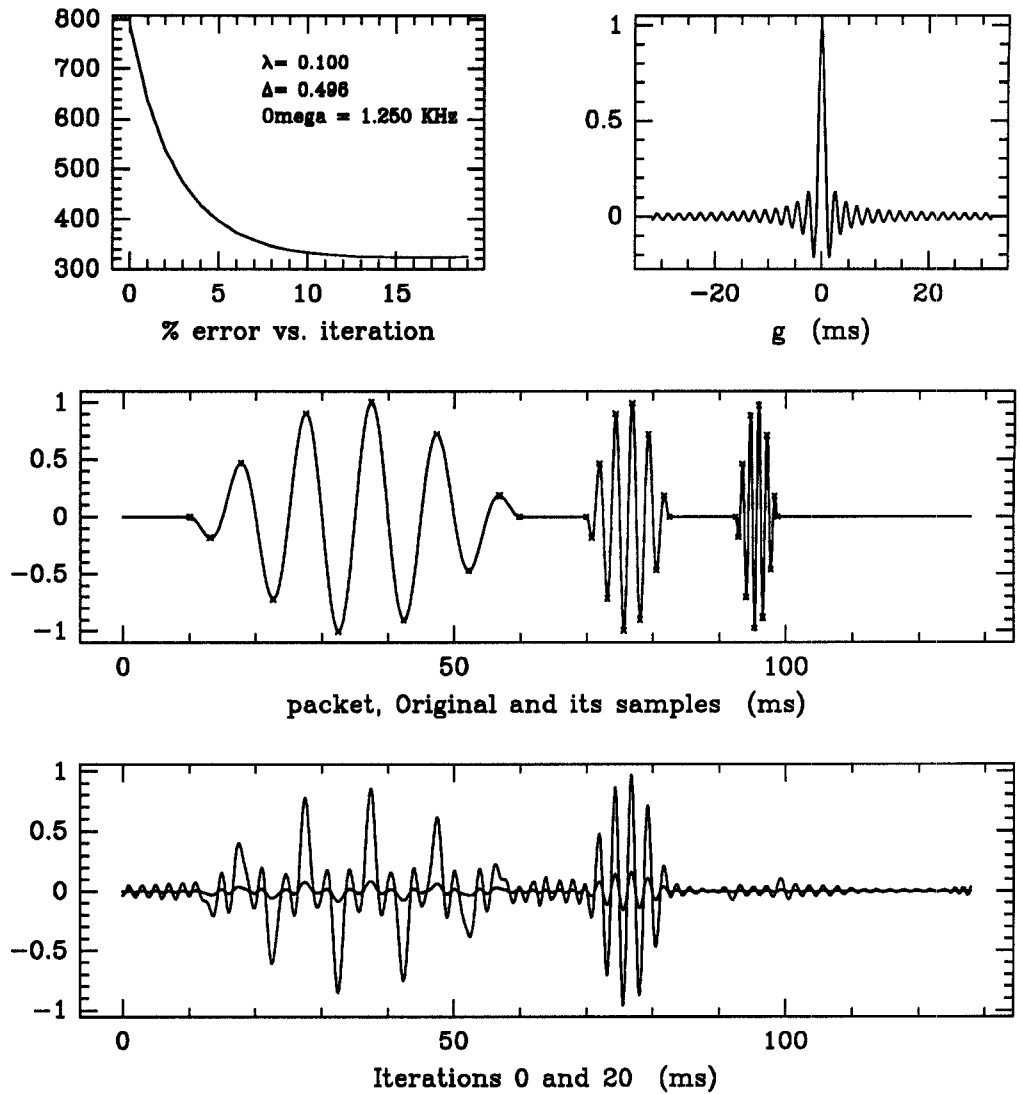
Figure 6.17: Reconstruction of "packet" from its extrema samples.

The above figure shows the extrema representation of the signal "packet" and its iterative reconstruction using Algorithm 3.4.3. The L^2-error is plotted as a function of the iteration number in the upper left graph which also contains the values of the simulation parameters. To its right is the reconstructing dirichlet function. The middle graph shows the original signal and its extrema samples and the iterative reconstruction is shown in the very bottom graph.
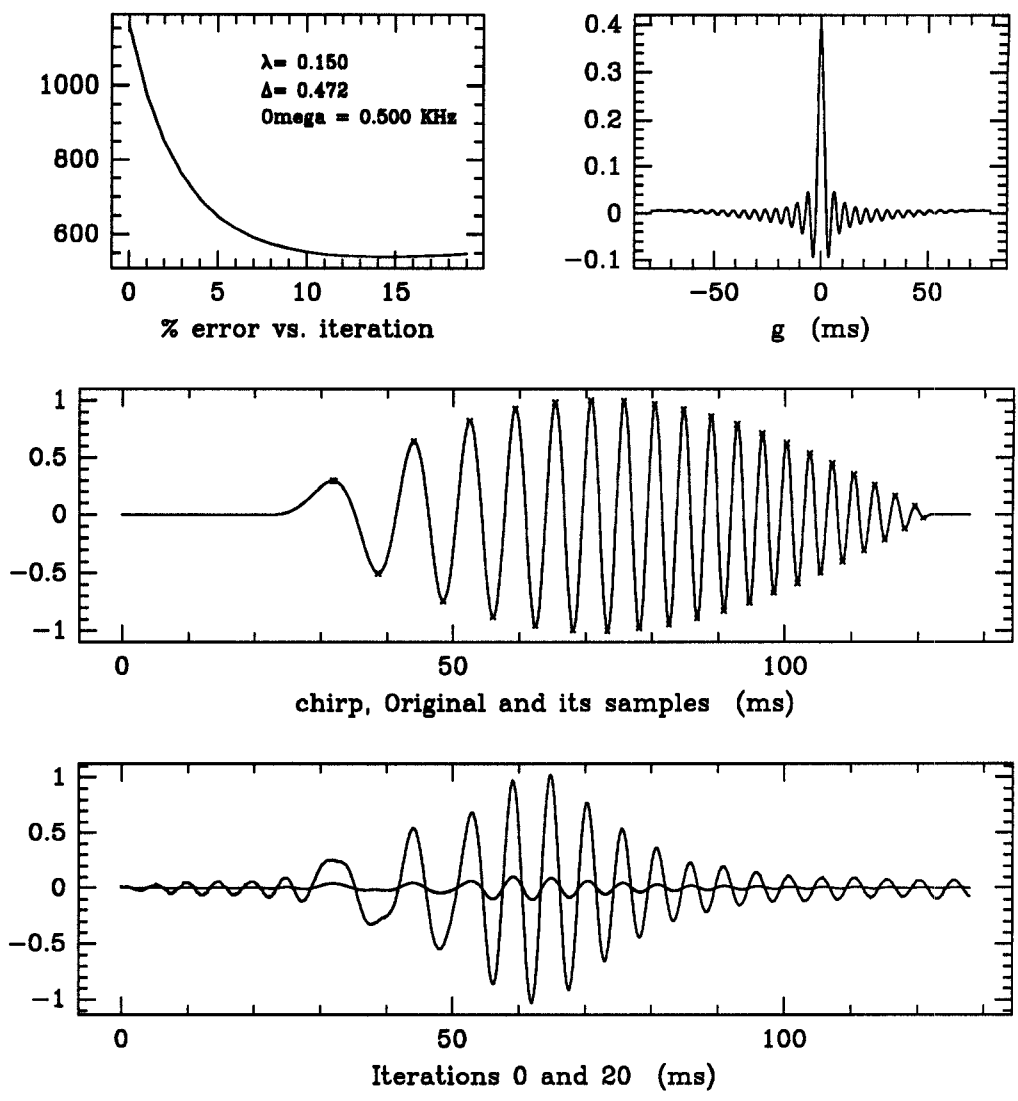
Figure 6.18: Reconstruction of "chirp" from its extrema samples.

The above figure shows the extrema representation of the signal "chirp" and its iterative reconstruction using Algorithm 3.4.3. The L^2-error is plotted as a function of the iteration number in the upper left graph which also contains the values of the simulation parameters. To its right is the reconstructing dirichlet function. The middle graph shows the original signal and its extrema samples and the iterative reconstruction is shown in the very bottom graph.
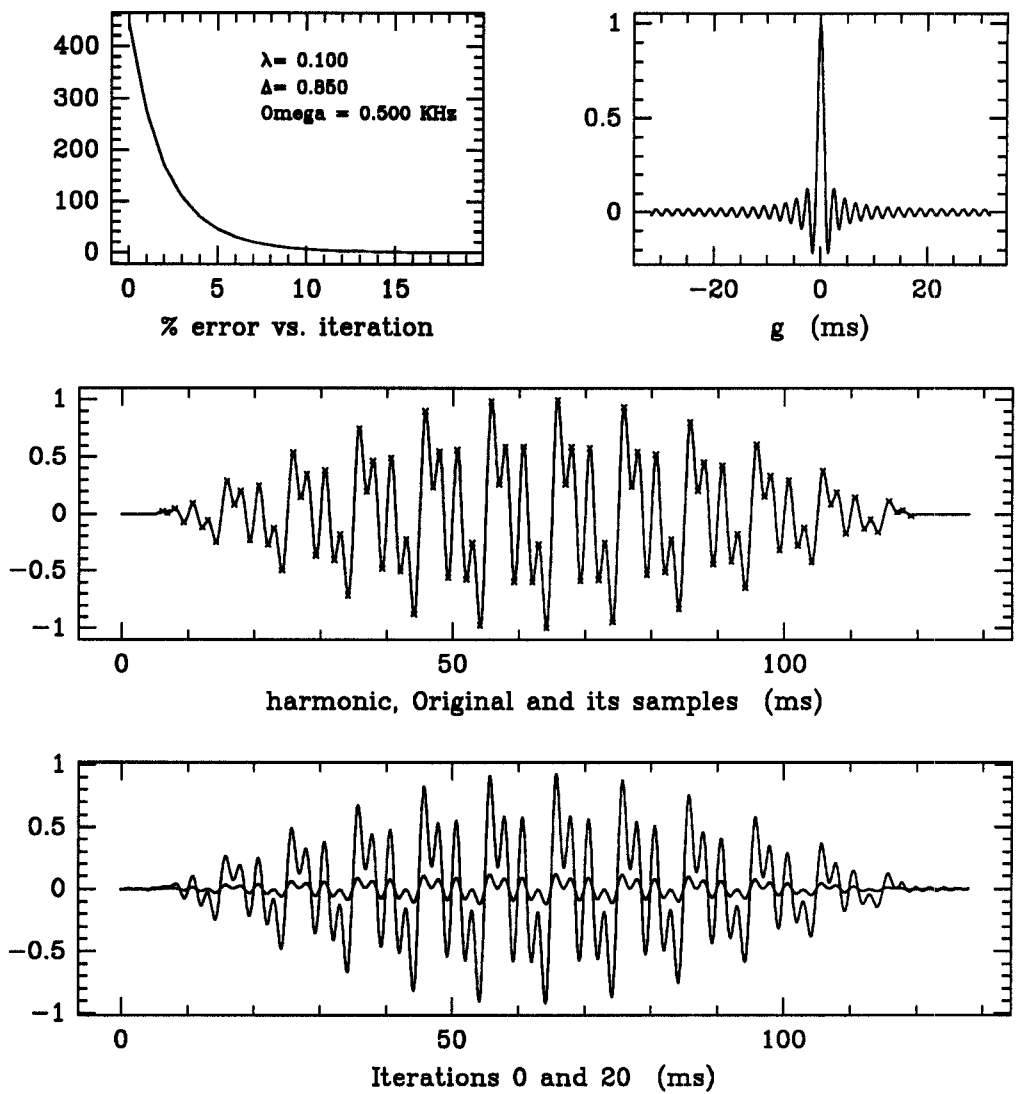
Figure 6.19: Reconstruction of "harmonic" from its extrema samples.

The above figure shows the extrema representation of the signal "harmonic" and its iterative reconstruction using Algorithm 3.4.3. The L^2-error is plotted as a function of the iteration number in the upper left graph which also contains the values of the simulation parameters. To its right is the reconstructing dirichlet function. The middle graph shows the original signal and its extrema samples and the iterative reconstruction is shown in the very bottom graph.

Figure 6.20: Reconstruction of "water" from its extrema samples.

The above figure shows the extrema representàtion of the signal "water" and its iterative reconstruction using Algorithm 3.4.3. The L^2-error is plotted as a function of the iteration number in the upper left graph which also contains the values of the simulation parameters. To its right is the reconstructing dirichlet function. The middle graph shows the original signal and its extrema samples and the iterative reconstruction is shown in the very bottom graph.

6.2.2 Discrete Wavelet Representation

In contrast to the orthogonal case, non-orthogonal wavelet frames with any specifiable shape and support in frequency are easily generated. In this section we present discrete wavelet representations of the signals in the test set and illustrate the frame reconstructions of Chapter 3.

Recall from Section 4.2.3 that the discrete wavelet representation of a signal f is $Lf = \{\langle f, \tau_{t_{m,n}} D_{s_m} g \rangle\}$ where $\Gamma = \{t_{m,n}, s_m\} \subseteq \mathcal{G}_A$ and g is the analyzing function. Alternatively, we may view this representation as the irregular sampling $W_g f(t_{m,n}, s_m)$ of the continuous wavelet transform $W_g f$ of f.

For demonstration purposes, we generate an analyzing function g which has good localization in both time and frequency. More specifically, let g_{ideal} be the real and even ideal bandpass filter specified as

$$\widehat{g}_{\text{ideal}} = 1_{[-b,-a]} + 1_{[a,b]},$$

for $0 < a < b < \infty$. This filter is clearly well localized in frequency, however its decay in time follows $1/t$. To achieve better decay in time we convolve in frequency the ideal bandpass filter with a dirichlet kernel $d_{2\pi c}$ where $c > 0$ is small compared to $b - a$, i.e. $c < b - a$. This yields the trapezoidal analyzing function $\widehat{g}_{\text{trap}}$ given as

$$\widehat{g}_{\text{trap}} = 1_{[-c,c]} * \widehat{g}_{\text{ideal}}.$$

The specific values we have used are $a = 0.4$, $b = 0.5$ and $c = 0.05$ KHz. The two sampling strategies which we examine are (i) regular with respect to the group structure of $\mathcal{G}_A$, and (ii) signal dependent positive extrema (PE).
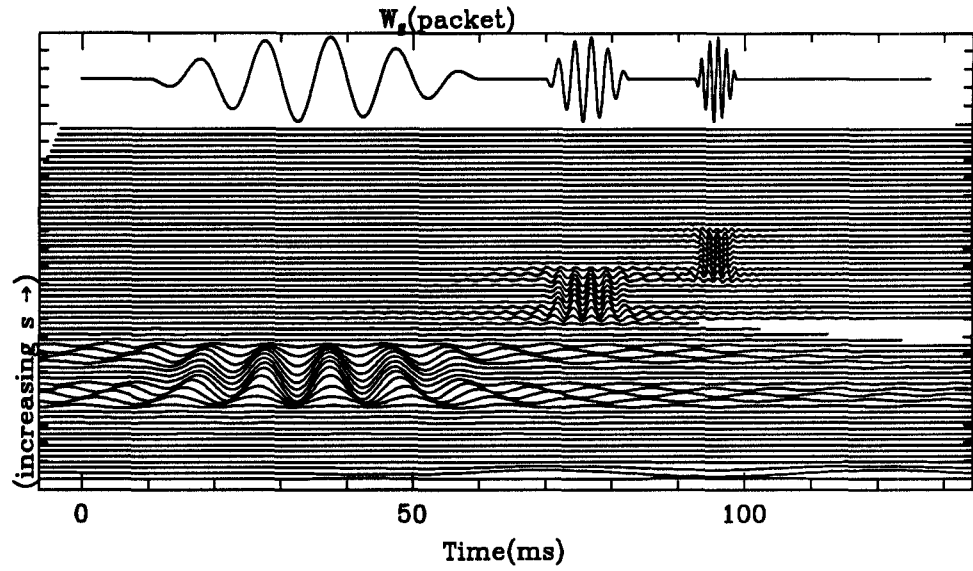
Figure 6.21: The continuous wavelet transform of the signal "packet"

6.2.2.1 Continuous Wavelet Transform

We have seen that the discrete wavelet representation of a signal f comes from samples of the continuous wavelet transform $W_g f(t, s)$, where $a_0 > 1$ is a representation parameter. For a given sampling structure $\{s_m\}_{m=1}^N$ on the scale axis s where N is a finite integer, the wavelet transform can be implemented as a bank of N linear filters. To see this note that

$$W_g f(t, s_m) = (f * D_{s_m} \tilde{g})(t),$$

so that the wavelet transform is the response of a bank of filters with impulse responses $\{D_{s_m} \tilde{g}\}_{m=1}^N$. For simplicity the simulations presented here have a sampling on the scale axis s which is fixed according to $\{s_m\}_{m=1}^N = \{a_0^m\}_{m=-N/2}^{N/2}$. As an example of a "continuous" wavelet transform we display in Figure 6.21 the "continuous" wavelet transform of the test signal "packet". Actually what is displayed in this figure is the "continuous" output of the wavelet filter bank $\{D_{s_m} \tilde{g}\}_{m=1}^N$ where $N = 64$. The figure displays the output of all 64 filters starting with the the response of $D_{s_1} g$ in the bottom most signal up to the response of $D_{s_{64}} g$ in the top most. In this figure $g = g_{\text{ideal}}$ where $a = 0.4$ and $b = 0.5$ KHz. The input signal is plotted at the very top of the figure for reference.

6.2.2.2 Regular Wavelet Representation

In this section we present a sequence of figures which display the discrete regular wavelet representation of the test signals. This representation is derived from the regular samples of the continuous wavelet transform. Signals are reconstructed from their regular wavelet representation via Algorithm 3.4.3. The regular wavelet representation of a signal f which we have used is

$$\left\{ W_g f(a_0^m, a_0^{-m} nT) \right\}$$

where a_0 and T are chosen so that this set is a regular wavelet frame.

105

Figures 6.22 through 6.33 illustrate the reconstruction of the test signals directly from their regular wavelet representations.

Figures 6.34 through 6.45 illustrate the reconstruction of the test signals from their quantized regular wavelet representations. Here, before reconstruction the sample coefficients are quantized according to $b_c = 2$ bits/coefficient, i.e. $c_Q = Q_2(c)$ is the quantized data where Q_b is the quantization function in (5.3.1) and the dynamic range (m, M) is signal dependent.
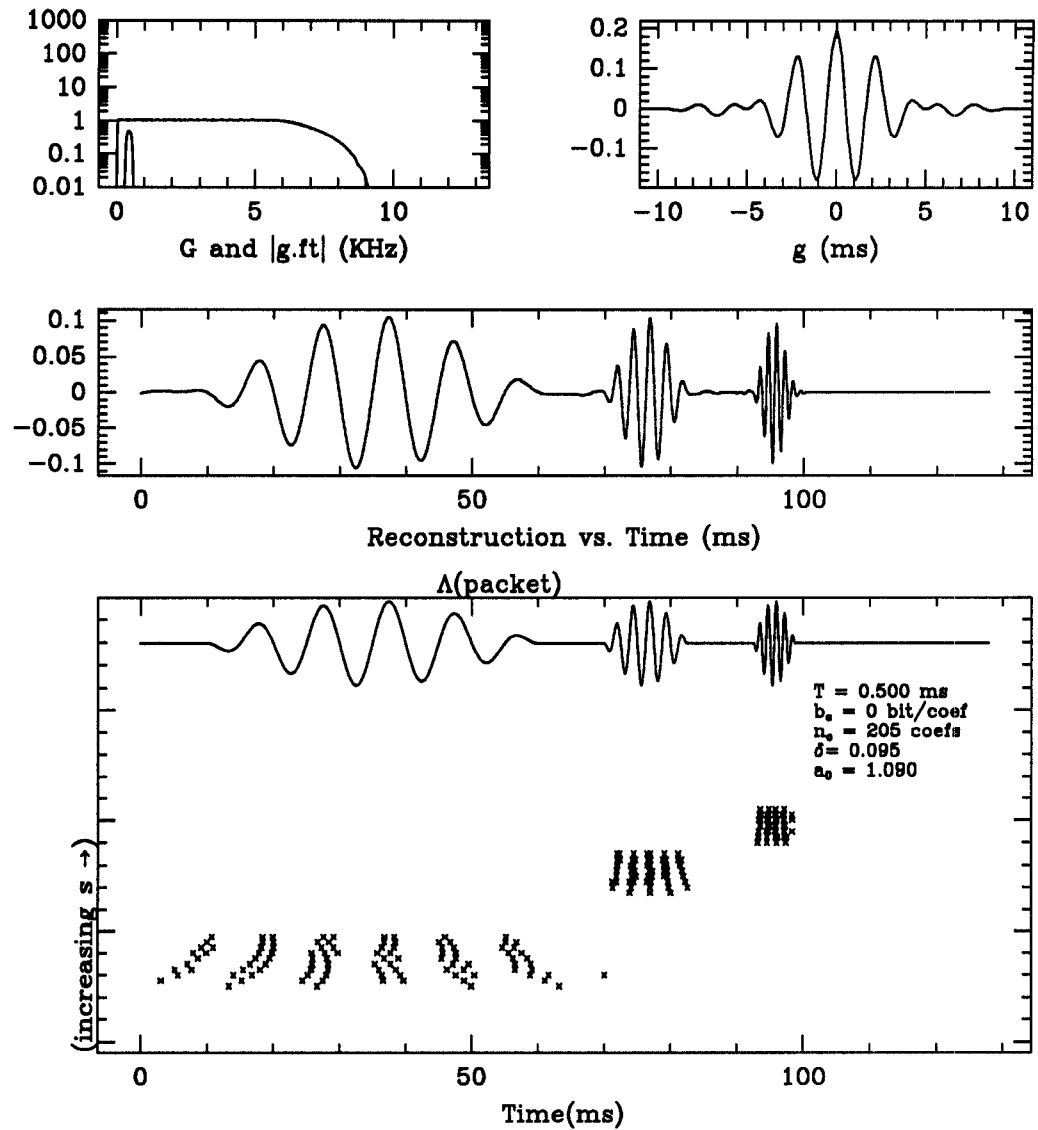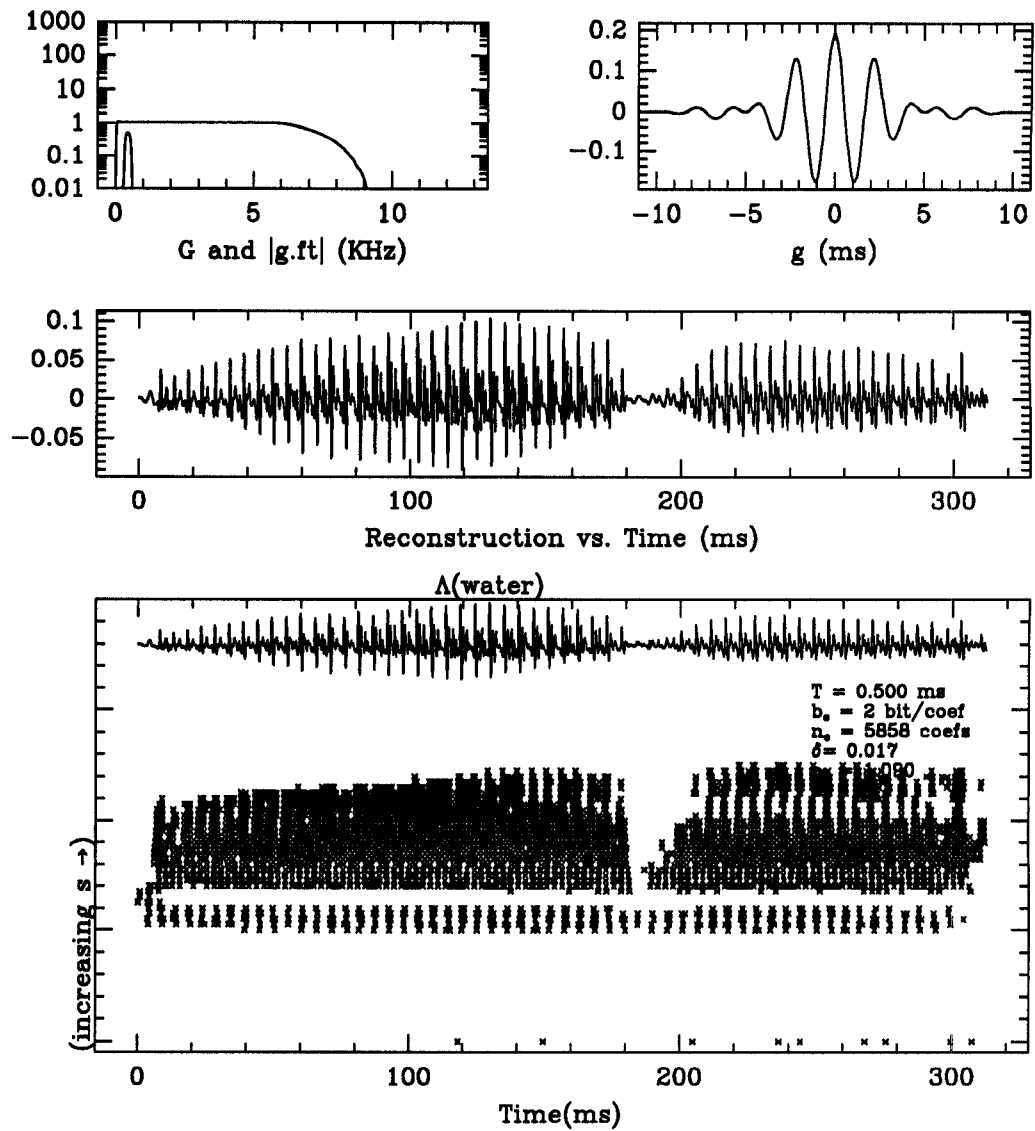
Figure 6.22: Regular wavelet representation for "packet".

Shown above is the wavelet regular representation and its reconstruction for the signal "packet". The trapezoidal analyzing function g appears in the top upper right. To its left are the functions $G = \sum_{m=1}^{N} |D_{s_m}\widehat{g}|^2$ and $\widehat{g}$. The middle graph displays the reconstruction of Algorithm 3.4.3. The lower most graph displays the sampling set Γ. At the top of the bottom graph is the input signal and to its lower right the values of the reconstruction parameters.
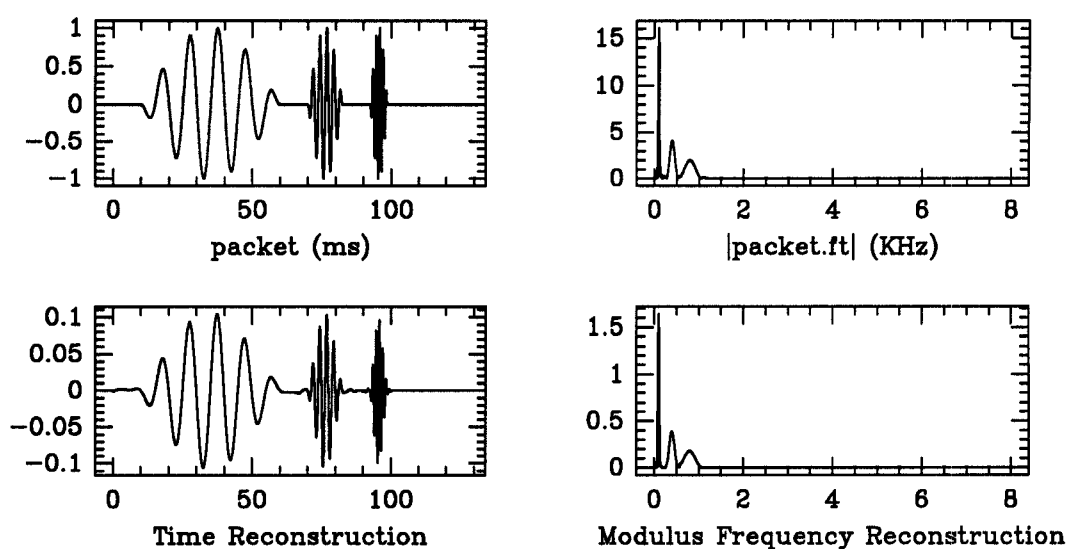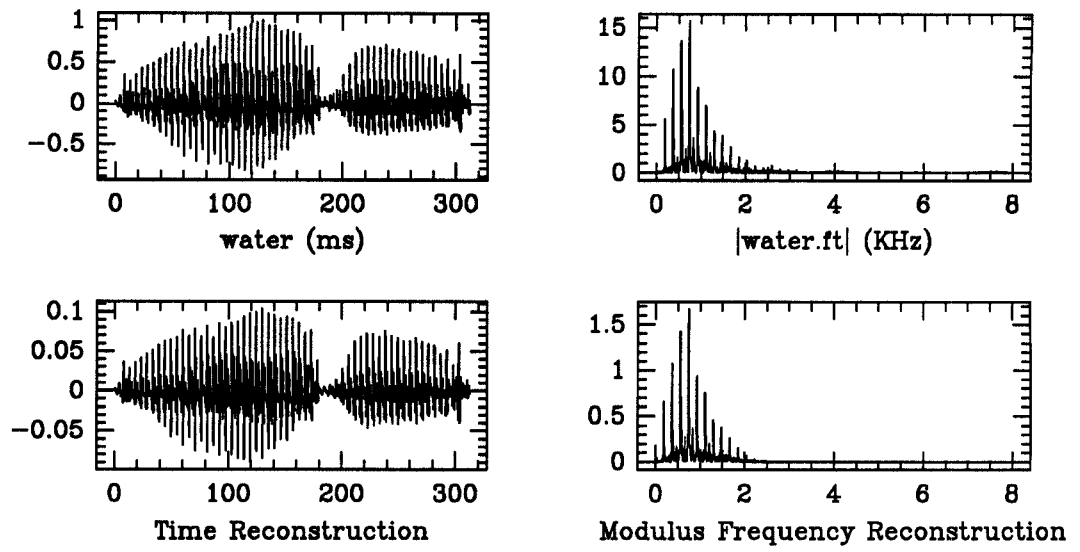
Figure 6.23: Reconstruction of "packet".

Above, the signal "packet"and its reconstructed versions in both time and frequency are displayed. Below, the associated coefficient distribution function λ_{packet} is plotted in the top graph while the lower graph shows the max and min value of the wavelet filter bank response as a function of the channel number.
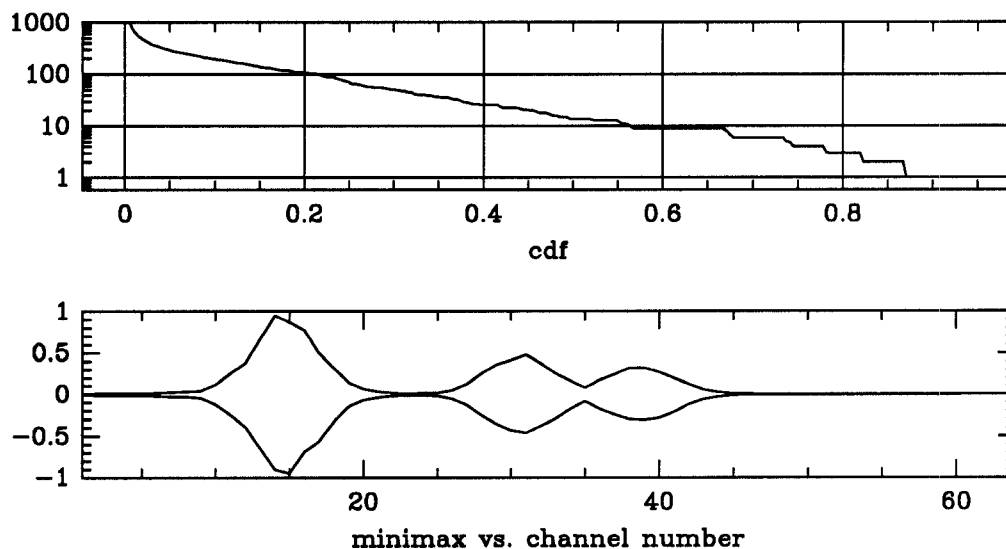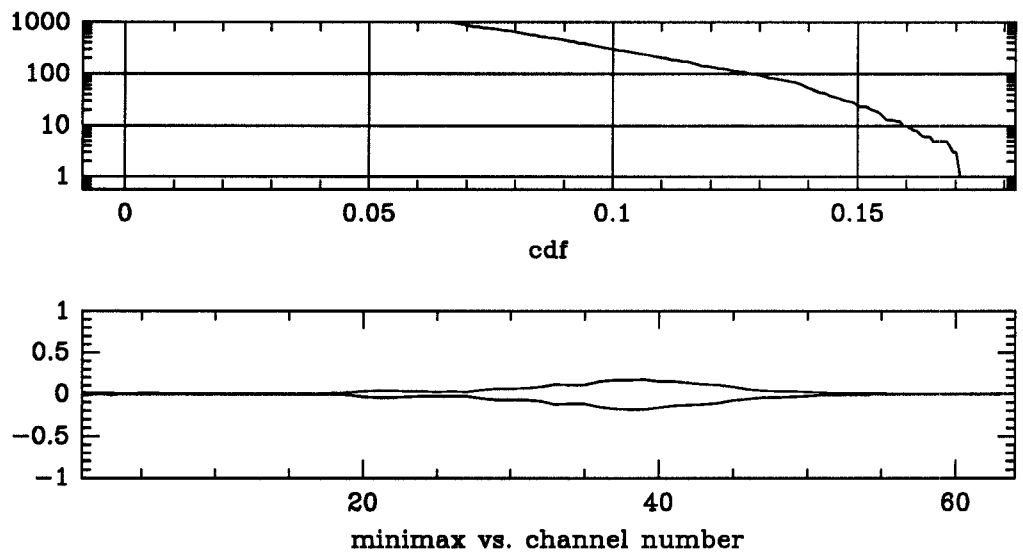

Figure 6.24: Cdf and minimax curves for "packet".
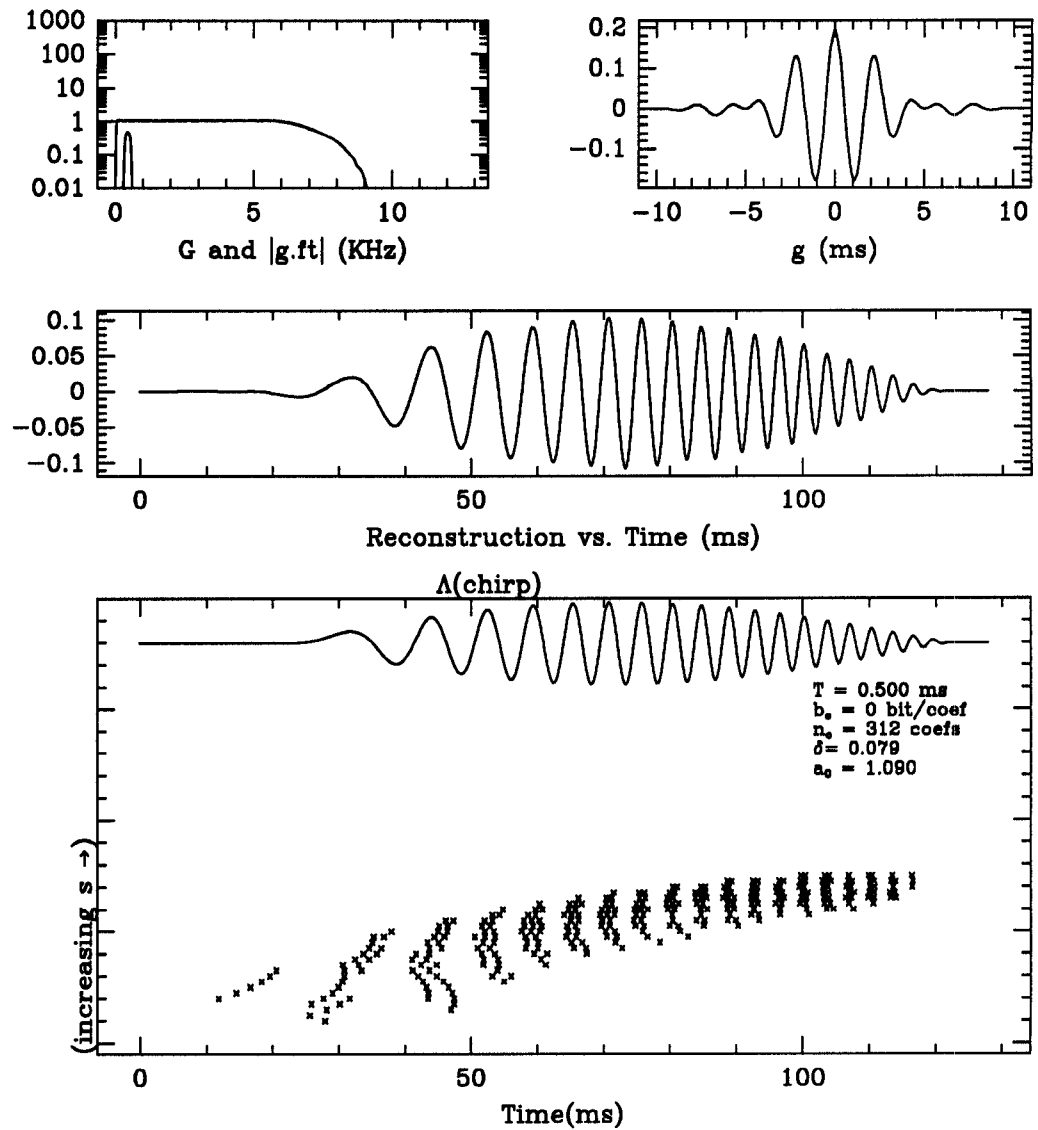
Figure 6.25: Regular wavelet representation for "chirp".

Shown above is the wavelet regular representation and its reconstruction for the signal "chirp". The trapezoidal analyzing function g appears in the top upper right. To its left are the functions $G = \sum_{m=1}^{N} |D_{s_m}\widehat{g}|^2$ and $\widehat{g}$. The middle graph displays the reconstruction of Algorithm 3.4.3. The lower most graph displays the sampling set Γ. At the top of the bottom graph is the input signal and to its lower right the values of the reconstruction parameters.
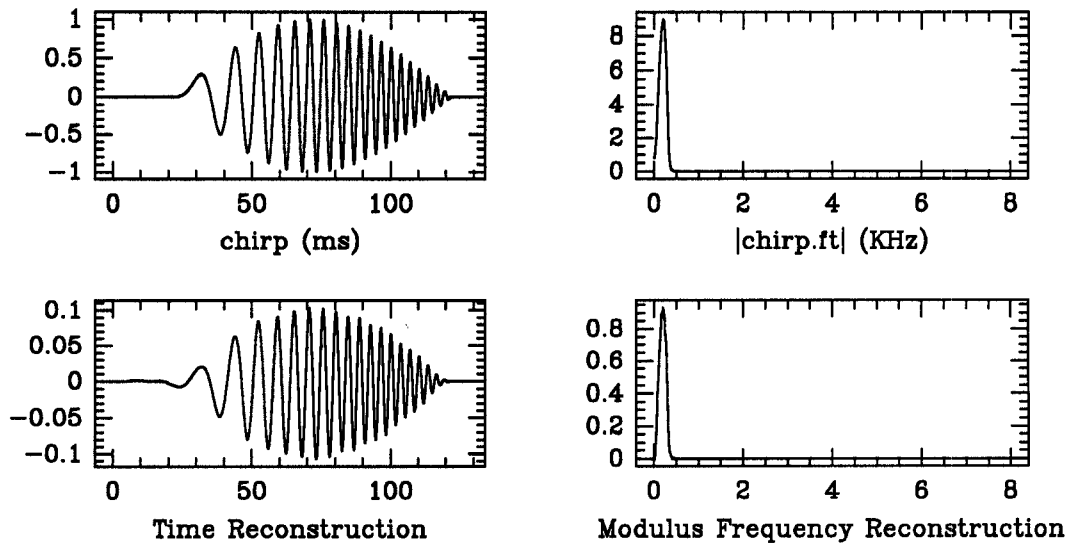
Figure 6.26: Reconstruction of "chirp".

Above, the signal "chirp"and its reconstructed versions in both time and frequency are displayed. Below, the associated coefficient distribution function λ_{chirp} is plotted in the top graph while the lower graph shows the max and min value of the wavelet filter bank response as a function of the channel number.
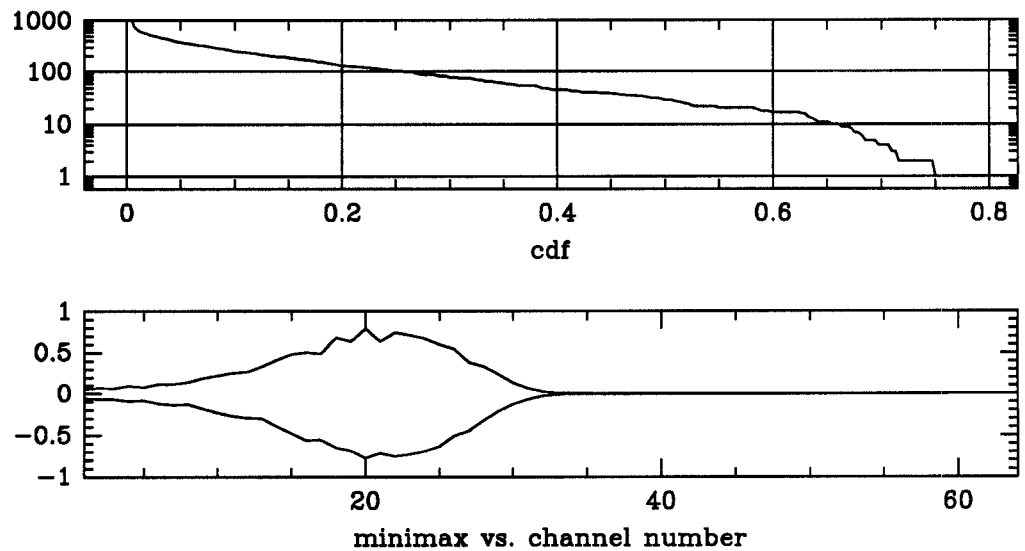
Figure 6.27: Cdf and minimax curves for "chirp".
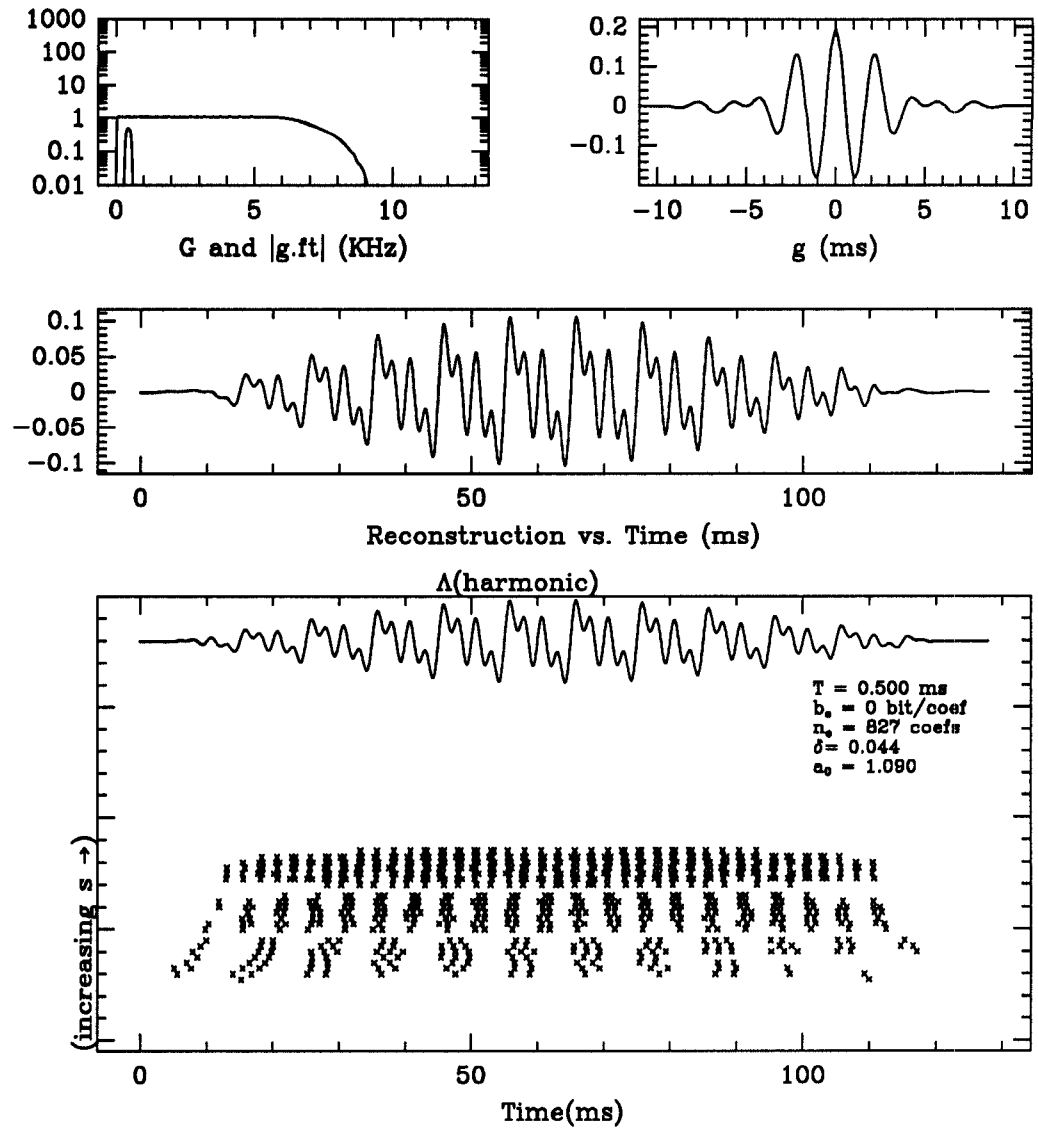
Figure 6.28: Regular wavelet representation for "harmonic".

Shown above is the wavelet regular representation and its reconstruction for the signal "harmonic". The trapezoidal analyzing function g appears in the top upper right. To its left are the functions $G = \sum_{m=1}^{N} |D_{s_m} \widehat{g}|^2$ and $\widehat{g}$. The middle graph displays the reconstruction of Algorithm 3.4.3. The lower most graph displays the sampling set Γ. At the top of the bottom graph is the input signal and to its lower right the values of the reconstruction parameters.
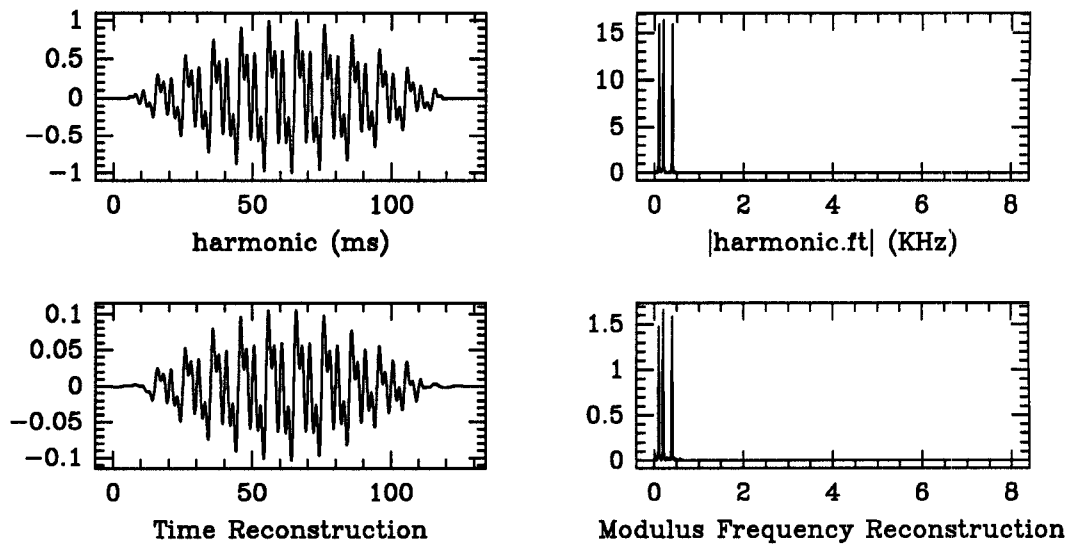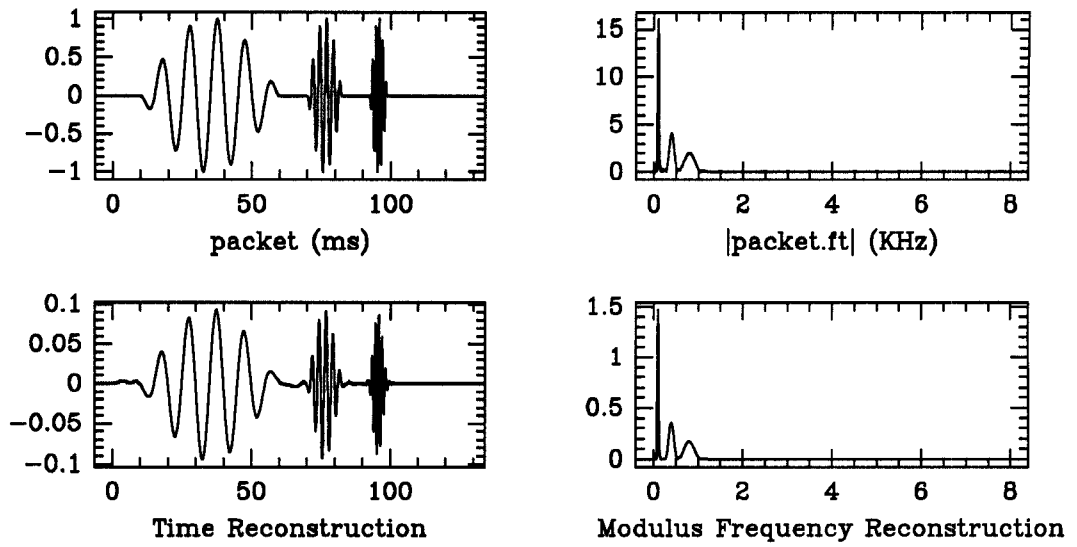
Figure 6.29: Reconstruction of "harmonic".

Above, the signal "harmonic"and its reconstructed versions in both time and frequency are displayed. Below, the associated coefficient distribution function $\lambda_{harmonic}$ is plotted in the top graph while the lower graph shows the max and min value of the wavelet filter bank response as a function of the channel number.
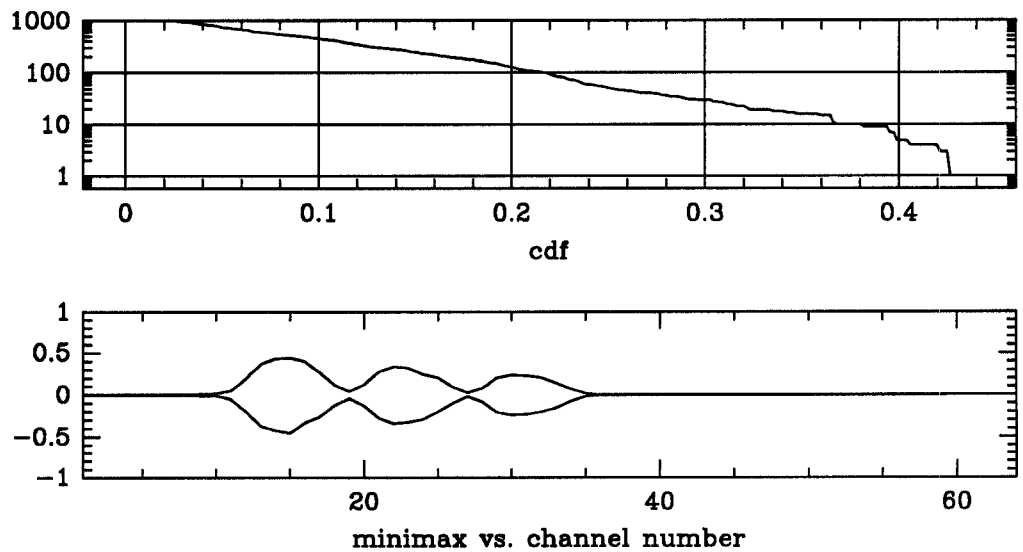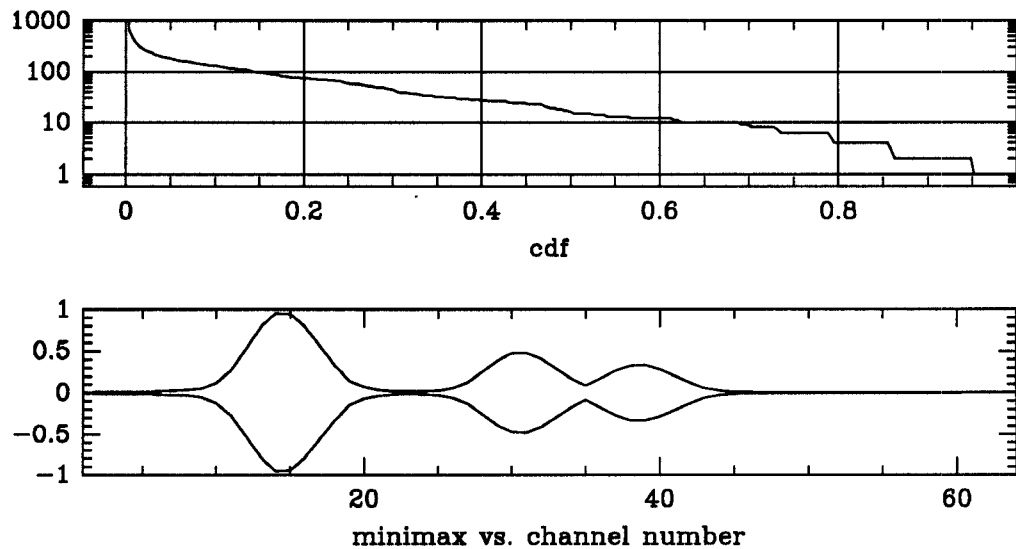
Figure 6.30: Cdf and minimax curves for "harmonic".
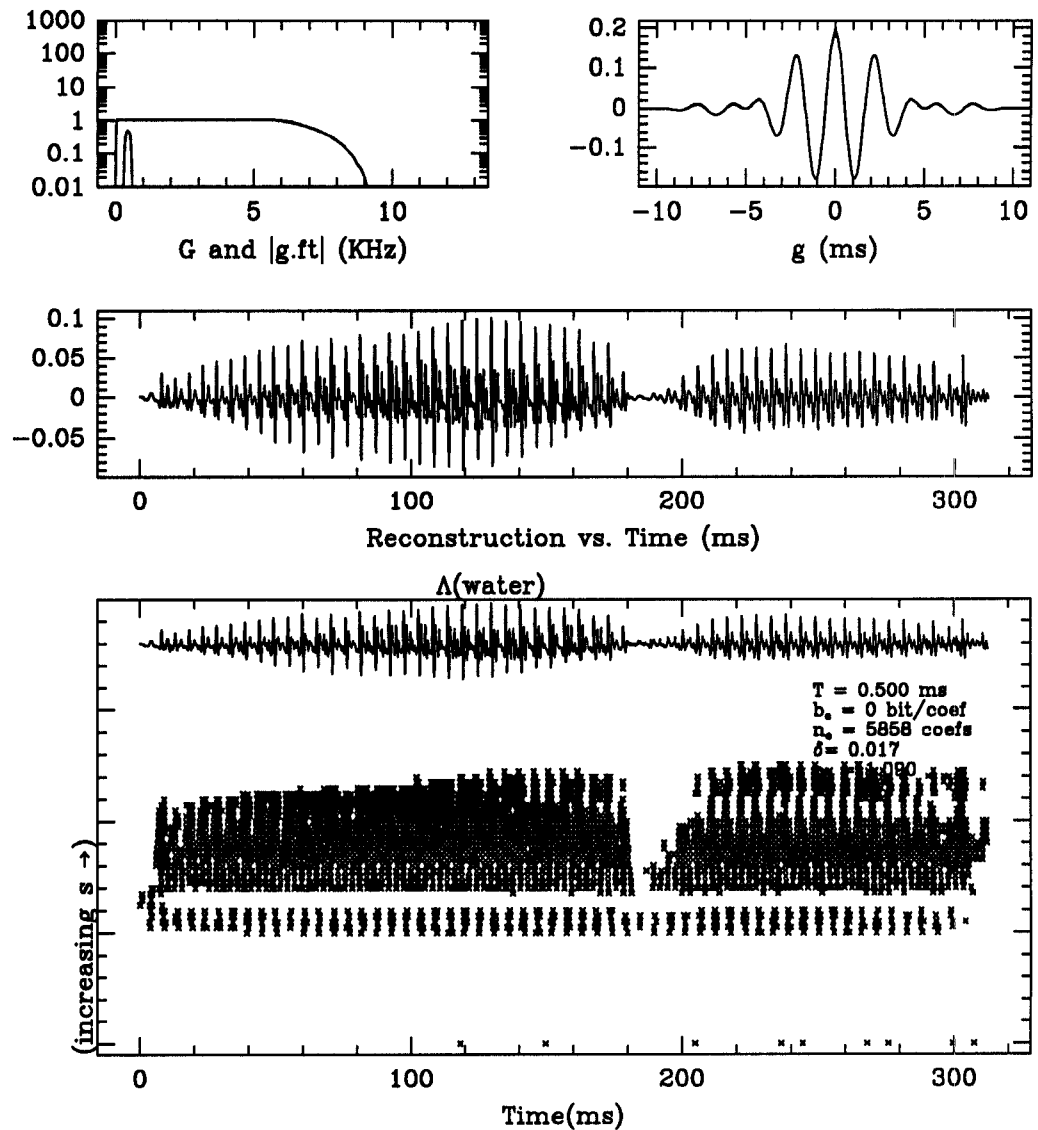
Figure 6.31: Regular wavelet representation for "water".

Shown above is the wavelet regular representation and its reconstruction for the signal "water". The trapezoidal analyzing function g appears in the top upper right. To its left are the functions $G = \sum_{m=1}^{N} |D_{s_m}\hat{g}|^2$ and $\hat{g}$. The middle graph displays the reconstruction of Algorithm 3.4.3. The lower most graph displays the sampling set Γ. At the top of the bottom graph is the input signal and to its lower right the values of the reconstruction parameters.
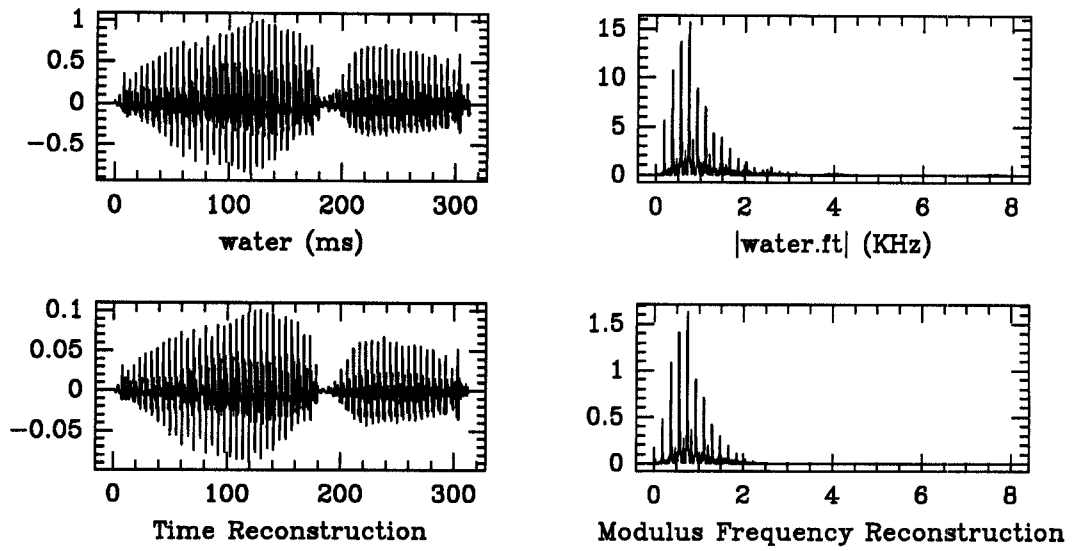
Figure 6.32: Reconstruction of "water".

Above, the signal "water"and its reconstructed versions in both time and frequency are displayed. Below, the associated coefficient distribution function λ_{water} is plotted in the top graph while the lower graph shows the max and min value of the wavelet filter bank response as a function of the channel number.
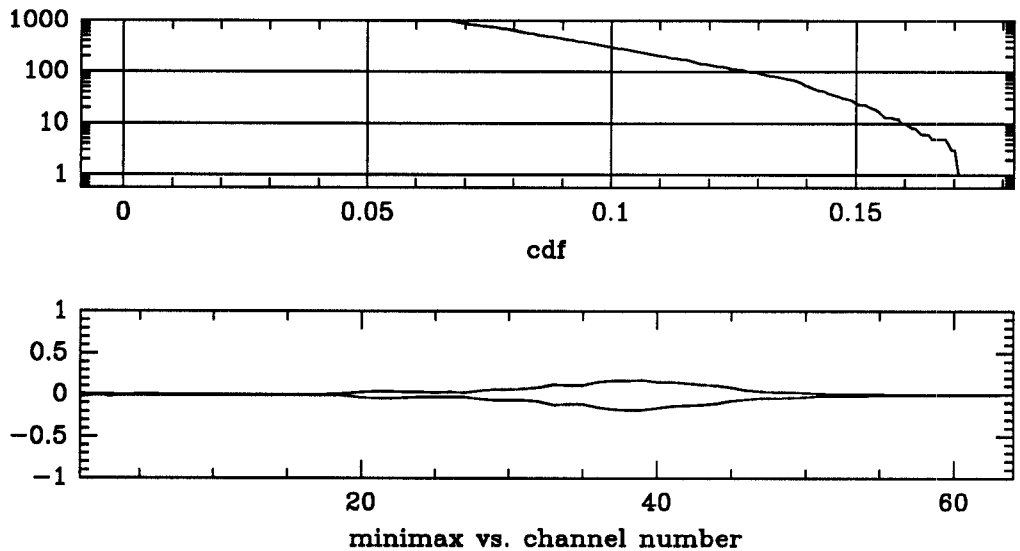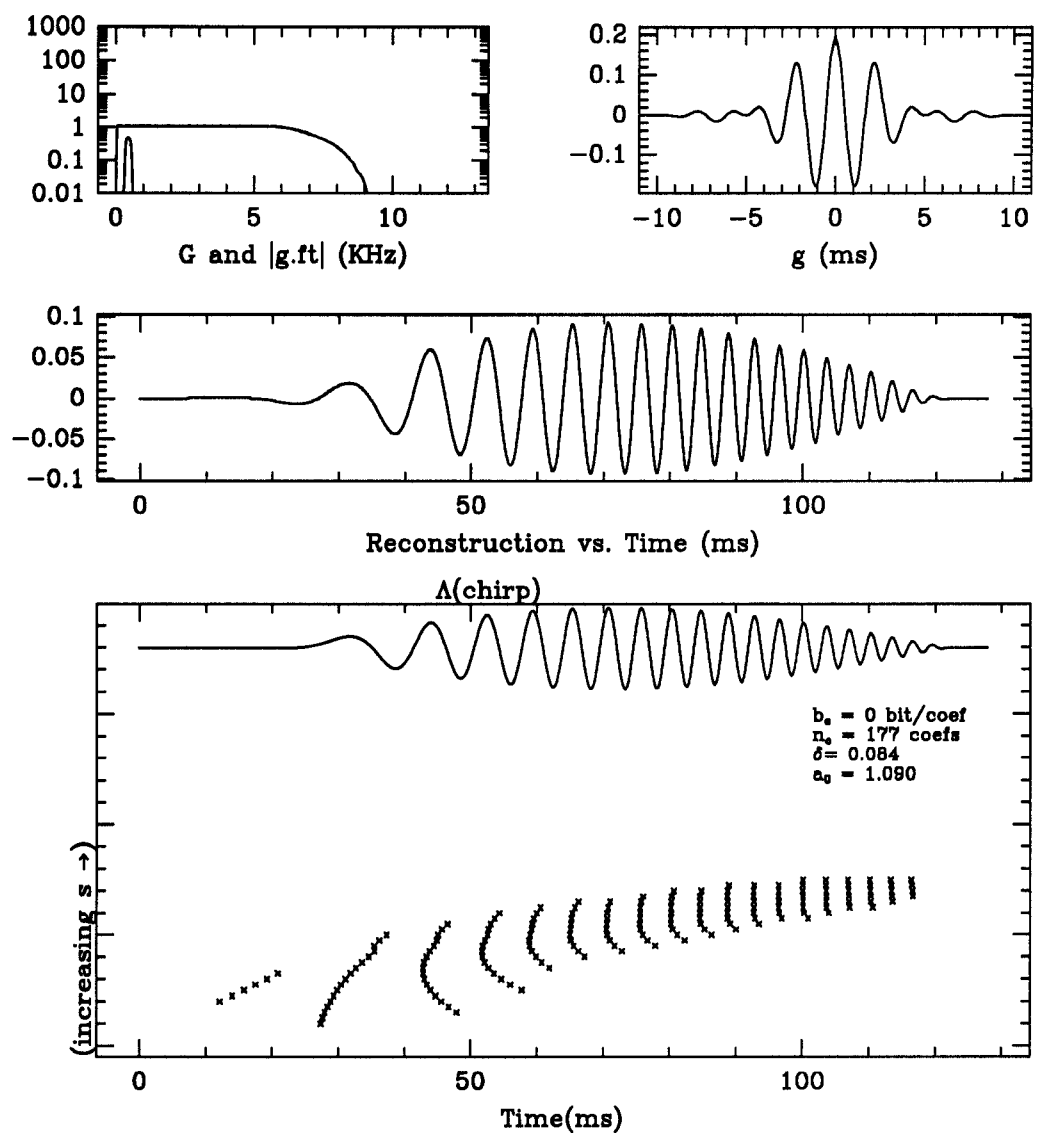

Figure 6.33: Cdf and minimax curves for "water".
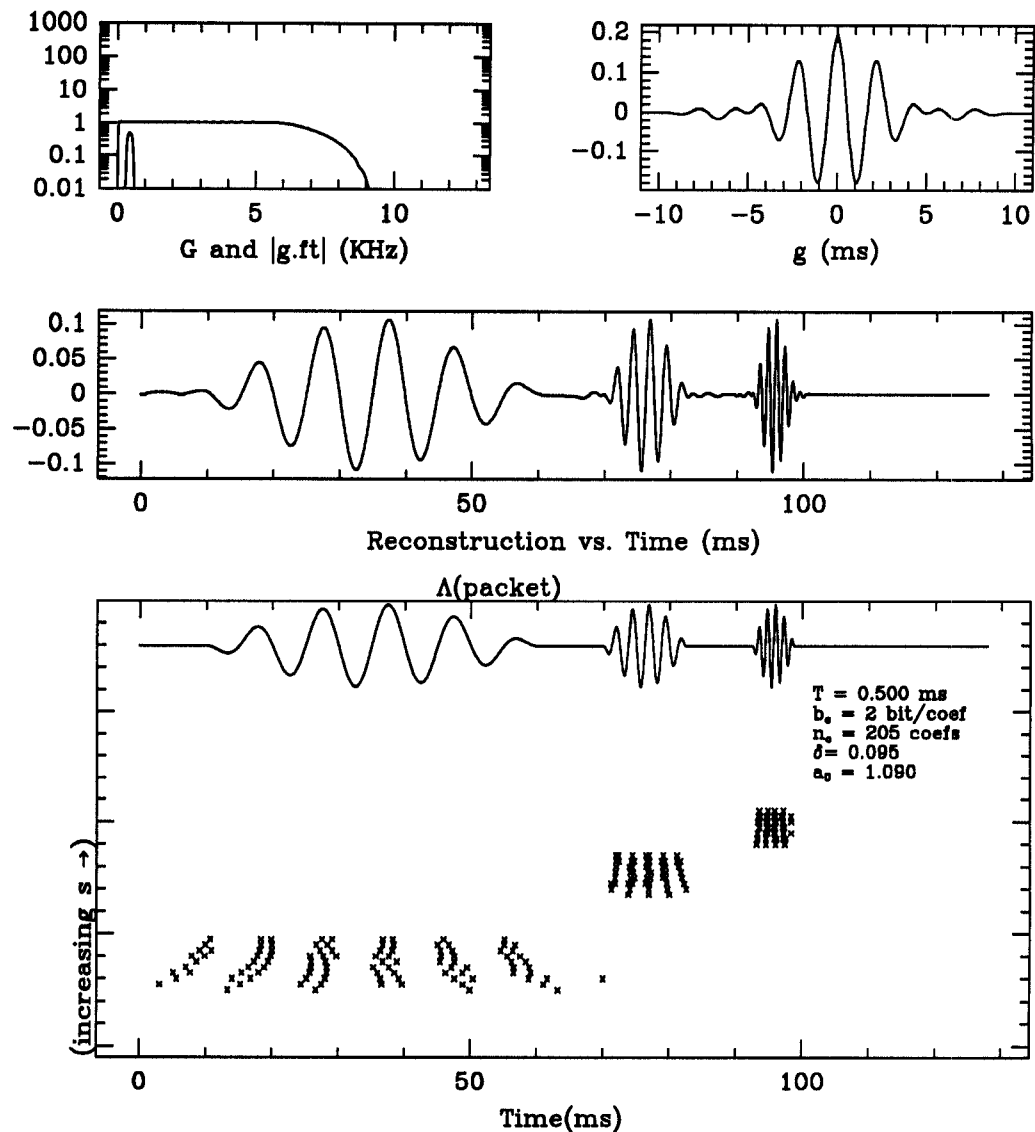
Figure 6.34: Regular wavelet representation for "packet".

Shown above is the wavelet regular representation and its reconstruction for the signal "packet". The trapezoidal analyzing function g appears in the top upper right. To its left are the functions $G = \sum_{m=1}^{N} |D_{s_m}\hat{g}|^2$ and $\hat{g}$. The middle graph displays the reconstruction of Algorithm 3.4.3. The lower most graph displays the sampling set Γ. At the top of the bottom graph is the input signal and to its lower right the values of the reconstruction parameters.
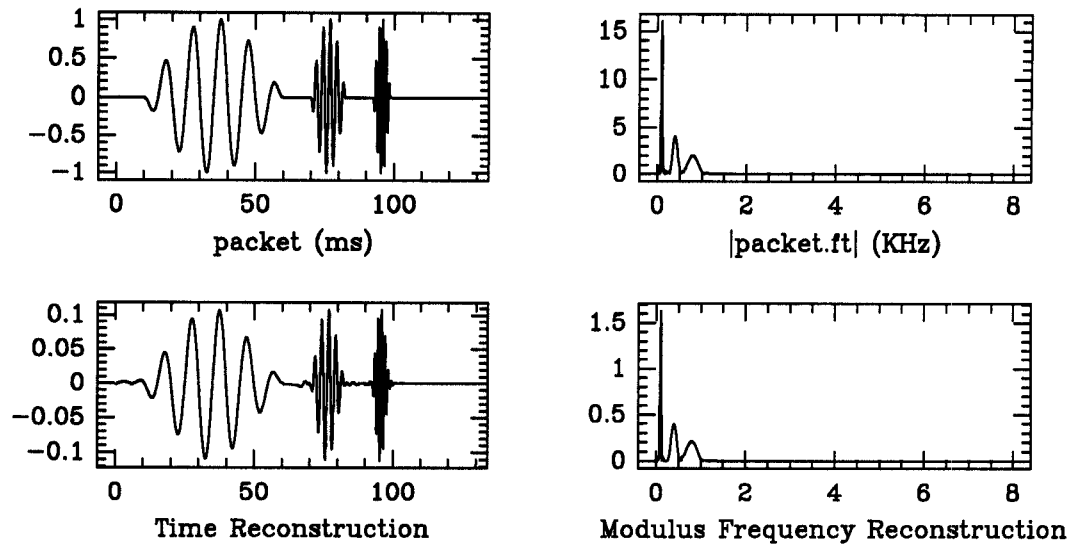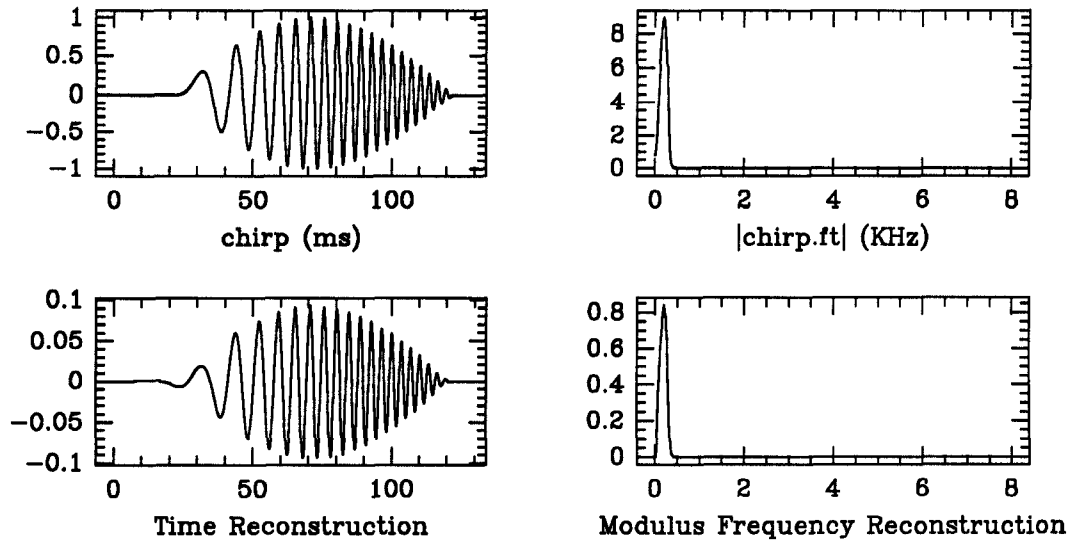
Figure 6.35: Reconstruction of "packet".

Above, the signal "packet"and its reconstructed versions in both time and frequency are displayed. Below, the associated coefficient distribution function λ_{packet} is plotted in the top graph while the lower graph shows the max and min value of the wavelet filter bank response as a function of the channel number.
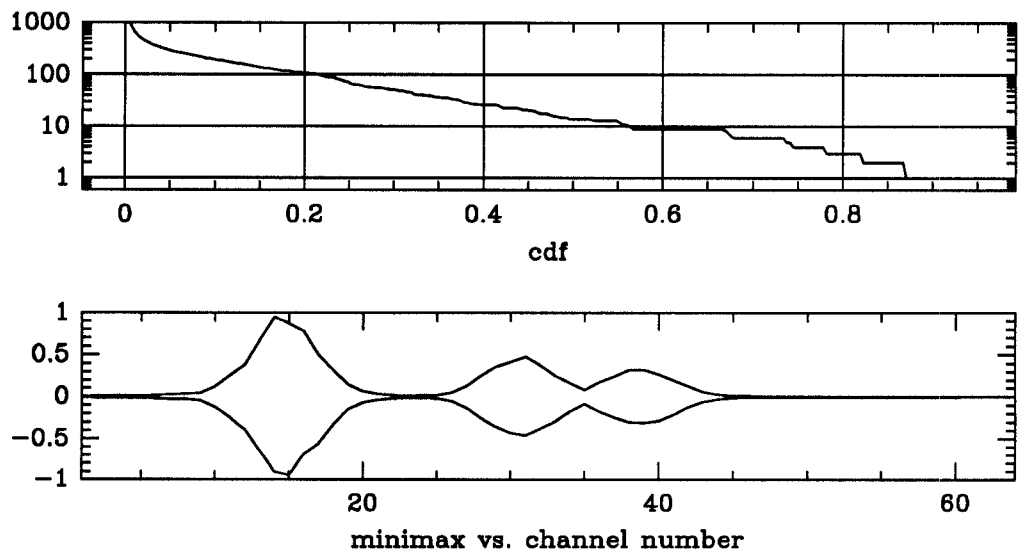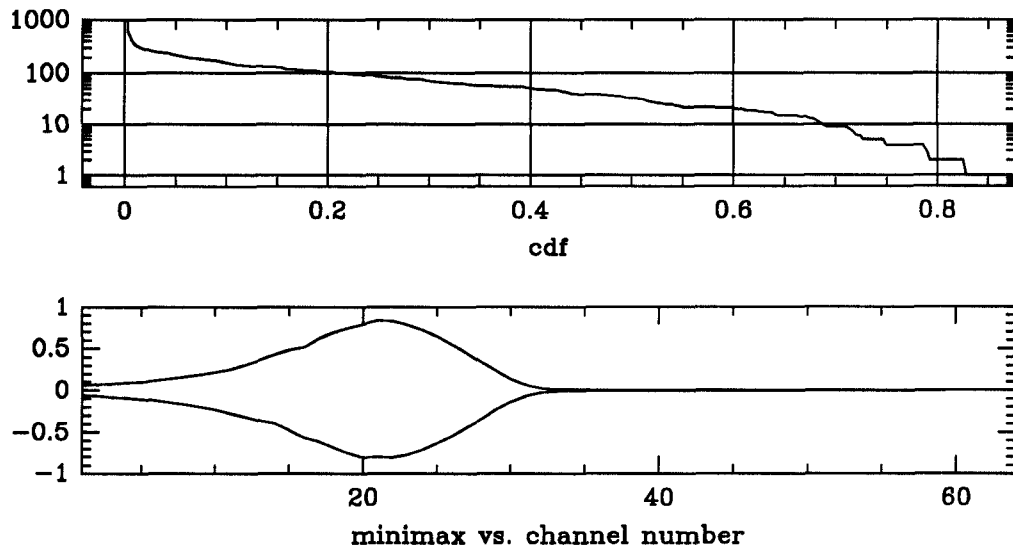

Figure 6.36: Cdf and minimax curves for "packet".
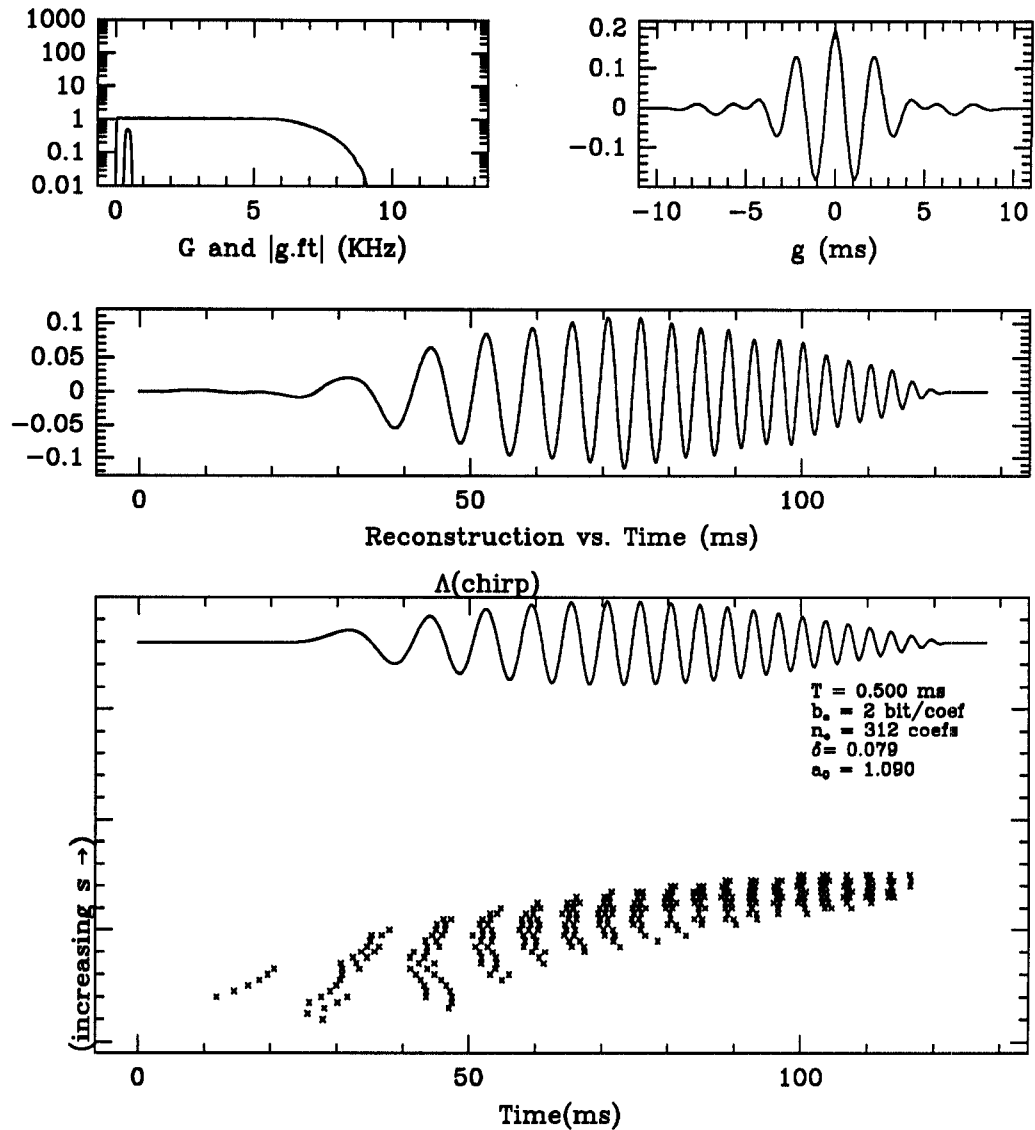
Figure 6.37: Regular wavelet representation for "chirp".

Shown above is the wavelet regular representation and its reconstruction for the signal "chirp". The trapezoidal analyzing function g appears in the top upper right. To its left are the functions $G = \sum_{m=1}^{N} |D_{s_m} \hat{g}|^2$ and $\hat{g}$. The middle graph displays the reconstruction of Algorithm 3.4.3. The lower most graph displays the sampling set Γ. At the top of the bottom graph is the input signal and to its lower right the values of the reconstruction parameters.
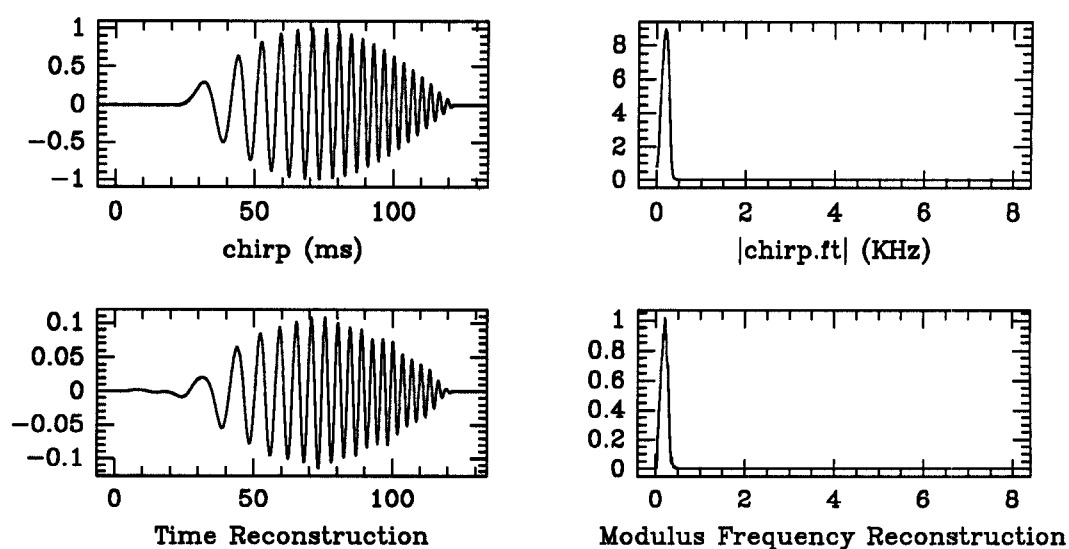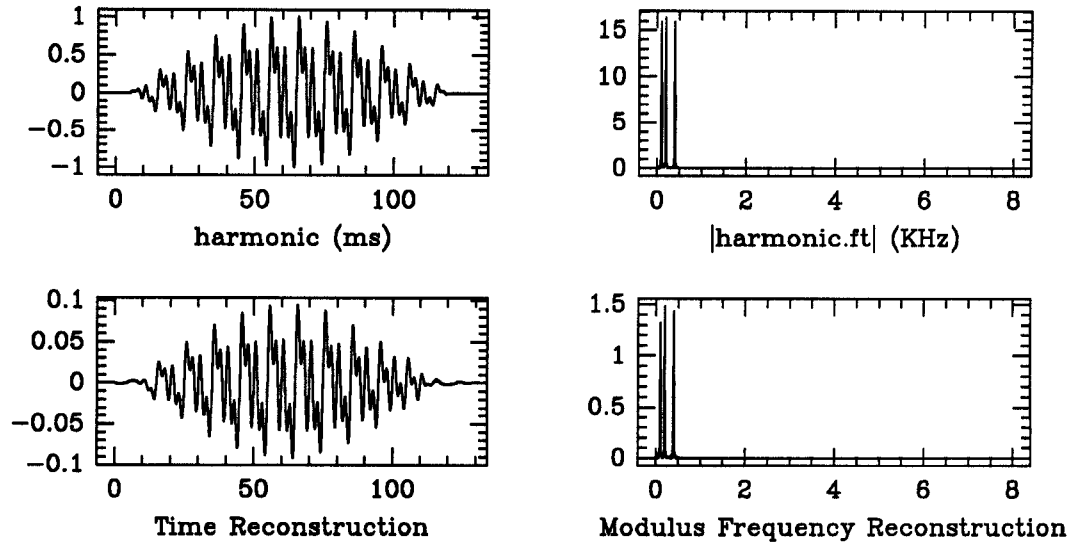
Figure 6.38: Reconstruction of "chirp".

Above, the signal "chirp"and its reconstructed versions in both time and frequency are displayed. Below, the associated coefficient distribution function λ_{chirp} is plotted in the top graph while the lower graph shows the max and min value of the wavelet filter bank response as a function of the channel number.
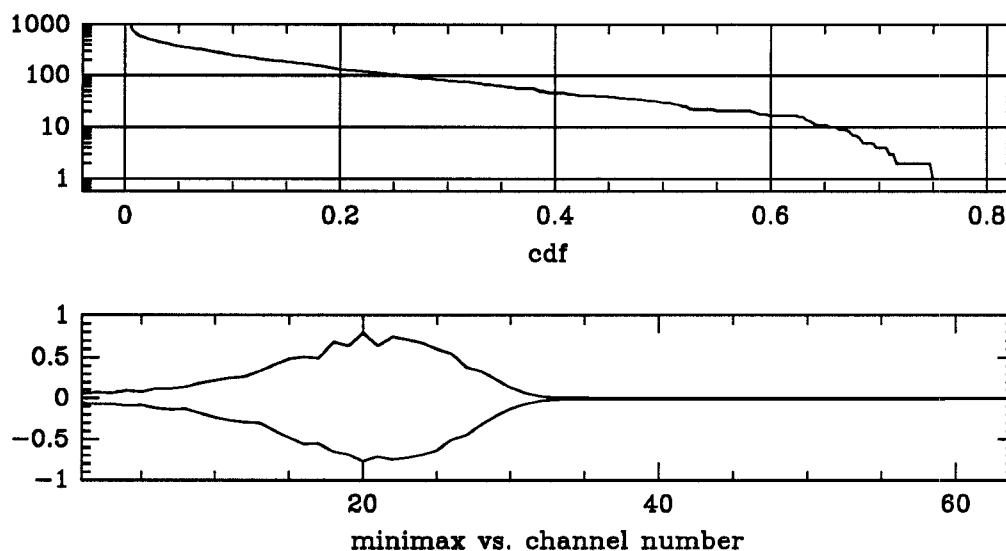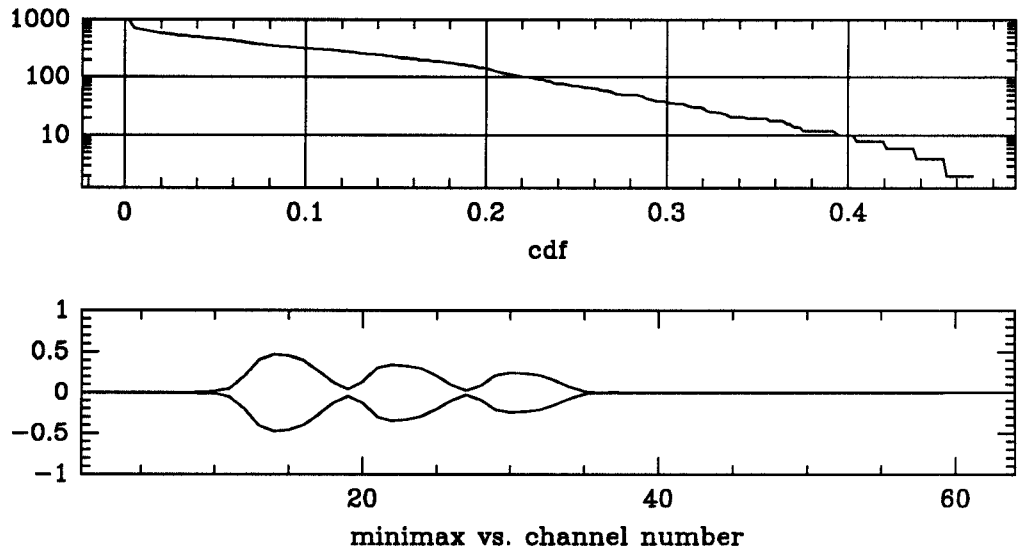

Figure 6.39: Cdf and minimax curves for "chirp".
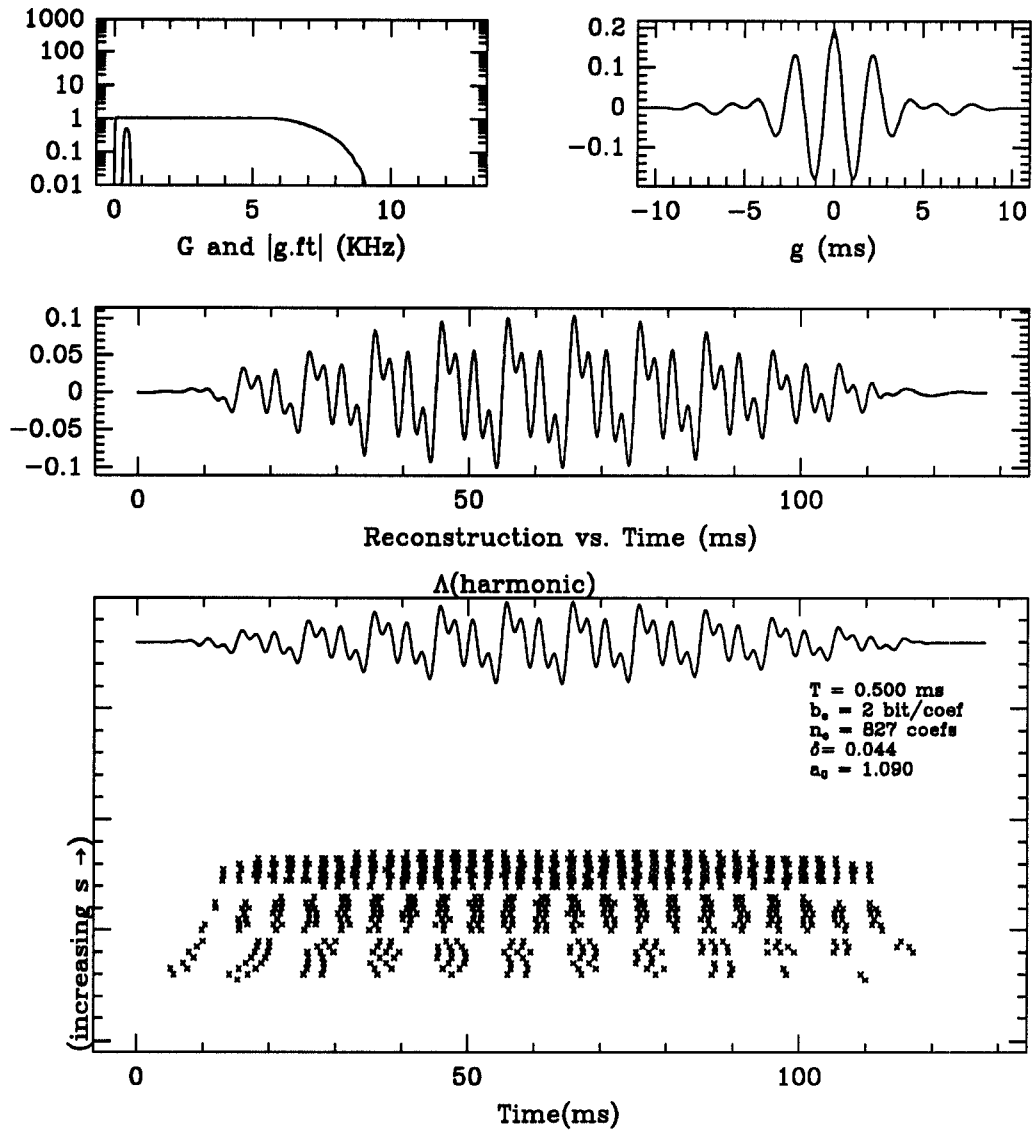
Figure 6.40: Regular wavelet representation for "harmonic".

Shown above is the wavelet regular representation and its reconstruction for the signal "harmonic". The trapezoidal analyzing function g appears in the top upper right. To its left are the functions $G = \sum_{m=1}^{N} |D_{s_m}\hat{g}|^2$ and $\hat{g}$. The middle graph displays the reconstruction of Algorithm 3.4.3. The lower most graph displays the sampling set Γ. At the top of the bottom graph is the input signal and to its lower right the values of the reconstruction parameters.
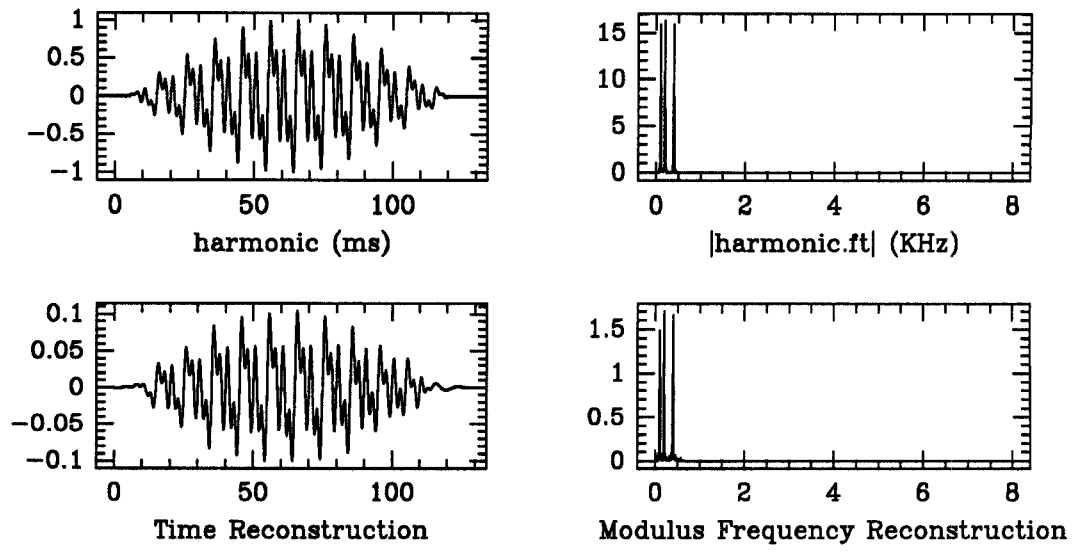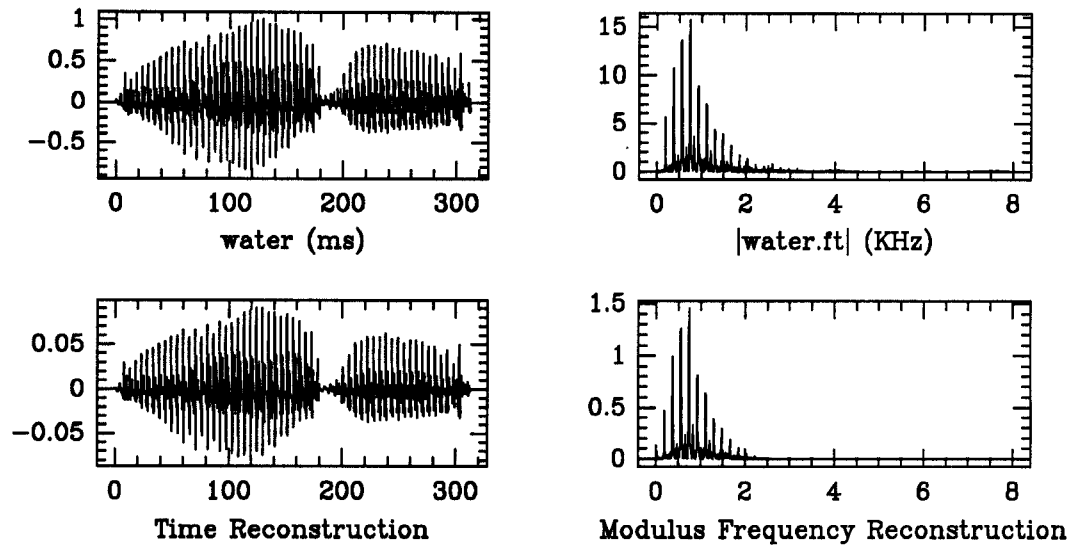
Figure 6.41: Reconstruction of "harmonic".

Above, the signal "harmonic"and its reconstructed versions in both time and frequency are displayed. Below, the associated coefficient distribution function $\lambda_{harmonic}$ is plotted in the top graph while the lower graph shows the max and min value of the wavelet filter bank response as a function of the channel number.
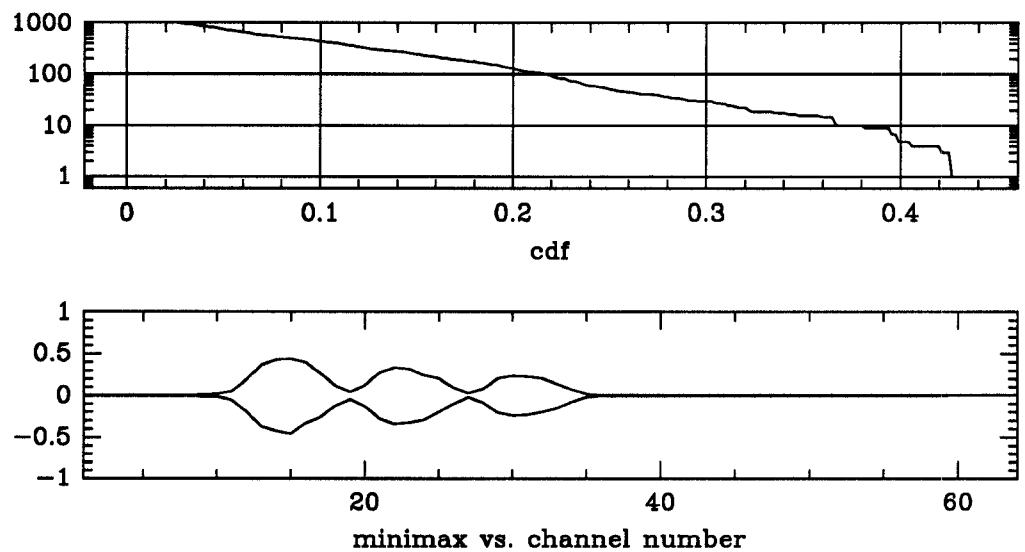
Figure 6.42: Cdf and minimax curves for "harmonic".

Figure 6.43: Regular wavelet representation for "water".

Shown above is the wavelet regular representation and its reconstruction for the signal "water". The trapezoidal analyzing function g appears in the top upper right. To its left are the functions $G = \sum_{m=1}^{N} |D_{s_m}\widehat{g}|^2$ and $\widehat{g}$. The middle graph displays the reconstruction of Algorithm 3.4.3. The lower most graph displays the sampling set Γ. At the top of the bottom graph is the input signal and to its lower right the values of the reconstruction parameters.

Figure 6.44: Reconstruction of "water".

Above, the signal "water"and its reconstructed versions in both time and frequency are displayed. Below, the associated coefficient distribution function λ_{water} is plotted in the top graph while the lower graph shows the max and min value of the wavelet filter bank response as a function of the channel number.
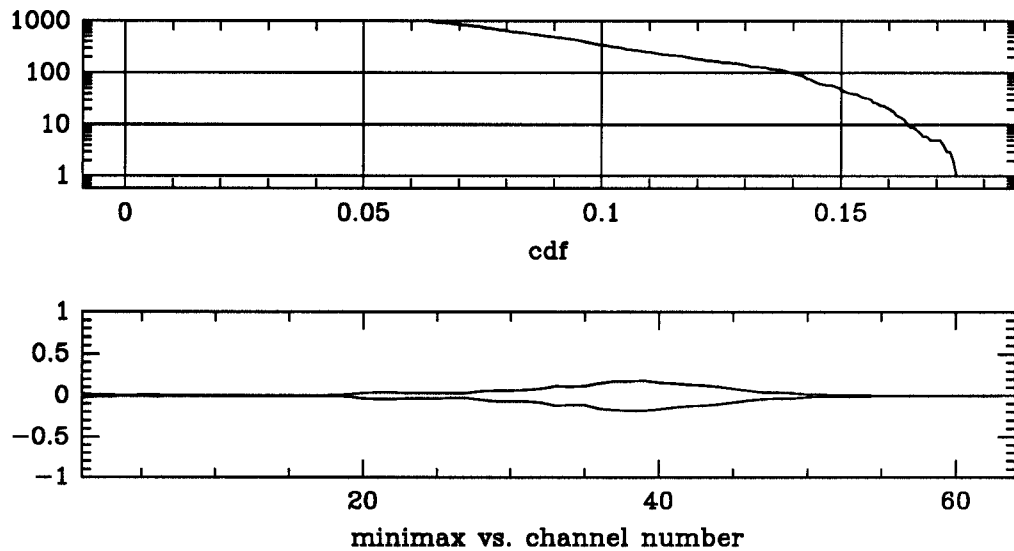

Figure 6.45: Cdf and minimax curves for "water".

6.2.2.3   Positive Extrema Wavelet Representation

In this section we present a sequence of figures which display the discrete positive extrema wavelet representation of the test signals. This representation is derived from the extrema samples of the continuous wavelet transform which are positive. Signals are reconstructed from their positive extrema (PE) wavelet representation via Algorithm 3.4.3. The PE wavelet representation of a signal f which we have used is

$$\{W_g f(a_0^m, t_{m,n})\}$$

where

$$\{t_{m,n}\} = \{t \ : \ W_g f(a_0^m, t) > 0, \ \ \partial_t W_g f(a_0^m, t) = 0\}.$$

Figures 6.46 through 6.57 illustrate the reconstruction of the signals in the test set from their positive extrema wavelet representations.
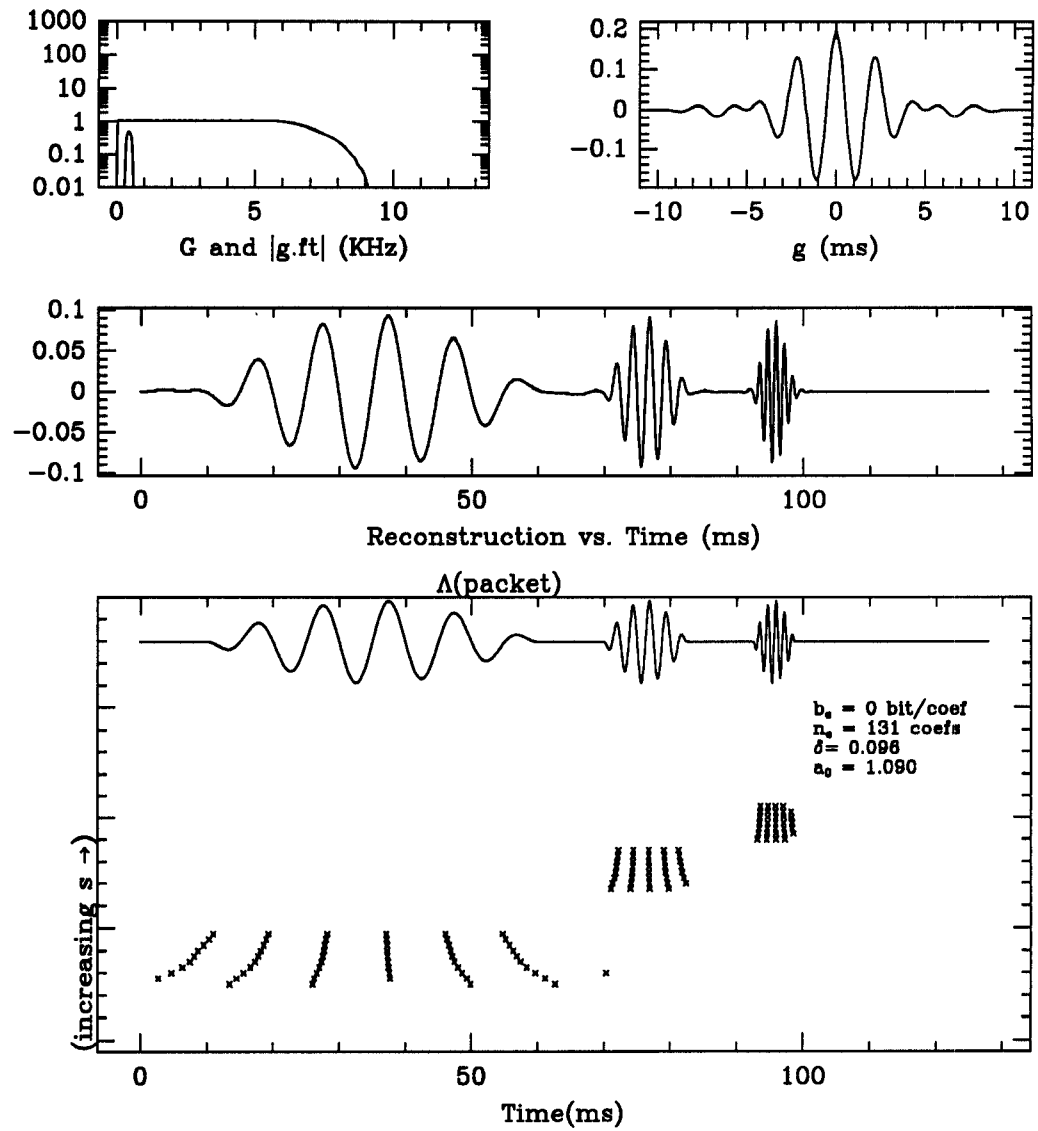
Figure 6.46: Positive extrema wavelet representation for "packet".

Shown above is the wavelet positive extrema representation and its reconstruction for the signal "packet". The trapezoidal analyzing function g appears in the top upper right. To its left are the functions $G = \sum_{m=1}^{N} |D_{s_m}\widehat{g}|^2$ and $\widehat{g}$. The middle graph displays the reconstruction of Algorithm 3.4.3. The lower most graph displays the sampling set Γ. At the top of the bottom graph is the input signal and to its lower right the values of the reconstruction parameters.

Figure 6.47: Reconstruction of "packet".

Above, the signal "packet"and its reconstructed versions in both time and frequency are displayed. Below, the associated coefficient distribution function λ_{packet} is plotted in the top graph while the lower graph shows the max and min value of the wavelet filter bank response as a function of the channel number.

Figure 6.48: Cdf and minimax curves for "packet".

1000
100
10
1
0.1
0.01

0   5   10

G and |g.ft| (KHz)

0.2
0.1
0
-0.1

-10   -5   0   5   10

g (ms)

0.1
0.05
0
-0.05
-0.1

0   50   100

Reconstruction vs. Time (ms)

Λ(chirp)

b_e = 0 bit/coef
n_e = 177 coefs
δ= 0.084
a_0 = 1.090

(increasing s →)

0   50   100

Time(ms)

Figure 6.49: Positive extrema wavelet representation for "chirp".

Shown above is the wavelet positive extrema representation and its reconstruction for the signal "chirp". The trapezoidal analyzing function g appears in the top upper right. To its left are the functions $G = \sum_{m=1}^{N} |D_{s_m}\hat{g}|^2$ and $\hat{g}$. The middle graph displays the reconstruction of Algorithm 3.4.3. The lower most graph displays the sampling set Γ. At the top of the bottom graph is the input signal and to its lower right the values of the reconstruction parameters.
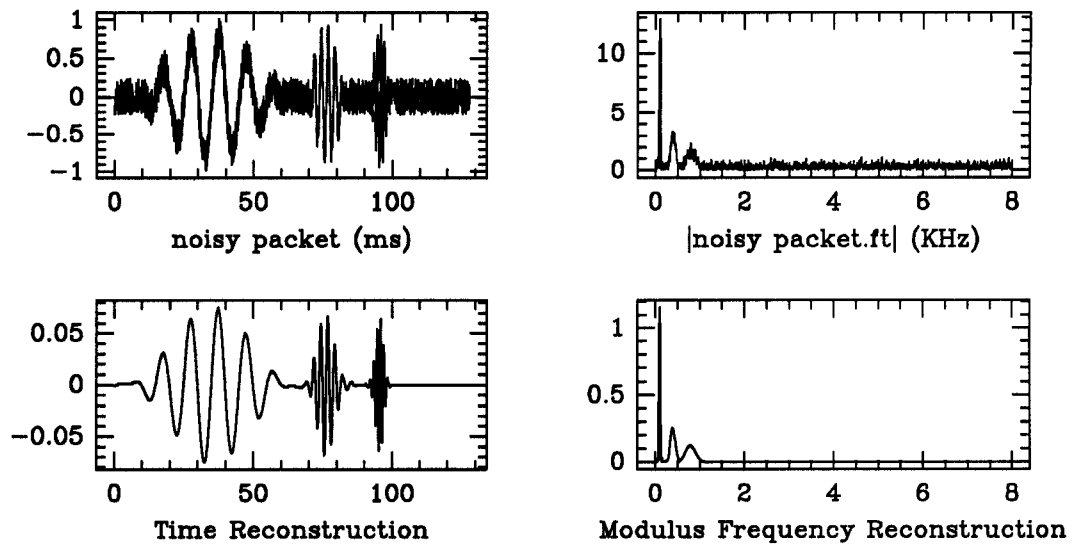
Figure 6.50: Reconstruction of "chirp".

Above, the signal "chirp"and its reconstructed versions in both time and frequency are displayed. Below, the associated coefficient distribution function λ_{chirp} is plotted in the top graph while the lower graph shows the max and min value of the wavelet filter bank response as a function of the channel number.
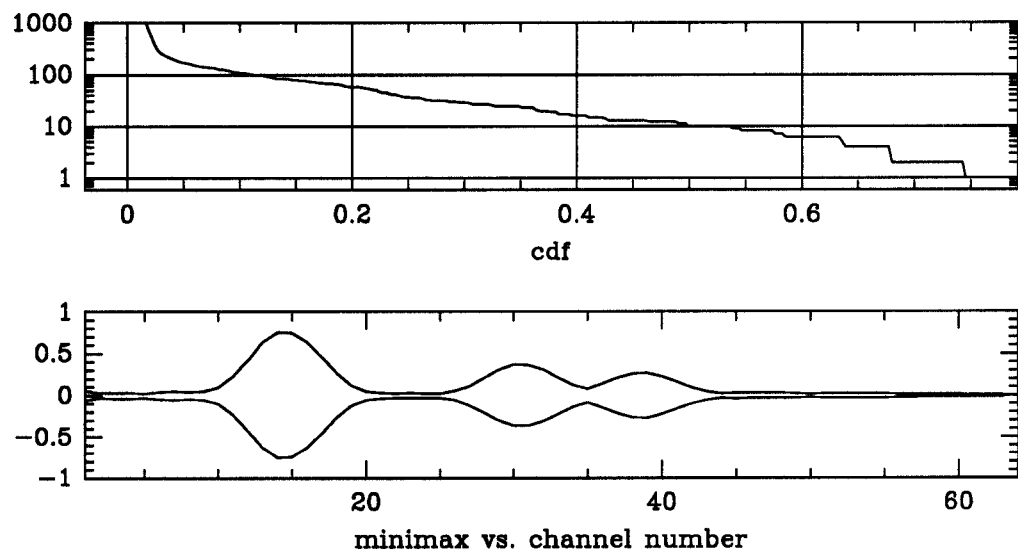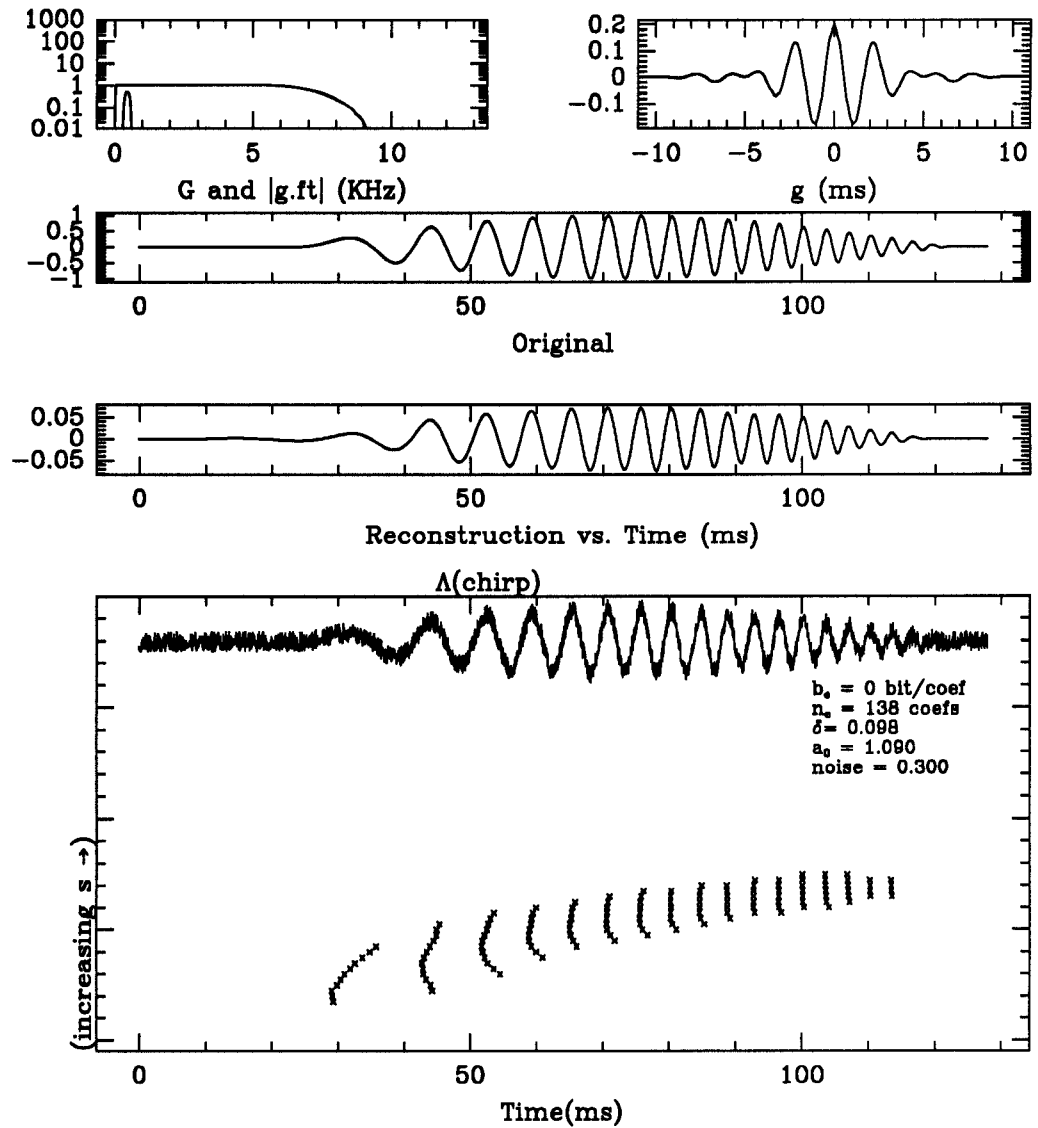

Figure 6.51: Cdf and minimax curves for "chirp".
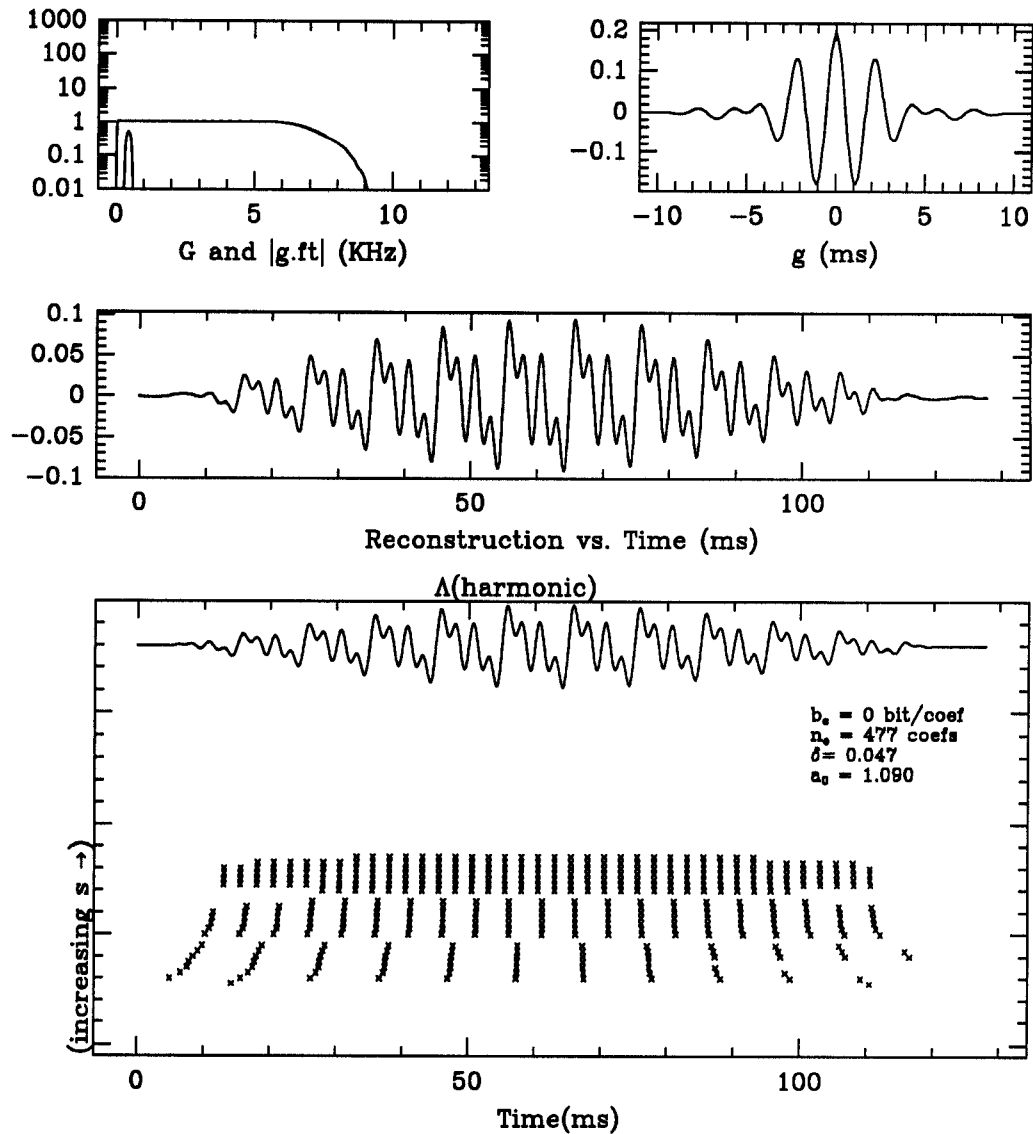
Figure 6.52: Positive extrema wavelet representation for "harmonic".

Shown above is the wavelet positive extrema representation and its reconstruction for the signal "harmonic". The trapezoidal analyzing function g appears in the top upper right. To its left are the functions $G = \sum_{m=1}^{N} |D_{s_m}\hat{g}|^2$ and $\hat{g}$. The middle graph displays the reconstruction of Algorithm 3.4.3. The lower most graph displays the sampling set Γ. At the top of the bottom graph is the input signal and to its lower right the values of the reconstruction parameters.
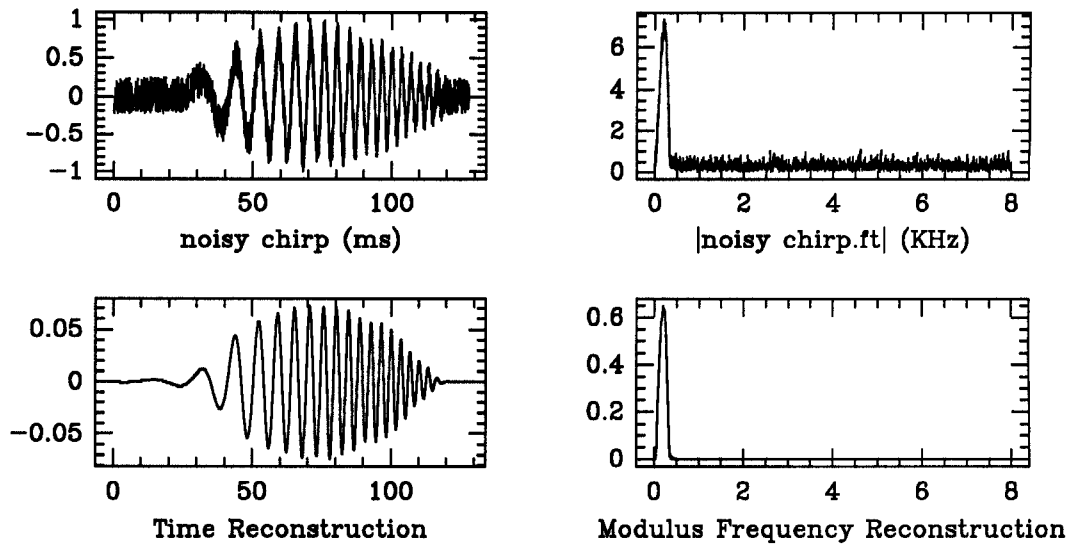
Figure 6.53: Reconstruction of "harmonic".

Above, the signal "harmonic"and its reconstructed versions in both time and frequency are displayed. Below, the associated coefficient distribution function $\lambda_{\text{harmonic}}$ is plotted in the top graph while the lower graph shows the max and min value of the wavelet filter bank response as a function of the channel number.

Figure 6.54: Cdf and minimax curves for "harmonic".
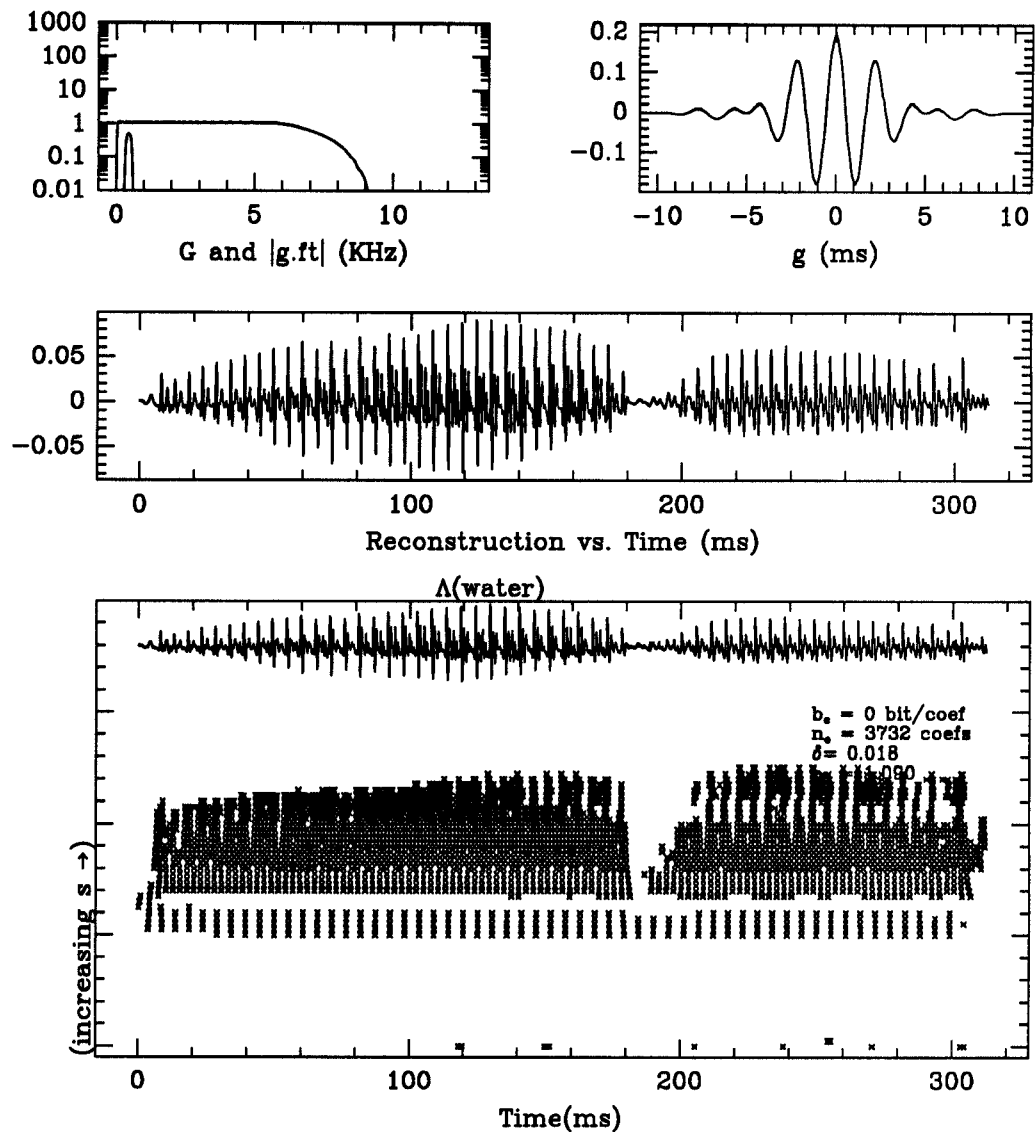
Figure 6.55: Positive extrema wavelet representation for "water".

Shown above is the wavelet positive extrema representation and its reconstruction for the signal "water". The trapezoidal analyzing function g appears in the top upper right. To its left are the functions $G = \sum_{m=1}^{N} |D_{s_m}\hat{g}|^2$ and $\hat{g}$. The middle graph displays the reconstruction of Algorithm 3.4.3. The lower most graph displays the sampling set Γ. At the top of the bottom graph is the input signal and to its lower right the values of the reconstruction parameters.

130

Figure 6.56: Reconstruction of "water".

Above, the signal "water"and its reconstructed versions in both time and frequency are displayed. Below, the associated coefficient distribution function λ_{water} is plotted in the top graph while the lower graph shows the max and min value of the wavelet filter bank response as a function of the channel number.
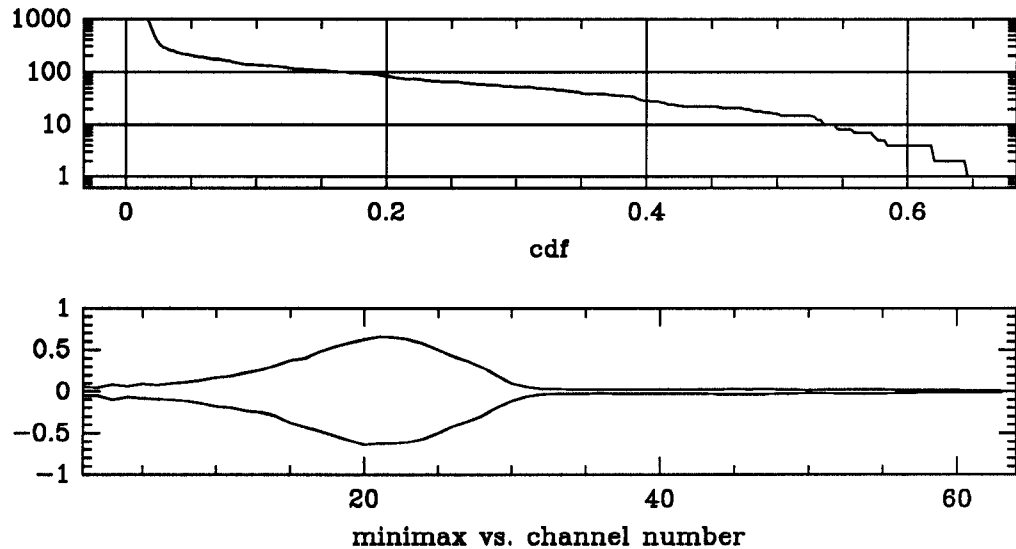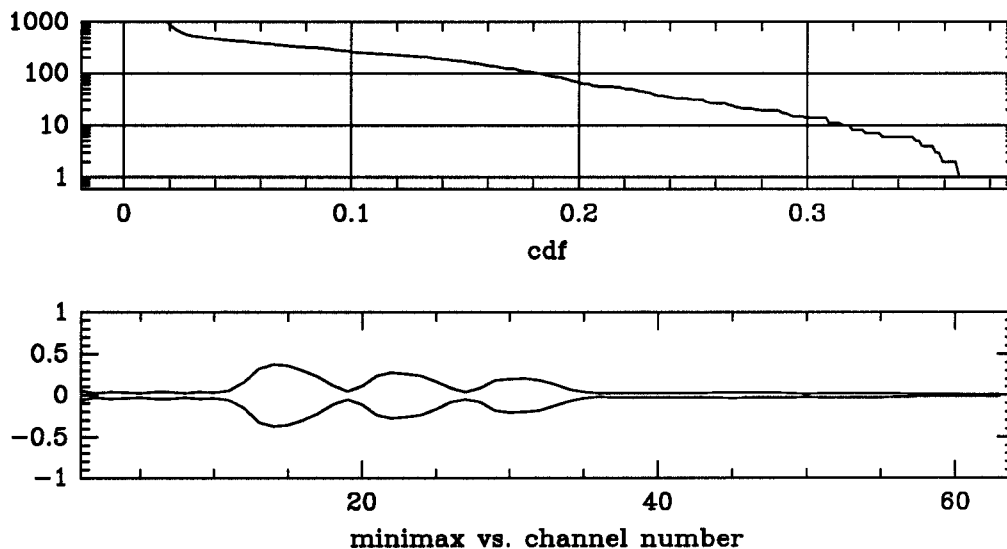

Figure 6.57: Cdf and minimax curves for "water".

6.3 Applications

We have seen numerous examples of discrete wavelet representations in the previous sections. From these examples it is seen that these discrete wavelet representations characterize signals in a manner which reflects their time-frequency behavior. A representation of this sort lends itself to numerous applications. Chapter 7 presents a partial list of such applications. In this section we limit ourselves to two applications: noise suppression and compression.

For the discrete positive extrema wavelet representation with the trapezoidal analyzing function g_{trap}, the next two sections display numerical results of (i) the noise suppression scheme discussed in Section 3.5.2 and (ii) the compression scheme discussed in Section 5.3.

6.3.1 Noise Suppression

For the noise suppression problem the goal is to reject noisy portions of corrupted signals and to recover their coherent portions. Based on the scheme discussed in Section 3.5.2, a numerical experiment is presented and its performance in various levels of random additive noise is displayed.

The noise suppression experiment can be summarized as follows. Fix a noise level $\sigma > 0$ and a threshold $\delta > 0$. For each f_* in the test set the following steps are performed:

(i) Generate a random noise signal $w(t)$ such that for each t, $w(t)$ is uniformly distributed in $[-1, 1]$.

(ii) Additively corrupt the signal f_* by σw yielding the noisy signal

$$f_w = f_* + \sigma w.$$

(iii) Compute the wavelet positive extrema representation of f_w:

$$\Lambda(f_w) \triangleq \{W_g f_w(t_{m,n}, s_m)\}.$$

(iv) Compute the distribution function λ_{f_w}.

(v) Threshold the wavelet positive extrema representation $\Lambda(f_*)$ by δ, yielding the truncated representation

$$\Lambda_\delta(f_w) \triangleq \{W_g f_w(t_{m,n}, s_m) \; : \; W_g f_w(t_{m,n}, s_m) \geq \delta\}.$$

(vi) Generate reconstruction of f_* using Algorithm 3.4.3 where initial data is

$$c_0 = \Lambda_\delta(f_w).$$

Figures 6.58 through 6.69 display the noise suppressed reconstructions for an additive noise level $\sigma = 0.3$ corresponding to a signal to noise ratio of $SNR \approx 5.2$dB.

Figures 6.70 through 6.81 display the noise suppressed reconstructions for an additive noise level $\sigma = 0.5$ corresponding to a signal to noise ratio of $SNR \approx 3.0$dB.

Figures 6.82 through 6.93 display the noise suppressed reconstructions for an additive noise level $\sigma = 0.7$ corresponding to a signal to noise ratio of $SNR \approx 1.5$dB.
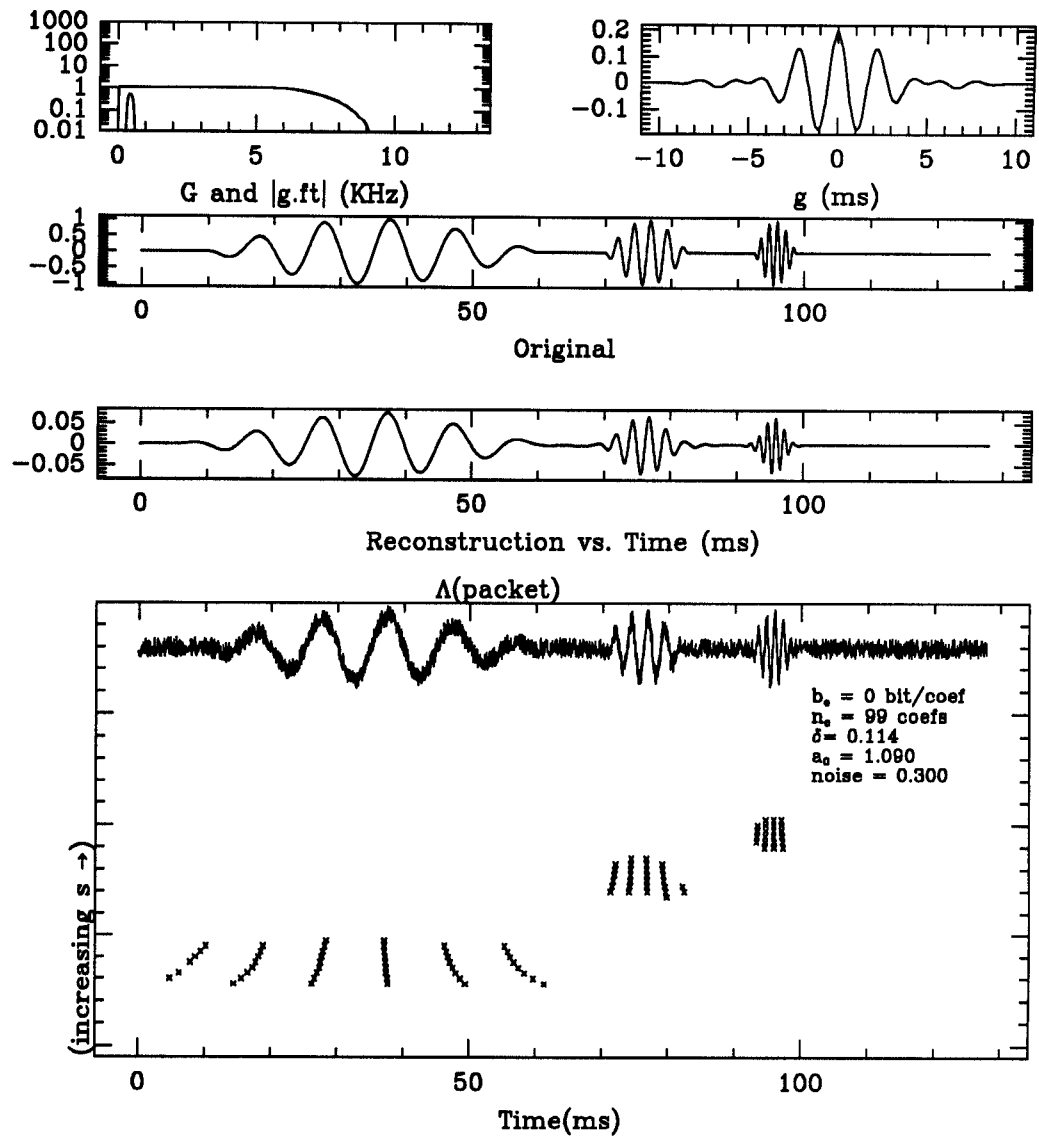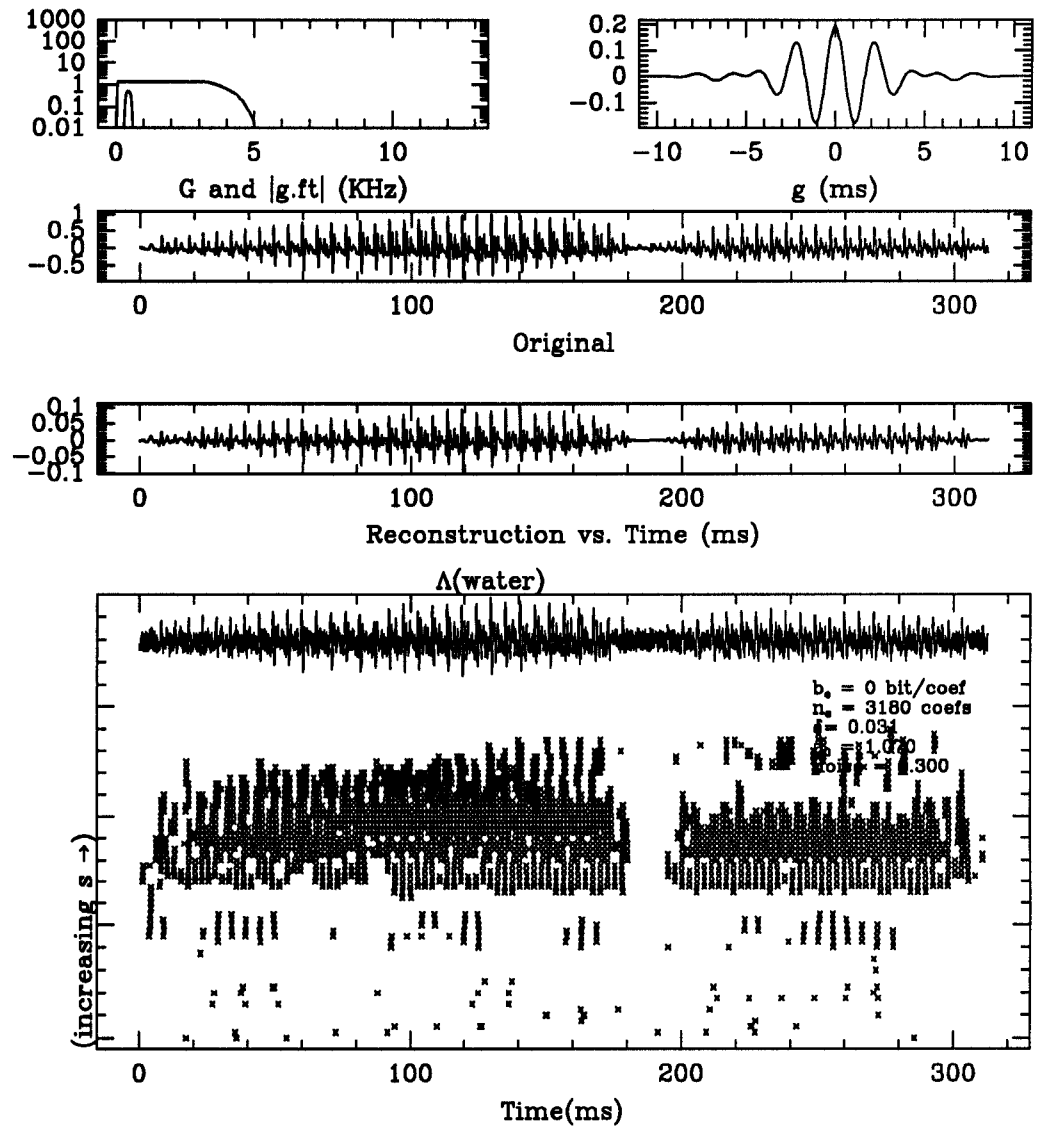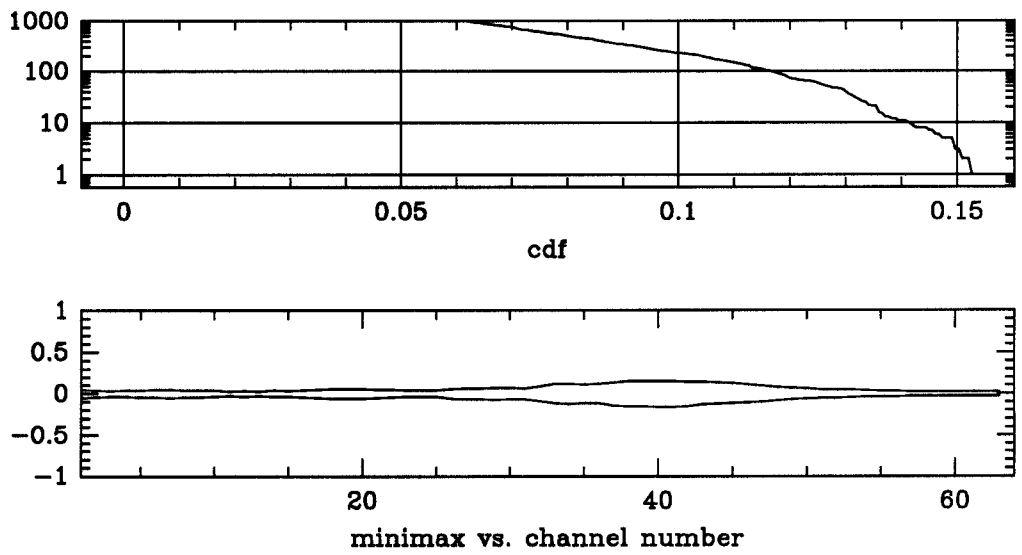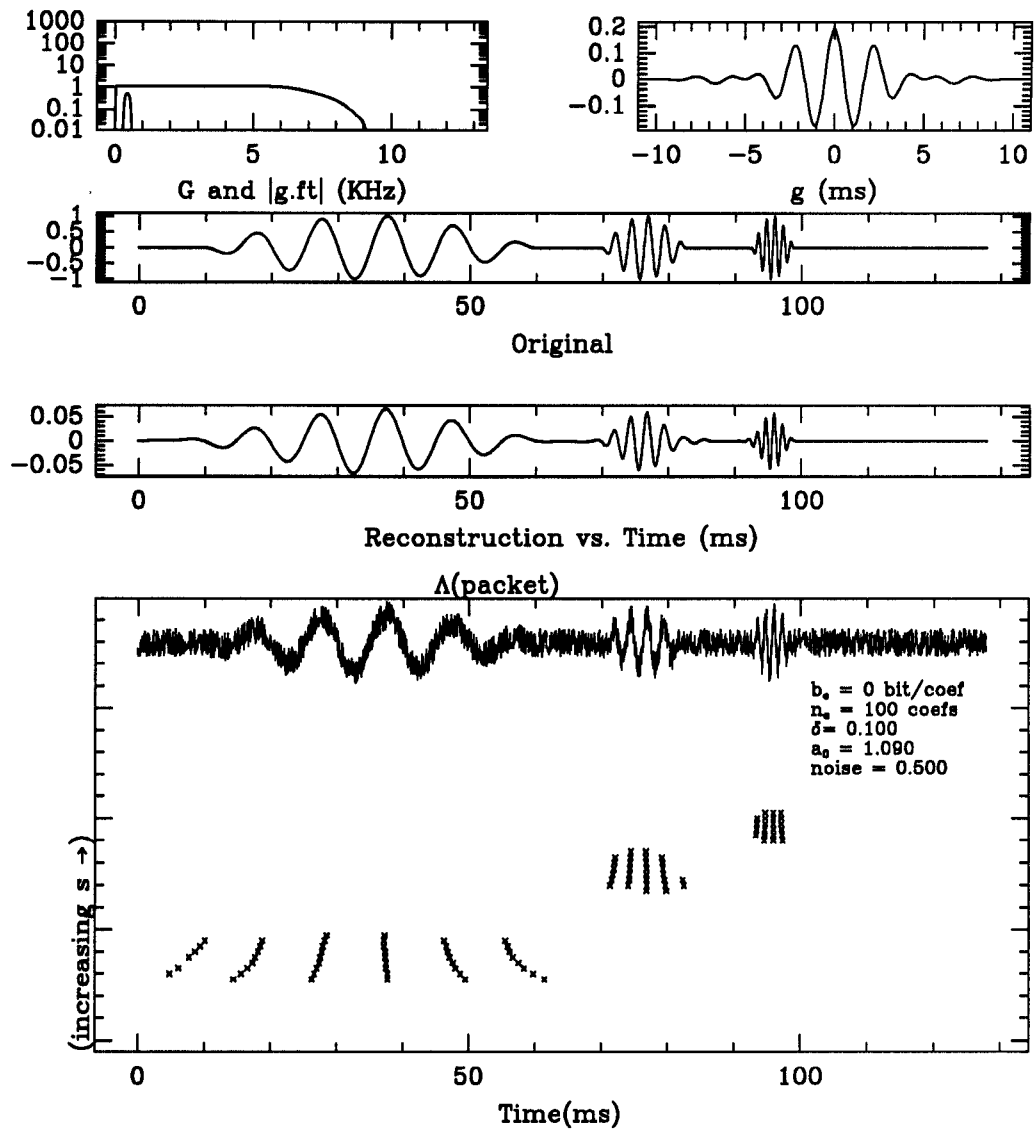
Figure 6.58: PE wavelet representation for "packet", $\sigma = 0.3$.

Shown above is the wavelet positive extrema representation and its reconstruction for the noisy signal "packet". The trapezoidal analyzing function g appears in the top upper right. To its left are the functions $G = \sum_{m=1}^{N} |D_{s_m}\hat{g}|^2$ and $\hat{g}$. The middle graph displays the reconstruction of Algorithm 3.4.3. The lower most graph displays the sampling set Γ. At the top of the bottom graph is the input signal and to its lower right the values of the reconstruction parameters.
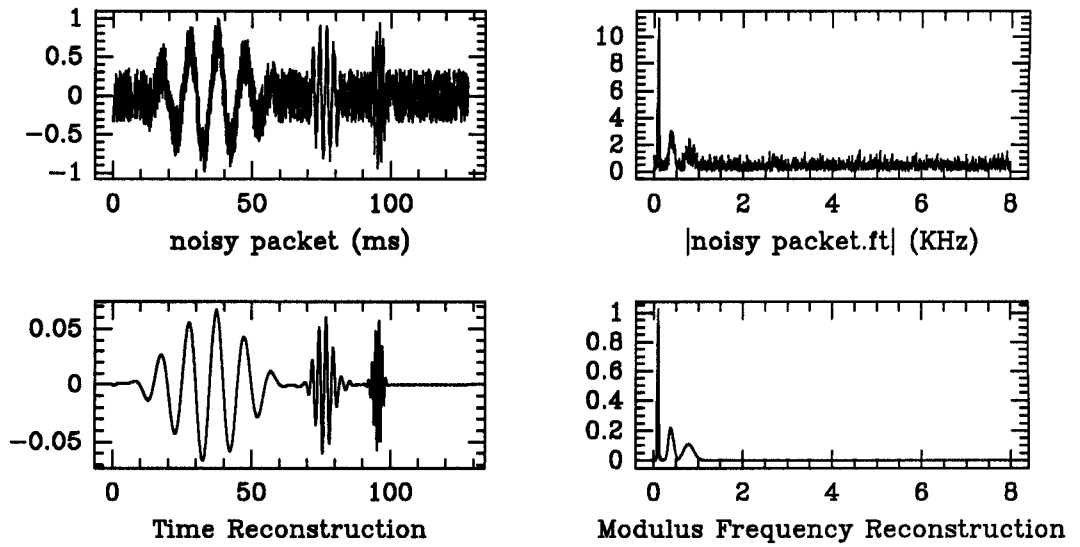
133

Figure 6.59: Reconstruction of noisy "packet", $\sigma = 0.3$.

Above, the signal "packet"and its reconstructed versions in both time and frequency are displayed. Below, the associated coefficient distribution function λ_{packet} is plotted in the top graph while the lower graph shows the max and min value of the wavelet filter bank response as a function of the channel number.
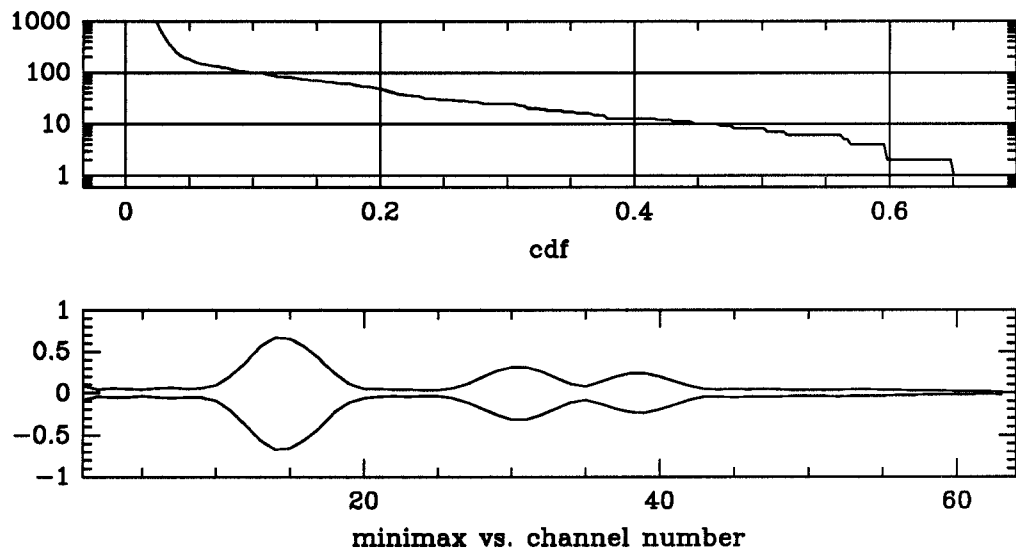

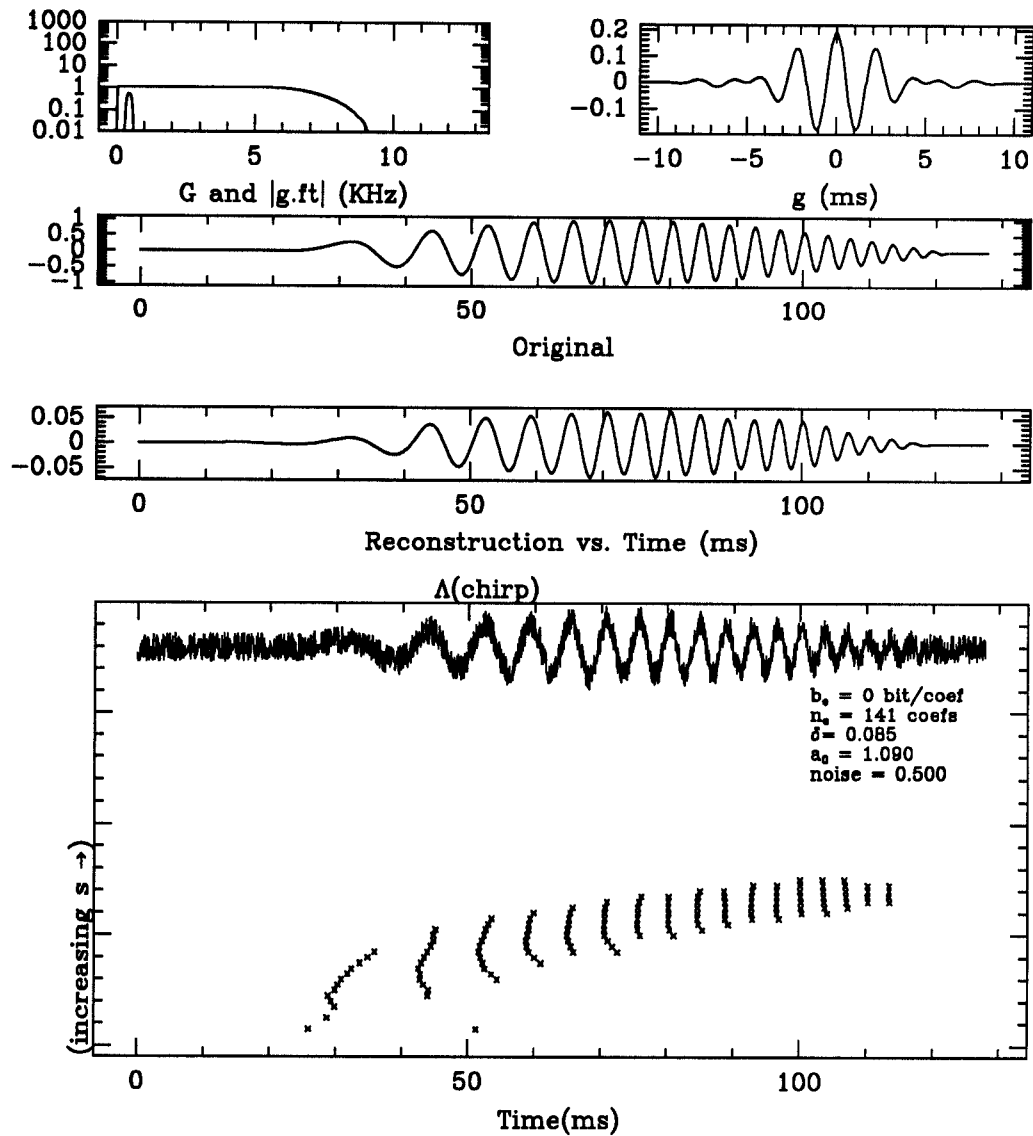Figure 6.60: Cdf and minimax curves for noisy "packet", $\sigma = 0.3$.

Figure 6.61: PE wavelet representation for "chirp", $\sigma = 0.3$.

Shown above is the wavelet positive extrema representation and its reconstruction for the noisy signal "chirp". The trapezoidal analyzing function g appears in the top upper right. To its left are the functions $G = \sum_{m=1}^{N} |D_{s_m}\widehat{g}|^2$ and $\widehat{g}$. The middle graph displays the reconstruction of Algorithm 3.4.3. The lower most graph displays the sampling set Γ. At the top of the bottom graph is the input signal and to its lower right the values of the reconstruction parameters.
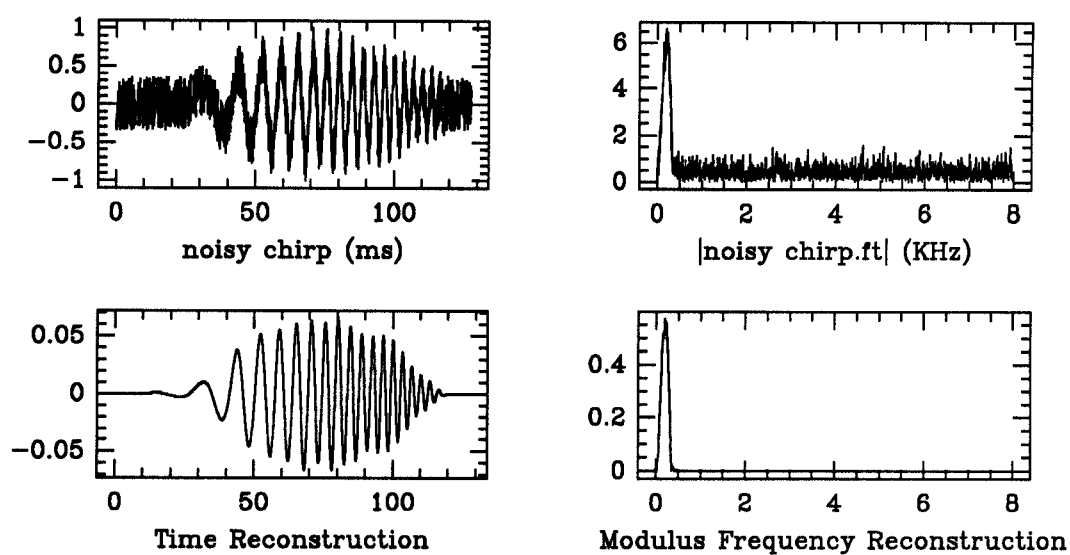
Figure 6.62: Reconstruction of noisy "chirp", $\sigma = 0.3$.

Above, the signal "chirp" and its reconstructed versions in both time and frequency are displayed. Below, the associated coefficient distribution function λ_{chirp} is plotted in the top graph while the lower graph shows the max and min value of the wavelet filter bank response as a function of the channel number.

Figure 6.63: Cdf and minimax curves for noisy "chirp", $\sigma = 0.3$.
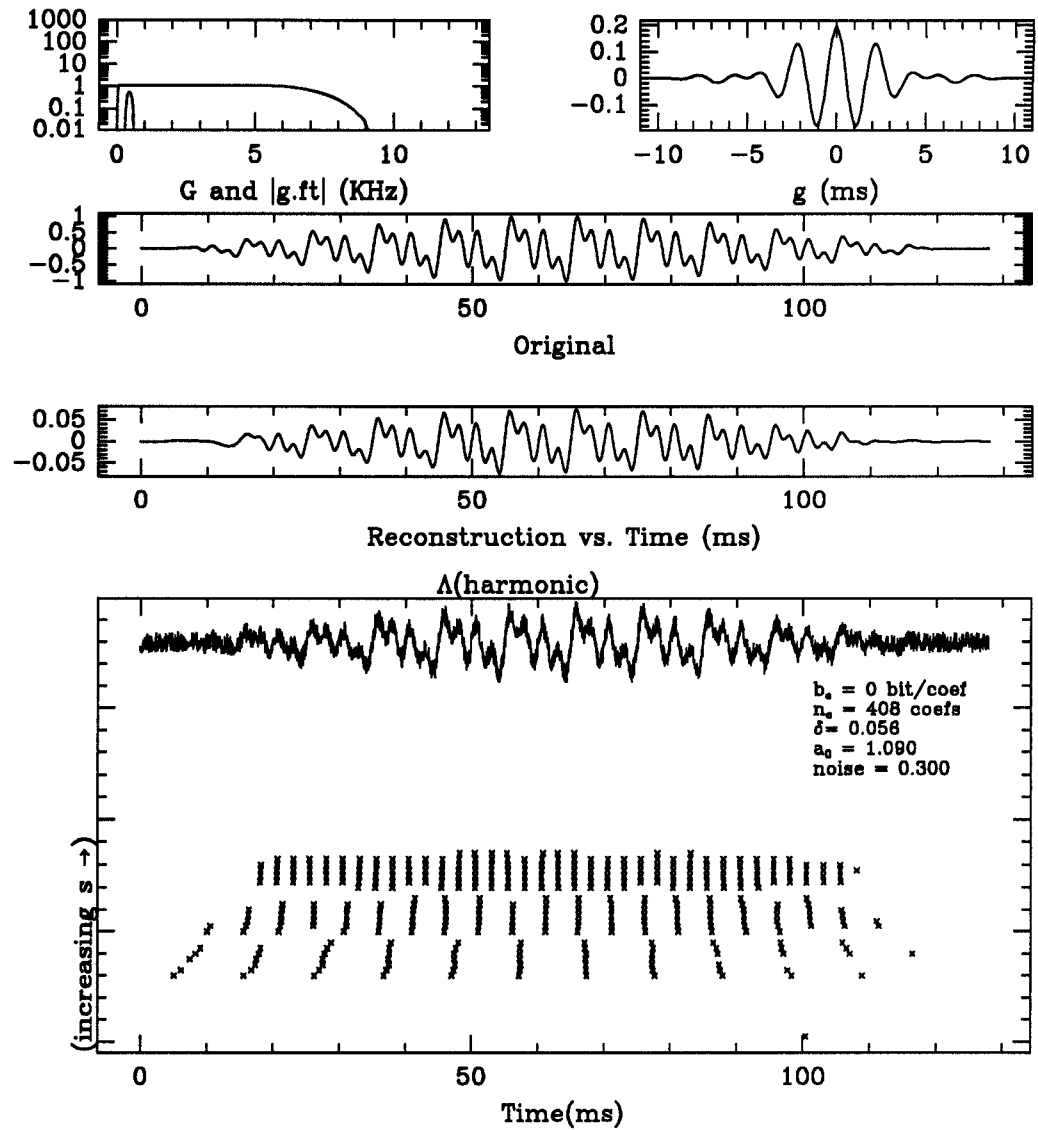
Figure 6.64: PE wavelet representation for "harmonic", $\sigma = 0.3$.

Shown above is the wavelet positive extrema representation and its reconstruction for the noisy signal "harmonic". The trapezoidal analyzing function g appears in the top upper right. To its left are the functions $G = \sum_{m=1}^{N} |D_{s_m}\hat{g}|^2$ and $\hat{g}$. The middle graph displays the reconstruction of Algorithm 3.4.3. The lower most graph displays the sampling set Γ. At the top of the bottom graph is the input signal and to its lower right the values of the reconstruction parameters.
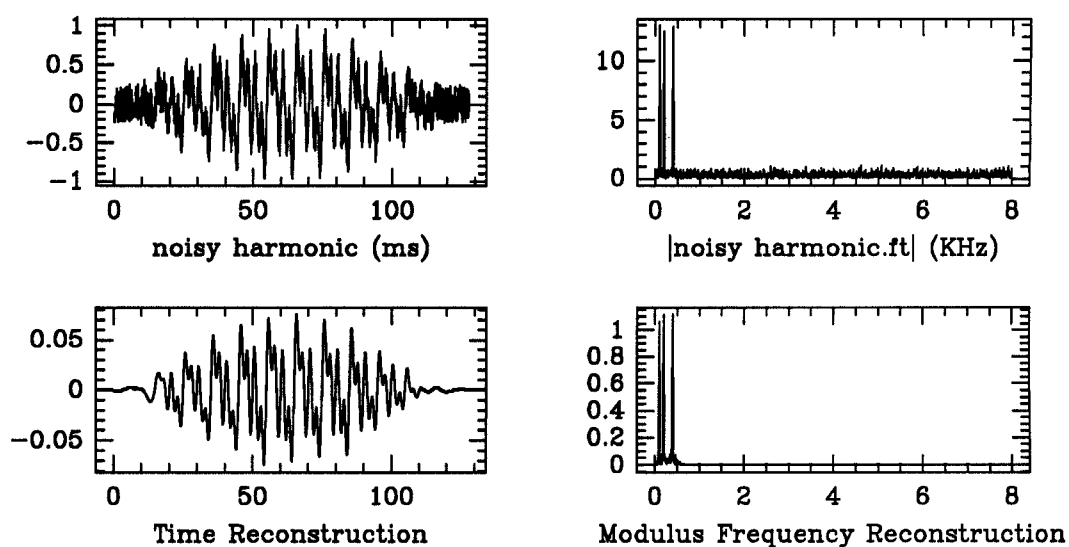
Figure 6.65: Reconstruction of noisy "harmonic", $\sigma = 0.3$.

Above, the signal "harmonic" and its reconstructed versions in both time and frequency are displayed. Below, the associated coefficient distribution function $\lambda_{\text{harmonic}}$ is plotted in the top graph while the lower graph shows the max and min value of the wavelet filter bank response as a function of the channel number.
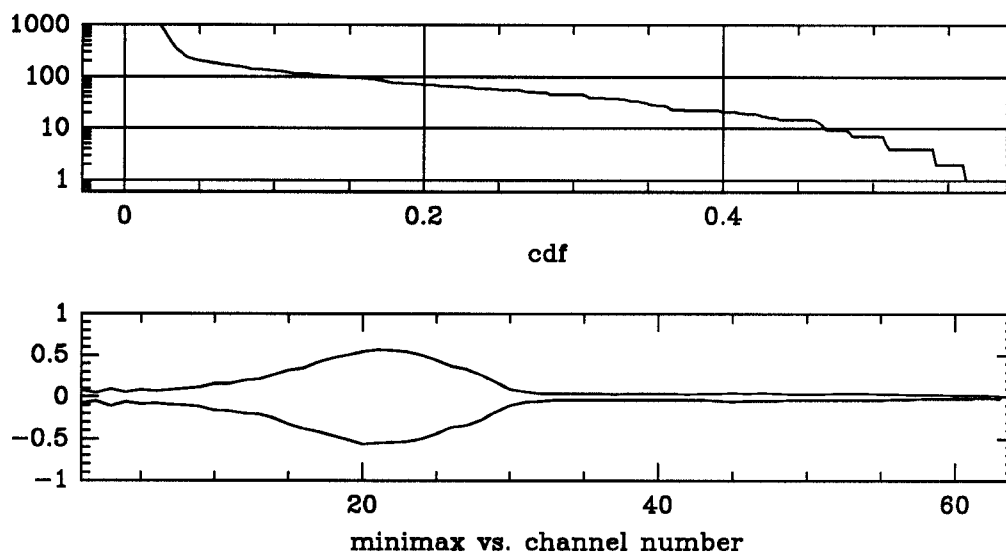

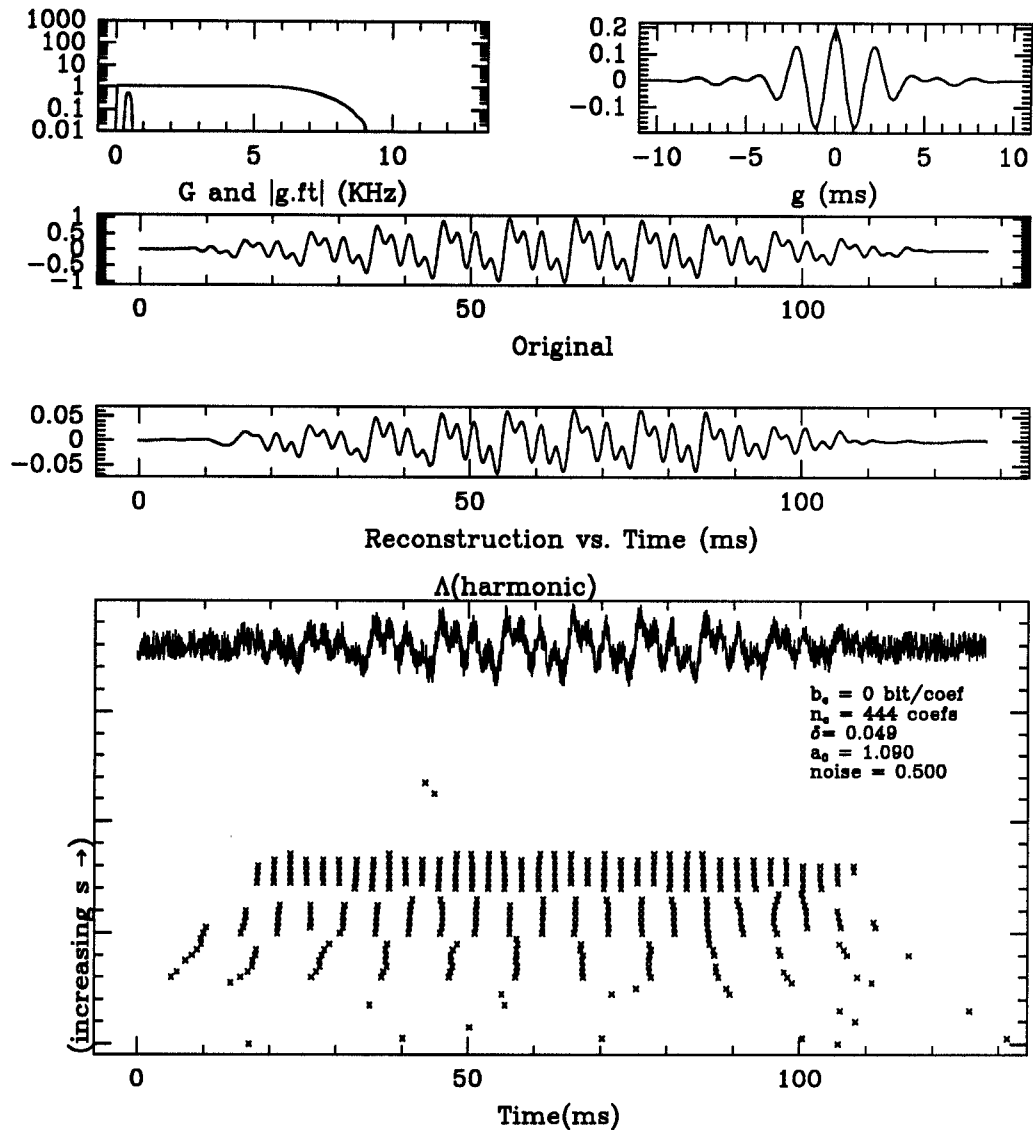Figure 6.66: Cdf and minimax curves for noisy "harmonic", $\sigma = 0.3$.

Figure 6.67: PE wavelet representation for "water", $\sigma = 0.3$.

Shown above is the wavelet positive extrema representation and its reconstruction for the noisy signal "water". The trapezoidal analyzing function g appears in the top upper right. To its left are the functions $G = \sum_{m=1}^{N} |D_{s_m}\widehat{g}|^2$ and $\widehat{g}$. The middle graph displays the reconstruction of Algorithm 3.4.3. The lower most graph displays the sampling set Γ. At the top of the bottom graph is the input signal and to its lower right the values of the reconstruction parameters.
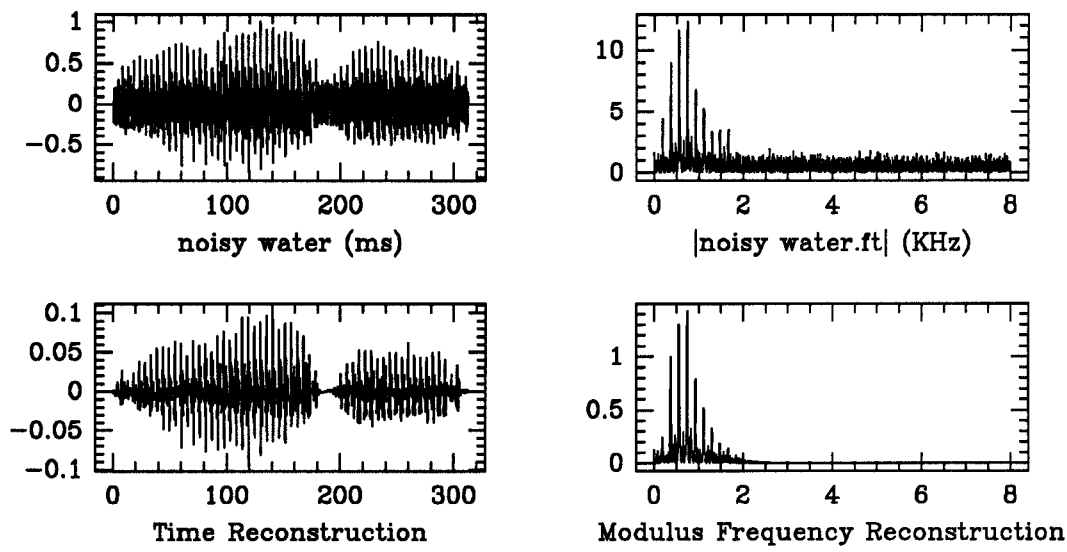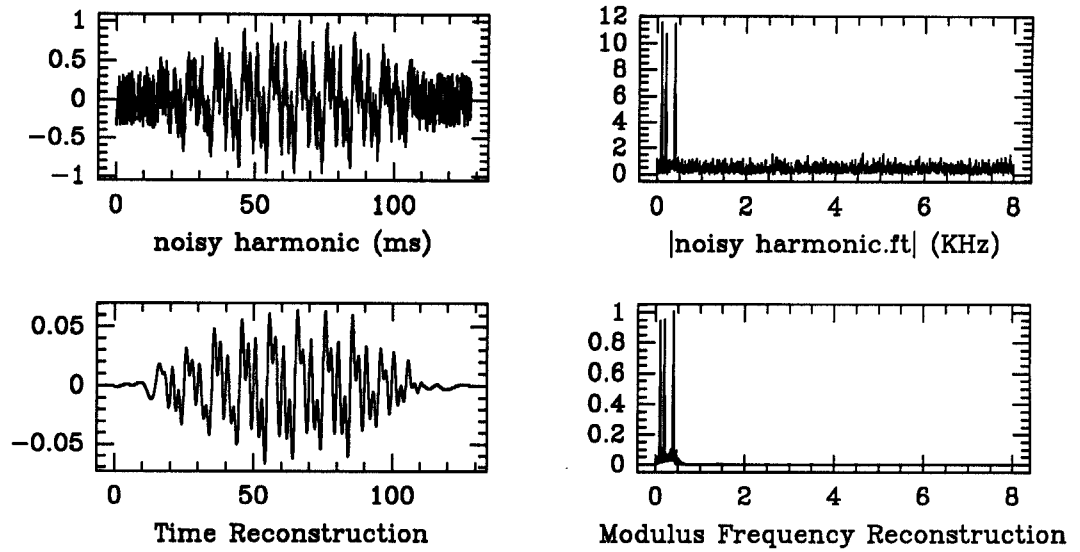
Figure 6.68: Reconstruction of noisy "water", $\sigma = 0.3$.

Above, the signal "water" and its reconstructed versions in both time and frequency are displayed. Below, the associated coefficient distribution function λ_{water} is plotted in the top graph while the lower graph shows the max and min value of the wavelet filter bank response as a function of the channel number.
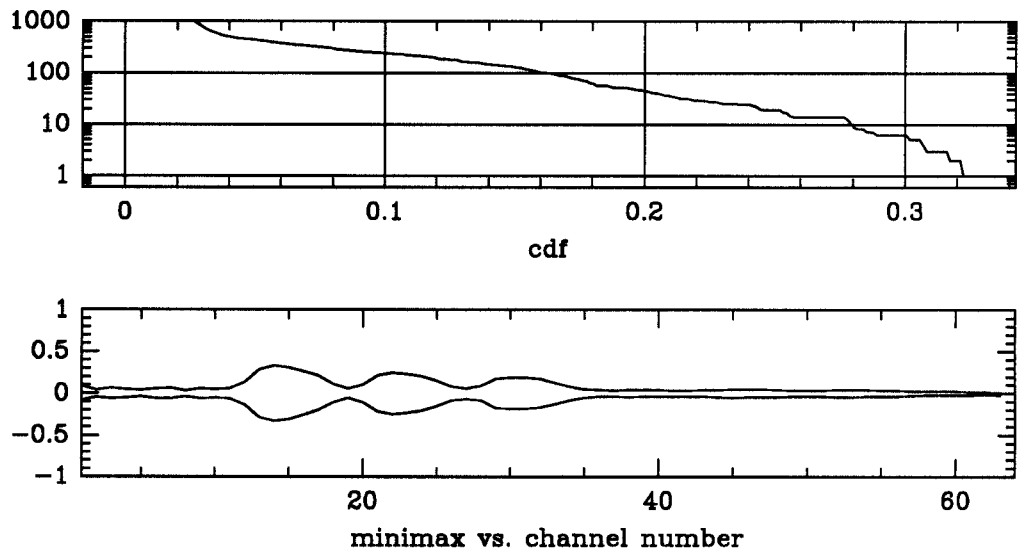

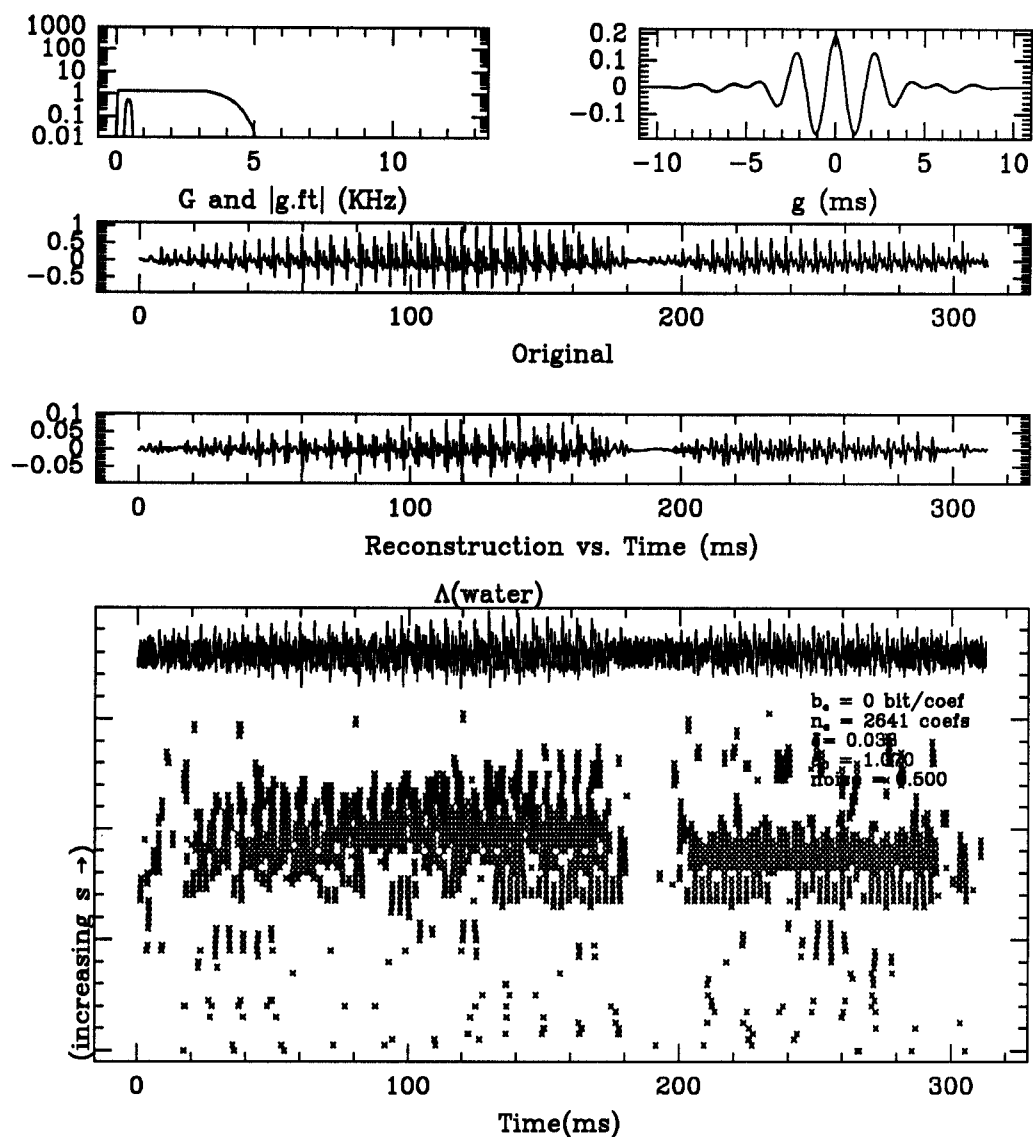Figure 6.69: Cdf and minimax curves for noisy "water", $\sigma = 0.3$.

Figure 6.70: PE wavelet representation for "packet", $\sigma = 0.5$.

Shown above is the wavelet positive extrema representation and its reconstruction for the noisy signal "packet". The trapezoidal analyzing function g appears in the top upper right. To its left are the functions $G = \sum_{m=1}^{N} |D_{s_m}\widehat{g}|^2$ and $\widehat{g}$. The middle graph displays the reconstruction of Algorithm 3.4.3. The lower most graph displays the sampling set Γ. At the top of the bottom graph is the input signal and to its lower right the values of the reconstruction parameters.
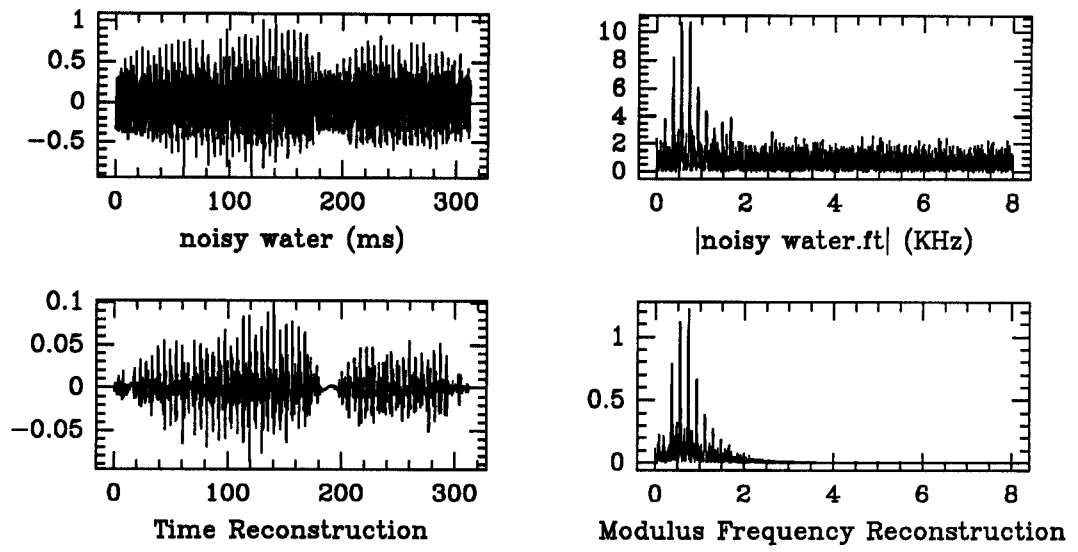
Figure 6.71: Reconstruction of noisy "packet", $\sigma = 0.5$.

Above, the signal "packet"and its reconstructed versions in both time and frequency are displayed. Below, the associated coefficient distribution function λ_{packet} is plotted in the top graph while the lower graph shows the max and min value of the wavelet filter bank response as a function of the channel number.
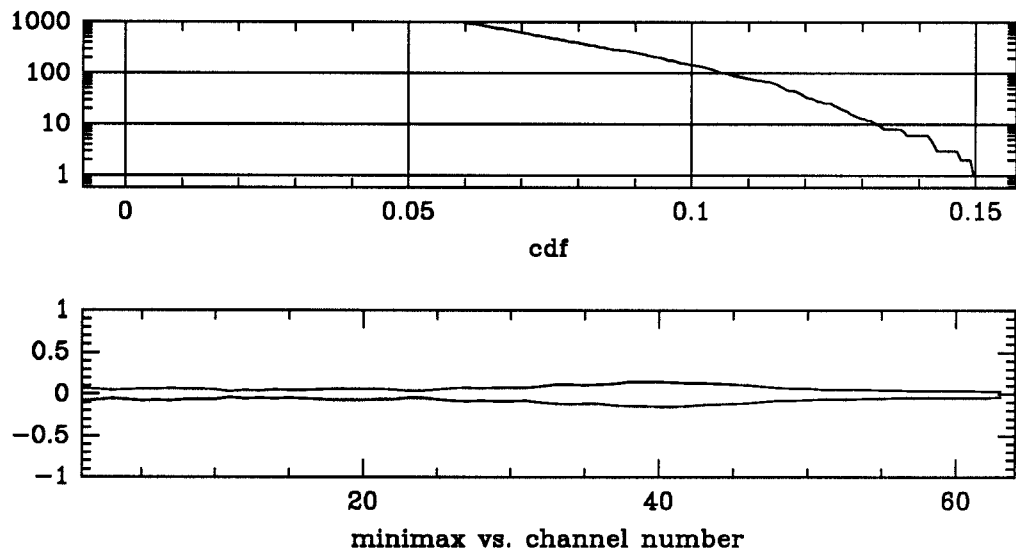

Figure 6.72: Cdf and minimax curves for noisy "packet", $\sigma = 0.5$.
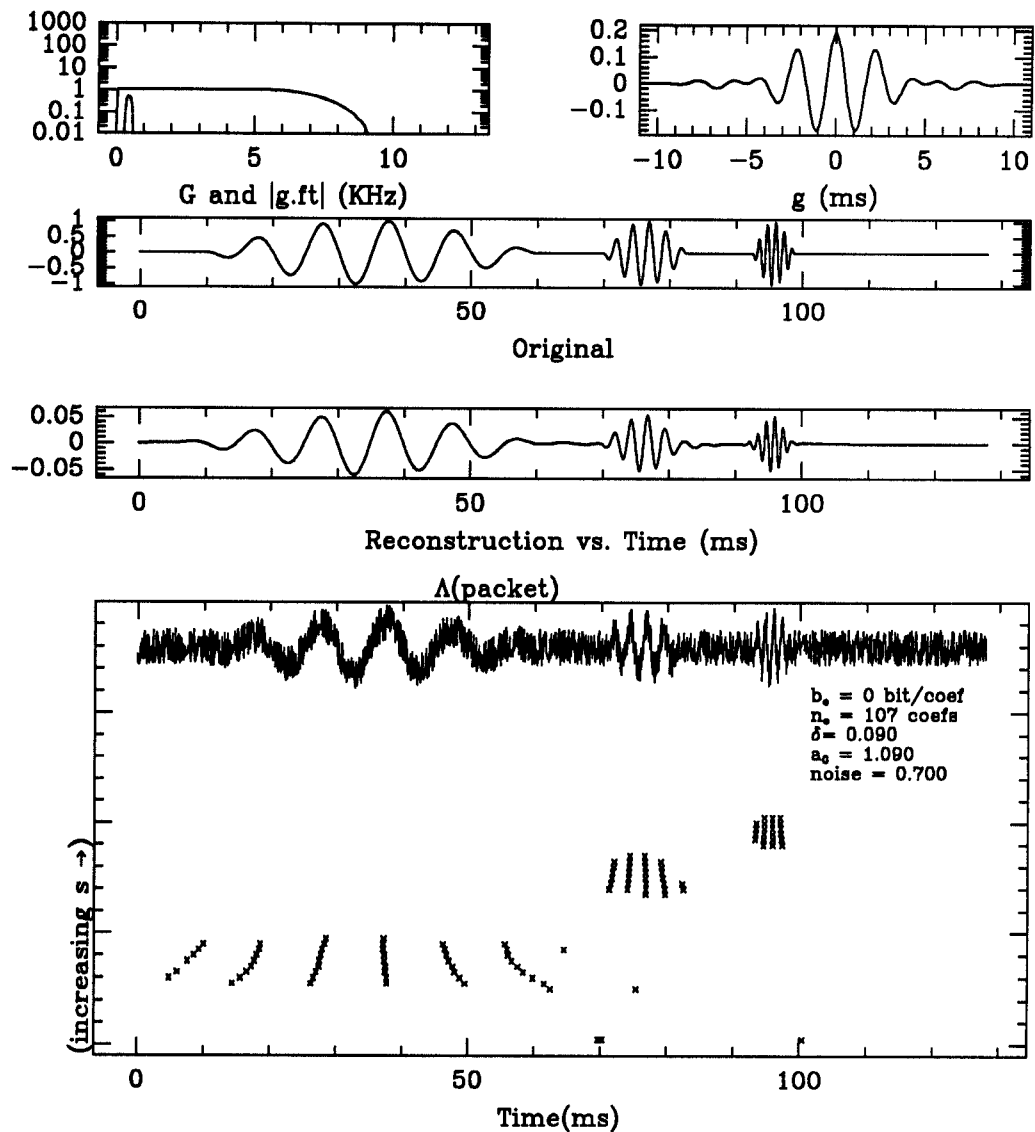
142

Figure 6.73: PE wavelet representation for "chirp", $\sigma = 0.5$.

Shown above is the wavelet positive extrema representation and its reconstruction for the noisy signal "chirp". The trapezoidal analyzing function g appears in the top upper right. To its left are the functions $G = \sum_{m=1}^{N} |D_{s_m}\widehat{g}|^2$ and $\widehat{g}$. The middle graph displays the reconstruction of Algorithm 3.4.3. The lower most graph displays the sampling set Γ. At the top of the bottom graph is the input signal and to its lower right the values of the reconstruction parameters.
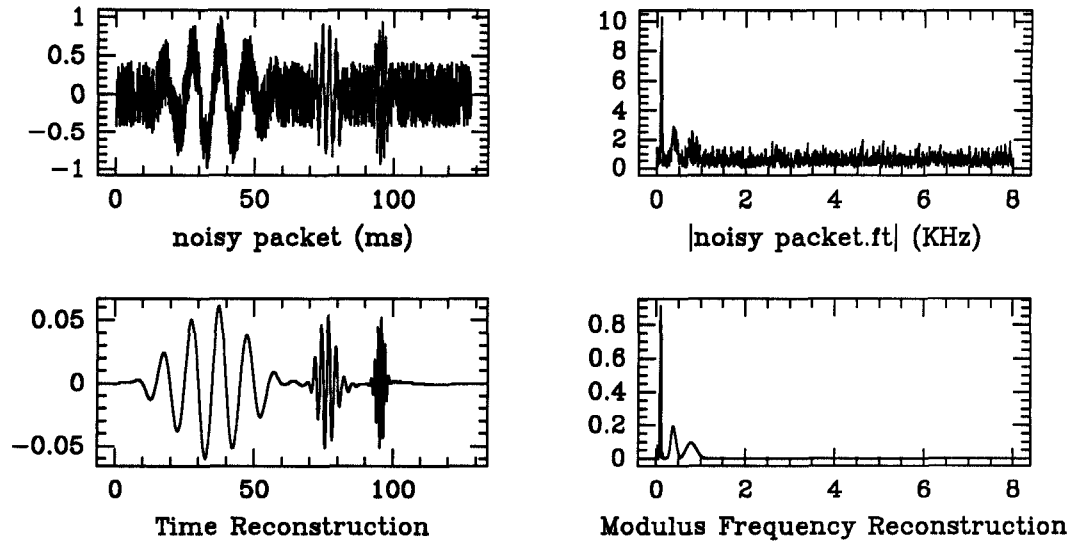
Figure 6.74: Reconstruction of noisy "chirp", $\sigma = 0.5$.

Above, the signal "chirp"and its reconstructed versions in both time and frequency are displayed. Below, the associated coefficient distribution function λ_{chirp} is plotted in the top graph while the lower graph shows the max and min value of the wavelet filter bank response as a function of the channel number.

Figure 6.75: Cdf and minimax curves for noisy "chirp", $\sigma = 0.5$.

144

Figure 6.76: PE wavelet representation for "harmonic", $\sigma = 0.5$.

Shown above is the wavelet positive extrema representation and its reconstruction for the noisy signal "harmonic". The trapezoidal analyzing function g appears in the top upper right. To its left are the functions $G = \sum_{m=1}^{N} |D_{s_m}\widehat{g}|^2$ and $\widehat{g}$. The middle graph displays the reconstruction of Algorithm 3.4.3. The lower most graph displays the sampling set Γ. At the top of the bottom graph is the input signal and to its lower right the values of the reconstruction parameters.

Figure 6.77: Reconstruction of noisy "harmonic", $\sigma = 0.5$.

Above, the signal "harmonic" and its reconstructed versions in both time and frequency are displayed. Below, the associated coefficient distribution function $\lambda_{harmonic}$ is plotted in the top graph while the lower graph shows the max and min value of the wavelet filter bank response as a function of the channel number.
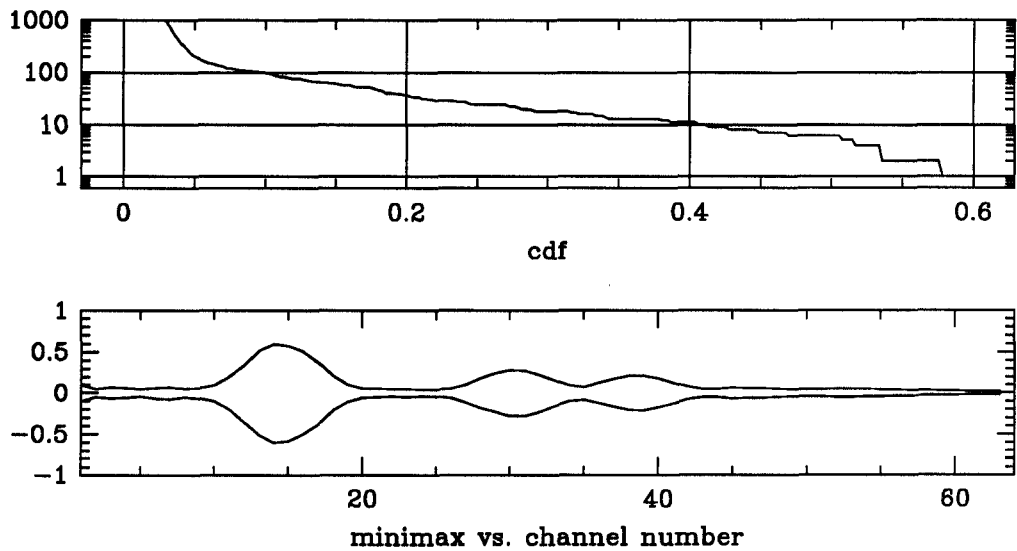

Figure 6.78: Cdf and minimax curves for noisy "harmonic", $\sigma = 0.5$.
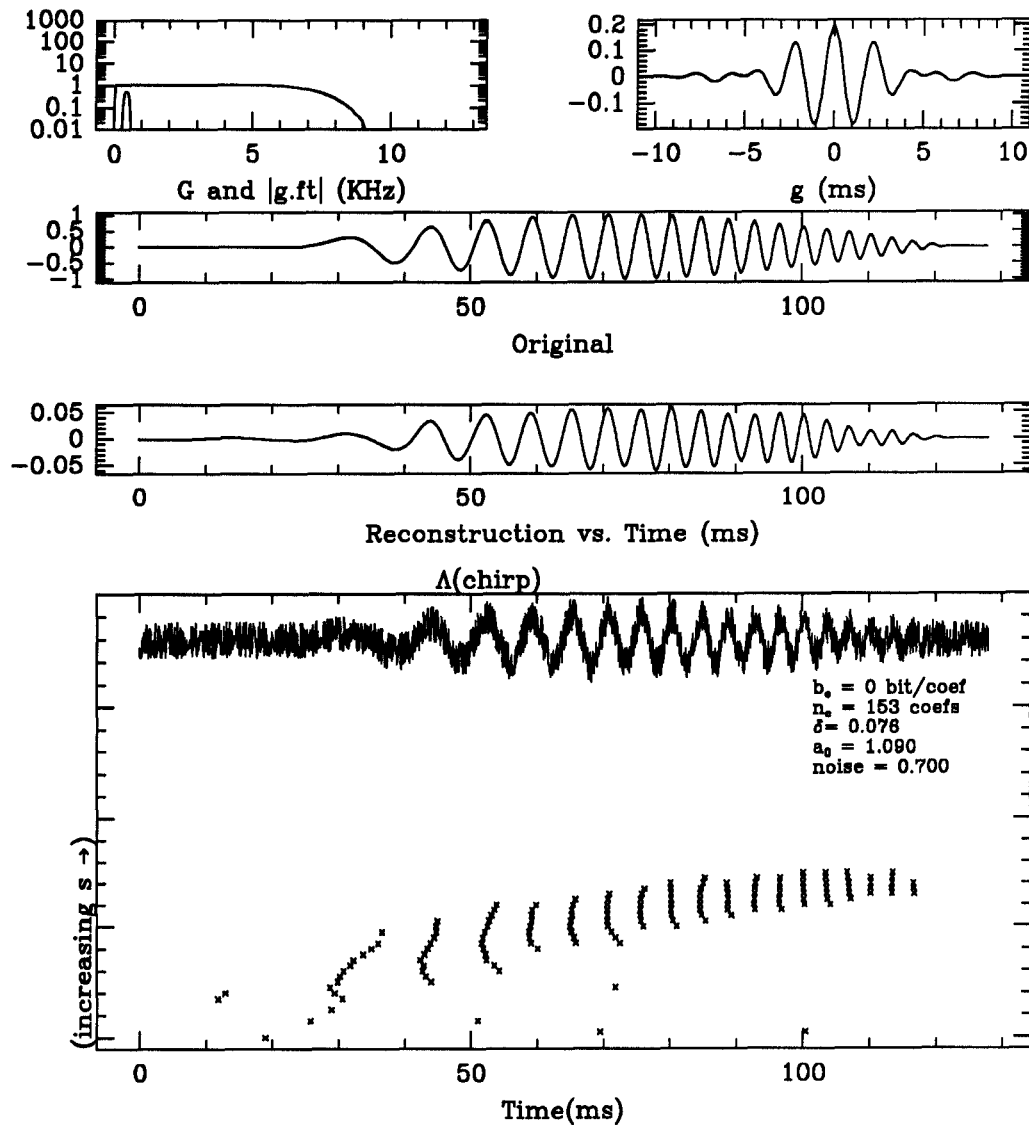
Figure 6.79: PE wavelet representation for "water", $\sigma = 0.5$.

Shown above is the wavelet positive extrema representation and its reconstruction for the noisy signal "water". The trapezoidal analyzing function g appears in the top upper right. To its left are the functions $G = \sum_{m=1}^{N} |D_{s_m}\widehat{g}|^2$ and $\widehat{g}$. The middle graph displays the reconstruction of Algorithm 3.4.3. The lower most graph displays the sampling set Γ. At the top of the bottom graph is the input signal and to its lower right the values of the reconstruction parameters.
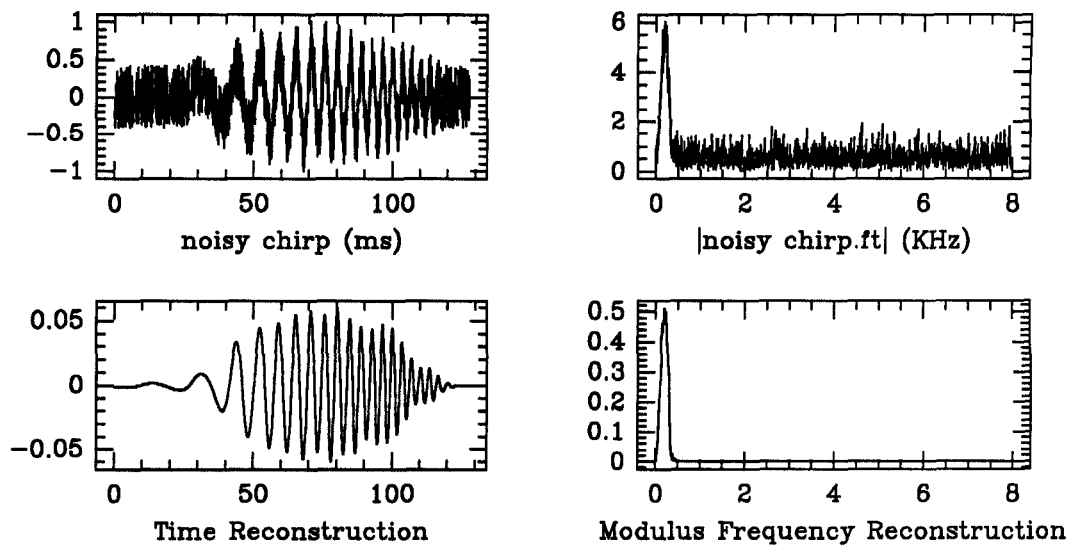
Figure 6.80: Reconstruction of noisy "water", $\sigma = 0.5$.

Above, the signal "water" and its reconstructed versions in both time and frequency are displayed. Below, the associated coefficient distribution function λ_{water} is plotted in the top graph while the lower graph shows the max and min value of the wavelet filter bank response as a function of the channel number.
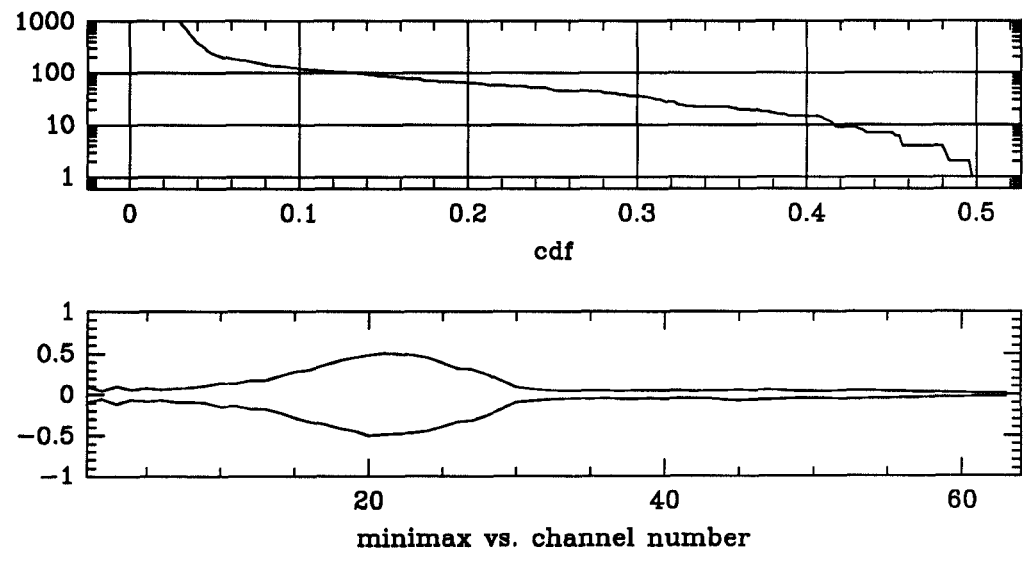

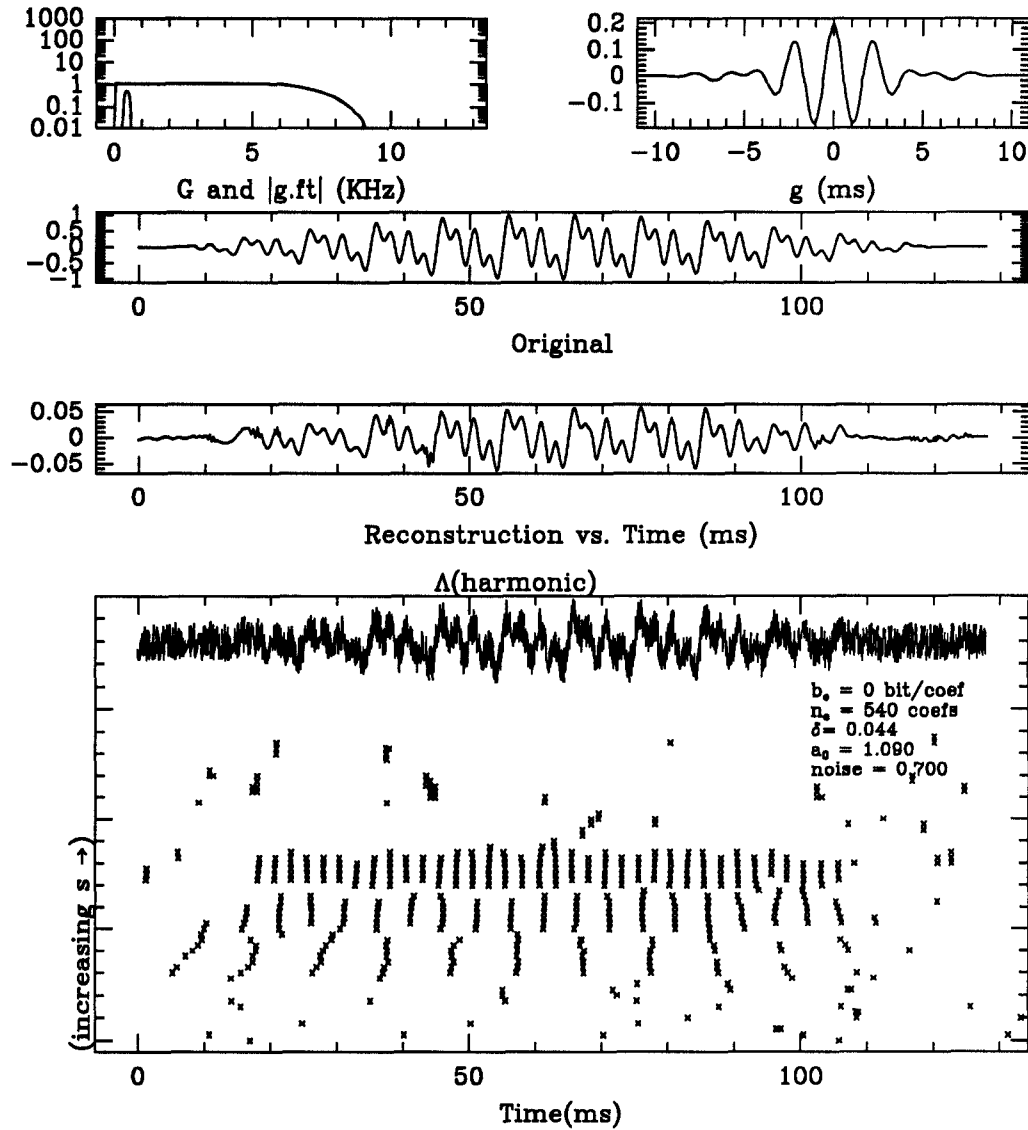Figure 6.81: Cdf and minimax curves for noisy "water", $\sigma = 0.5$.

Figure 6.82: PE wavelet representation for "packet", $\sigma = 0.7$.

Shown above is the wavelet positive extrema representation and its reconstruction for the noisy signal "packet". The trapezoidal analyzing function g appears in the top upper right. To its left are the functions $G = \sum_{m=1}^{N} |D_{s_m}\widehat{g}|^2$ and $\widehat{g}$. The middle graph displays the reconstruction of Algorithm 3.4.3. The lower most graph displays the sampling set Γ. At the top of the bottom graph is the input signal and to its lower right the values of the reconstruction parameters.
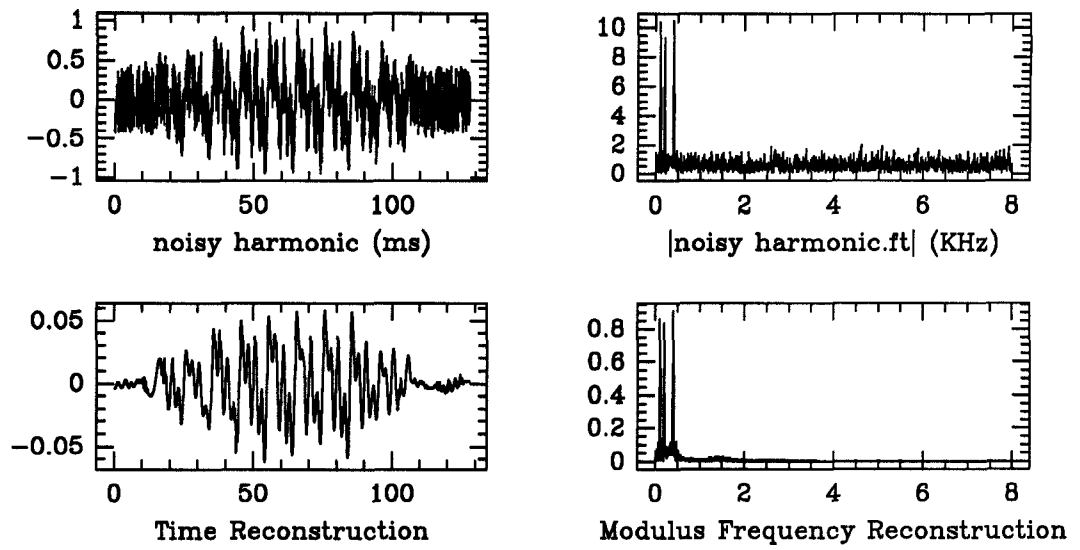
Figure 6.83: Reconstruction of noisy "packet", $\sigma = 0.7$.

Above, the signal "packet" and its reconstructed versions in both time and frequency are displayed. Below, the associated coefficient distribution function λ_{packet} is plotted in the top graph while the lower graph shows the max and min value of the wavelet filter bank response as a function of the channel number.
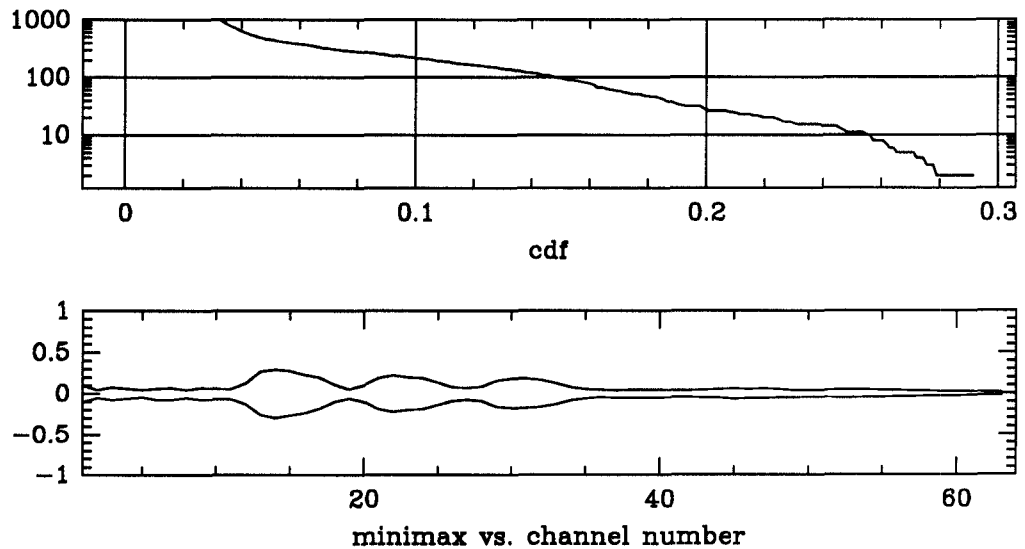

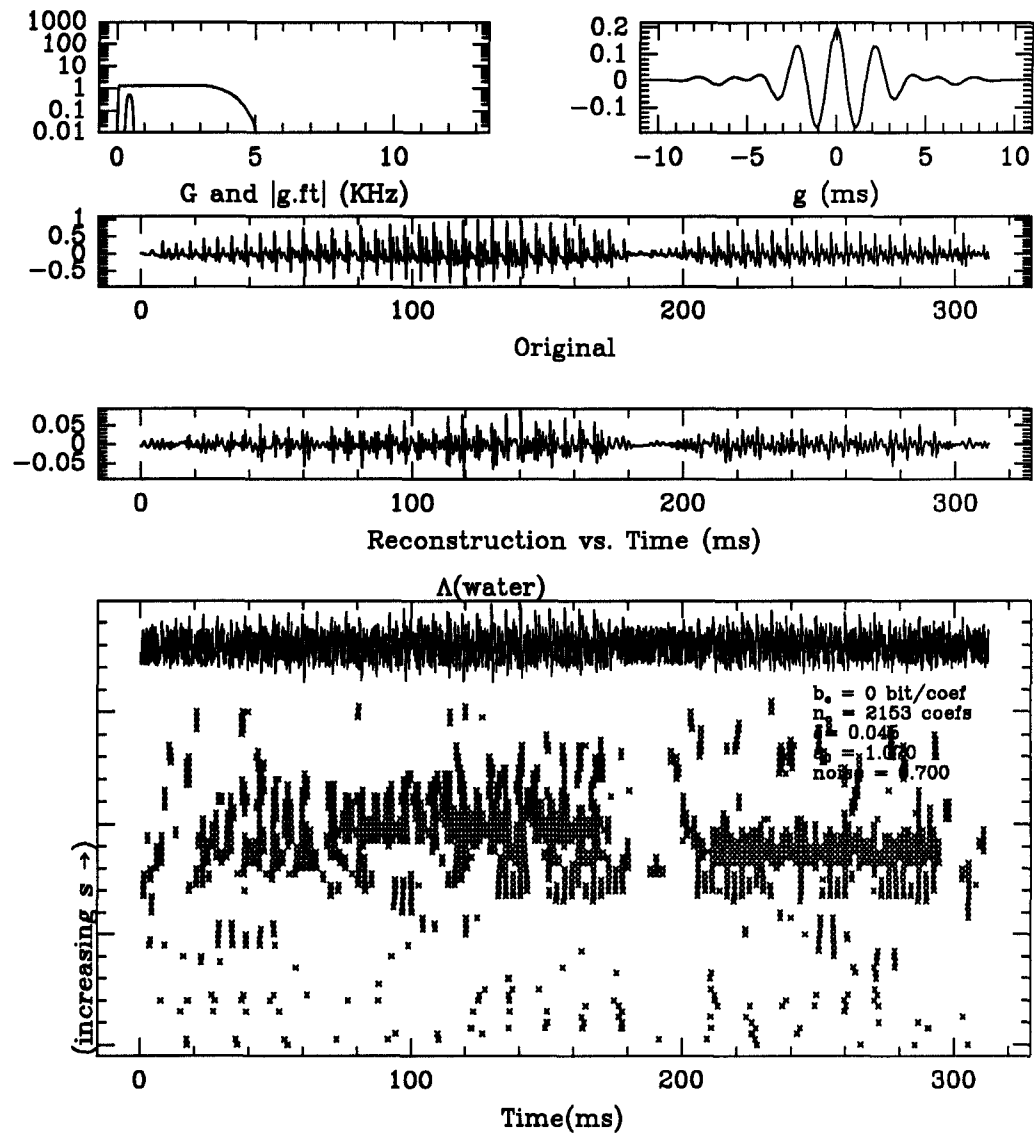Figure 6.84: Cdf and minimax curves for noisy "packet", $\sigma = 0.7$.

Figure 6.85: PE wavelet representation for "chirp", $\sigma = 0.7$.

Shown above is the wavelet positive extrema representation and its reconstruction for the noisy signal "chirp". The trapezoidal analyzing function g appears in the top upper right. To its left are the functions $G = \sum_{m=1}^{N} |D_{s_m}\widehat{g}|^2$ and $\widehat{g}$. The middle graph displays the reconstruction of Algorithm 3.4.3. The lower most graph displays the sampling set Γ. At the top of the bottom graph is the input signal and to its lower right the values of the reconstruction parameters.
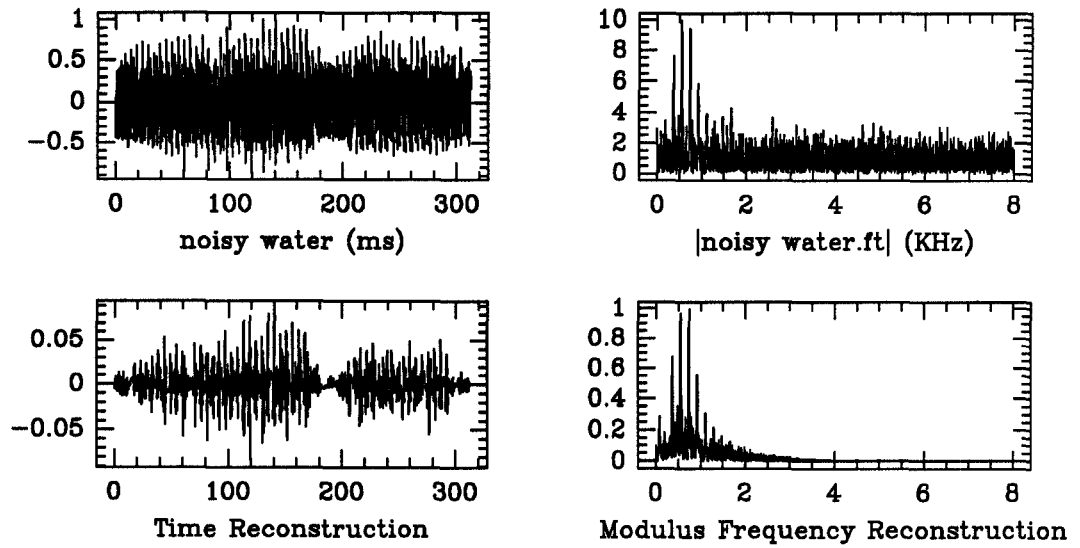
Figure 6.86: Reconstruction of noisy "chirp", $\sigma = 0.7$.

Above, the signal "chirp"and its reconstructed versions in both time and frequency are displayed. Below, the associated coefficient distribution function λ_{chirp} is plotted in the top graph while the lower graph shows the max and min value of the wavelet filter bank response as a function of the channel number.

Figure 6.87: Cdf and minimax curves for noisy "chirp", $\sigma = 0.7$.

Figure 6.88: PE wavelet representation for "harmonic", $\sigma = 0.7$.

Shown above is the wavelet positive extrema representation and its reconstruction for the noisy signal "harmonic". The trapezoidal analyzing function g appears in the top upper right. To its left are the functions $G = \sum_{m=1}^{N} |D_{s_m}\widehat{g}|^2$ and $\widehat{g}$. The middle graph displays the reconstruction of Algorithm 3.4.3. The lower most graph displays the sampling set Γ. At the top of the bottom graph is the input signal and to its lower right the values of the reconstruction parameters.

Figure 6.89: Reconstruction of noisy "harmonic", $\sigma = 0.7$.

Above, the signal "harmonic"and its reconstructed versions in both time and frequency are displayed. Below, the associated coefficient distribution function $\lambda_{\text{harmonic}}$ is plotted in the top graph while the lower graph shows the max and min value of the wavelet filter bank response as a function of the channel number.
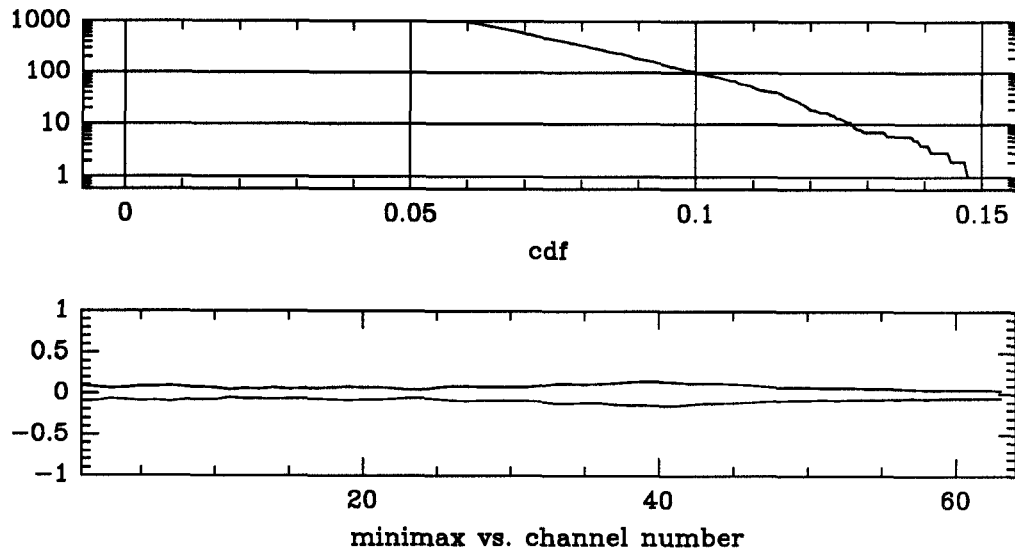

Figure 6.90: Cdf and minimax curves for noisy "harmonic", $\sigma = 0.7$.

Figure 6.91: PE wavelet representation for "water", $\sigma = 0.7$.

Shown above is the wavelet positive extrema representation and its reconstruction for the noisy signal "water". The trapezoidal analyzing function g appears in the top upper right. To its left are the functions $G = \sum_{m=1}^{N} |D_{s_m} \widehat{g}|^2$ and $\widehat{g}$. The middle graph displays the reconstruction of Algorithm 3.4.3. The lower most graph displays the sampling set Γ. At the top of the bottom graph is the input signal and to its lower right the values of the reconstruction parameters.

Figure 6.92: Reconstruction of noisy "water", $\sigma = 0.7$.

Above, the signal "water"and its reconstructed versions in both time and frequency are displayed. Below, the associated coefficient distribution function λ_{water} is plotted in the top graph while the lower graph shows the max and min value of the wavelet filter bank response as a function of the channel number.

Figure 6.93: Cdf and minimax curves for noisy "water", $\sigma = 0.7$.

6.3.2 Compression

In speech, the goal of compression is to represent speech signals in a way which minimizes storage and transmission bandwidth requirements under the constraint that sufficiently high "quality" approximations of the original speech signal can be recovered from the representation. The meaning of the 'quality' of a reconstruction is a criterion which is difficult to specify precisely. In vague terms we would like our representation to preserve pertinent perceptual information in the speech signal, e.g., timbre, emotional state of the speaker, inflections, etc. Intelligibility is a less stringent criterion by which to judge reconstructions. In this case, we require only that listeners be able to determine the textual content of the original speech signal purely from audition of the reconstruction.

We detail a compression experiment based on the discussion in Section 5.3. Let $g = g_{\text{trap}}$. Fix a coefficient rate c_r, e.g., $c_r = 4800$ coef/sec. For each f_* in the test set and for each value of b_c, the following steps are performed:

(i) Compute the wavelet positive extrema representation of f_*:

$$\Lambda(f_*) \triangleq \{W_g f_*(t_{m,n}, s_m)\}.$$

(ii) Determine the maximum number of coefficients n_c with which f_* can be represented and still met coefficient rate constraint:

$$n_c = c_r \cdot |I(f_*)|,$$

where $|I(f_*)|$ is the duration of f_*.

(iii) Compute the distribution function λ_{f_*}.

(iv) Threshold the wavelet positive extrema representation $\Lambda(f_*)$ by $\delta = \lambda^{-1}(n_c)$, yielding the truncated representation

$$\Lambda_\delta(f_*) \triangleq \{W_g f_*(t_{m,n}, s_m) : W_g f_*(t_{m,n}, s_m) \geq \delta\}.$$

(v) Quantize the thresholded wavelet positive extrema representation, yielding the sequence

$$Q_{b_c}(\Lambda_\delta(f_*)).$$

(vi) Generate reconstruction of f_* using Algorithm 3.5.3 where initial data is

$$c_0 = Q_{b_c}(\Lambda_\delta(f_*)).$$

Synthetic Data

For the compression of the non-speech signals in the test set we have chosen the discretization parameters $g = g_{\text{trap}}$ and $a_0 = 1.09$.

Figures 6.94 through 6.102 display the compressed reconstructions for a bit rate constraint of $b_r = 1.2$ coefs/msec and a quantization of $b_c = 2$ bits/coef, i.e., 2.4 Kbits/sec.

Figures 6.103 through 6.111 display the compressed reconstructions for a bit rate constraint of $b_r = 1.2$ coefs/msec and a quantization of $b_c = 1$ bit/coef, i.e., 1.2 Kbits/sec.

Speech Data

The discretization parameters we have chosen for the speech data are $a_0 = 1.1$ and $g = g_{trap}$. Note that to achieve greater compression we have resampled the s-axis effectively eliminating every other channel.

Figures 6.112 through 6.120 display the compressed reconstructions for a bit rate constraint of $b_r = 9.6$ coefs/msec and a quantization levels of $b_c = 4, 2$ and 1 bit/coef respectively, corresponding to bit rates of 38.4, 19.2, and 9.6 Kbits/sec.

Figures 6.121 through 6.129 display the compressed reconstructions for a bit rate constraint of $b_r = 4.8$ coefs/msec and a quantization levels of $b_c = 4, 2$ and 1 bit/coef respectively, corresponding to bit rates of 19.2, 9.6, and 4.8 Kbits/sec.

Figures 6.130 through 6.138 display the compressed reconstructions for a bit rate constraint of $b_r = 2.4$ coefs/msec and a quantization levels of $b_c = 4, 2$ and 1 bit/coef respectively, corresponding to bit rates of 9.6, 4.8 and 2.4 Kbits/sec.
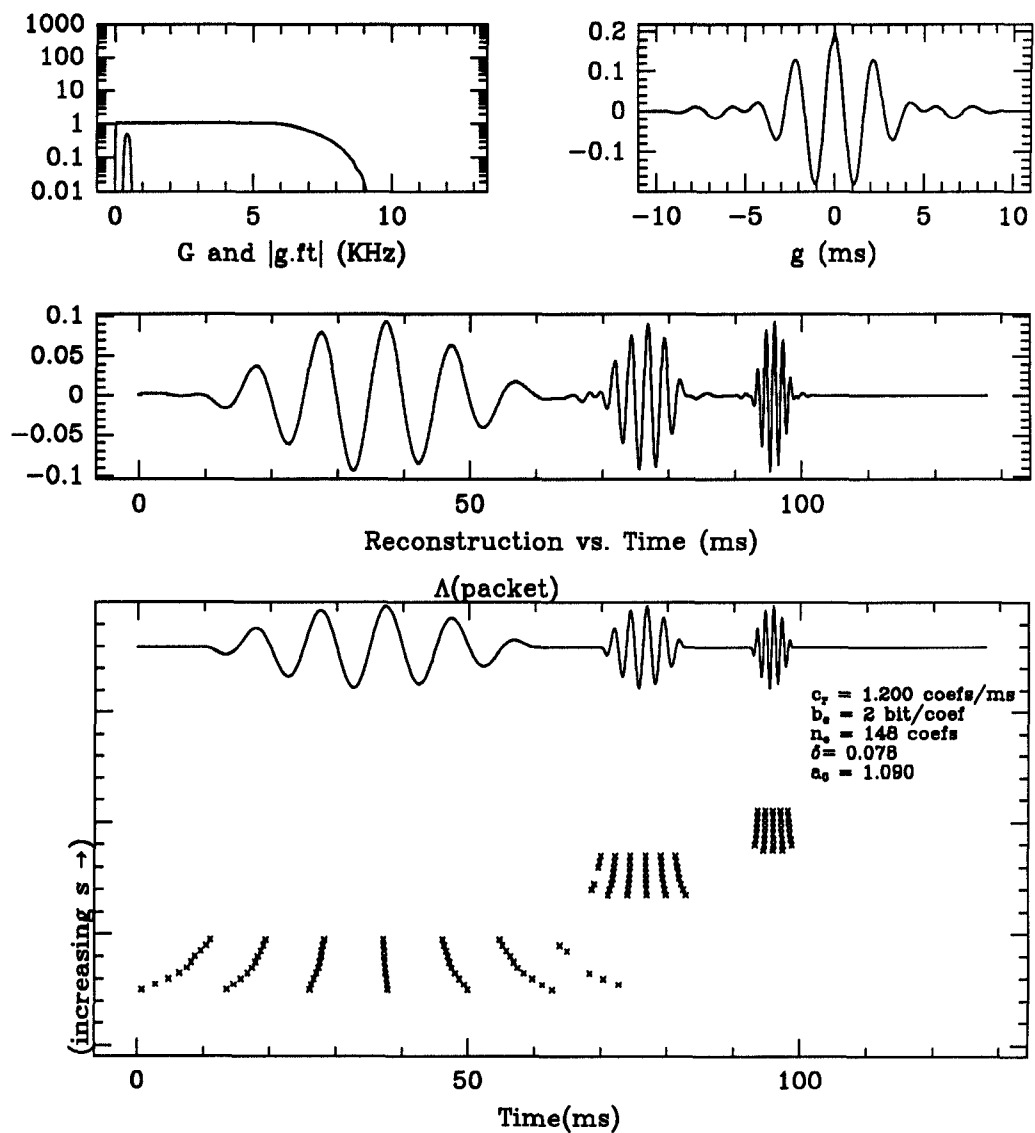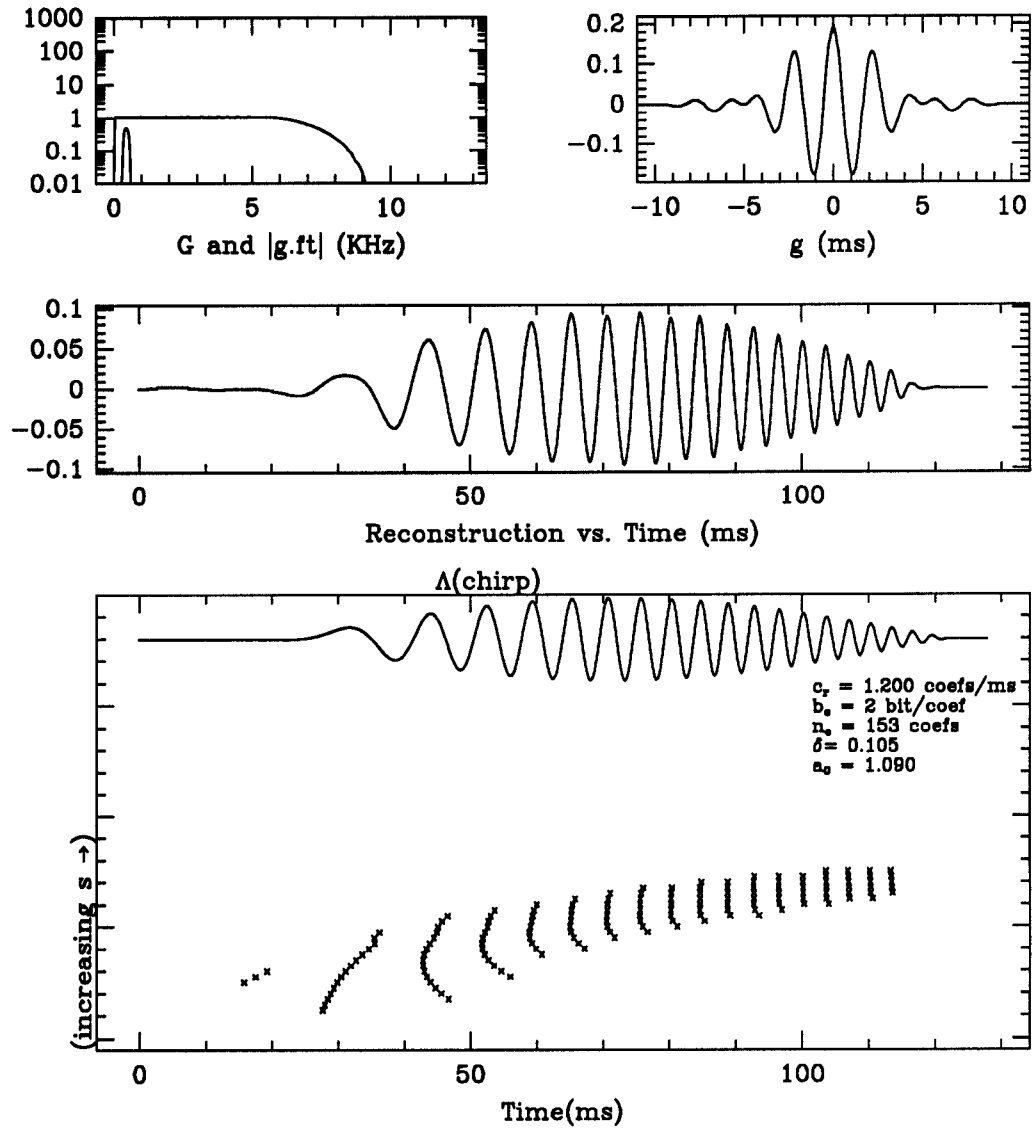
Figure 6.94: PE wavelet representation for "packet", $(b_c, b_r) = (2, 1.2)$.

Shown above is the wavelet positive extrema representation and its reconstruction for the compressed signal "packet". The trapezoidal analyzing function g appears in the top upper right. To its left are the functions $G = \sum_{m=1}^{N} |D_{s_m} \widehat{g}|^2$ and $\widehat{g}$. The middle graph displays the reconstruction of Algorithm 3.4.3. The lower most graph displays the sampling set Γ. At the top of the bottom graph is the input signal and to its lower right the values of the reconstruction parameters.
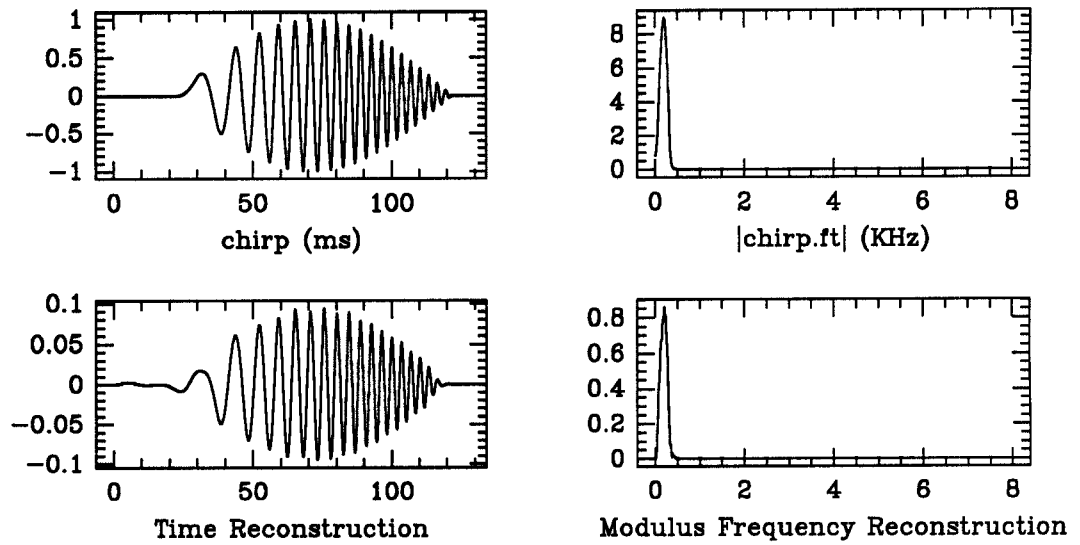
159
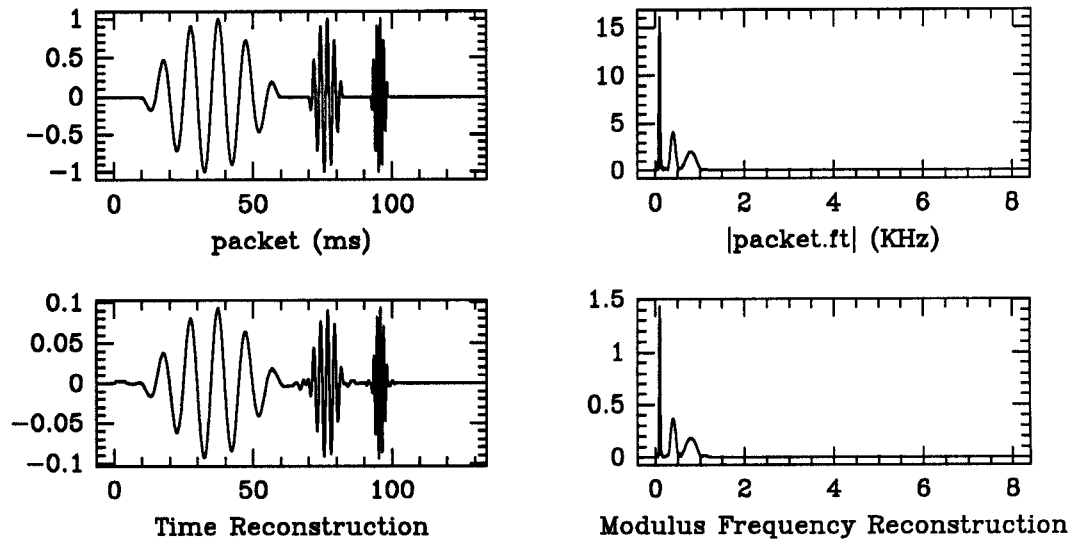
Figure 6.95: Reconstruction of compressed "packet", $(b_c, b_r) = (2, 1.2)$.

Above, the signal "packet"and its reconstructed versions in both time and frequency are displayed. Below, the associated coefficient distribution function λ_{packet} is plotted in the top graph while the lower graph shows the max and min value of the wavelet filter bank response as a function of the channel number.
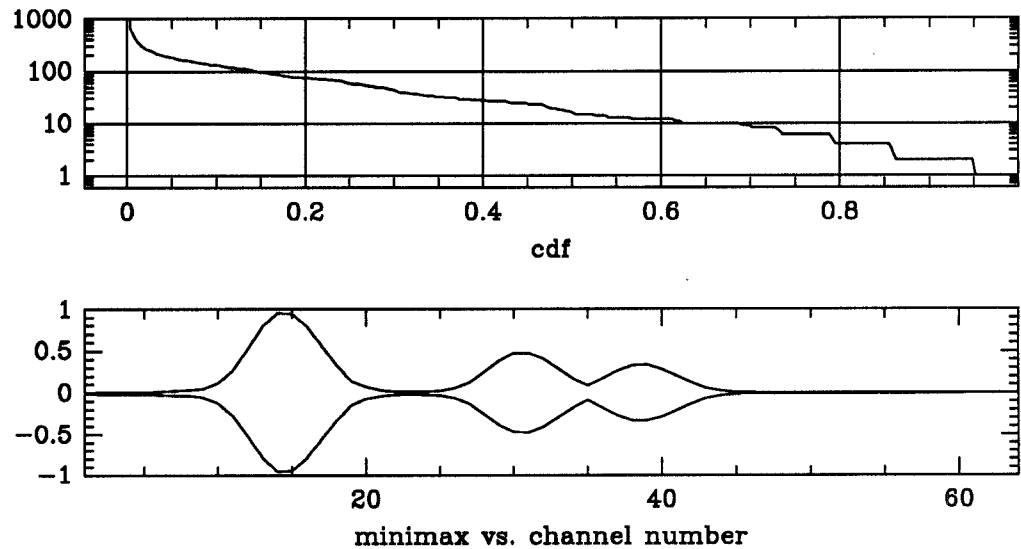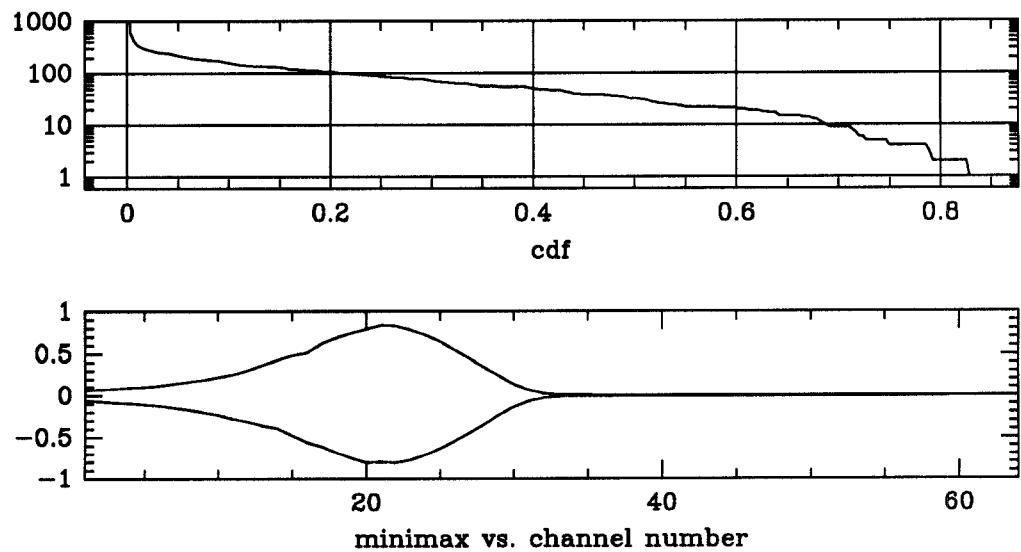

Figure 6.96: Cdf and minimax curves for compressed "packet", $(b_c, b_r) = (2, 1.2)$.
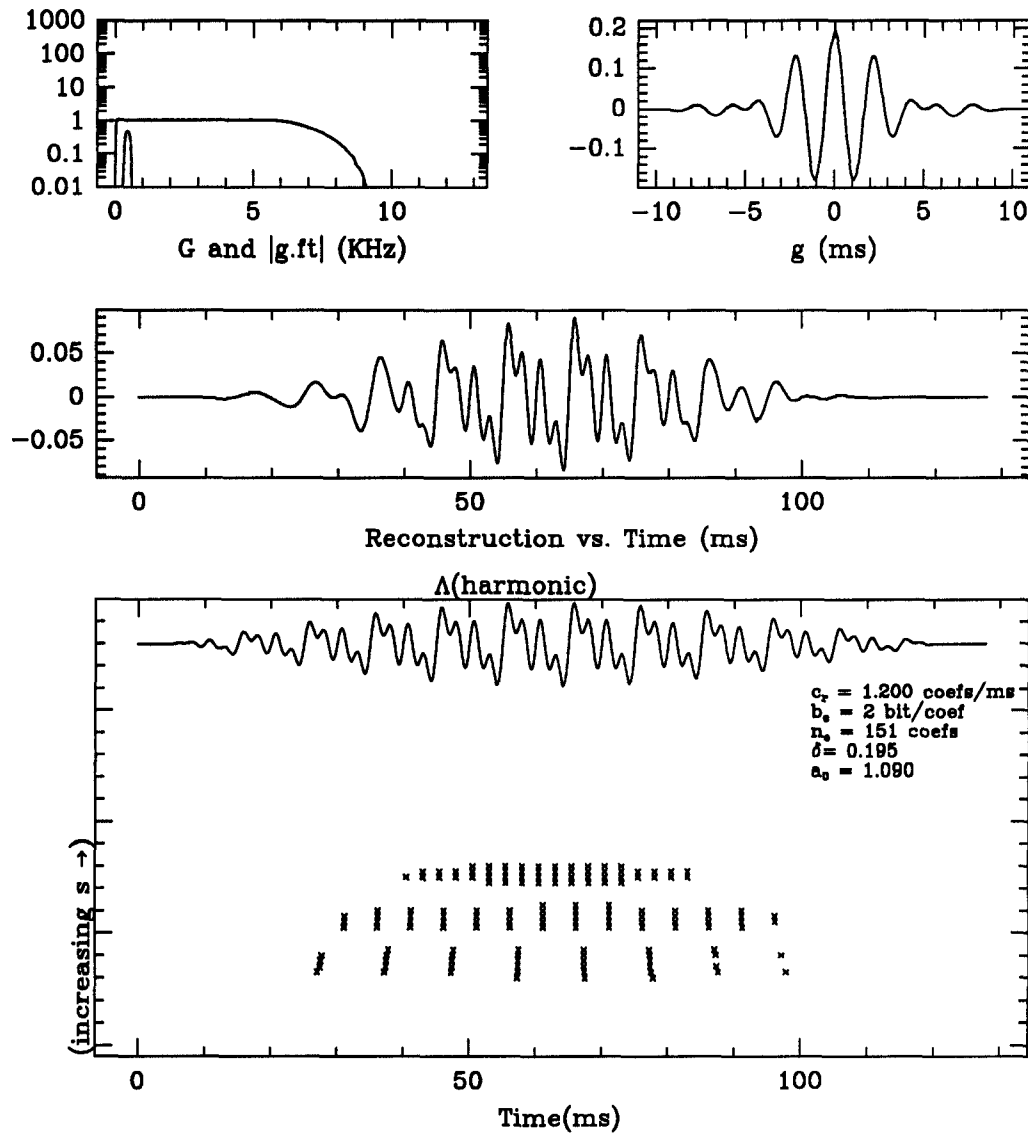
Figure 6.97: PE wavelet representation for "chirp", $(b_c, b_r) = (2, 1.2)$.

Shown above is the wavelet positive extrema representation and its reconstruction for the compressed signal "chirp". The trapezoidal analyzing function g appears in the top upper right. To its left are the functions $G = \sum_{m=1}^{N} |D_{s_m} \widehat{g}|^2$ and $\widehat{g}$. The middle graph displays the reconstruction of Algorithm 3.4.3. The lower most graph displays the sampling set Γ. At the top of the bottom graph is the input signal and to its lower right the values of the reconstruction parameters.
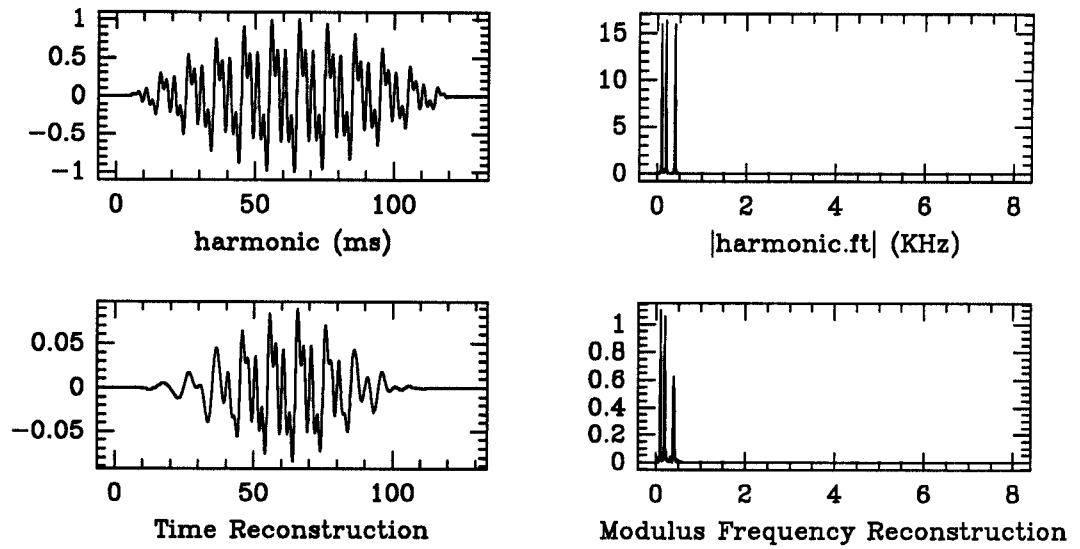
161

Figure 6.98: Reconstruction of compressed "chirp", $(b_c, b_r) = (2, 1.2)$.

Above, the signal "chirp"and its reconstructed versions in both time and frequency are displayed. Below, the associated coefficient distribution function λ_{chirp} is plotted in the top graph while the lower graph shows the max and min value of the wavelet filter bank response as a function of the channel number.
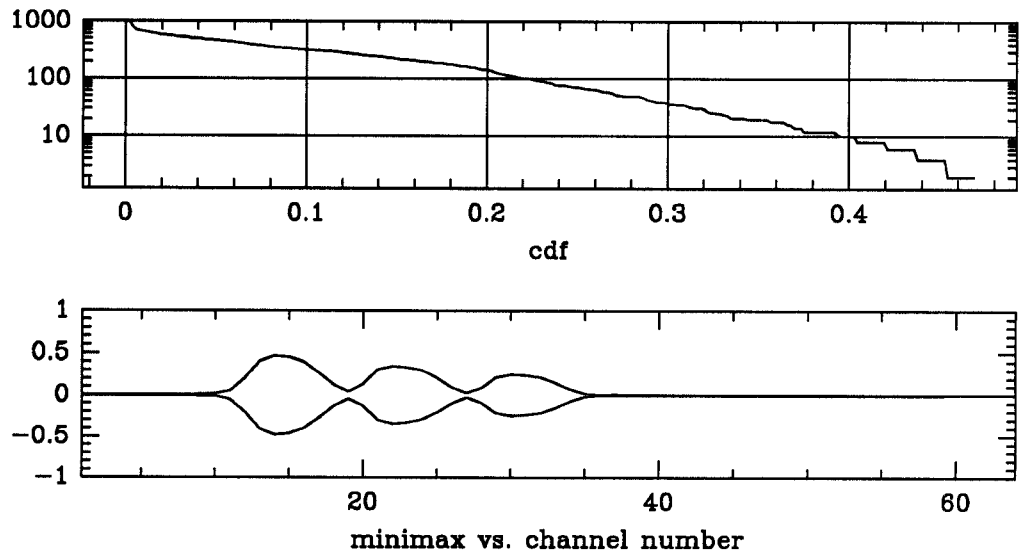

Figure 6.99: Cdf and minimax curves for compressed "chirp", $(b_c, b_r) = (2, 1.2)$.

Figure 6.100: PE wavelet representation for "harmonic", $(b_c, b_r) = (2, 1.2)$.

Shown above is the wavelet positive extrema representation and its reconstruction for the compressed signal "harmonic". The trapezoidal analyzing function g appears in the top upper right. To its left are the functions $G = \sum_{m=1}^{N} |D_{s_m}\widehat{g}|^2$ and $\widehat{g}$. The middle graph displays the reconstruction of Algorithm 3.4.3. The lower most graph displays the sampling set Γ. At the top of the bottom graph is the input signal and to its lower right the values of the reconstruction parameters.
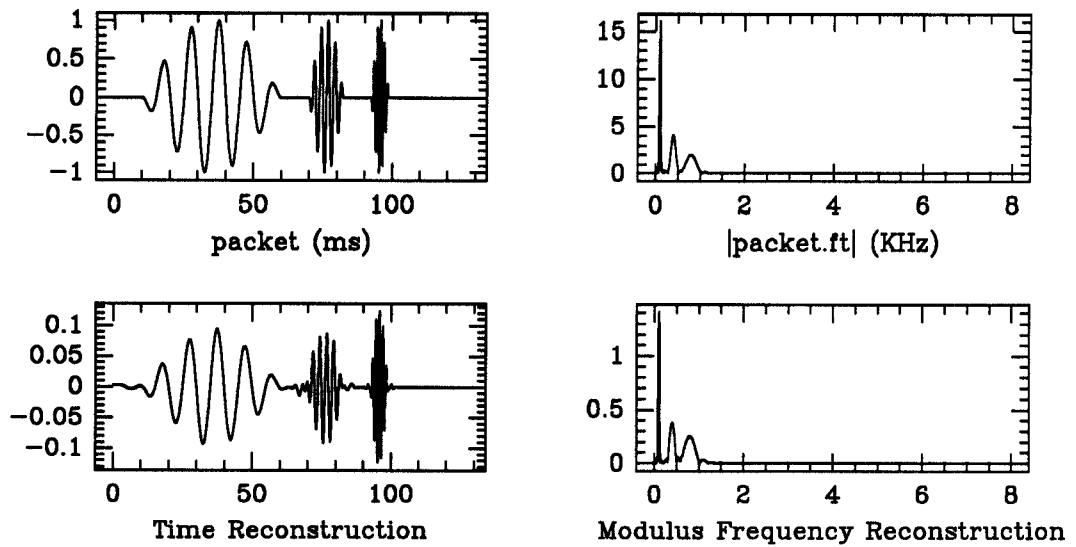
Figure 6.101: Reconstruction of compressed "harmonic", $(b_c, b_r) = (2, 1.2)$.

Above, the signal "harmonic" and its reconstructed versions in both time and frequency are displayed. Below, the associated coefficient distribution function $\lambda_{\text{harmonic}}$ is plotted in the top graph while the lower graph shows the max and min value of the wavelet filter bank response as a function of the channel number.

Figure 6.102: Cdf and minimax curves for compressed "harmonic", $(b_c, b_r) = (2, 1.2)$.

164
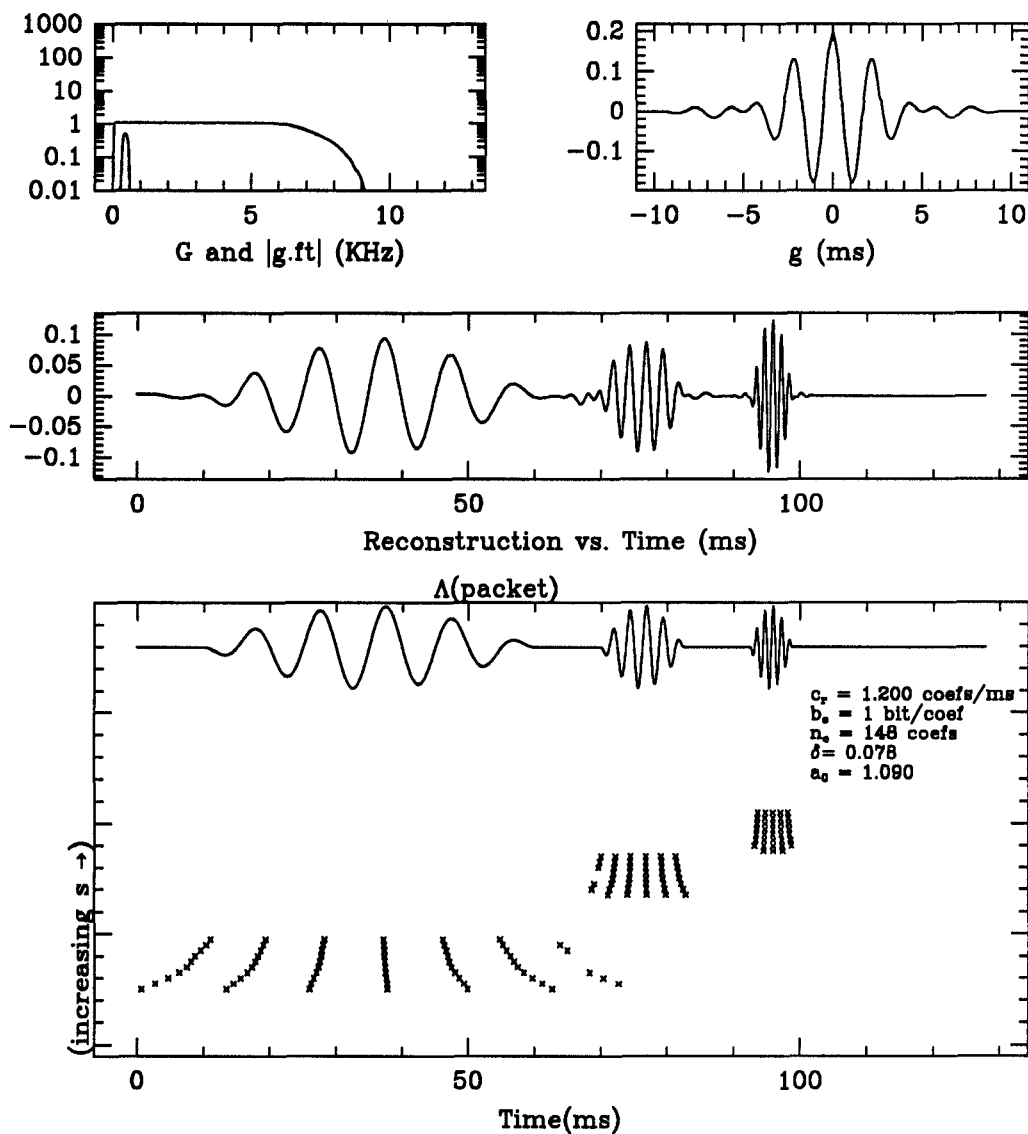
Figure 6.103: PE wavelet representation for "packet", $(b_c, b_r) = (1, 1.2)$.

Shown above is the wavelet positive extrema representation and its reconstruction for the compressed signal "packet". The trapezoidal analyzing function g appears in the top upper right. To its left are the functions $G = \sum_{m=1}^{N} |D_{s_m} \widehat{g}|^2$ and $\widehat{g}$. The middle graph displays the reconstruction of Algorithm 3.4.3. The lower most graph displays the sampling set Γ. At the top of the bottom graph is the input signal and to its lower right the values of the reconstruction parameters.

Figure 6.104: Reconstruction of compressed "packet", $(b_c, b_r) = (1, 1.2)$.

Above, the signal "packet"and its reconstructed versions in both time and frequency are displayed. Below, the associated coefficient distribution function λ_{packet} is plotted in the top graph while the lower graph shows the max and min value of the wavelet filter bank response as a function of the channel number.
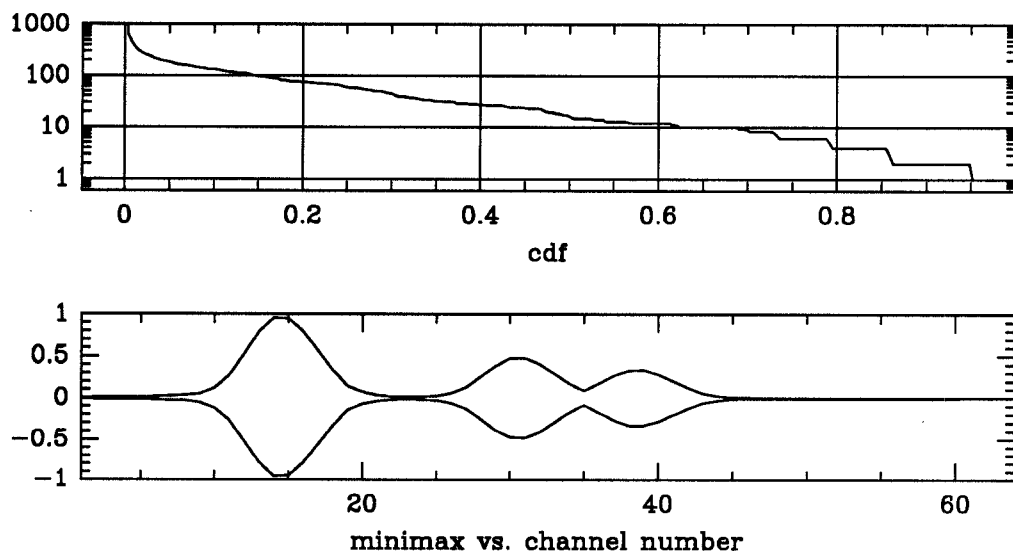

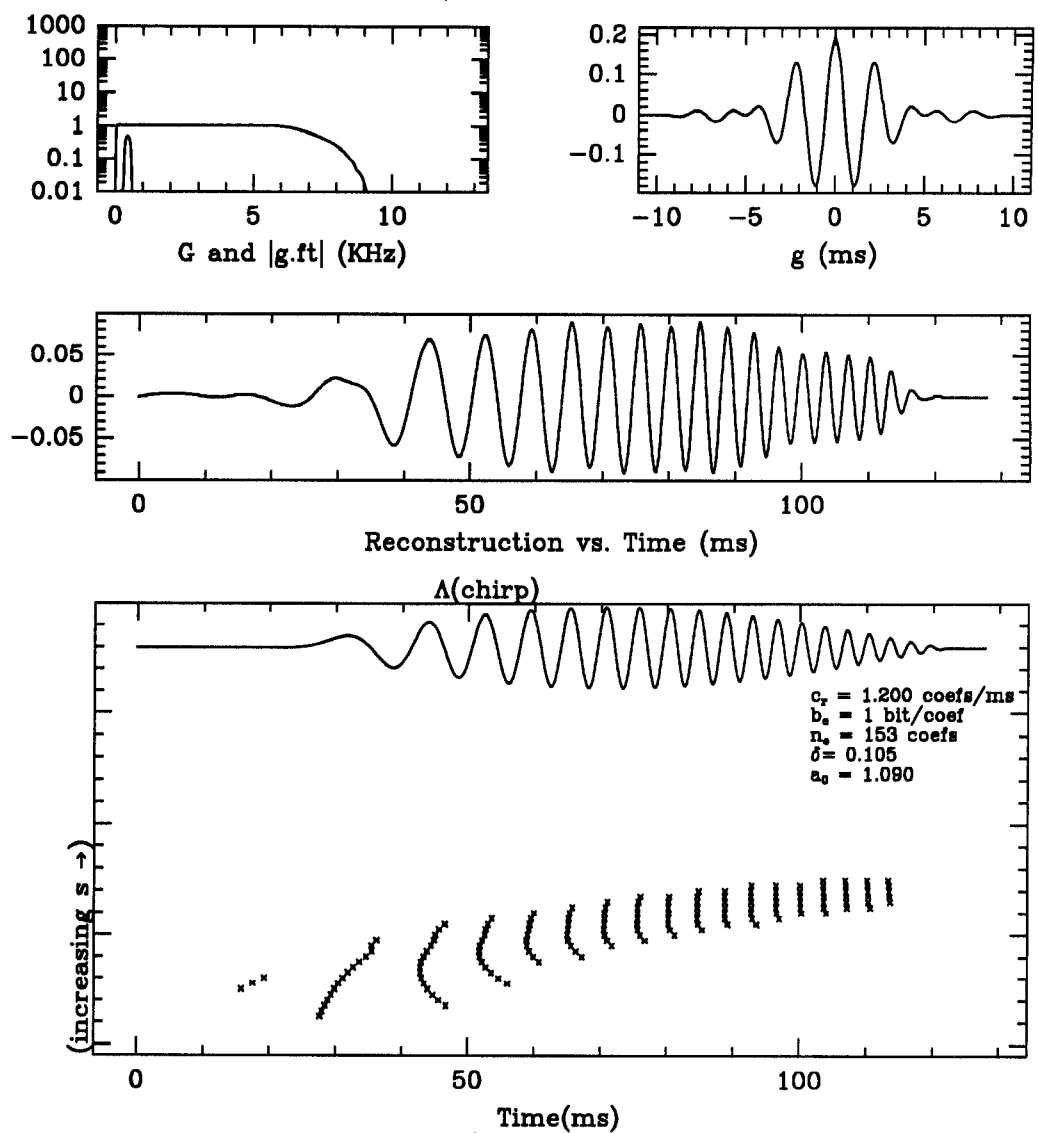Figure 6.105: Cdf and minimax curves for compressed "packet", $(b_c, b_r) = (1, 1.2)$.

Figure 6.106: PE wavelet representation for "chirp", $(b_c, b_r) = (1, 1.2)$.

Shown above is the wavelet positive extrema representation and its reconstruction for the compressed signal "chirp". The trapezoidal analyzing function g appears in the top upper right. To its left are the functions $G = \sum_{m=1}^{N} |D_{s_m} \widehat{g}|^2$ and $\widehat{g}$. The middle graph displays the reconstruction of Algorithm 3.4.3. The lower most graph displays the sampling set Γ. At the top of the bottom graph is the input signal and to its lower right the values of the reconstruction parameters.
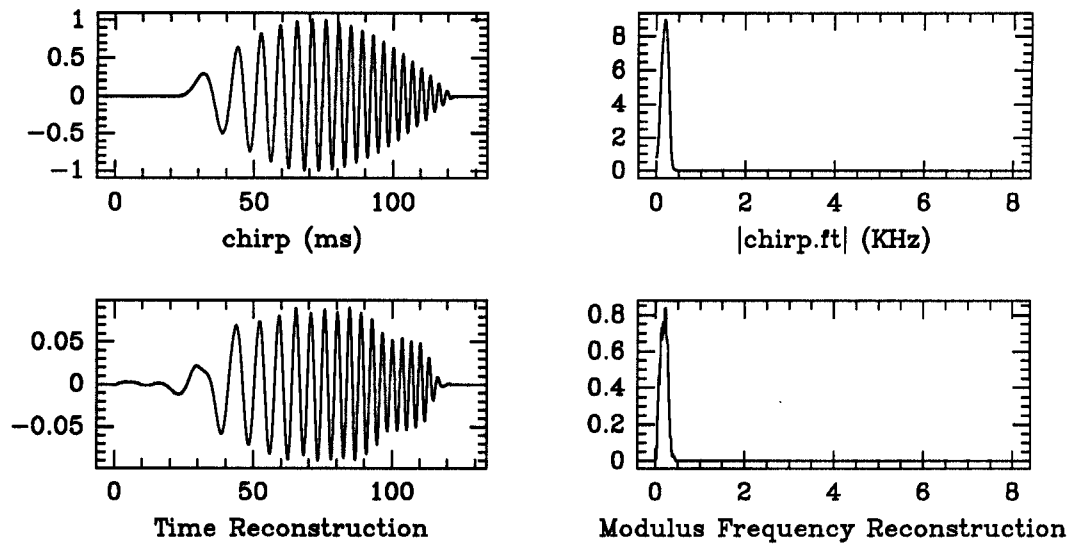
Figure 6.107: Reconstruction of compressed "chirp", $(b_c, b_r) = (1, 1.2)$.

Above, the signal "chirp" and its reconstructed versions in both time and frequency are displayed. Below, the associated coefficient distribution function λ_{chirp} is plotted in the top graph while the lower graph shows the max and min value of the wavelet filter bank response as a function of the channel number.
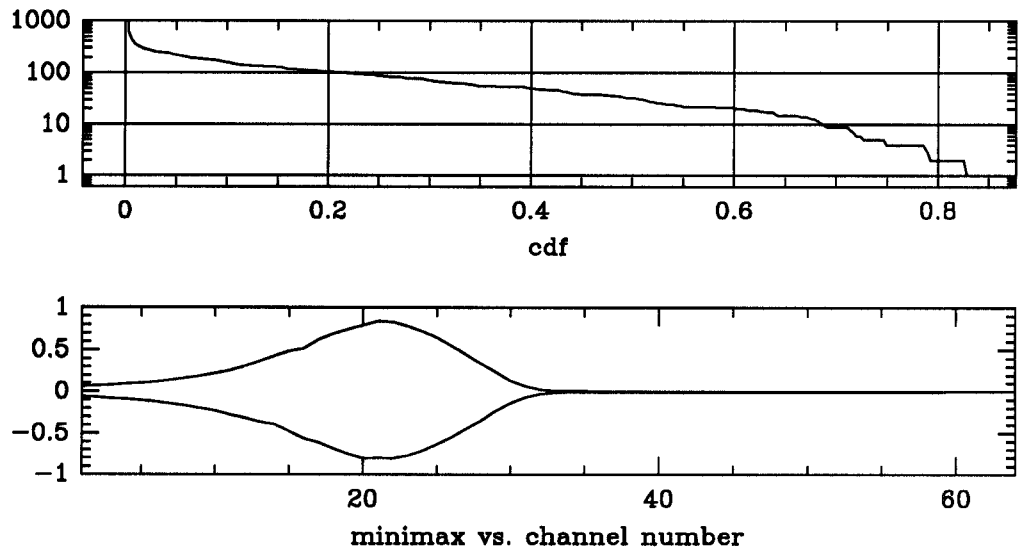

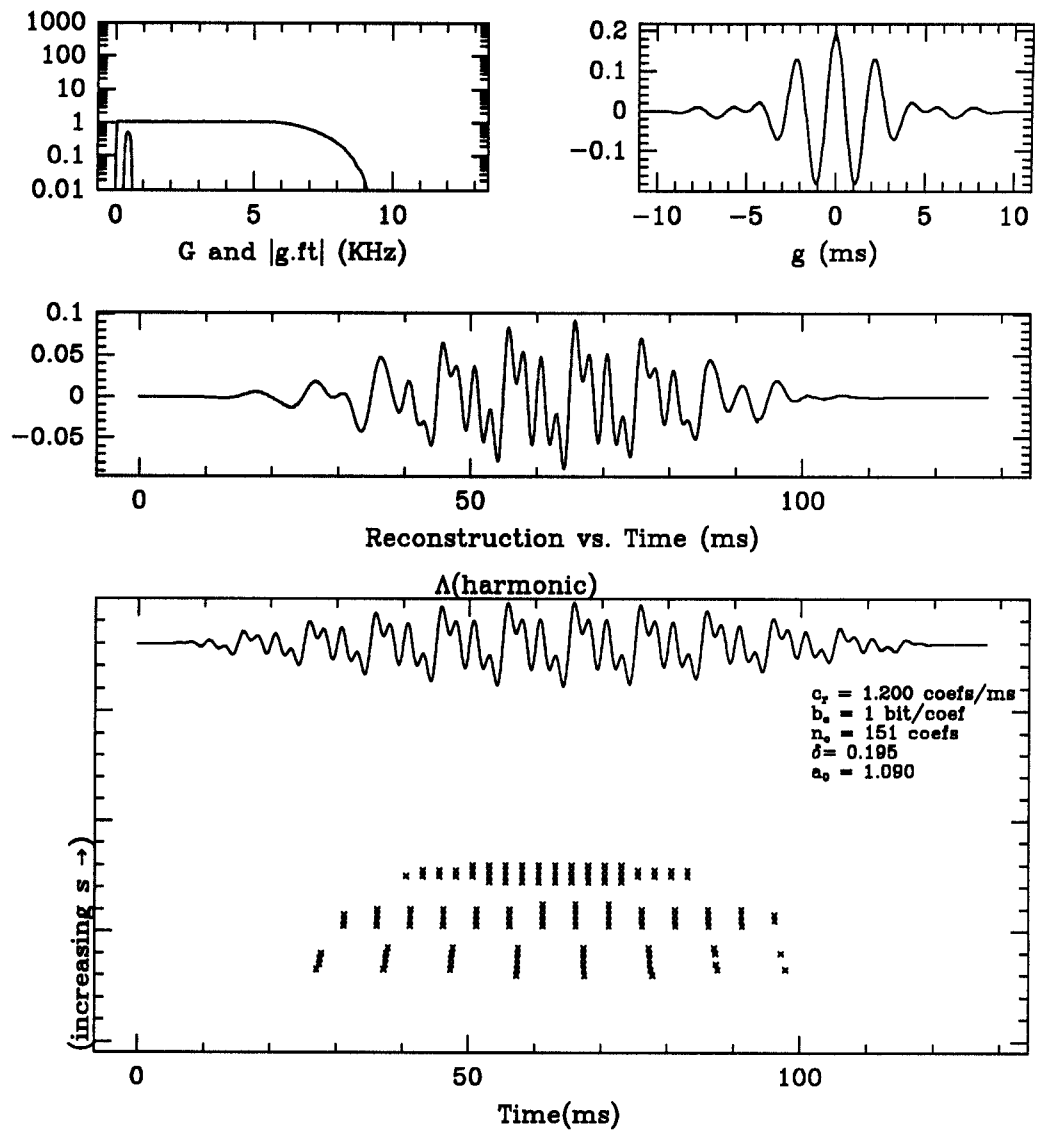Figure 6.108: Cdf and minimax curves for compressed "chirp", $(b_c, b_r) = (1, 1.2)$.

168

Figure 6.109: PE wavelet representation for "harmonic", $(b_c, b_r) = (1, 1.2)$.

Shown above is the wavelet positive extrema representation and its reconstruction for the compressed signal "harmonic". The trapezoidal analyzing function g appears in the top upper right. To its left are the functions $G = \sum_{m=1}^{N} |D_{s_m} \widehat{g}|^2$ and $\widehat{g}$. The middle graph displays the reconstruction of Algorithm 3.4.3. The lower most graph displays the sampling set Γ. At the top of the bottom graph is the input signal and to its lower right the values of the reconstruction parameters.
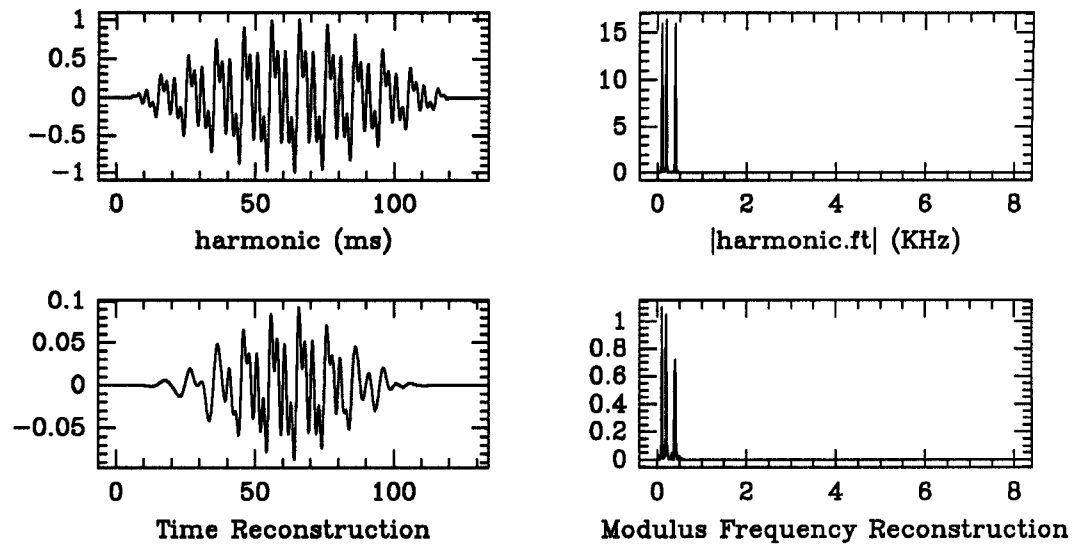
Figure 6.110: Reconstruction of compressed "harmonic", $(b_c, b_r) = (1, 1.2)$.

Above, the signal "harmonic" and its reconstructed versions in both time and frequency are displayed. Below, the associated coefficient distribution function $\lambda_{harmonic}$ is plotted in the top graph while the lower graph shows the max and min value of the wavelet filter bank response as a function of the channel number.
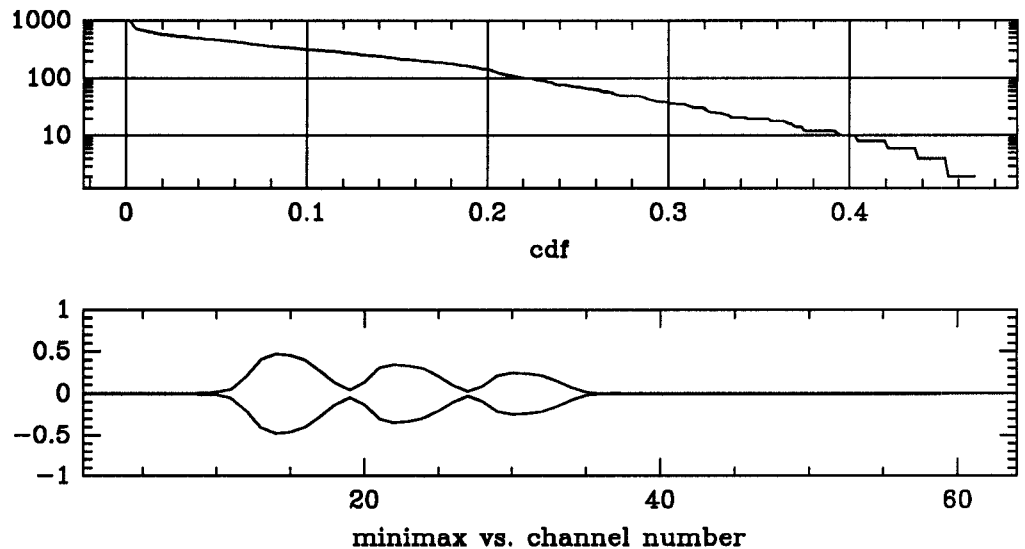

Figure 6.111: Cdf and minimax curves for compressed "harmonic", $(b_c, b_r) = (1, 1.2)$.
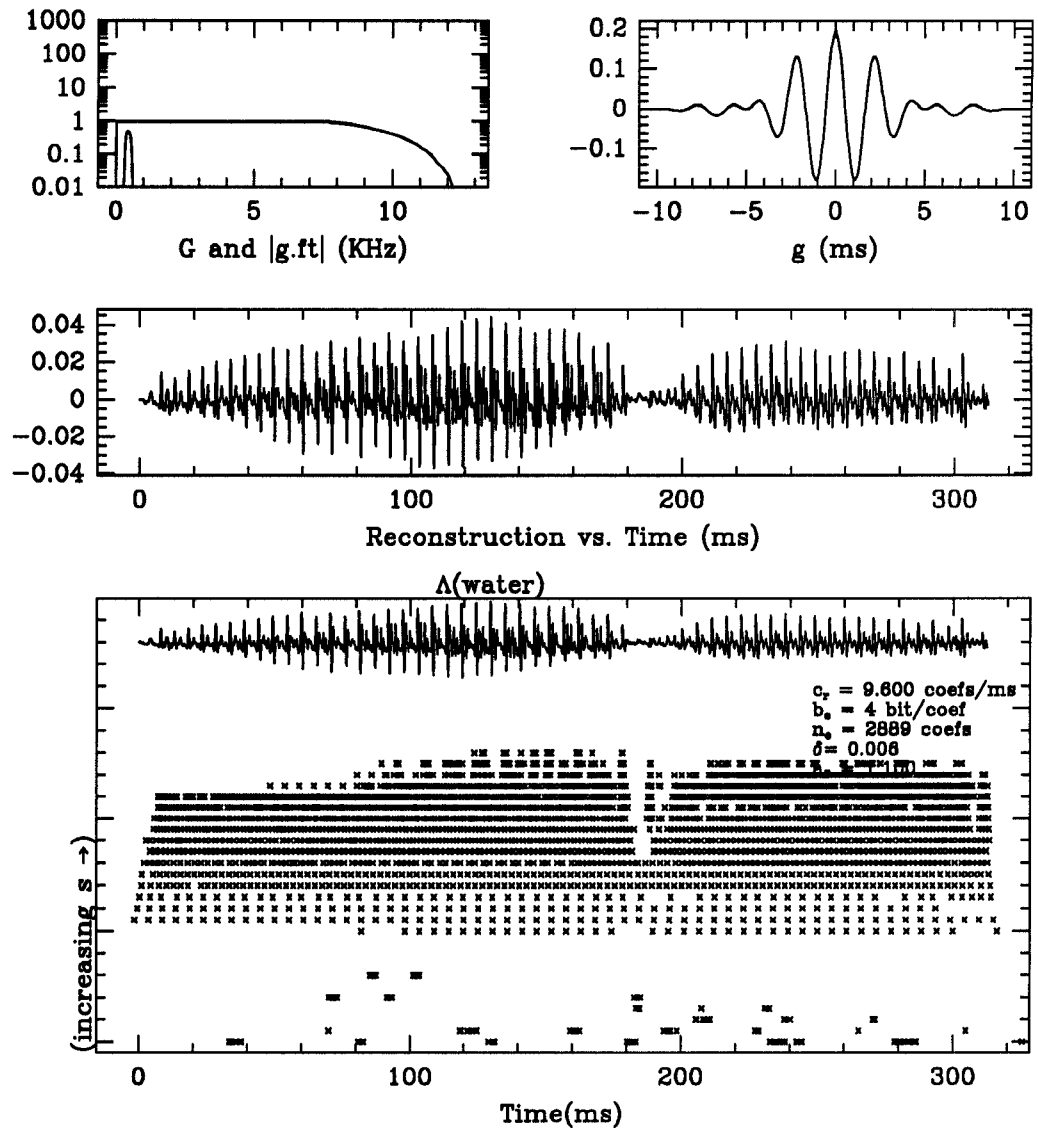
Figure 6.112: PE wavelet representation for "water", $(b_c, b_r) = (4, 9.6)$.

Shown above is the wavelet positive extrema representation and its reconstruction for the compressed signal "water". The trapezoidal analyzing function g appears in the top upper right. To its left are the functions $G = \sum_{m=1}^{N} |D_{s_m} \hat{g}|^2$ and $\hat{g}$. The middle graph displays the reconstruction of Algorithm 3.4.3. The lower most graph displays the sampling set Γ. At the top of the bottom graph is the input signal and to its lower right the values of the reconstruction parameters.
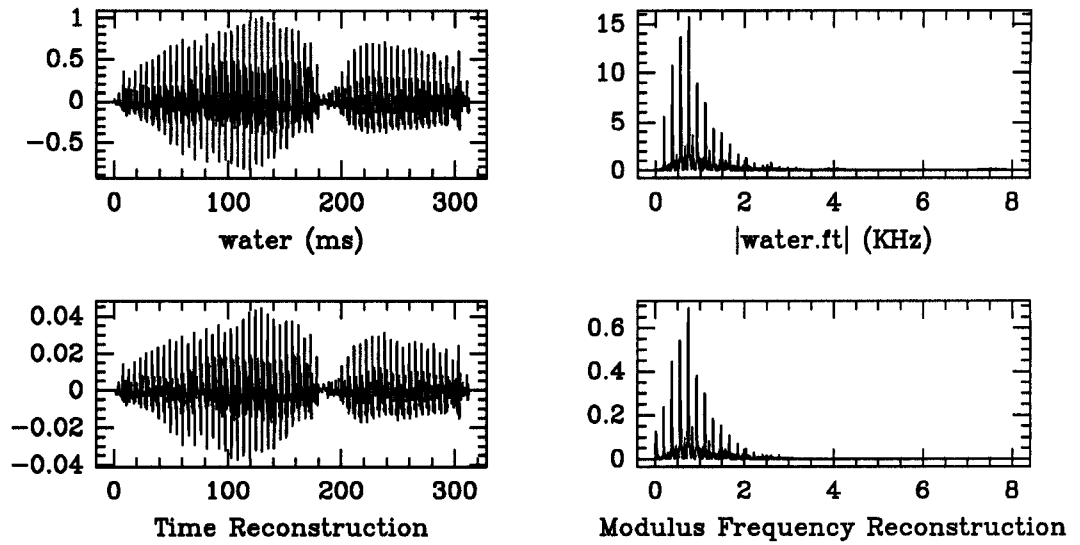
Figure 6.113: Reconstruction of compressed "water", $(b_c, b_r) = (4, 9.6)$.

Above, the signal "water"and its reconstructed versions in both time and frequency are displayed. Below, the associated coefficient distribution function λ_{water} is plotted in the top graph while the lower graph shows the max and min value of the wavelet filter bank response as a function of the channel number.

Figure 6.114: Cdf and minimax curves for compressed "water", $(b_c, b_r) = (4, 9.6)$.

172

Figure 6.115: PE wavelet representation for "water", $(b_c, b_r) = (2, 9.6)$.

Shown above is the wavelet positive extrema representation and its reconstruction for the compressed signal "water". The trapezoidal analyzing function g appears in the top upper right. To its left are the functions $G = \sum_{m=1}^{N} |D_{s_m}\widehat{g}|^2$ and $\widehat{g}$. The middle graph displays the reconstruction of Algorithm 3.4.3. The lower most graph displays the sampling set Γ. At the top of the bottom graph is the input signal and to its lower right the values of the reconstruction parameters.

Figure 6.116: Reconstruction of compressed "water", $(b_c, b_r) = (2, 9.6)$.

Above, the signal "water" and its reconstructed versions in both time and frequency are displayed. Below, the associated coefficient distribution function λ_{water} is plotted in the top graph while the lower graph shows the max and min value of the wavelet filter bank response as a function of the channel number.
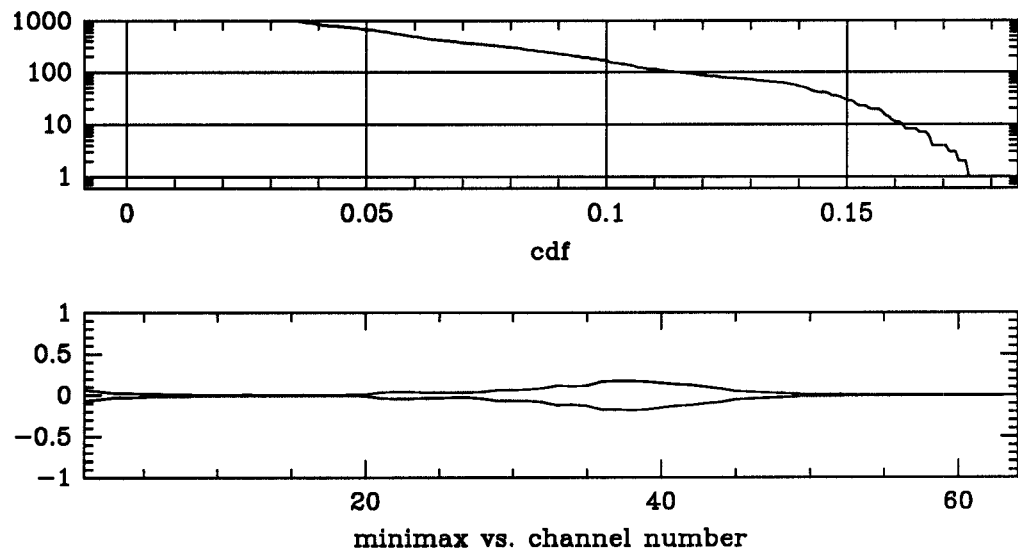

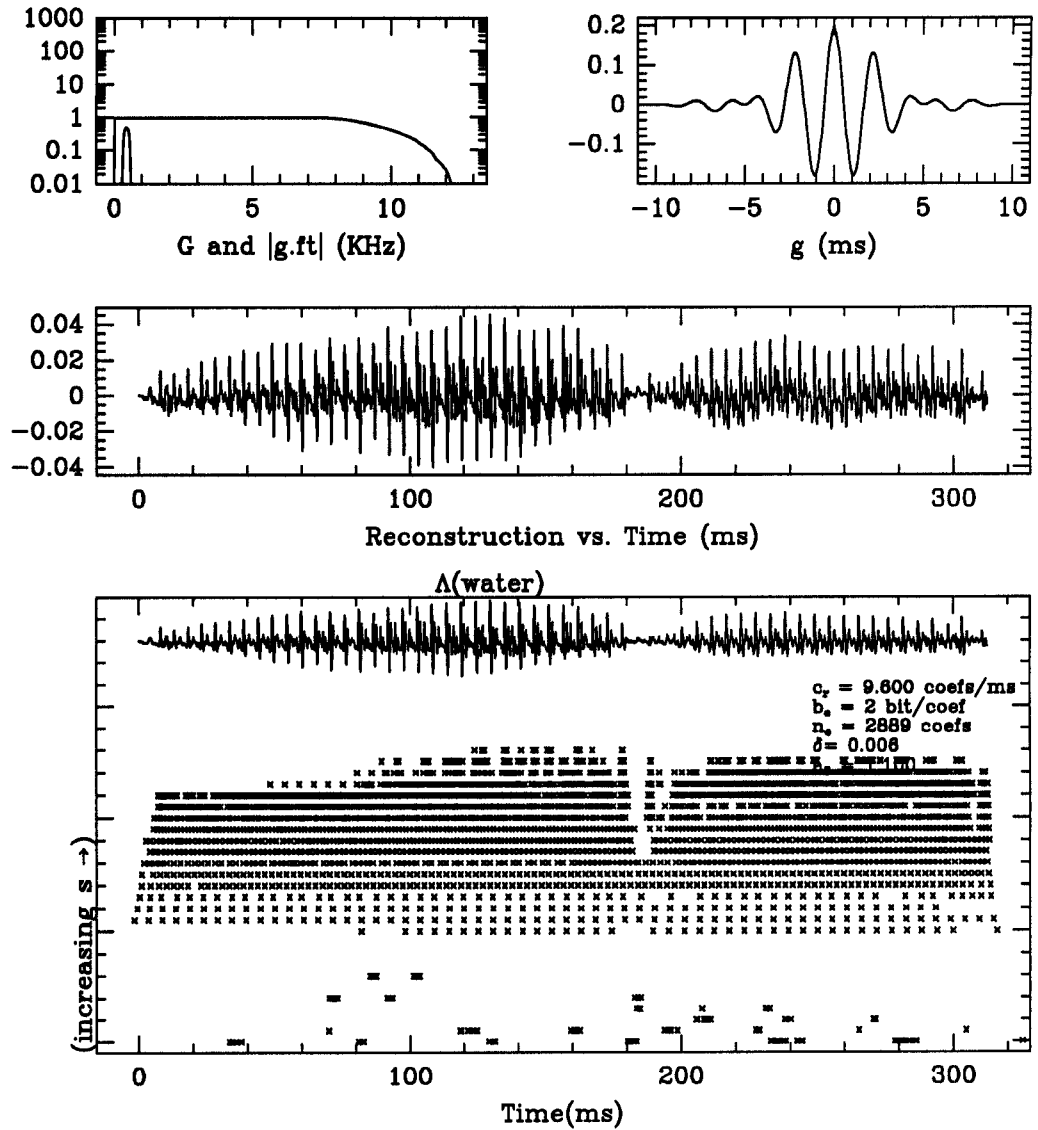Figure 6.117: Cdf and minimax curves for compressed "water", $(b_c, b_r) = (2, 9.6)$.

Figure 6.118: PE wavelet representation for "water", $(b_c, b_r) = (1, 9.6)$.

Shown above is the wavelet positive extrema representation and its reconstruction for the compressed signal "water". The trapezoidal analyzing function g appears in the top upper right. To its left are the functions $G = \sum_{m=1}^{N} |D_{s_m}\hat{g}|^2$ and $\hat{g}$. The middle graph displays the reconstruction of Algorithm 3.4.3. The lower most graph displays the sampling set Γ. At the top of the bottom graph is the input signal and to its lower right the values of the reconstruction parameters.
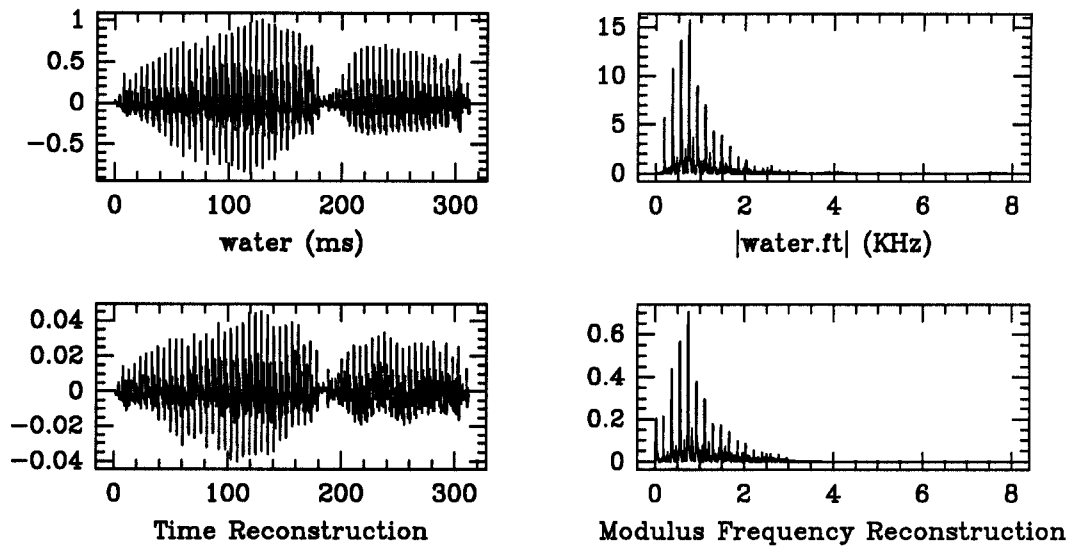
Figure 6.119: Reconstruction of compressed "water", $(b_c, b_r) = (1, 9.6)$.

Above, the signal "water"and its reconstructed versions in both time and frequency are displayed. Below, the associated coefficient distribution function λ_{water} is plotted in the top graph while the lower graph shows the max and min value of the wavelet filter bank response as a function of the channel number.
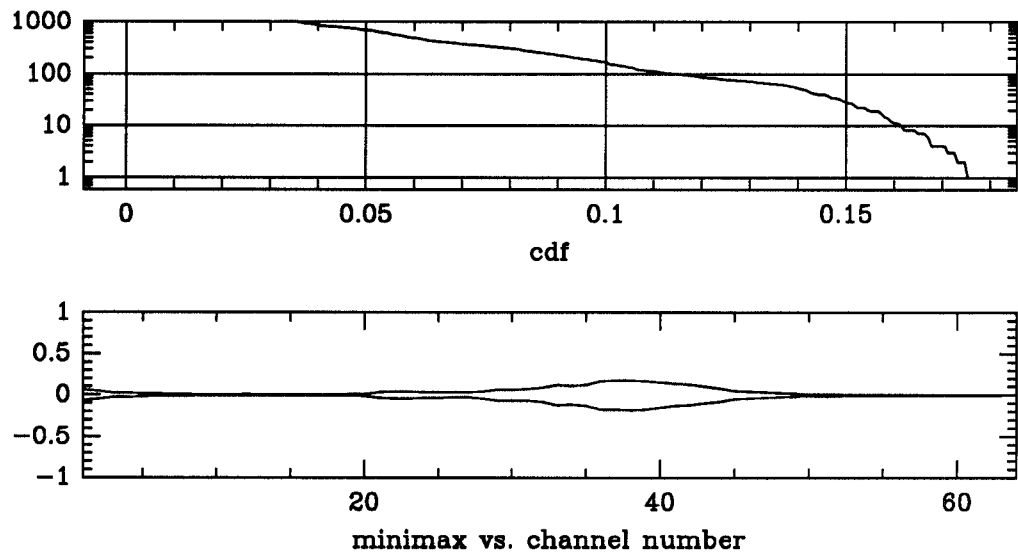

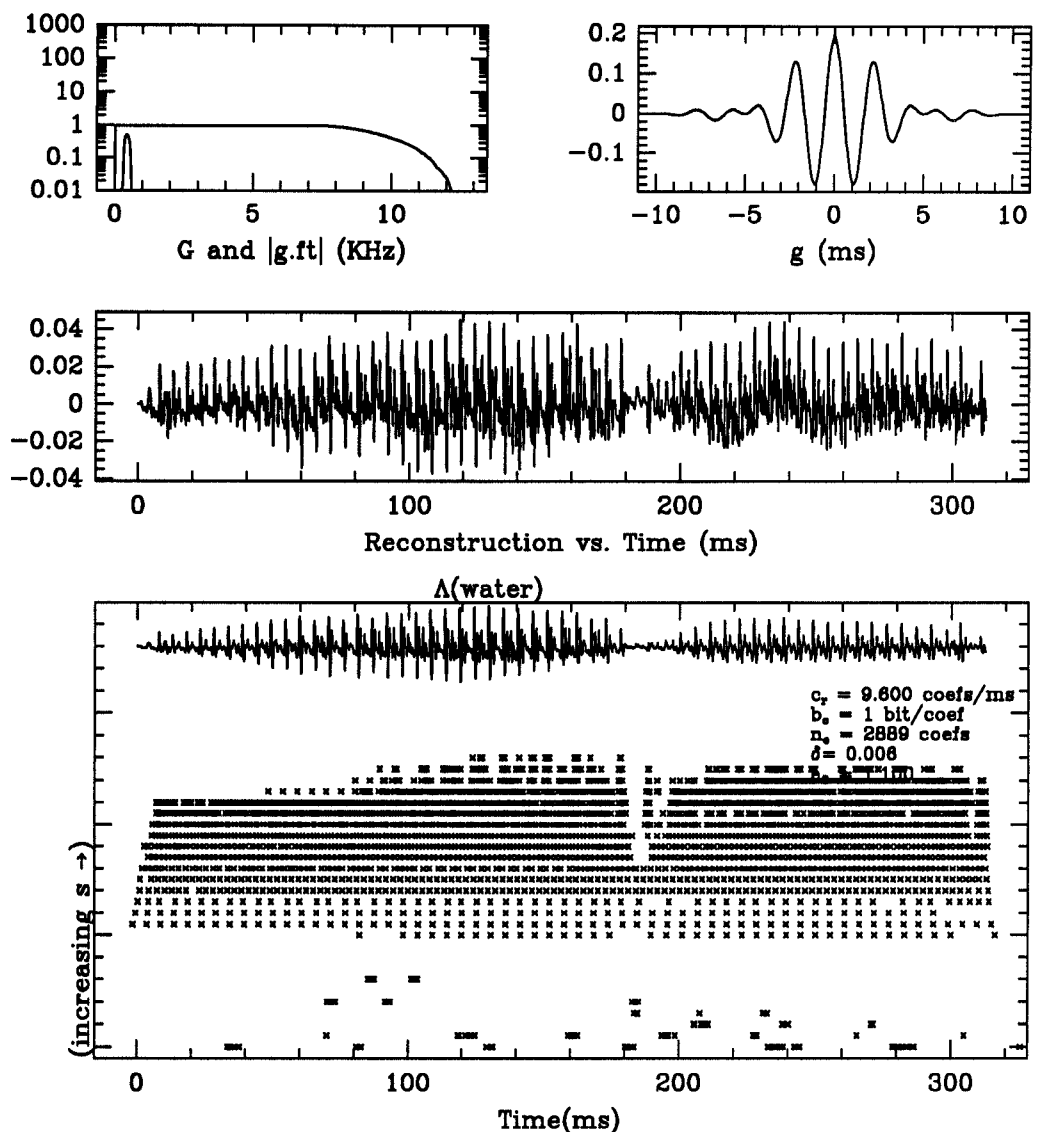Figure 6.120: Cdf and minimax curves for compressed "water", $(b_c, b_r) = (1, 9.6)$.

Figure 6.121: PE wavelet representation for "water", $(b_c, b_r) = (4, 4.8)$.

Shown above is the wavelet positive extrema representation and its reconstruction for the compressed signal "water". The trapezoidal analyzing function g appears in the top upper right. To its left are the functions $G = \sum_{m=1}^{N} |D_{s_m}\widehat{g}|^2$ and $\widehat{g}$. The middle graph displays the reconstruction of Algorithm 3.4.3. The lower most graph displays the sampling set Γ. At the top of the bottom graph is the input signal and to its lower right the values of the reconstruction parameters.
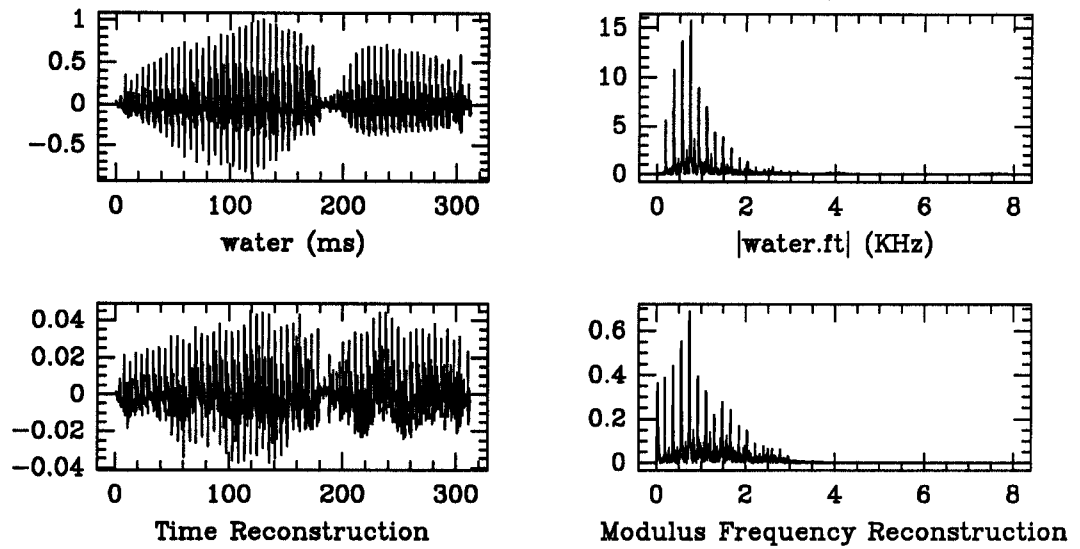
Figure 6.122: Reconstruction of compressed "water", $(b_c, b_r) = (4, 4.8)$.

Above, the signal "water" and its reconstructed versions in both time and frequency are displayed. Below, the associated coefficient distribution function λ_{water} is plotted in the top graph while the lower graph shows the max and min value of the wavelet filter bank response as a function of the channel number.
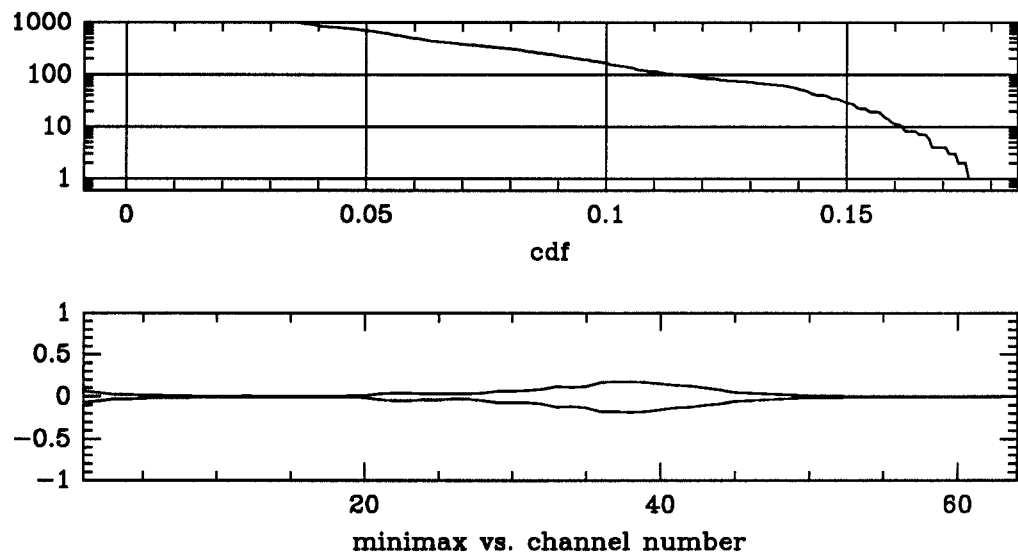

Figure 6.123: Cdf and minimax curves for compressed "water", $(b_c, b_r) = (4, 4.8)$.
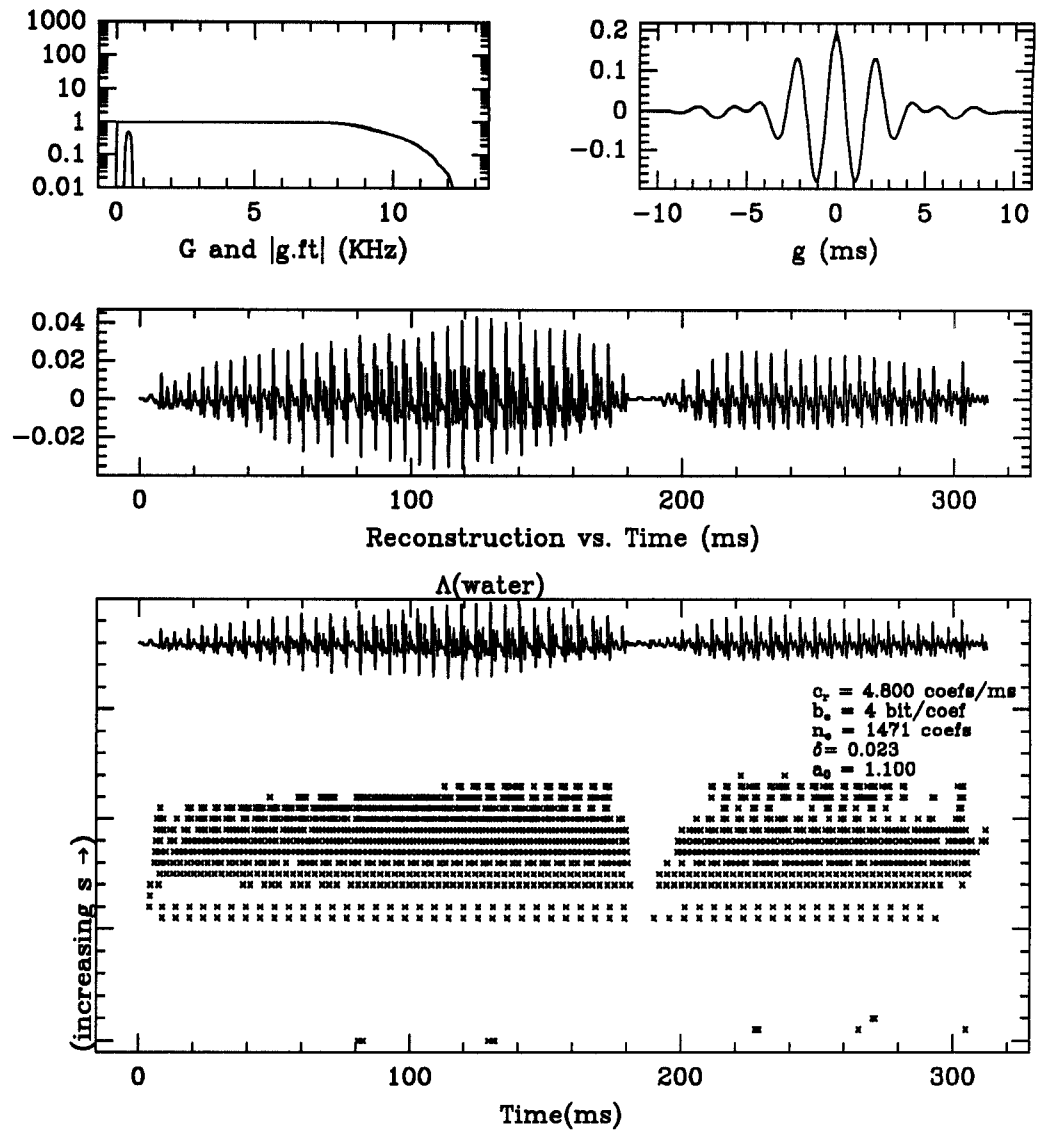
Figure 6.124: PE wavelet representation for "water", $(b_c, b_r) = (2, 4.8)$.

Shown above is the wavelet positive extrema representation and its reconstruction for the compressed signal "water". The trapezoidal analyzing function g appears in the top upper right. To its left are the functions $G = \sum_{m=1}^{N} |D_{s_m}\hat{g}|^2$ and $\hat{g}$. The middle graph displays the reconstruction of Algorithm 3.4.3. The lower most graph displays the sampling set Γ. At the top of the bottom graph is the input signal and to its lower right the values of the reconstruction parameters.
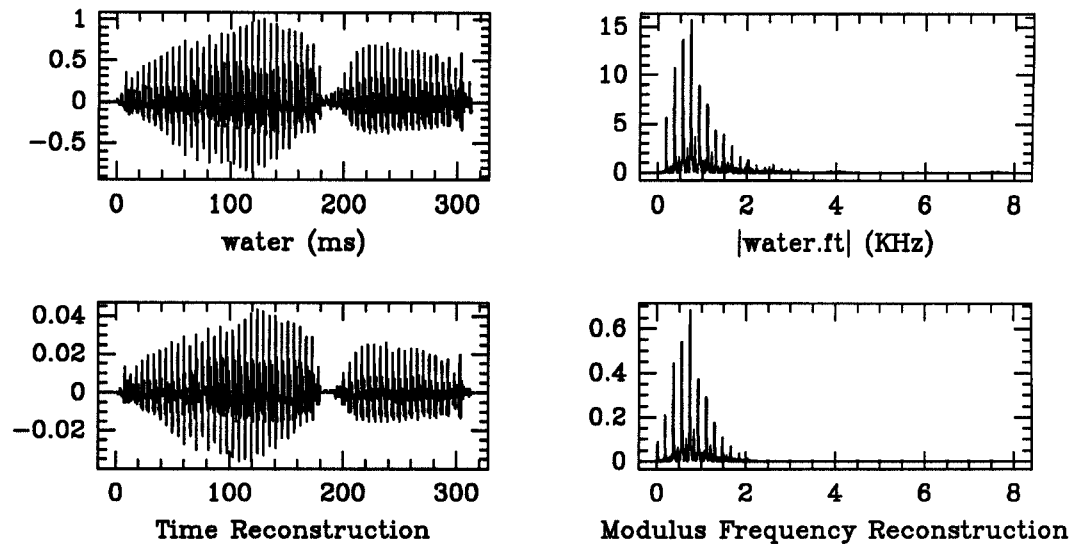
Figure 6.125: Reconstruction of compressed "water", $(b_c, b_r) = (2, 4.8)$.

Above, the signal "water"and its reconstructed versions in both time and frequency are displayed. Below, the associated coefficient distribution function λ_{water} is plotted in the top graph while the lower graph shows the max and min value of the wavelet filter bank response as a function of the channel number.

Figure 6.126: Cdf and minimax curves for compressed "water", $(b_c, b_r) = (2, 4.8)$.

Figure 6.127: PE wavelet representation for "water", $(b_c, b_r) = (1, 4.8)$.

Shown above is the wavelet positive extrema representation and its reconstruction for the compressed signal "water". The trapezoidal analyzing function g appears in the top upper right. To its left are the functions $G = \sum_{m=1}^{N} |D_{s_m} \hat{g}|^2$ and $\hat{g}$. The middle graph displays the reconstruction of Algorithm 3.4.3. The lower most graph displays the sampling set Γ. At the top of the bottom graph is the input signal and to its lower right the values of the reconstruction parameters.

Figure 6.128: Reconstruction of compressed "water", $(b_c, b_r) = (1, 4.8)$.

Above, the signal "water" and its reconstructed versions in both time and frequency are displayed. Below, the associated coefficient distribution function λ_{water} is plotted in the top graph while the lower graph shows the max and min value of the wavelet filter bank response as a function of the channel number.
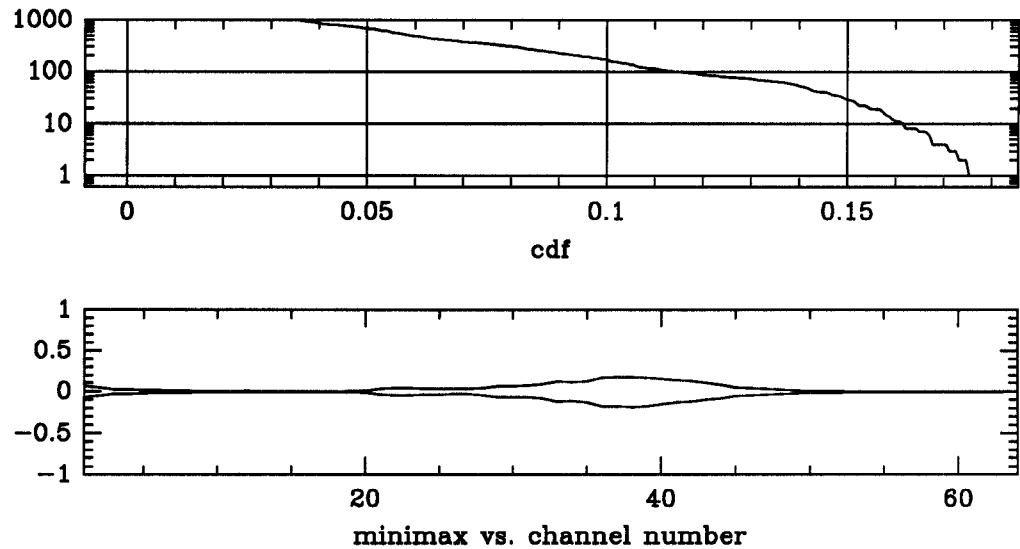

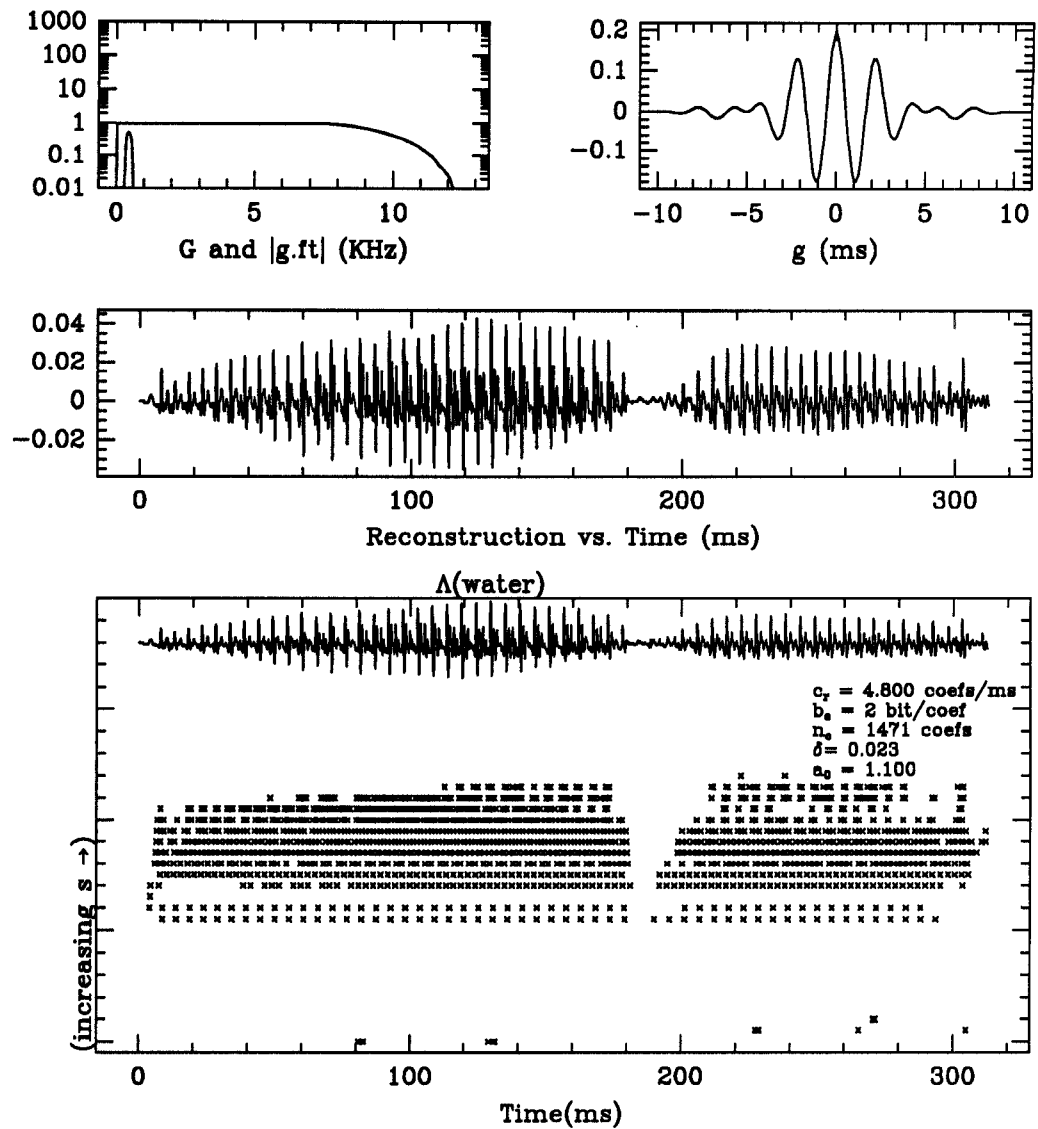Figure 6.129: Cdf and minimax curves for compressed "water", $(b_c, b_r) = (1, 4.8)$.

Figure 6.130: PE wavelet representation for "water", $(b_c, b_r) = (4, 2.4)$.

Shown above is the wavelet positive extrema representation and its reconstruction for the compressed signal "water". The trapezoidal analyzing function g appears in the top upper right. To its left are the functions $G = \sum_{m=1}^{N} |D_{s_m}\widehat{g}|^2$ and $\widehat{g}$. The middle graph displays the reconstruction of Algorithm 3.4.3. The lower most graph displays the sampling set Γ. At the top of the bottom graph is the input signal and to its lower right the values of the reconstruction parameters.
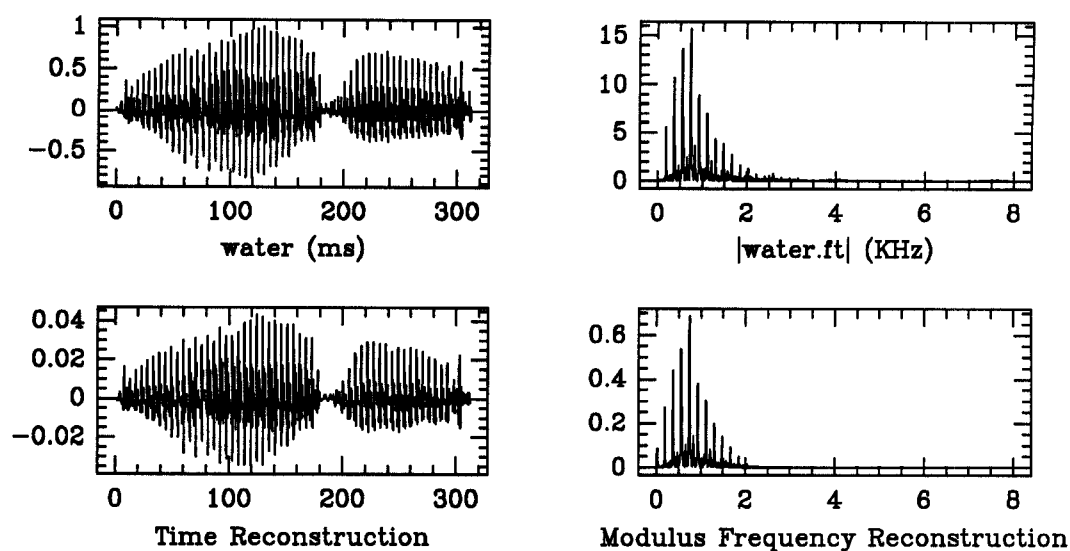
Figure 6.131: Reconstruction of compressed "water", $(b_c, b_r) = (4, 2.4)$.

Above, the signal "water"and its reconstructed versions in both time and frequency are displayed. Below, the associated coefficient distribution function λ_{water} is plotted in the top graph while the lower graph shows the max and min value of the wavelet filter bank response as a function of the channel number.
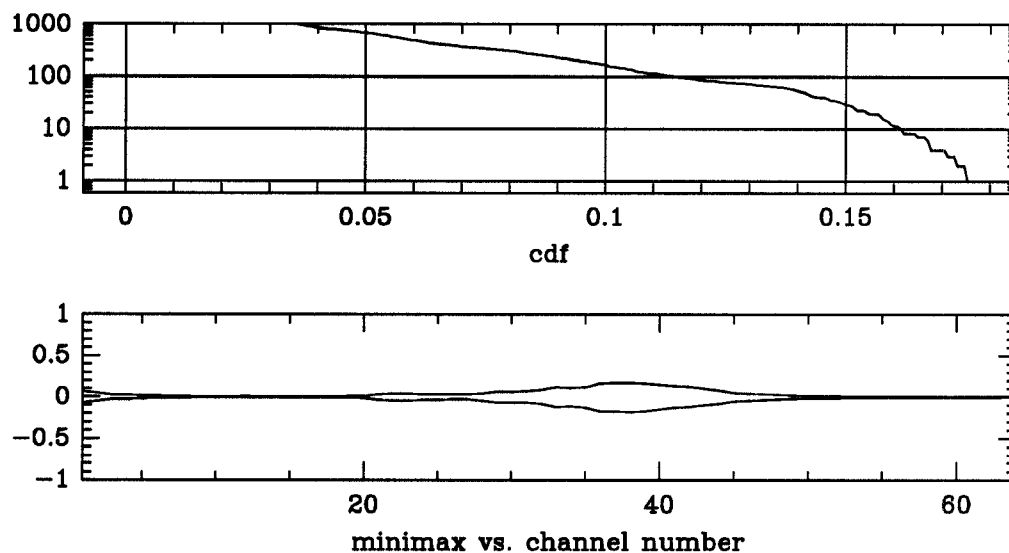

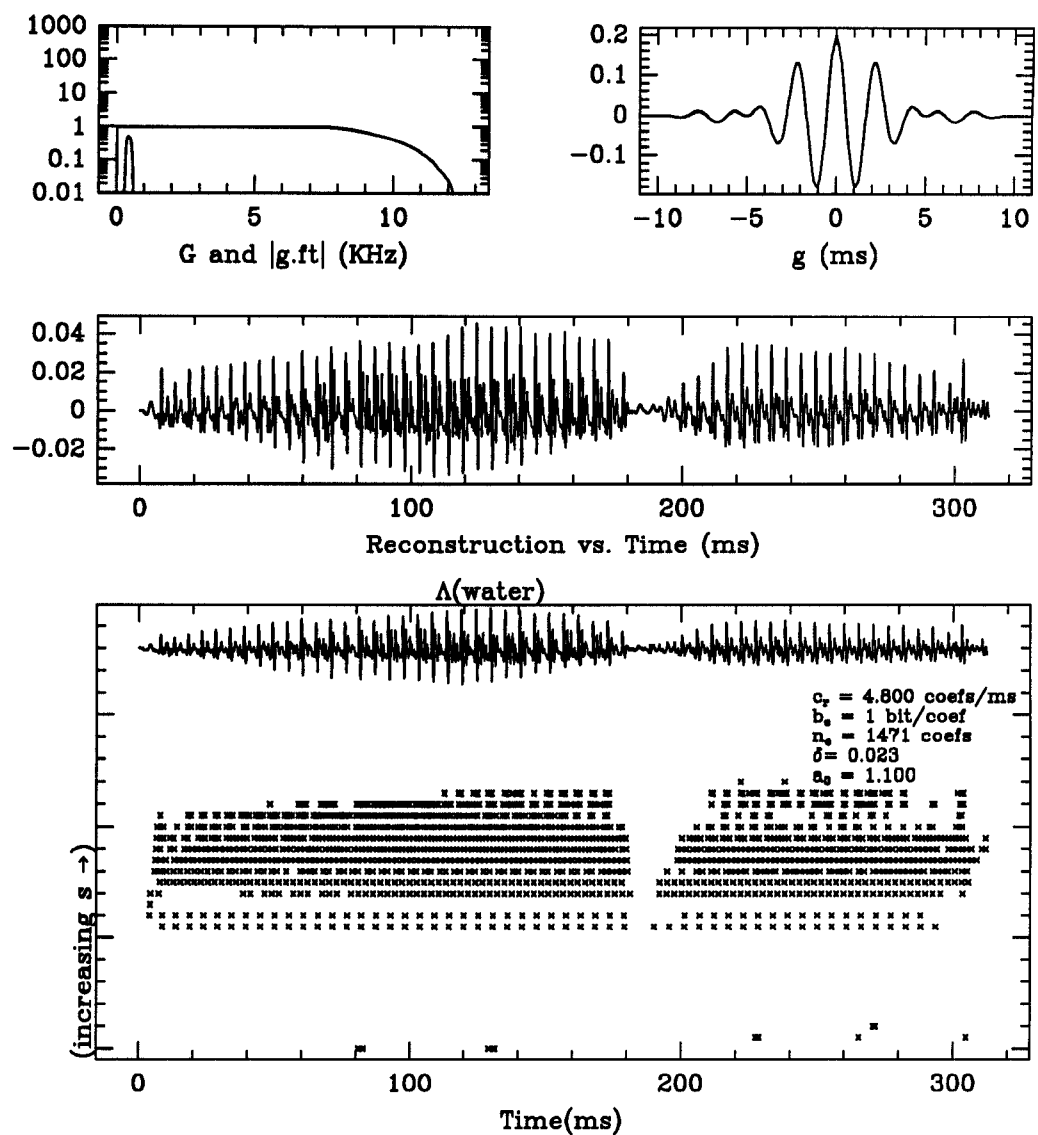Figure 6.132: Cdf and minimax curves for compressed "water", $(b_c, b_r) = (4, 2.4)$.
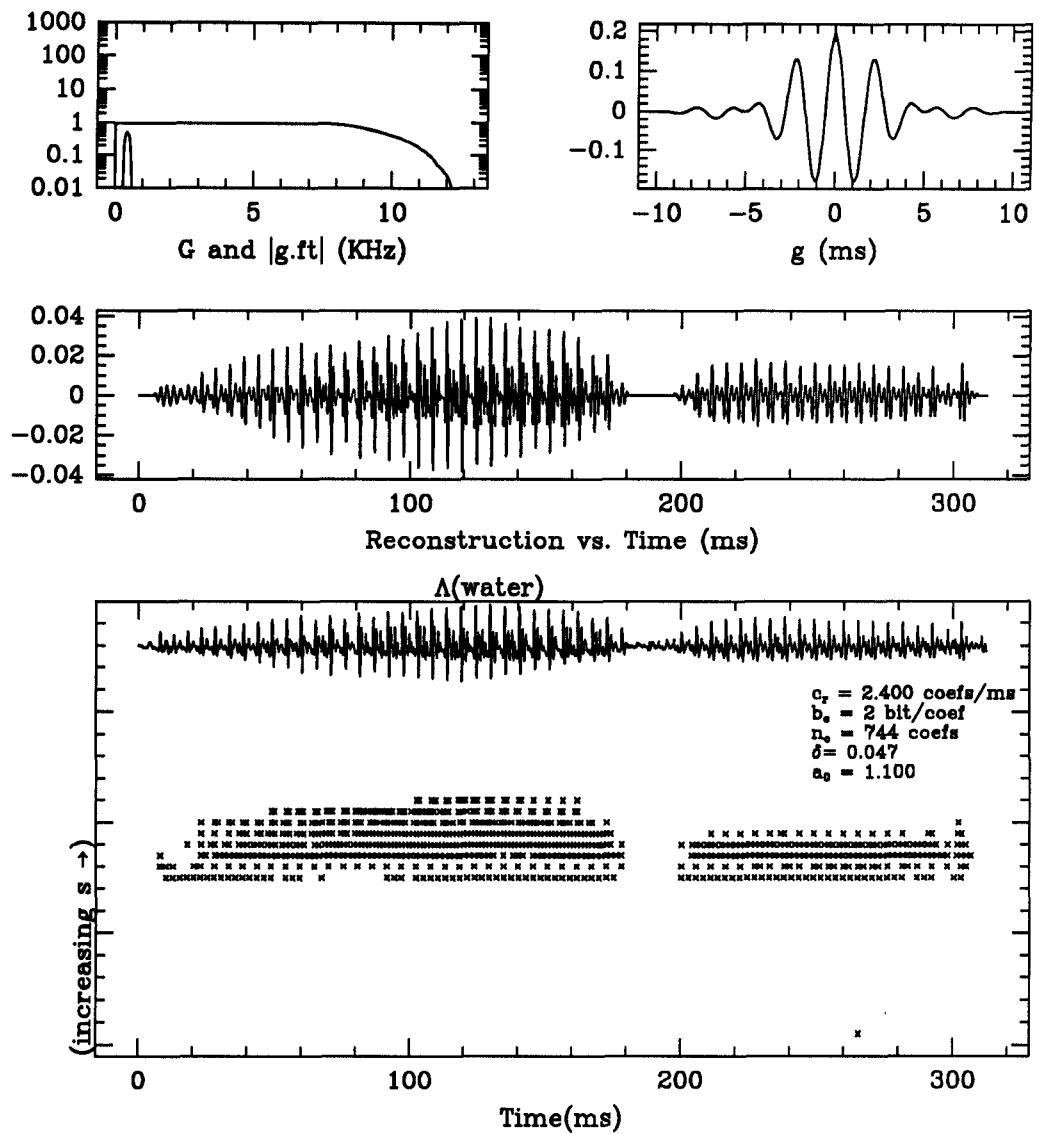
Figure 6.133: PE wavelet representation for "water", $(b_c, b_r) = (2, 2.4)$.

Shown above is the wavelet positive extrema representation and its reconstruction for the compressed signal "water". The trapezoidal analyzing function g appears in the top upper right. To its left are the functions $G = \sum_{m=1}^{N} |D_{s_m}\widehat{g}|^2$ and $\widehat{g}$. The middle graph displays the reconstruction of Algorithm 3.4.3. The lower most graph displays the sampling set Γ. At the top of the bottom graph is the input signal and to its lower right the values of the reconstruction parameters.
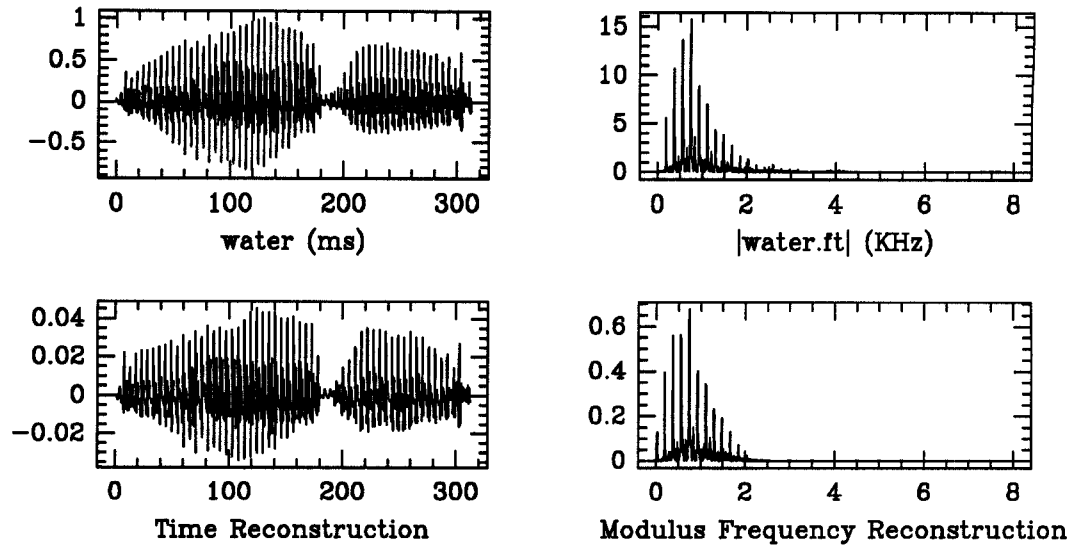
185
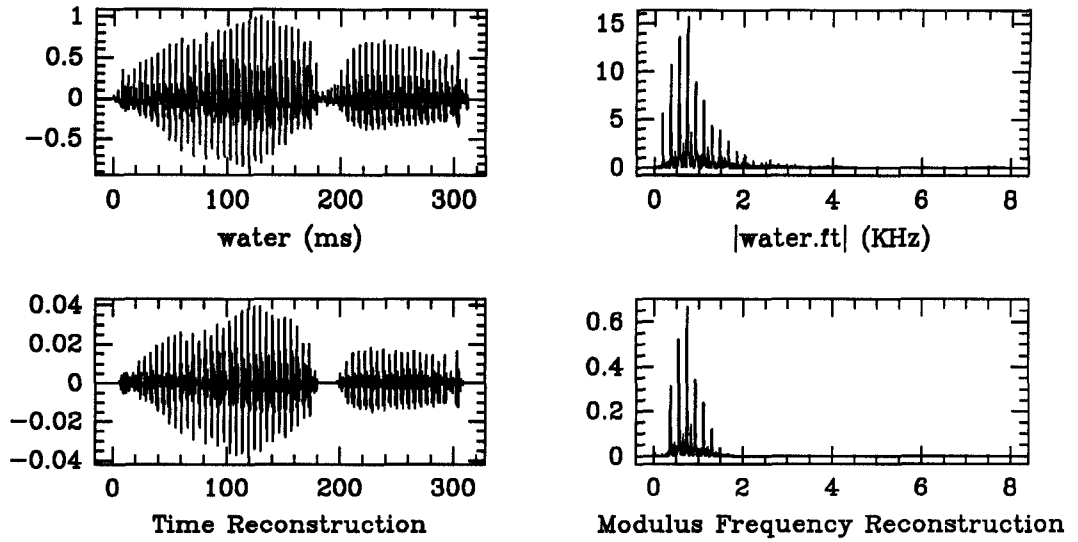
Figure 6.134: Reconstruction of compressed "water", $(b_c, b_r) = (2, 2.4)$.

Above, the signal "water" and its reconstructed versions in both time and frequency are displayed. Below, the associated coefficient distribution function λ_{water} is plotted in the top graph while the lower graph shows the max and min value of the wavelet filter bank response as a function of the channel number.
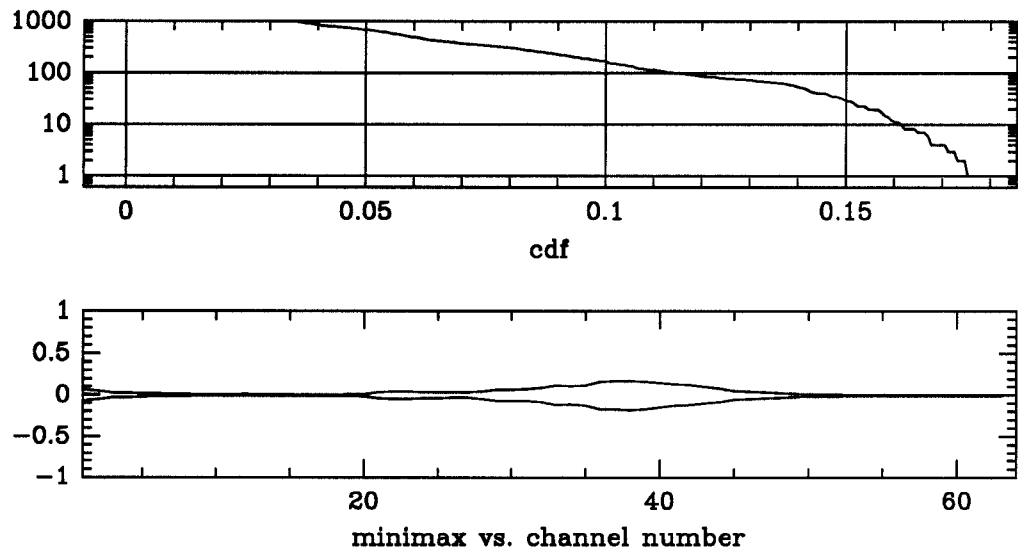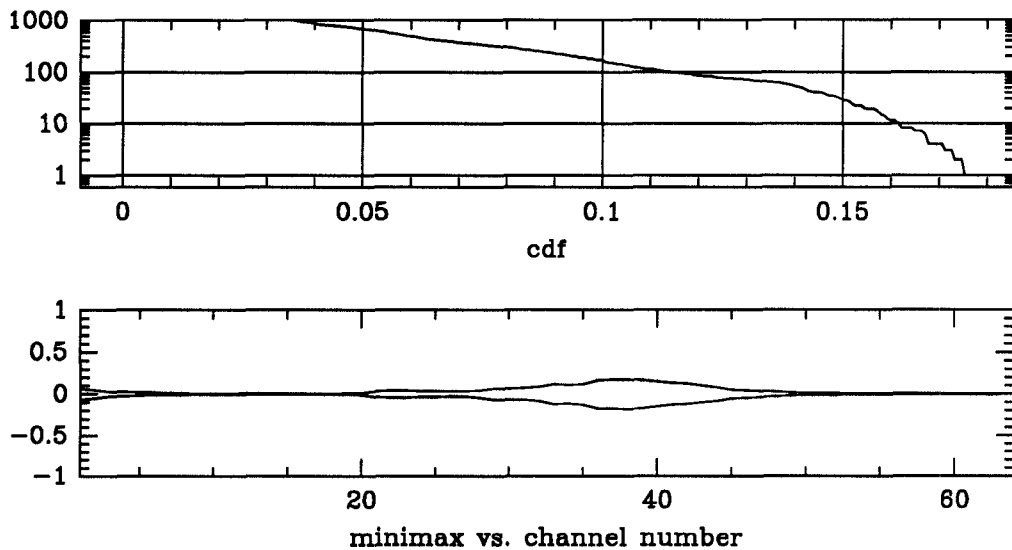

Figure 6.135: Cdf and minimax curves for compressed "water", $(b_c, b_r) = (2, 2.4)$.
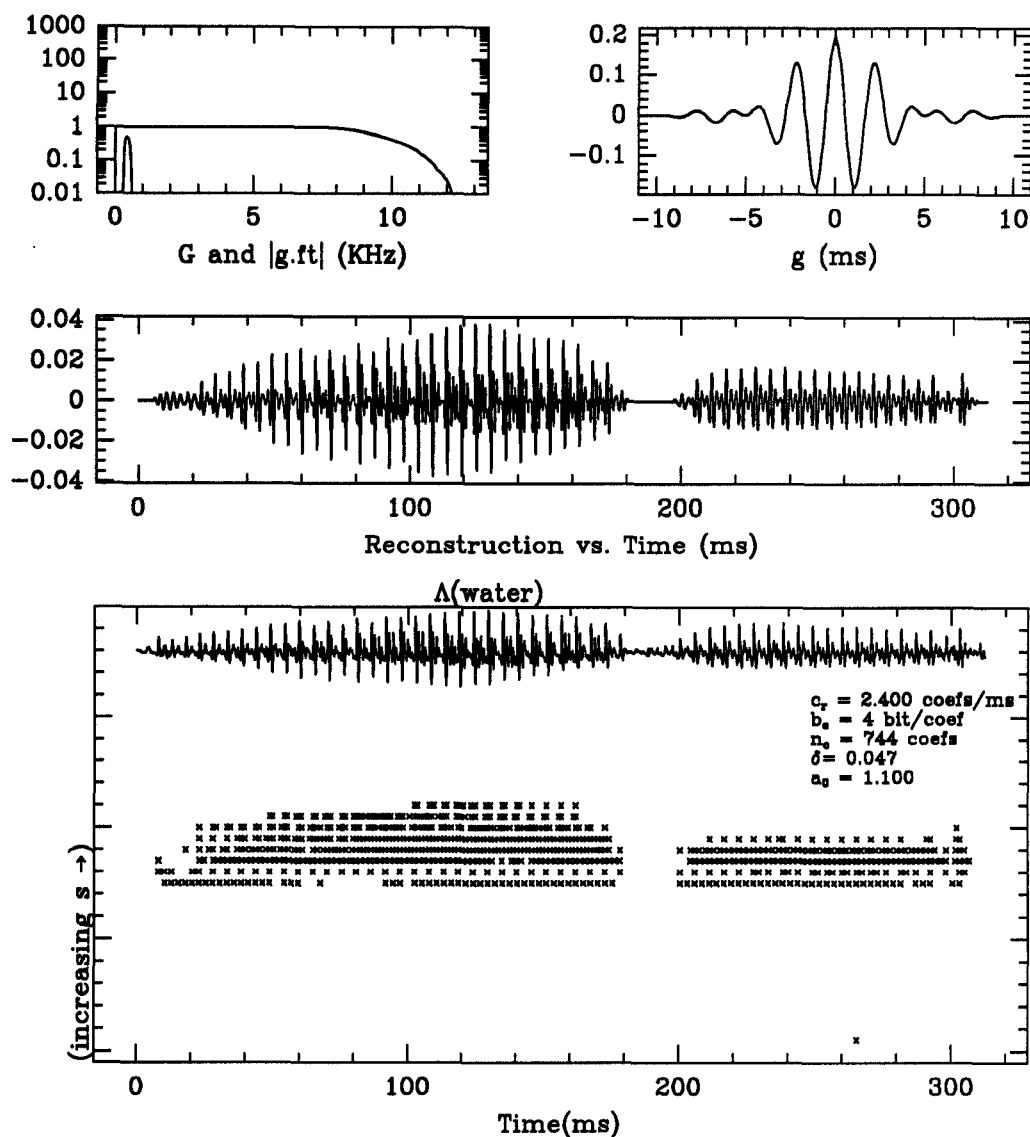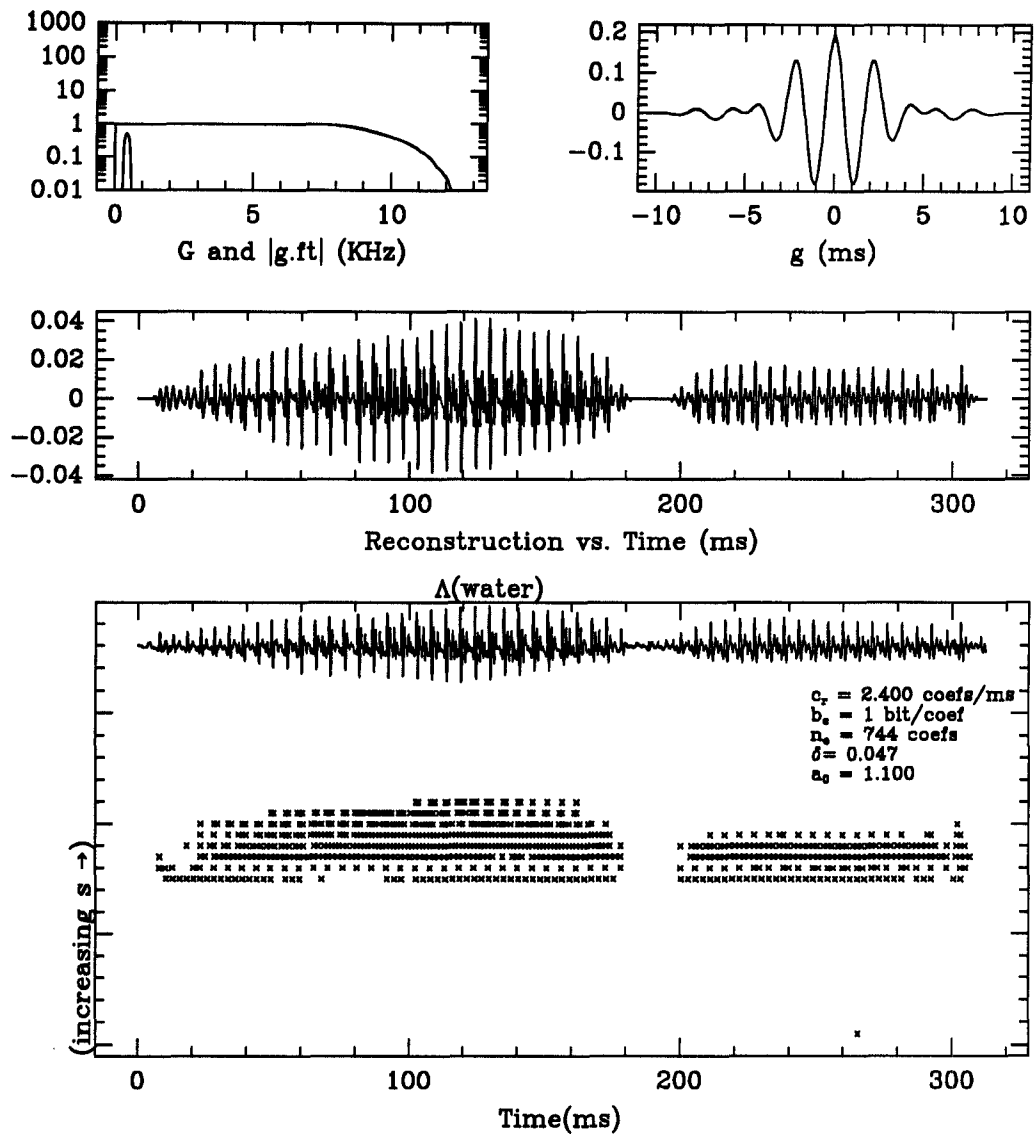
Figure 6.136: PE wavelet representation for "water", $(b_c, b_r) = (1, 2.4)$.

Shown above is the wavelet positive extrema representation and its reconstruction for the compressed signal "water". The trapezoidal analyzing function g appears in the top upper right. To its left are the functions $G = \sum_{m=1}^{N} |D_{s_m} \widehat{g}|^2$ and $\widehat{g}$. The middle graph displays the reconstruction of Algorithm 3.4.3. The lower most graph displays the sampling set Γ. At the top of the bottom graph is the input signal and to its lower right the values of the reconstruction parameters.
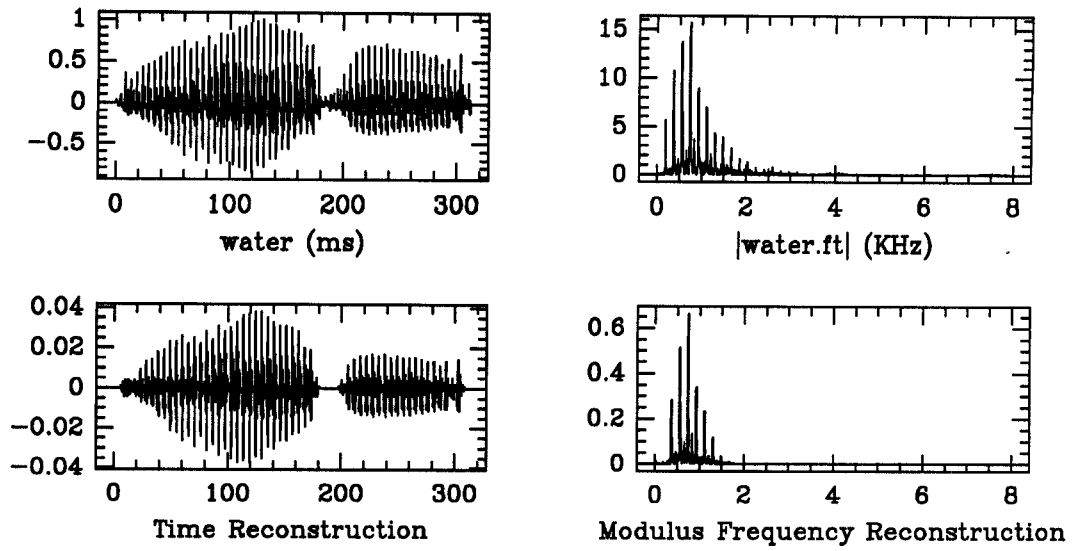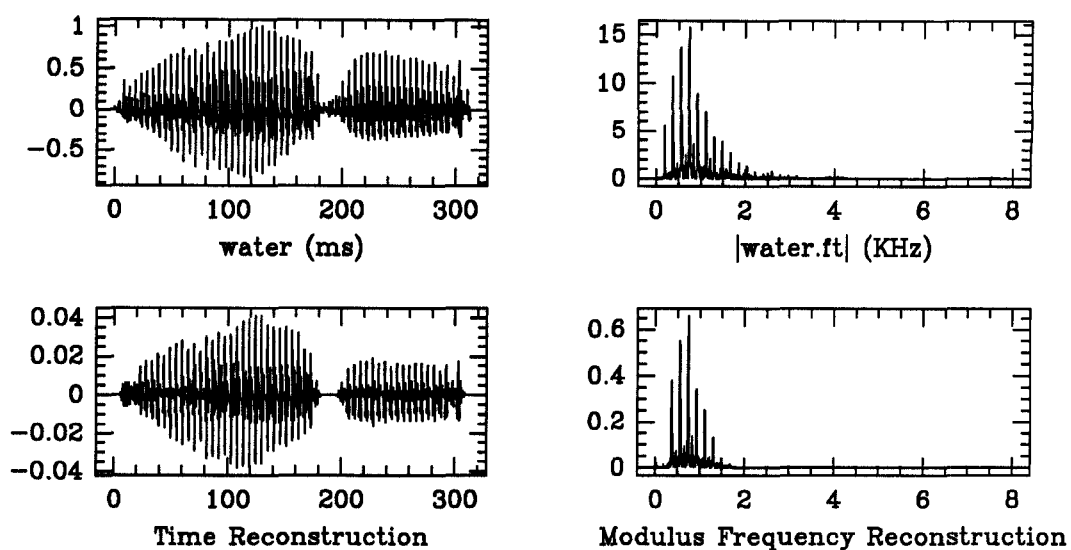
Figure 6.137: Reconstruction of compressed "water", $(b_c, b_r) = (1, 2.4)$.

Above, the signal "water"and its reconstructed versions in both time and frequency are displayed. Below, the associated coefficient distribution function λ_{water} is plotted in the top graph while the lower graph shows the max and min value of the wavelet filter bank response as a function of the channel number.
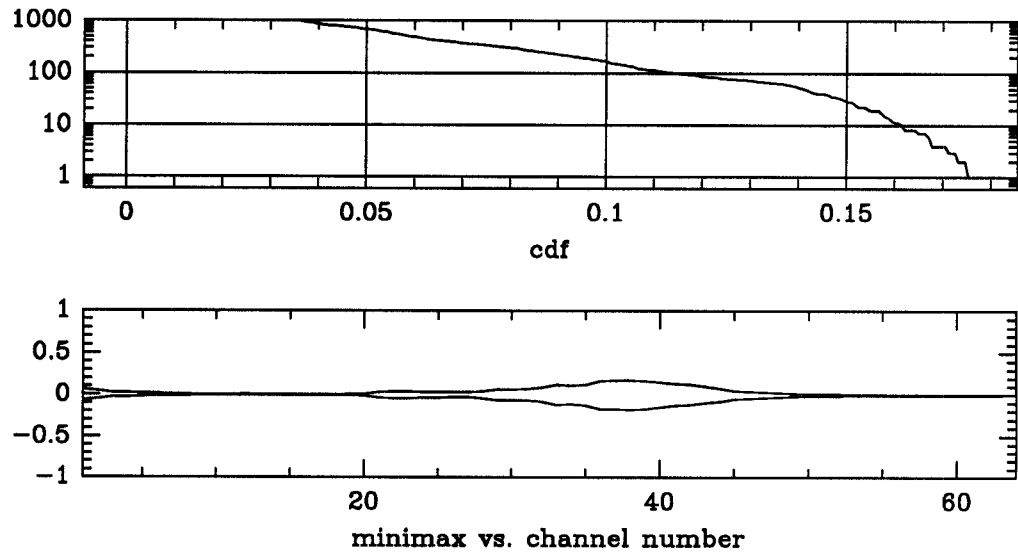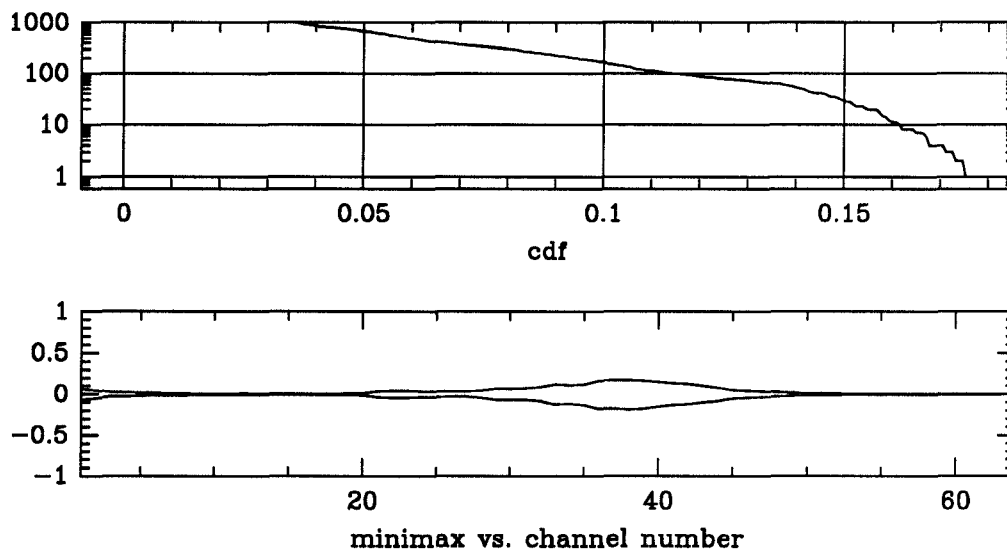

Figure 6.138: Cdf and minimax curves for compressed "water", $(b_c, b_r) = (1, 2.4)$.

6.4 Discussion

In this chapter we have presented numerous examples of discrete signal representations. Examples have been computed and displayed for cases from uniform sampling representations in Paley-Wiener spaces to positive extrema wavelet representations in $L^2(\mathbb{R})$ or $H_+^2(\mathbb{R})$. Moreover, we have applied the notions of local frames and frame coherence to the applications of compression and noise suppression.

6.4.1 Paley Wiener Sampling

We have provided examples which illustrate the reconstruction of bandlimited signals from their irregular samples using Algorithm 3.4.3.

A sufficient condition given by the Duffin-Schaeffer Theorem 4.2.4 for the reconstruction of a bandlimited signal from its irregular samples is that the sample set be dense enough, i.e., the uniform density of the sampling set be larger than twice the bandlimit. For signals with complex time-frequency behavior, e.g. the signal "packet" or "chirp", the Duffin-Schaeffer condition may lead to intuitively unsatisfactory sampling sets. For example for the "packet" signal we are required to sample at a density consistent with the highest frequency sine packet in the signal. For the other lower frequency sine packets this density is clearly excessive. Hence, for Paley-Wiener sampling there is no mechanism for time localization. In other words it is necessary to sample densely over the entire duration of the signal even if the high frequency components of the signal are well localized in time. This situation naturally suggests a joint time-frequency analysis such as afforded by the wavelet transform.

6.4.2 PE wavelet Representation

Some of the general properties of the PE wavelet representations with trapezoidal analyzing function which have been observed here are listed below. Recall that the trapezoidal analyzing has very good localization in both time and frequency.

Fast Convergence For all reconstructions based on the PE wavelet extrema representation we have exhibited only the first iteration of Algorithm 3.4.3 with relaxation parameter $\lambda = 0.1$. As can be seen from the previous simulations the first iteration in every case is already a high quality, though multiplicatively scaled (by λ), version of the original. It has been experimentally observed that further iterations serve only to scale the reconstruction properly. We attribute this situation to the choice of well localized time-frequency analyzing function $g = g_{trap}$ and the fact that the function G of Lemma 4.2.1 is essentially constant over the frequency range of interest.

Quantization robustness Reconstructions via Algorithm 3.4.3 exhibit a high degree of robustness to quantization of coefficients. Quantization of the coefficients at levels as low as one or two bits per coefficient still result in high quality approximations of the original signal. This suggests the applicability of such representations to data and speech compression.

Embedded truncated representations An appealing property of the truncated wavelet representation of a signal f is that the truncated representations

$$\Lambda_\delta \;\triangleq\; \{W_g f_*(t_{m,n}, s_m) \;:\; W_g f_*(t_{m,n}, s_m) \geq \delta\}$$

form a decreasing continuum of sets with respect to the threshold parameter δ. In other words, if $\delta_1 < \delta_2$ then $\Lambda_{\delta_2} \subseteq \Lambda_{\delta_1}$. Thus, the truncation is hierarchical in the sense that representations with small information content Λ_{δ_2} are embedded in ones with higher information content Λ_{δ_1}.

Robust truncation It has been experimentally observed that (for coherent signals) as the PE representation is truncated through the application of smaller thresholds δ that reconstructions based on initializing Algorithm 3.4.3 with the data Λ_δ degrade in a robust way. Because the truncated representations are naturally embedded (see above), the increase of the threshold δ from δ_1 to δ_2 ($\delta_1 < \delta_2$) corresponds to the removal of some elements of Λ_{δ_1}. This in turn corresponds to removing the least significant components of the reconstruction based on Λ_{δ_1}. This insures that a small change in δ will not lead to a catastrophic change in the reconstruction.

Time Translation Invariance The PE wavelet representation is translation invariant in the sense that a time shifted version of a signal will yield a corresponding time shifted PE wavelet representation. This is simply because the extrema points of a function are translation invariant, i.e., if a signal is time shifted one unit to the left so are its extrema. Translation invariance is an important property in pattern recognition schemes where it is desirable for time shifted versions of signals to yield identical representations.

6.4.2.1 Noise Suppression

From the numerical experiments we have observed the ability to reject wide band random noise in signals with coherent time-frequency structure. The basic approach to noise suppression has been founded on the notion of frame coherence, viz. Section 3.5.1, and localization through application of a thresholding operation on the (frame) representation of a noise corrupted signal.

The minimax curves in the simulations illustrate the notion of coherence. Recall that the minimax curves show the minimum and maximum values attained by the output of a specific filter in the continuous wavelet representation of the signal. Comparing the minimax curves for a specific signal it can be seen that as the noise level is increased the overall shape of the curve due to the coherent portion is retained while the gap between the minimum and maximum curves is increased uniformly over all channels due to the incoherent portion. This is because the incoherent portion must necessarily spread its energy throughout the entire filter bank. For this reason we should choose a threshold which rejects the gap area. Clearly, in high noise situations this procedure will break down since the non-coherent portion may rise to a level comparable to the signal.

6.4.2.2 Compression

Examining the results of our compression experiment we can make the following observations:

(i) In general, reconstructions are 'good' for all values of b_c=1,2 or 4. We use the term 'good' in the sense that both the time and frequency magnitude reconstructions are judged to be close to their original counterparts.

(ii) Frequency magnitude reconstructions degrade less severely than time reconstructions as b_c varies from 4 to 1 bit per coefficient.

(iii) Strong frequency components (peaks) are replicated faithfully.

The results of the experiment also indicate that the PE representation is highly robust to quantization effects. Allocating just one or two bits per coefficient ($b_c = 1, 2$) still allows for good quality reconstructions. It is here that we see one benefit of non-orthogonal highly redundant systems, viz. Section 3.5.1. All of these observations suggest that the proposed data compression scheme is a promising one for speech.

There are other variables, trade-offs, and issues for evaluating the compression scheme. We list some of them here.

(i) Besides coefficient quantization, time quantization must also be addressed. Each PE wavelet coefficient for a signal f is a sample $W_g f(s_m, t_{m,n})$ of the wavelet transform $W_g f$. Since the sequence $\{t_{m,n}\}$ is signal dependent for the PE representation, the reconstruction process (receiver) must have knowledge of these values. In our reconstructions we have assumed complete knowledge of the sequence $\{t_{m,n}\}$.

(ii) Essentially, we have circumvented the issue of windowing of the signal by taking the window to be of a length equal to the duration of the signal. In practice, windowing plays a finer role, e.g., in narrowband speech compression systems going back to Dudley (1939), speech coders divide the speech signal into intervals of duration 10 to 25 ms.

(iii) The dilation parameter a_0 effectively changes the frequency support of each filter in the filter bank $\left\{ (D_{a_0^k} \partial \widehat{g}) \right\}$. In particular, increasing the value of a_0 decreases the bandwidth of each filter in the bank. A decrease in bandwidth necessarily implies that a particular filter will respond to a smaller band in frequency. Thus, keeping f the same, an increase in the value of a_0 will cause the bands of activity in the original a_0 representation to become compressed along the s-axis in the new increased a_0 representation. Thus, with δ fixed, larger a_0 will lead to smaller data sets. On the other hand, larger values of a_0 will cause the function G in 4.2.1 to have greater variation from constant value. This condition necessarily implies a spread between possible frame bounds, i.e., movement away from tightness. This, in turn, can be related to a slowing of the rate of convergence of the reconstruction Algorithm 3.4.3.

(iv) An interesting inherent feature of the compression scheme and representation is that, in a communication setting, all of the available bandwidth can be used for the transmission of information about the underlying signal. Suppose a fixed information transmission rate limit, e.g., the bit rate constraint b_r. Further, suppose that a threshold of $\delta = 0$ yields a finite PE wavelet representation $\Lambda_0(f_*)$ from which it is possible to reconstruct perfectly the original signal f_*. Clearly, the cardinality of the representation $\Lambda_0(f_*)$ depends on the information content of the underlying signal f_*. For example, if $f_* \equiv 0$ then card $\Lambda_\delta = 0$ for all values of δ. For signals with low enough information content,

i.e., $b_c \cdot \text{card } \Lambda_0 < b_r \cdot |I(f_*)|$, the information rate constraint poses no problem. For more complex signals, though, a threshold of zero will not suffice to meet the information constraint. Suppose we have such a signal. In this case, an appropriate threshold must be found via the distribution function in (5.3.3). Since the thresholded representations are embedded (see above), the PE wavelet compression scheme can be viewed as a method to remove the least significant coefficients from the set Λ_0 to meet the information rate constraint. Removing the least significant coefficients insures that the least amount of information will be lost. The significance of this is that (i) the PE wavelet compression scheme yields the best thresholded representation which meets the information constraint; and (ii) if the information constraint b_r were increased, the new PE wavelet compressed representation would contain the old PE wavelet compressed representation. This is a consequence of the fact that the information constraint b_r can be related directly to the threshold δ by the relation

$$b_c \text{ card } \Lambda_\delta / |I(f_*)| \leq b_r,$$

and that card Λ_δ is a decreasing function of δ. If $b_1 < b_2$ are two information rate constraints, the two corresponding thresholded representations generated by the PE wavelet compression scheme will be Λ_{δ_1} and Λ_{δ_2}, and $\delta_1 \geq \delta_2$ so that $\Lambda_{\delta_1} \subseteq \Lambda_{\delta_2}$. Consequently, over different signals (or pieces of signals) it is always possible to transmit at a rate up to the information limit b_r by adjusting the threshold δ.

(v) We have not dealt with the issue of the choice of the analyzing function aside from designing it to have good time and frequency localization. For the compression of speech data it seems reasonable to suspect that analyzing functions which come from a model of the auditory system will provide better results. This issue has been studied by Benedetto and Teolis [BT92a], [BT92b].

Chapter 7

Conclusion

We conclude this thesis with a brief summary and list of directions for future research. Highlighted in the summary is a list of some of the contributions made by this research.

7.1 Summary

In this thesis we have presented a constructive theory for the discrete representation of analog signals from infinite dimensional Hilbert spaces. The approach to discrete representation which we have taken has its fundamental roots in the theory of frames and may be analyzed in terms of irregular sampling in certain reproducing kernel Hilbert spaces. In its most general form the discrete representation of a signal is the irregular samples of a signal dependent function whose domain is a group, e.g., the real line under addition, or the affine group. Special cases of this general transform are the Gabor and Wavelet transform.

With the perspective of digital implementation, we have developed algorithms for the reconstruction of signals from their discrete representations. In addition, we have studied the effects of quantization and perturbations in the representation domain with respect to reconstructions.

We have introduced the notion of frame localization with respect to a specific signal. Localization leads to finite discrete representations which efficiently capture the essential characteristics of a signal.

Further, we have implemented the theory and provided numerous examples of representations and their reconstructions. For the particular case of the positive wavelet extrema representation we have implemented schemes for noise suppression and compression. Results of these applications can be viewed in Chapter 6.

In the following list we indicate some of the main contributions of this research:

- A general reproducing kernel Hilbert space frame representation approach to the representation of signals from infinite dimensional Hilbert spaces.

- The development of iterative algorithms for the reconstruction of a signal from its discrete representation which is cast in terms of the frame correlation operator, viz. Section 3.3.

- Identification of the role of the pseudo-inverse frame correlation operator in reconstruction from perturbed representations and its relation to the underlying frame bounds in infinite dimensional spaces, viz. Theorem 3.3.6.

- The development of an iterative algorithm for the reconstruction of a signal from its *perturbed* representation, e.g., from quantization of the representation.

- Introduction of the notion of frame localization through truncation and signal dependent sampling sets.

- Introduction of the positive extrema wavelet representation for the efficient representation of signals with complex time-frequency behavior.

- A discrete representation method for the suppression of noise based on the notion of frame coherence, viz. Section 6.3.1.

- A discrete representation method for the compression of signals, viz. Section 6.3.2.

7.2 Future Directions

Future research efforts may be thought of in two broad areas. First, there are extensions of the theory and second, there is the investigation and development of further applications.

7.2.1 Theory

Some potential theoretical directions on which future research could focus are listed below.

Extension of the theory to higher dimensions In particular a two dimensional extension of the theory would find immediate applicability in image processing.

Incorporation of auxiliary information In many applications there is auxiliary information known about a signal. For example, the signal may be known to be positive in certain intervals. In such cases, we expect that signals should be able to be represented more efficiently with side information than without it.

Investigation of zero crossing sets In [Log77] Logan shows that certain classes of (octave) bandlimited functions may be reconstructed from knowledge of only their zero crossings to within a multiplicative constant; however, Logan's original work is non-constructive in nature. The analysis of zero crossings in terms of the frame approach we have taken in this thesis may lead to a constructive theory of reconstruction from zero crossing sets for octave bandlimited functions. Moreover, extensions to larger spaces may be attacked with an approach similar to that of Lemma 4.2.1.

Analysis/Design of discrete representations There are many free parameters present in the generic discrete representations which we have developed here, viz. Chapter 4. These free parameters include the group, group representation, analyzing function g, and discrete sampling lattice in the group. In many cases some or all of these parameters will be fixed independent of the class of signals of interest. For a given problem, however, it may prove fruitful to tailor some of these parameters. A detailed analysis of these sorts of considerations could lead to efficient and useful representations of signals. For example, the positive extrema wavelet representation illustrated in Chapter 6 is based on signal dependent samplings where

the group, group representation, and analyzing function are all fixed apriori. There, the group and group representation have been selected to yield the wavelet transform. In this case, one direction of future research would involve the investigation of the design of analyzing functions to better suit the signals to be analyzed.

7.2.2 Application

In this thesis we have explored only two potential applications of the discretization theory. Namely, we have examined applications to compression and noise suppression. There are a vast number of other areas in signal and speech processing for which discrete representations have applicability. A partial list of some of these is given below.

Signal Detection/Recognition   From the simulations provided in Chapter 6 for the case of the positive extrema wavelet representation, there is an indication that such a representation captures the time-frequency content of the signal. Moreover, we have seen that these representations are robust to noise and enjoy the property of translation invariance. These observations indicate that such a representation is well suited for detection or recognition.

Parameter Estimation   For signals which may be described by one or more parameters discrete representations offer a method of estimating the signal parameter(s). In Chapter 6 we have seen that for the case of the positive extrema wavelet representation the time-frequency evolution of a signal is captured. For signals whose time-frequency behavior may be parameterized, e.g. frequency modulated (FM) signals, the positive extrema wavelet representation should provide enough information to estimate the modulation parameters. For example the parameter α in the chirp signal $\sin(\alpha t^2)$ can be estimated from any one of its representations in Section 6.2.2.3.

Synthesis/Resynthesis   We have heretofore focused on the process of representing a signal in a discrete manner. We may turn the situation around and ask if it is possible to directly construct discrete representations which when reconstructed have desirable or interesting properties. Or in a related question we may ask the following: given a discrete representation of a signal may that representation be altered to achieve some desired effect in the signal domain? Respectively, these two tasks are called synthesis and resynthesis. Development of such techniques may prove useful in music for the synthesis/resynthesis of interesting timbres.

Time Dilation   An interesting problem in sound processing is the speeding up or slowing down of recorded sound while preserving the frequency support of the signal. A possible approach to this problem is to develop processing techniques in the representation domain which perform the requisite speeding or slowing of signals. For instance, for the positive extrema representations of Chapter 6 a simple time dilation in the coefficient domain would change the speed in signal domain but not the frequency support.

Appendix A

Assorted Items

Proposition A.1 If $K : \mathcal{H}_1 \mapsto \mathcal{H}_2$ is a bounded linear operator mapping the Hilbert space $\mathcal{H}_1$ *into* the *closed* Hilbert space $\mathcal{H}_2$ then the adjoint operator K^* maps H_2 *onto* H_1.

Proof:

We first prove that the range $K^*(\mathcal{H}_2)$ is closed. Since $\mathcal{H}_2$ is closed, any converging sequence $\{y_n\} \subseteq \mathcal{H}_2$ converges to a $y = \lim y_n \in \mathcal{H}_2$. Through application of K^* we may generate another sequence $x_n = K^* y_n$ so that $\{x_n\} \subseteq K^*(\mathcal{H}_2)$. Because K^* is bounded and linear and therefore continuous we have that x_n converges and

$$x \overset{\triangle}{=} \lim x_n = \lim K^* y_n = K^*(\lim y_n) = K^* y$$

where the exchange of limit is justified since K^* is continuous. We conclude that $x \in K^*(\mathcal{H}_1)$ because $y \in \mathcal{H}_2$. Thus we have proven that $K^*(\mathcal{H}_2)$ is closed.

Using the basic fact from operator theory that

$$\overline{K^*(\mathcal{H}_2)} = (\ker K)^\perp,$$

and that K is 1-1, i.e. $\ker K = \{0\}$, we have

$$\overline{K^*(\mathcal{H}_2)} = K^*(\mathcal{H}_2) = \{0\}^\perp = \mathcal{H}_1.$$

This proves that K^* is onto $\mathcal{H}_1$.

∎

Corollary A.2 If in addition to the hypotheses of A.1 K is self adjoint ($\mathcal{H} \overset{\triangle}{=} \mathcal{H}_1 = \mathcal{H}_2$ is closed) then K^* is both surjective and injective, i.e. bijective, and therefore invertible on $K(\mathcal{H})$.

Appendix B

Group Representation

In this appendix we detail the computations which confirm that Π_H and Π_A are group representations of $\mathcal{G}_H$ and $\mathcal{G}_A$ respectively on $L^2(\mathbb{R})$ with the group operations indicated in Section 2.3.

B.1 Weyl-Heisenberg

The Weyl-Heisenberg group $\mathcal{G}_H$ is $\mathbb{T} \times \mathbb{R} \times \widehat{\mathbb{R}}$ and the representation we are using is $\Pi_G(z, t, \gamma) = z e_\gamma \tau_t$. For this to be a valid representation we must have $\Pi(x)\Pi(y) = \Pi(x \cdot y)$ for all $x, y \in \mathcal{G}_H$. Note the operator identity

$$\tau_b e_a = e^{-2\pi i a b} e_a \tau_b,$$

where a and b are real numbers. Let $x_1 = (z_1, t_1, \gamma_1)$ and $x_2 = (z_2, t_2, \gamma_2)$ be arbitrary members of $\mathcal{G}_H$. Then

$$
\begin{aligned}
\Pi_H(x_1)\Pi_H(x_2) &= z_1 e_{\gamma_1} \tau_{t_1} z_2 e_{\gamma_2} \tau_{t_2} \\
&= z_1 z_2 e^{-2\pi i \gamma_2 t_1} e_{\gamma_1} e_{\gamma_2} \tau_{t_1} \tau_{t_2} \\
&= z_1 z_2 e^{-2\pi i \gamma_2 t_1} e_{\gamma_1 + \gamma_2} \tau_{t_1 + t_2}.
\end{aligned}
$$

Thus, the group operation must be

$$(z_1, t_1, \gamma_1) \cdot (z_2, t_2, \gamma_2) = (z_1 z_2 e^{-2\pi i \gamma_2 t_1}, t_1 + t_2, \gamma_1 + \gamma_2).$$

With this operation it is easy to check that the identity is $e = (1, 0, 0)$, i.e. $\forall x \in \mathcal{G}_H$, $x \cdot e = e \cdot x = x$. If $x_2 = x_1^{-1}$ is the inverse of x_1 we must have $e = x_1 \cdot x_2$ or

$$(1, 0, 0) = (z_1 z_2 e^{-2\pi i \gamma_2 t_1}, t_1 + t_2, \gamma_1 + \gamma_2).$$

By direct substitution it can be seen that this is satisfied by

$$x_1^{-1} = (z_1^{-1} e^{-2\pi i \gamma_1 t_1}, -t_1, -\gamma_1).$$

B.2 Affine

The affine group $\mathcal{G}_A$ is $\mathbb{R} \times \mathbb{R}^+$ and the representation we are using is $\Pi_A(t,s) = \tau_t D_s$. For this to be a valid representation we must have $\Pi(x)\Pi(y) = \Pi(x \cdot y)$ for all $x, y \in \mathcal{G}_H$. Note the operator identity

$$D_a \tau_b = \tau_{a^{-1}b} D_a,$$

where $a > 0$ and b are real numbers. Let $x_1 = (s_1, t_1)$ and $x_2 = (s_2, t_2)$ be arbitrary members of $\mathcal{G}_A$. Then

$$\begin{aligned}
\Pi_H(x_1)\Pi_H(x_2) &= \tau_{t_1} D_{s_1} \tau_{t_2} D_{s_2} \\
&= \tau_{t_1} \tau_{s_1^{-1} t_2} D_{s_1} D_{s_2} \\
&= \tau_{t_1 + s_1^{-1} t_2} D_{s_1 s_2}
\end{aligned}$$

Thus, the group operation must be

$$(s_1, t_1) \cdot (s_2, t_2) = (t_1 + s_1^{-1} t_2, s_1 s_2).$$

With this operation it is easy to check that the identity is $e = (0,1)$, i.e. $\forall x \in \mathcal{G}_H$, $x \cdot e = e \cdot x = x$. If $x_2 = x_1^{-1}$ is the inverse of x_1 we must have $e = x_1 \cdot x_2$ or

$$(0,1) = (t_1 + s_1^{-1} t_2, s_1 s_2).$$

By direct substitution it can be seen that this is satisfied by

$$x_1^{-1} = (-s_1 t_1, s_1^{-1}).$$

Appendix C

Generalized Inverses

This appendix provides some of the basic concepts associated with generalized inverses of linear operators which are pertinent to frame representations and reconstructions. For a detailed treatment of the subject the reader is referred to [Gro77].

There are several equivalent definitions of a "generalized inverse" of a linear operator. We adopt the definition attributed to Penrose [Pen55] and use the terms "generalized inverse" and "pseudo inverse" interchangeably.

Definition C.1[Gro77, Definition (P)] If $A \in \mathcal{B}(\mathcal{H}_1, \mathcal{H}_2)$ has closed range, then $A^\dagger$ is the unique operator in $\mathcal{B}(\mathcal{H}_2, \mathcal{H}_1)$ satisfying

  (1) $AA^\dagger$ is self adjoint,

  (2) $A^\dagger A$ is self adjoint,

  (3) $AA^\dagger A = A$, and

  (4) $A^\dagger A A^\dagger = A^\dagger$.

Fact C.2 Let $A \in \mathcal{B}(\mathcal{H}_1, \mathcal{H}_2)$ have closed range. The mapping $A^\dagger : \mathcal{H}_2 \mapsto \mathcal{H}_1$ defined by

$$A^\dagger x = \operatorname*{argmin}_{y \in \mathcal{H}_2} \|y - Ax\|$$

is the generalized inverse of A.

Bibliography

[Alt60]   M. Altman, An optimum cubically convergent iterative method of inverting a bounded linear operator in Hilbert space, *Pacific J. Math.*, 10:1107–1114, 1960.

[Bal81]   R. Balian, Un principe d'incertitude fort en théorie du signal ou en mécanique quantique, *C. R. Acad. Sci. Paris*, 292:1357–1362, 1981.

[Ben92]   J. Benedetto, Irregular sampling and frames, In C. Chui, editor, *Wavelets: A Tutorial in Theory and Applications*, pages 445–507. Academic Press, Boston, MA, 1992.

[Ben93]   J. Benedetto, Frame decompositions, sampling and uncertainty principle inequalities, In J. Benedetto and M. Frazier, editors, *Wavelets: Mathematics and Applications*. CRC Press, Boca Raton, FL, 1993.

[Beu61]   F. Beutler, Sampling theorems and bases in Hilbert spaces, *Inf. Contr.*, 4:97–117, 1961.

[Beu66]   F. Beutler, Error-free recovery of signals from irregularly spaced samples, *SIAM Rev.*, 8:328–335, 1966.

[BH90]   J. Benedetto and W. Heller, Irregular sampling and the theory of frames, *Mat. note 10 suppl. n. 1*, pages 103–125, 1990.

[BHW90] J. Benedetto, C. Heil, and D. Walnut, Remarks on the proof of the balian-low theorem, Technical report, MITRE Corp., McLean, Virginia, 1990.

[BT92a]   J. Benedetto and A. Teolis, An auditory motivated time-scale signal representation, *IEEE-SP International Symposium on Time-Frequency and Time-Scale analysis*, October 1992.

[BT92b]   J. Benedetto and A. Teolis, A wavelet auditory model and data compression, submitted, 1992.

[CA87]   D. S. Chen and J. P. Allebach, Analysis of error in reconstructions of two-dimensional irregularly spaced samples, *IEEE Trans. ASSP*, ASSP-35:173–180, 1987.

[CFS]   C. Cenker, H. G. Feichtinger, and H. Steier, Fast iterative and non-iterative reconstruction of band-limited functions from irregular sampling values.

[Dau]   I. Daubechies, The wavelet transform: a tool for time-frequency localization, preprint.

[Dau88] I. Daubechies, Orthonormal bases of compactly supported wavelets, *Comm. Pure Appl. Math.*, 41:909–996, 1988.

[Dau90] I. Daubechies, The wavelet transform, time-frequency localization and signal analysis, *IEEE Trans. Information Theory*, 36(5):961–1005, 1990.

[Dau92] I. Daubechies, *Ten Lectures on Wavelets*, CBMS-NSF, SIAM, 1992.

[DGM86] I. Daubechies, A. Grossman, and Y. Meyer, Painless nonorthogonal expansions, *J. Math. Phys.*, 27(5):1271–1283, May 1986.

[DS52] R. Duffin and S. Schaeffer, A class of nonharmonic Fourier series, *Trans. Amer. Math. Soc.*, 72:341–366, 1952.

[FG89] H. G. Feichtinger and K. Gröchenig, Banach spaces related to integrable group representations and their atomic decompositions, i, *J. Functional Analy.*, 86:307–340, 1989.

[FG92] H. G. Feichtinger and K. Gröchenig, Iterative reconstruction of multivariate band-limited functions from irregular sampling values, *SIAM J. Math Anal.*, 23(1):1–18, January 1992.

[Gab46] D. Gabor, Theory of communication, *J. IEE*, 93:429–457, 1946.

[GG80] Israel Gohberg and Seymour Goldberg, *Basic Operator Theory*, Birkhauser, Boston, MA., 1980.

[Gib93] Jerry D. Gibson, *Principles of Digital and Analog Communications*, Macmillan, second edition, 1993.

[GM84] A. Grossman and J. Morlet, Decomposition of Hardy functions into square integrable wavelets of constant shape, *SIAM J. Math. Anal.*, 15:723–736, 1984.

[GMP85] A. Grossman, J. Morlet, and T. Paul, Transforms associated to square integrable group representations, I, General Results, *J. Math. Phys.*, 26:2473–2579, 1985.

[Gro77] C.W. Groetsch, *Generalized Inverses of Linear Operators*, marcel dekker, Inc., New York, 1977.

[Grö91] K. Gröchenig, Reconstruction algorithms in irregular sampling, NATO ASI, 1991.

[Grö92] K. Gröchenig, Irregular sampling of wavelet and short time Fourier transforms, preprint, 1992.

[Hel91] W. Heller, *Frames of exponentials and applications*, PhD thesis, University of Maryland, College Park, MD, 1991.

[HW89] C. Heil and D. Walnut, Continuous and discrete wavelet transforms, *SIAM Review*, 31:628–666, 1989.

[Jaf91] S. Jaffard, A density criterion for frames of complex exponentials, *Michigan Math. J.*, 38:339–348, 1991.

[Jer77]   A. J. Jerri, The Shannon sampling theorem-Its various extensions and applications: A tutorial review, *Proc. IEEE*, 65:1565–1596, 1977.

[Kad64]   M. I. Kadec, The exact value of the Paley-Wiener constant, *Soviet Math. Dokl.*, 5:559–561, 1964.

[Kot33]   V. A. Kotel'nikov, On the transmission capacity of 'ether' and wire in electro-communications, *Izd. Red. Upr. Svyazi RKKA*, 1933.

[Lev40]   N. Levinson, Gap and density theorems, *Am. Math. Soc. Colloq. Publ.*, 26, 1940.

[Log77]   Logan, Information contained in zero crossings, *Bell System Tech. J.*, 56(4):487–510, 1977.

[Low85]   F. Low, Complete sets of wave packets, In et al. C. DeTar, editor, *A Passion for Physics–Essays in Honor of Goeffrey Chew*, pages 17–22. World Scientific, Singapore, 1985.

[Mal89a] S. Mallat, Multifrequency channel decomposition of images and wavelet models, *IEEE Trans. ASSP*, 315:2091–2110, 1989.

[Mal89b] S. Mallat, Multiresolution approximations and wavelet orthonormal bases of $L^2(\mathbb{R})$, *Trans. Amer. Math. Soc.*, 315:69–87, 1989.

[Mal89c] S. Mallat, A theory for multiresolution signal decomposition: The wavelet representation, *IEEE Trans. on Pattern Anal. Machine Intell.*, 11:674–693, 1989.

[Mar87]   F. A. Marvasti, *A Unified Approach to zero-crossings and nonuniform sampling*, Nonuniform, Oak Park, Illinois, 1987.

[Mey90]   Y. Meyer, Ondelettes et Opérateurs, vol. I, II, and III, Hermann, 1990.

[MZ92a]   S. Mallat and Z. Zhang, Matching pursuits with time-frequency dictionaries, Technical report, 1992.

[MZ92b]   S. Mallat and S. Zhong, Wavelet transform maxima and multiscale edges, In M.B. Ruskai et al., editor, *Wavelets and their Applications*. Jones and Bartlett, Boston, 1992.

[Oga89]   Hidemitsu Ogawa, A generalized sampling theorem, *Electronics and Communications in Japan, Part 3*, 72(3):97–105, 1989.

[OS92]   Peder A. Olsen and Kristian Seip, A note on irregular discrete wavelet transforms, *IEEE Trans. on Information Theory*, 38(2):861–863, March 1992.

[Pat92]   Y. C. Pati, *Wavelets and Time-Frequency Methods in Linear Systems and Neural Networks*, PhD thesis, University of Maryland, College Park, MD, 1992.

[Pen55]   R. Penrose, A generalized inverse for matrices, *Proc. Cambridge Philos. Soc.*, 51:406–413, 1955.

[Pet67]   W. V. Petryshyn, On generalized inverses and uniform convergence of $(I - \beta K)^n$ with applications to iterative methods, *J. Math. Anal. Appl.*, 18:417–439, 1967.

[PW34]   R. Paley and N. Wiener, Fourier Transforms in the Complex Domain, *Am. Math. Soc. Colloq. Publ.*, 19, 1934.

[Roy68]   H. L. Royden, *Real Analysis*, Macmillan, second edition, 1968.

[Sei92a]   Kristian Seip, Density theorems for sampling and interpolation in the Bargmann-Fock space, *Bull. of the AMS*, 26(2):322–328, 1992.

[Sei92b]   Kristian Seip, Sampling and interpolation in the bargmann-fock space, preprint, 1992.

[Sha49]   C. E. Shannon, Communications in the presence of noise, *Proc. IRE*, 37:10–21, January 1949.

[Sho67]   D. Showalter, Representation and computation of the pseudoinverse, *Proc. Amer. Math. Soc.*, 18:584–586, 1967.

[Whi15]   E. T. Whittaker, On the functions which are represented by the expansion of interpolating theory, *Proc. Roy. Soc. Edinburgh*, 35:181–194, 1915.

[Yao67]   K. Yao, Applications of reproducing kernel Hilbert spaces-Bandlimited signal models, *Inform. Contr.*, 11:429–444, 1967.

[Yen56]   J. L. Yen, On nonuniform sampling of bandlimited signals, *IRE Trans. Circuit Theory*, CT-3:251–257, 1956.

[You80]   R. M. Young, *An Introduction to Nonharmonic Fourier Series*, Academic Press, New York, 1980.

[YT67]   K. Yao and J. Thomas, On some stability and interpolatory properties of nonuniform sampling expansions, *IEEE Trans. on Circuit Theory*, 14:404–408, 1967.

[YW91]   D. Youla and H. Webb, Image restoration by the method of convex projection, *IEEE Trans. on Medical Imaging*, 1:81–101, October 1991.